

# **HYDROGEN ATOM FORMATION IN THE GAMMA AND HEAVY ION RADIOLYSIS OF AQUEOUS SYSTEMS**

A thesis submitted to The University of Manchester for the  
degree of Doctor of Philosophy in the Faculty of Engineering  
and Physical Sciences.

**2010**

**Mónica Huerta Parajón**

**School of Chemistry**

---

# List of contents

<b>Chapter 1</b>	<b>Introduction</b>	<b>25</b>
1.1	Background	26
1.2	Objectives	26
1.3	References	27
<b>Chapter 2</b>	<b>An introduction to radiation chemistry and water radiolysis</b>	<b>29</b>
2.1	Introduction	30
2.2	Definition	30
2.3	Radiation from radioactive nuclei	30
2.4	Interaction of radiation with matter	32
2.5	Ionization and excitation produced by radiation	34
2.6	Reactions due to excited molecules, ions and free radicals	36
2.6.1	Reactions of excited molecules	36
2.6.2	Reactions of ions	36
2.6.3	Reactions of free radicals	37
2.7	Primary radiation processes in water	37
2.8	Summary	40
2.9	References	41
<b>Chapter 3</b>	<b>Facilities, Equipment &amp; Techniques</b>	<b>42</b>
3.1	Introduction	43
3.2	Chemicals	43
3.3	Radiation sources	43
3.3.1	The FN Tandem Van de Graaff accelerator	44
3.3.2	The Shepherd $^{60}\text{Co}$ source	53
3.4	Analytical techniques	55
3.4.1	The SRI 8610C gas chromatograph	55
3.4.2	The Balzers Mass Spectrometer	57
3.5	Set up and Data Collection	58
3.6	Summary	61
3.7	References	61

---

<b>Chapter 4</b>	<b>Stochastic Models</b> .....	63
4.1	Introduction.....	64
4.2	Radiation processes.....	64
4.3	Monte Carlo simulation of track structure.....	65
4.3.1	Monte Carlo simulation of electron track structure.....	65
4.3.1.1	Cross sections.....	68
4.3.2	Monte Carlo simulation of heavy ion track structure.....	72
4.4	Monte Carlo simulation of chemical evolution of the track.....	73
4.5	Summary.....	78
4.6	References.....	78
<b>Chapter 5</b>	<b>H atom determination in the radiolysis of water</b> .....	80
5.1	Introduction.....	81
5.2	Background to the H atom determination in the radiolysis of water.....	81
5.3	Experimental work.....	83
5.4	Supporting calculations.....	84
5.5	Results and discussion.....	84
5.5.1	Formate & nitrate addition.....	85
5.5.2	Deuterated formate & nitrate addition.....	91
5.5.3	Formate & selenate addition.....	93
5.5.4	Methanol & nitrate addition.....	95
5.5.5	Deuterated methanol & nitrate addition.....	96
5.6	Summary.....	97
5.7	References.....	100
<b>Chapter 6</b>	<b>Influence of scavengers of the <math>e_{aq}^-</math> and its precursors on the H atom yield</b> .....	102
6.1	Introduction.....	103
6.2	Introduction to the H atom determination in the radiolysis of water.....	103
6.3	Experimental work.....	106
6.4	Supporting calculations.....	107
6.5	Results and discussion.....	107
6.5.1	Total molecular hydrogen production.....	108

---

6.5.1.1	Gamma radiolysis	108
6.5.1.2	$^1\text{H}$ radiolysis	117
6.5.1.3	$^4\text{He}$ radiolysis	120
6.5.1.4	Conclusions	125
6.5.2	H atom production	126
6.5.2.1	Gamma radiolysis	126
6.5.2.2	$^1\text{H}$ radiolysis	135
6.5.2.3	$^4\text{He}$ radiolysis	139
6.5.3.4	Conclusions	147
6.5.3	Experimental and stochastic modeled yields	148
6.5.3.1	Gamma radiolysis	149
6.5.3.2	$^1\text{H}$ radiolysis	152
6.5.3.3	$^4\text{He}$ radiolysis	154
6.5.3.4	Discussion	159
6.6	Summary	161
6.7	References	161
<b>Chapter 7 Conclusions and Further Work</b>		<b>163</b>
7.1	Conclusions	164
7.1.1	H atom determination	164
7.1.2	H atom formation	164
7.1.3	H atom yield dependence	165
7.2	Future work	165
7.3	References	166
<b>Appendix A: Publications &amp; Conference Papers</b>		<b>167</b>
1.1	Publications	168
1.2	Conference Posters	168
<b>Appendix B: Yields and Standard Errors</b>		<b>178</b>
1.1	Introduction	179
1.2	Gamma radiolysis	179
1.2.1	Variation of formate	179

---

1.2.2	Variation of nitrate	180
1.2.3	Variation of selenate	183
1.3	$^1\text{H}$ radiolysis	185
1.3.1	No addition of hydrogen atom scavenger	185
1.3.2	Variation of nitrate	186
1.3.3	Variation of selenate	187
1.4	$^4\text{He}$ radiolysis	189
1.4.1	No addition of hydrogen atom scavenger	189
1.4.2	Variation of nitrate	190
1.4.3	Variation of selenate	193
<b>Appendix C: Command Scripts</b>		<b>195</b>
1.1	Ravenglass layout	196
1.2	TS_MHP.com	197
1.3	run_ravenglass.com	199

---

List of tables

<b>Table 3.1</b>	Parameters of the energy beam.....	52
<b>Table 5.1</b>	$e_{aq}^-$ Scavenger capacities in terms of the scavenger and its concentration.....	89
<b>Table 5.2</b>	Differences between experimental and modeled results at each concentration of nitrate.....	92
<b>Table 5.3</b>	H atom scavenging kinetic ratios among $Br^-$ , $NO_3^-$ , $CH_3OH$ and $HCO_2^-$ .....	96
<b>Table 6.1</b>	Formate, nitrate and bromide reaction rates with the hydrogen atom.....	105
<b>Table 6.2</b>	Deuterated formate, nitrate and bromide reaction rates with the hydrogen atom.....	105
<b>Table 6.3</b>	Variation of the H atom scavenging capacity.....	116
<b>Table 6.4</b>	Molecular hydrogen yields variation in the gamma, $^1H$ and $^4He$ radiolysis of 10 mM $HCO_2^-$ with $NaNO_3$ at the lowest considered electron precursor scavenging capacity.....	121
<b>Table 6.5</b>	Total molecular hydrogen yields variation in the gamma, $^1H$ and $^4He$ radiolysis of 10 mM $HCO_2^-$ or 1 M $HCO_2^-$ with $NaNO_3$ at the lowest considered electron precursor scavenging capacity.....	123
<b>Table 6.6</b>	$G(Total H_2)$ in the $\gamma$ , $^1H$ and $^4He$ radiolysis of 1 M $DCO_2^-$ solutions with $NaNO_3$ at the lowest considered electron precursor scavenging capacity.....	124
<b>Table 6.7</b>	Percentage of energy received by solute.....	133
<b>Table 6.8</b>	Hydrogen atom yields variation in the gamma, $^1H$ and $^4He$ radiolysis of 10 mM $HCO_2^-$ with $NaNO_3$ at the lowest considered electron precursor scavenging capacity.....	139

---

<b>Table 6.9</b>	Hydrogen atom yields in the gamma, $^1\text{H}$ and $^4\text{He}$ radiolysis of 10 mM $\text{HCO}_2^-$ or 1 M $\text{HCO}_2^-$ with $\text{NaNO}_3$ at the lowest considered electron precursor scavenging capacity.....	144
<b>Table 6.10</b>	Hydrogen atom yields in the gamma, $^1\text{H}$ and $^4\text{He}$ radiolysis of 1 M $\text{DCO}_2^-$ solutions with $\text{NaNO}_3$ at the lowest considered electron precursor scavenging capacity.....	146

## List of figures

<b>Figure 2.1</b>	The penetration, path length and range are equivalent for alpha particles.....	31
<b>Figure 2.2</b>	The penetration, path length and range are not equivalent for beta particles.....	32
<b>Figure 2.3</b>	Schematic representation of heavy ion track structure.....	35
<b>Figure 2.4</b>	Fast electrons track structure.....	35
<b>Figure 2.5</b>	Early processes in the radiolysis of water.....	37
<b>Figure 2.6</b>	Decay of the water excited states.....	38
<b>Figure 2.7</b>	Spin states of a two pair spurs accessible.....	39
<b>Figure 2.8</b>	Evolution of $e_{aq}^-$ , OH, H, $H_2O_2$ and $H_2$ yields with time following $\gamma$ or fast $e^-$ radiolysis of water.....	39
<b>Figure 2.9</b>	Main primary products in the radiolysis of water.....	40
<b>Figure 3.1</b>	Layout of the FN Tandem Van de Graaff accelerator.....	44
<b>Figure 3.2</b>	Beam trajectory within the accelerator.....	45
<b>Figure 3.3</b>	SNICS II Ion Source.....	45
<b>Figure 3.4</b>	Helium Ion Source.....	46
<b>Figure 3.5</b>	Acceleration tank.....	47
<b>Figure 3.6</b>	Resistors.....	47
<b>Figure 3.7</b>	Acceleration tube and column.....	48
<b>Figure 3.8</b>	Pelletron charging system.....	49
<b>Figure 3.9</b>	The analyzing Magnet.....	51
<b>Figure 3.10</b>	Slit control mode.....	51
<b>Figure 3.11</b>	Calculation of the energy received by a sample irradiated with heavy ions.....	52
<b>Figure 3.12</b>	Decay scheme of $^{60}\text{Co}$ .....	53
<b>Figure 3.13</b>	The Shepherd 109 Cobalt-60 source.....	54
<b>Figure 3.14</b>	Cobalt-60 rods layout.....	54
<b>Figure 3.15</b>	Gas chromatograph layout.....	55
<b>Figure 3.16</b>	Four-way valve.....	56
<b>Figure 3.17</b>	Thermal conductivity detector.....	57
<b>Figure 3.18</b>	Schematic design of an ordinary Mass Spectrometer.....	57
<b>Figure 3.19</b>	Titanium rods within the Quadrapole mass analyzer.....	57



<b>Figure 3.20</b>	Pyrex cell filled with 20 milliliters of the sample.....	58
<b>Figure 3.21</b>	A gas chromatograph and a mass spectrometer are connected inline with the sample cell placed on the heavy ions accelerator.....	59
<b>Figure 3.22</b>	Cuvette filled with four milliliters of the sample.....	60
<b>Figure 3.23</b>	Gas chromatograph and mass spectrometer connected in line with the sample cell placed in the gamma source.....	60
<b>Figure 4.1</b>	Physical and chemical processes in the evolution of radiation tracks.....	64
<b>Figure 4.2</b>	Physico-chemical processes in a radiation track.....	65
<b>Figure 4.3</b>	Diagrammatic representation of the probability distribution of elastic and inelastic events.....	67
<b>Figure 4.4</b>	Stopping power for electrons, hydrogen and helium in terms of the particle energy.....	72
<b>Figure 4.5</b>	Heavy ion track structure is calculated at consecutive track segments.....	73
<b>Figure 4.6</b>	The triangle relationship of three particles.....	75
<b>Figure 4.7</b>	Independent Reaction Times simulation method.....	75
<b>Figure 4.8</b>	Example of the IRT model.....	76
<b>Figure 5.1</b>	Atomic and molecular hydrogen production in the radiolysis of water.....	81
<b>Figure 5.2</b>	Production of H <sub>2</sub> and H atom in the $\gamma$ -radiolysis of aqueous formate solutions with 1 mM NaNO <sub>3</sub> and 1 mM KBr as a function of the formate scavenging capacity for H atoms. Go(H <sub>2</sub> ) is the yield of H <sub>2</sub> from a 1 mM NaNO <sub>3</sub> / 1 mM KBr solution in the absence of HCO <sub>2</sub> <sup>-</sup> .....	85
<b>Figure 5.3</b>	Production of H <sub>2</sub> and H atom in the $\gamma$ -radiolysis of aqueous formate solutions with 24 mM NaNO <sub>3</sub> as a function of the formate scavenging capacity for H atoms.....	86
<b>Figure 5.4</b>	Production of and H atom in the $\gamma$ -radiolysis of aqueous formate solutions with 1 / 24 mM NaNO <sub>3</sub> as a function of the formate scavenging capacity for H atoms.....	87
<b>Figure 5.5</b>	Production of H <sub>2</sub> in the $\gamma$ -radiolysis of aqueous formate solutions with different concentrations of NaNO <sub>3</sub> or N <sub>2</sub> O as a function of the formate scavenging capacity for H atoms.....	88
<b>Figure 5.6</b>	Production of H <sub>2</sub> in the $\gamma$ -radiolysis of aqueous deuterated formate solutions with 1 mM NaNO <sub>3</sub> as a function of the formate scavenging capacity for H atoms.....	92

<b>Figure 5.7</b>	Production of H <sub>2</sub> and H atom in the $\gamma$ -radiolysis of aqueous formate solutions with 1 mM Na <sub>2</sub> SeO <sub>4</sub> as a function of the formate scavenging capacity for H atoms. G <sup>o</sup> (H <sub>2</sub> ) is the yield of H <sub>2</sub> from a 1mM Na <sub>2</sub> SeO <sub>4</sub> solution in the absence of HCO <sub>2</sub> <sup>-</sup> .....	93
<b>Figure 5.8</b>	Production of H <sub>2</sub> in the $\gamma$ -radiolysis of aqueous formate solutions with 100 mM Na <sub>2</sub> SeO <sub>4</sub> as a function of the formate scavenging capacity for H atoms. G <sup>o</sup> (H <sub>2</sub> ) is the yield of H <sub>2</sub> from a 1mM NaNO <sub>3</sub> solution in the absence of HCO <sub>2</sub> <sup>-</sup> .....	94
<b>Figure 5.9</b>	Production of H <sub>2</sub> and H atom in the $\gamma$ -radiolysis of aqueous methanol solutions with 1 mM NaNO <sub>3</sub> as a function of the formate scavenging capacity for H atoms.....	95
<b>Figure 5.10</b>	Production of H <sub>2</sub> and H atom in the $\gamma$ -radiolysis of aqueous deuterated methanol solutions with 1 mM NaNO <sub>3</sub> as a function of the formate scavenging capacity for H atoms.....	97
<b>Figure 5.11</b>	Production of H atom in the $\gamma$ -radiolysis of aqueous HCO <sub>2</sub> <sup>-</sup> , DCO <sub>2</sub> <sup>-</sup> , CH <sub>3</sub> OH or CD <sub>3</sub> OH with 1 mM NaNO <sub>3</sub> and 1 mM KBr as a function of the H atom scavenging capacity for H atoms.....	98
<b>Figure 5.12</b>	Hydrogen atom production as a function of time.....	99
<b>Figure 6.1</b>	Production of H <sub>2</sub> in the $\gamma$ -radiolysis of aqueous 10 mM formate solutions with NaNO <sub>3</sub> or Na <sub>2</sub> SeO <sub>4</sub> as a function of the hydrated electron scavenging capacity. G <sup>o</sup> (H <sub>2</sub> ) is the yield of H <sub>2</sub> at different concentrations of the electron scavengers in the absence of any H atom scavenger.....	108
<b>Figure 6.2</b>	Production of H <sub>2</sub> in the $\gamma$ -radiolysis of aqueous 10 mM formate solutions with NaNO <sub>3</sub> or Na <sub>2</sub> SeO <sub>4</sub> as a function of the precursor to the hydrated electron scavenging capacity. G <sup>o</sup> (H <sub>2</sub> ) is the yield of H <sub>2</sub> at different concentrations of the electron scavengers in the absence of any H atom scavenger.....	109
<b>Figure 6.3</b>	Production of H <sub>2</sub> in the $\gamma$ -radiolysis of aqueous 1 M formate solutions with NaNO <sub>3</sub> or Na <sub>2</sub> SeO <sub>4</sub> as a function of the hydrated electron scavenging capacity. G <sup>o</sup> (H <sub>2</sub> ) is the yield of H <sub>2</sub> at different concentrations of the electron scavengers in the absence of any H atom scavenger.....	110
<b>Figure 6.4</b>	Production of H <sub>2</sub> in the $\gamma$ -radiolysis of aqueous 1 M formate solutions with NaNO <sub>3</sub> or Na <sub>2</sub> SeO <sub>4</sub> as a function of the precursor to the hydrated electron scavenging capacity. G <sup>o</sup> (H <sub>2</sub> ) is the yield of H <sub>2</sub> at different concentrations of the electron scavengers in the absence of any H atom scavenger.....	111

- Figure 6.5** Hydrogen atom and molecular hydrogen production in the  $\gamma$ -radiolysis of aqueous 10 mM deuterated formate solutions with  $\text{NaNO}_3$  or  $\text{Na}_2\text{SeO}_4$  as a function of the precursor to the hydrated electron scavenging capacity.  $G^{\circ}(\text{H}_2)$  is the yield of  $\text{H}_2$  at different concentrations of the electron scavengers in the absence of any H atom scavenger. ....113
- Figure 6.6** Hydrogen production in the  $\gamma$ -radiolysis of aqueous 1 M deuterated formate solutions with  $\text{NaNO}_3$  as a function of the precursor to the hydrated electron scavenging capacity.  $G^{\circ}(\text{H}_2)$  is the yield of  $\text{H}_2$  at different concentrations of the electron scavengers in the absence of any H atom scavenger. ....114
- Figure 6.7**  $\text{H}_2$  yields behavior in the gamma radiolysis of aqueous systems and in terms of the H atom scavenging capacity and the electron precursor scavenging capacity.  $G^{\circ}(\text{H}_2)$  is the yield of  $\text{H}_2$  at different concentrations of the electron scavengers in the absence of any H atom scavenger. ....115
- Figure 6.8** Molecular hydrogen production in the  $^1\text{H}$ -radiolysis of aqueous 10 mM formate solutions with  $\text{NaNO}_3$  as a function of the precursor to the hydrated electron scavenging capacity.  $G^{\circ}(\text{H}_2)$  is the yield of  $\text{H}_2$  at different concentrations of the electron scavengers in the absence of any H atom scavenger. ....117
- Figure 6.9** Hydrogen production in the  $^1\text{H}$ -radiolysis of aqueous 1 M deuterated formate solutions with  $\text{NaNO}_3$  as a function of the precursor to the hydrated electron scavenging capacity.  $G^{\circ}(\text{H}_2)$  is the yield of  $\text{H}_2$  at different concentrations of the electron scavengers in the absence of any H atom scavenger. ....118
- Figure 6.10**  $\text{H}_2$  yields behavior in the  $^1\text{H}$  radiolysis of aqueous systems and in terms of the H atom scavenging capacity and the concentration of the electron scavenger.  $G^{\circ}(\text{H}_2)$  is the yield of  $\text{H}_2$  at different concentrations of the electron scavengers in the absence of any H atom scavenger. ....119
- Figure 6.11** Molecular hydrogen production in the  $^4\text{He}$ -radiolysis of aqueous 10 mM formate solutions with  $\text{NaNO}_3$  as a function of the precursor to the hydrated electron scavenging capacity.  $G^{\circ}(\text{H}_2)$  is the yield of  $\text{H}_2$  at different concentrations of the electron scavengers in the absence of any H atom scavenger. ....120
- Figure 6.12** Molecular hydrogen and hydrogen atom production in the  $^4\text{He}$ -radiolysis of aqueous 10 mM deuterated formate solutions with  $\text{NaNO}_3$  or  $\text{Na}_2\text{SeO}_4$  as a function of the precursor to the hydrated electron scavenging capacity.  $G^{\circ}(\text{H}_2)$  is

the yield of H <sub>2</sub> at different concentrations of the electron scavengers in the absence of any H atom scavenger.....	121
<b>Figure 6.13</b> Production of H <sub>2</sub> in the <sup>4</sup> He-radiolysis of aqueous 1 M formate solutions with NaNO <sub>3</sub> or Na <sub>2</sub> SeO <sub>4</sub> as a function of the precursor to the hydrated electron scavenging capacity. G <sup>o</sup> (H <sub>2</sub> ) is the yield of H <sub>2</sub> at different concentrations of the electron scavengers in the absence of any H atom scavenger.....	122
<b>Figure 6.14</b> Molecular hydrogen yields in the <sup>4</sup> He-radiolysis of aqueous 1 M formate solutions with NaNO <sub>3</sub> as a function of the precursor to the hydrated electron scavenging capacity. G <sup>o</sup> (H <sub>2</sub> ) is the yield of H <sub>2</sub> at different concentrations of the electron scavengers in the absence of any H atom scavenger.....	123
<b>Figure 6.15</b> H <sub>2</sub> yields behavior in the <sup>4</sup> He radiolysis of aqueous systems and in terms of the H atom scavenging capacity and the concentration of the electron scavenger. G <sup>o</sup> (H <sub>2</sub> ) is the yield of H <sub>2</sub> at different concentrations of the electron scavengers in the absence of any H atom scavenger.....	124
<b>Figure 6.16</b> Total molecular hydrogen yields behavior in terms of the LET value of the radiation source and the concentration of the electron scavenger.....	125
<b>Figure 6.17</b> Hydrogen atom predictions in the γ-radiolysis of aqueous 10 mM formate solutions with NaNO <sub>3</sub> or Na <sub>2</sub> SeO <sub>4</sub> as a function of the precursor to the hydrated electron scavenging capacity (a) and the hydrated electron scavenging capacity (b).....	126
<b>Figure 6.18</b> Hydrogen atom predictions in the γ-radiolysis of aqueous 1 M formate solutions with NaNO <sub>3</sub> or Na <sub>2</sub> SeO <sub>4</sub> as a function of the precursor to the hydrated electron (a) and the hydrated electron scavenging capacity (b).....	127
<b>Figure 6.19</b> Hydrogen atom and molecular hydrogen production in the γ-radiolysis of aqueous 10 mM deuterated formate solutions with NaNO <sub>3</sub> or Na <sub>2</sub> SeO <sub>4</sub> as a function of the precursor to the hydrated electron scavenging capacity. G <sup>o</sup> (H <sub>2</sub> ) is the yield of H <sub>2</sub> at different concentrations of the electron scavengers in the absence of any H atom scavenger.....	128
<b>Figure 6.20</b> Hydrogen production in the γ-radiolysis of aqueous 10 mM deuterated formate solutions with NaNO <sub>3</sub> as a function of the precursor to the hydrated electron scavenging capacity. G <sup>o</sup> (H <sub>2</sub> ) is the yield of H <sub>2</sub> at different concentrations of the electron scavengers in the absence of any H atom scavenger.....	129

<b>Figure 6.21</b> Hydrogen production in the $\gamma$ -radiolysis of aqueous 10 mM deuterated formate solutions with $\text{Na}_2\text{SeO}_4$ as a function of the precursor to the hydrated electron scavenging capacity. $G^0(\text{H}_2)$ is the yield of $\text{H}_2$ at different concentrations of the electron scavengers in the absence of any H atom scavenger.....	130
<b>Figure 6.22</b> Production of HD in the $\gamma$ -radiolysis of aqueous 10 mM deuterated formate solutions with $\text{NaNO}_3$ or $\text{Na}_2\text{SeO}_4$ as a function of the precursor to the hydrated electron scavenging capacity.....	131
<b>Figure 6.23</b> Hydrogen production in the $\gamma$ -radiolysis of aqueous 1 M deuterated formate solutions with $\text{NaNO}_3$ as a function of the precursor to the hydrated electron scavenging capacity. $G(\text{H atom}) = G(\text{Total H}_2) - G^0(\text{H}_2)$ . $G^0(\text{H}_2)$ is the yield of $\text{H}_2$ at different concentrations of the electron scavengers in the absence of any H atom scavenger.....	132
<b>Figure 6.24</b> Hydrogen atom yields behavior in the gamma radiolysis of aqueous systems and in terms of the H atom scavenging capacity and the scavenging capacity of the electron scavenger.....	134
<b>Figure 6.25</b> Hydrogen atom production as a function of time in the gamma radiolysis of aqueous systems. Where times are estimated as: $t = \ln 2 / (k_{\text{NaNO}_3+\text{epre}}[\text{NaNO}_3])$ .....	135
<b>Figure 6.26</b> Hydrogen production in the $^1\text{H}$ -radiolysis of aqueous 10 mM formate solutions with $\text{NaNO}_3$ as a function of the precursor to the hydrated electron scavenging capacity.....	136
<b>Figure 6.27</b> Hydrogen production in the $^1\text{H}$ -radiolysis of aqueous 1 M deuterated formate solutions with $\text{NaNO}_3$ as a function of the precursor to the hydrated electron scavenging capacity. $G^0(\text{H}_2)$ is the yield of $\text{H}_2$ at different concentrations of the electron scavengers in the absence of any H atom scavenger.....	137
<b>Figure 6.28</b> Hydrogen atom yields in the $^1\text{H}$ radiolysis of aqueous systems and in terms of the H atom scavenging capacity and the concentration of the electron scavenger.....	138
<b>Figure 6.29</b> Hydrogen production in the $^4\text{He}$ -radiolysis of aqueous 10 mM formate solutions with $\text{NaNO}_3$ as a function of the precursor to the hydrated electron scavenging capacity.....	139
<b>Figure 6.30</b> $\text{H}_2$ and H atom production in the $^4\text{He}$ -radiolysis of aqueous 10 mM deuterated formate solutions with $\text{NaNO}_3$ or $\text{Na}_2\text{SeO}_4$ as a function of the precursor	

to the hydrated electron scavenging capacity. $G^{\circ}(\text{H}_2)$ is the yield of $\text{H}_2$ at different concentrations of the electron scavengers in the absence of any H atom scavenger.	140
<b>Figure 6.31</b> Hydrogen yields in the $^4\text{He}$ -radiolysis of aqueous 10 mM deuterated formate solutions with $\text{NaNO}_3$ as a function of the precursor to the hydrated electron scavenging capacity. $G^{\circ}(\text{H}_2)$ is the yield of $\text{H}_2$ at different concentrations of the electron scavengers in the absence of any H atom scavenger.	141
<b>Figure 6.32</b> Hydrogen yields in the $^4\text{He}$ -radiolysis of aqueous 10 mM deuterated formate solutions with $\text{Na}_2\text{SeO}_4$ as a function of the precursor to the hydrated electron scavenging capacity. $G^{\circ}(\text{H}_2)$ is the yield of $\text{H}_2$ at different concentrations of the electron scavengers in the absence of any H atom scavenger.	142
<b>Figure 6.33</b> Hydrogen atom predictions in the $^4\text{He}$ -radiolysis of aqueous 1 M formate solutions with $\text{NaNO}_3$ as a function of the precursor to the hydrated electron scavenging capacity.	143
<b>Figure 6.34</b> Hydrogen atom predictions in the $^4\text{He}$ -radiolysis of aqueous 1 M formate solutions with $\text{Na}_2\text{SeO}_4$ as a function of the precursor to the hydrated electron scavenging capacity.	144
<b>Figure 6.35</b> Hydrogen yields in the $^4\text{He}$ -radiolysis of aqueous 1 M formate solutions with $\text{NaNO}_3$ as a function of the precursor to the hydrated electron scavenging capacity. $G^{\circ}(\text{H}_2)$ is the yield of $\text{H}_2$ at different concentrations of the electron scavengers in the absence of any H atom scavenger.	145
<b>Figure 6.36</b> Hydrogen atom yields in the $^4\text{He}$ radiolysis of aqueous systems and in the $^4\text{He}$ radiolysis of aqueous solutions and in terms of the H atom scavenging capacity and the concentration of the electron scavenger.	147
<b>Figure 6.37</b> Total molecular hydrogen yields behavior in terms of the LET value of the radiation source and the concentration of the electron scavenger.	148
<b>Figure 6.38</b> Water radiolysis pathway	149
<b>Figure 6.39</b> Experimental $\text{H}_2$ yields combined with simulations in the $\gamma$ -radiolysis of aqueous 10 mM (a) and 1 M (b) formate solutions with added $\text{NaNO}_3$ . $G^{\circ}(\text{H}_2)$ is the yield of $\text{H}_2$ at different concentrations of the electron scavengers in the absence of any H atom scavenger.	149
<b>Figure 6.40</b> Experimental $\text{H}_2$ yields combined with simulations in the $\gamma$ -radiolysis of aqueous 10 mM (a) and 1 M (b) M formate solutions with added $\text{Na}_2\text{SeO}_4$ . $G^{\circ}(\text{H}_2)$	

is the yield of H <sub>2</sub> at different concentrations of the electron scavengers in the absence of any H atom scavenger.....	150
<b>Figure 6.41</b> Experimental results combined with simulations in the $\gamma$ -radiolysis of aqueous 10 mM deuterated formate solutions with NaNO <sub>3</sub> as a function of the precursor to the hydrated electron scavenging capacity. G <sup>o</sup> (H <sub>2</sub> ) is the yield of H <sub>2</sub> at different concentrations of the electron scavengers in the absence of any H atom scavenger.....	151
<b>Figure 6.42</b> Experimental results combined with simulations in the $\gamma$ -radiolysis of aqueous 10 mM deuterated formate solutions with Na <sub>2</sub> SeO <sub>4</sub> as a function of the precursor to the hydrated electron scavenging capacity. G <sup>o</sup> (H <sub>2</sub> ) is the yield of H <sub>2</sub> at different concentrations of the electron scavengers in the absence of any H atom scavenger.....	151
<b>Figure 6.43</b> Experimental results combined with simulations in the $\gamma$ -radiolysis of aqueous 1 M deuterated formate solutions with NaNO <sub>3</sub> as a function of the precursor to the hydrated electron scavenging capacity. G <sup>o</sup> (H <sub>2</sub> ) is the yield of H <sub>2</sub> at different concentrations of the electron scavengers in the absence of any H atom scavenger.....	152
<b>Figure 6.44</b> Experimental results combined with simulations in the <sup>1</sup> H-radiolysis of aqueous 10 mM formate solutions with NaNO <sub>3</sub> as a function of the precursor to the hydrated electron scavenging capacity. G <sup>o</sup> (H <sub>2</sub> ) is the yield of H <sub>2</sub> at different concentrations of the electron scavengers in the absence of any H atom scavenger.....	153
<b>Figure 6.45</b> Experimental results combined with simulations in the <sup>1</sup> H-radiolysis of aqueous 1 M deuterated formate solutions with NaNO <sub>3</sub> as a function of the precursor to the hydrated electron scavenging capacity. G <sup>o</sup> (H <sub>2</sub> ) is the yield of H <sub>2</sub> at different concentrations of the electron scavengers in the absence of any H atom scavenger.....	154
<b>Figure 6.46</b> Experimental results combined with simulations in the <sup>4</sup> He-radiolysis of aqueous 10 mM (a) and 1 M (b) formate solutions with NaNO <sub>3</sub> as a function of the precursor to the hydrated electron scavenging capacity. G <sup>o</sup> (H <sub>2</sub> ) is the yield of H <sub>2</sub> at different concentrations of the electron scavengers in the absence of any H atom scavenger.....	155
<b>Figure 6.47</b> Experimental results combined with simulations in the <sup>4</sup> He-radiolysis of aqueous 10 mM deuterated formate solutions with NaNO <sub>3</sub> as a function of the precursor to the hydrated electron scavenging capacity. G <sup>o</sup> (H <sub>2</sub> ) is the yield of H <sub>2</sub> at	

---

different concentrations of the electron scavengers in the absence of any H atom scavenger.....	156
<b>Figure 6.48</b> Experimental results combined with simulations in the $^4\text{He}$ -radiolysis of aqueous 10 mM deuterated formate solutions with $\text{Na}_2\text{SeO}_4$ as a function of the precursor to the hydrated electron scavenging capacity. $G^0(\text{H}_2)$ is the yield of $\text{H}_2$ at different concentrations of the electron scavengers in the absence of any H atom scavenger.....	156
<b>Figure 6.49</b> Experimental results combined with simulations in the $^4\text{He}$ -radiolysis of aqueous 1 M formate solutions with $\text{NaNO}_3$ as a function of the precursor to the hydrated electron scavenging capacity. $G^0(\text{H}_2)$ is the yield of $\text{H}_2$ at different concentrations of the electron scavengers in the absence of any H atom scavenger.	157
<b>Figure 6.50</b> Experimental results combined with simulations in the $^4\text{He}$ -radiolysis of aqueous 1 M formate solutions with $\text{Na}_2\text{SeO}_4$ as a function of the precursor to the hydrated electron scavenging capacity. $G^0(\text{H}_2)$ is the yield of $\text{H}_2$ at different concentrations of the electron scavengers in the absence of any H atom scavenger.	158
<b>Figure 6.51</b> Experimental results combined with simulations in the $^4\text{He}$ -radiolysis of aqueous 1 M deuterated formate solutions with $\text{NaNO}_3$ as a function of the precursor to the hydrated electron scavenging capacity. $G^0(\text{H}_2)$ is the yield of $\text{H}_2$ at different concentrations of the electron scavengers in the absence of any H atom scavenger.....	159
<b>Figure 6.52</b> Alternative water radiolysis pathway.....	160



## Abbreviations & acronyms

<i>a</i>	Acceleration
ACS	American Chemical Society
<i>B</i>	Magnetic field
<i>D'</i>	Relative diffusion coefficient
<i>e</i>	Electron's charge
$e_{\text{aq}}^-$	Hydrated electron
<i>E</i>	Energy
$f(\Delta E')$	Dipole oscillator strength distribution
<i>q</i>	Momentum transfer
G	Yield value or the number of molecules produced for each 100 eV absorbed by a substance from ionizing radiation
G(D <sub>2</sub> )	Molecular deuterium yield
G(H <sub>2</sub> )	Yield of molecular hydrogen formed by intra track chemistry when deuterated formate is added
G <sup>o</sup> (H <sub>2</sub> )	Yield of molecular hydrogen formed by intra track chemistry
G(H atom)	Hydrogen atom yield obtained through the molecular hydrogen difference method
G(HD)	Hydrogen atom yield obtained through the direct measurement of the HD yield
G(Total H <sub>2</sub> )	Molecular hydrogen yield due to the addition of G <sup>o</sup> (H <sub>2</sub> ) and G(H <sub>2</sub> )
GV	Generating Voltmeter Control
GVM	Generating Voltmeter
H <sub>2</sub> O*	Water excited state
H <sub>aq</sub> <sup>+</sup>	Hydrated proton
HIS	Helium Ion Source
HE	High Energy column
Im	Imaginary part
IRT	Independent Reaction Times
LE	Low Energy column
LET	Linear Energy Transfer
<i>N</i>	Number density of molecules
<i>m</i>	Mass

---

$p$	Momentum
$Q$	Charge
QMA	Quantum Resonance Magnetic Analyzer
$r$	Radius of curvature or interparticle distance (depending on the circumstances)
$r_c$	Onsager distance
$r_{eff}$	Effective separation
$r_m$	Final interparticles distance
$r'_m$	Initial interparticle distance
$R$	Reaction distance
$R_{eff}$	Effective reaction distance
$R_m$	Encounter distance
SNICS	Source of Negative Ions by Cesium Sputtering
$t$	Time
$T$	Temperature
TCD	Thermal Conductivity Detector
$U$	Random number
$v$	Velocity
$V$	Number of beam pulses
$W_{Br}$	Brownian bridge probability
$W(t)$	Random reaction times distribution function
$x$	Displacement
$z$	Position
$\alpha$	Alpha radiation
$\beta$	Beta radiation
$\gamma$	Gamma radiation
$\delta t$	Time step
$\Delta E$	Energy transfer
$\Delta E'$	Binding Energy
$\Delta z$	Distance travelled before collision
$\varepsilon(q, \Delta E)$	Complex dielectric response function
$\theta$	Angle
$\lambda$	Wavelength

$\Lambda_{\text{total}}$	Mean free path
$\sigma$	Cross section
$\tau(E, \Delta E)$	Probability of an energy loss of magnitude $\Delta E$ for a radiation particle of energy $E$

## Abstract

Experimental measurements in conjunction with stochastic simulations are used to determine hydrogen atom yields in the gamma and heavy ions radiolysis of aqueous solutions of formate and deuterated formate ions.

In radiolysis, the hydrogen atom is produced directly by the fragmentation of water excited states, and during the diffusion-kinetic evolution of the radiation track by the intra-track reaction of  $e_{\text{aq}}^-$  with  $\text{H}_{\text{aq}}^+$  up to the microsecond timescale. The yield of  $\text{H}\bullet$  is relatively small, but it is fundamentally very important. An accurate examination of the H atom yields after radiolysis will make possible a better understanding of the initial steps of the radiolytic decomposition of water. The competition between H atom combination reactions and its formation by reaction of  $e_{\text{aq}}^-$  with  $\text{H}_{\text{aq}}^+$  makes predictions of the H atom kinetics very difficult. Hydrogen atom yields were determined by difference measurements of  $\text{H}_2$  yields and direct measurements of HD yields when using deuterated formate as  $\text{H}\bullet$  scavenger. While the total  $\text{H}_2$  yield measured is always greater for alpha than for gamma radiolysis, the H atom yield is observed to be smaller. The addition of selected scavengers of the hydrated electron and its precursors reveals a stronger correlation of the H atom formation on the precursor to the hydrated electron rather than the hydrated electron itself. Scavengable  $\text{H}\bullet$  yields strongly decrease as the concentration of the electron scavenger increases.

Stochastic track chemistry calculations were used to analyze the measured experimental yields and to elucidate the underlying kinetics.

## Declaration

I declare that no portion of the work referred to in the thesis has been submitted in support of an application for another degree or qualification of this or any other university or other institute of learning.

.....

Monica Huerta Parajon

December 2010

## Copyright Statement

- i. The author of this thesis (including any appendices and/or schedules to this thesis) owns any copyright in it (the “Copyright”) and s/he has given The University of Manchester the right to use such Copyright for any administrative, promotional, educational and/or teaching purposes.
- ii. Copies of this thesis, either in full or in extracts, may be made only in accordance with the regulations of the John Rylands University Library of Manchester. Details of these regulations may be obtained from the Librarian. This page must form part of any such copies made.
- iii. The ownership of any patents, designs, trademarks and any and all other intellectual property rights except for the Copyright (the “Intellectual Property Rights”) and any reproductions of copyright works, for example graphs and tables (“Reproductions”), which may be described in this thesis, may not be owned by the author and may be owned by third parties. Such Intellectual Property Rights and Reproductions cannot and must not be made available for use without the prior written permission of the owner(s) of the relevant Intellectual Property Rights and/or Reproductions.
- iv. Further information on the conditions under which disclosure, publication and exploitation of this thesis, the Copyright and any Intellectual Property Rights and/or Reproductions described in it may take place is available from the Head of School of Chemistry.

## Acknowledgements

I would like to express my sincere gratitude to those whom contributed to this thesis, without whose help I would not have been able to carry out these intense years full of new knowledge, challenges and experiences.

In particular, I would like to thank my supervisor Prof. Simon M. Pimblott for giving me the opportunity to undertake this project and providing me with support and guidance in many aspects of my academic and personal life.

Thanks also to all members of the Radiation Chemistry Group, and in particular Dr. Sven Koehler, Pavlina Schmitz and Rafal Feliga for their help and the experiences we shared.

I would also like to extend my gratitude to all the members of the computational group for offering a pleasant work environment.

My special acknowledgement to Prof. Jay A. LaVerne and all the members of the Radiation Laboratory at The University of Notre Dame (Indiana, USA) for their invaluable guidance both academically and personally.

Thanks to The Nuclear Decommissioning Authority (NDA), The University of Manchester and The Office of Basic Energy Sciences of the U.S. Department of Energy for funding this project.

I would like to thank Dr. Howard Sims from NNL for his useful discussions and suggestions.

Finally, my family and close friends deserve a special mention for their unconditional love and support.

## The Author

Monica Huerta Parajon graduated from the Universidad de Oviedo (Spain) in 2007 with a MChem degree in Chemistry specially focused on the physical chemistry field. This degree included one year Erasmus international exchange in the Chemistry department of The University of Liverpool.

From April 2007 until September 2010 research was undertaken in The University of Manchester and under the supervision of Prof. Simon M. Pimblott in the field of H atom determination in the gamma and heavy ions radiolysis of aqueous systems. The project is funded by the Nuclear Decommission Authority (NDA) and presented in this thesis.

My experiments were carried out in the Radiation Laboratory at the University of Notre Dame (USA) in collaboration with Prof. Jay A. LaVerne's group and co-funded by the Office of Basic Energy Sciences of the U.S. Department of Energy.



# Chapter 1

## Introduction

1.1	Background.....	26
1.2	Objectives.....	26
1.3	References.....	27

## 1.1 Background

Energy production and its environmental cost is a topic of considerable importance [1-3]. Nuclear power represents a significant energy resource, however, its production generates relatively small amounts of highly toxic waste. Common components of this waste are hydrocarbons, which are derived from nuclear power plant infrastructure or reprocessing and storage materials, in contact with water. Generation of species of a considerable interest are expected when radiolysis of water-hydrocarbon systems occurs. While the radiolysis of many aqueous systems have been studied [4-10], mechanisms and product yields due to different types of radiation and concentrations of solutes are still unknown for a large number of aqueous systems.

Hydrogen atoms are formed by the decay of water excited states and by the reaction of the hydrated electron reaction,  $e_{aq}^-$ , with the hydrated hydrogen ion,  $H_{aq}^+$ , during the diffusion-kinetic evolution of the radiation track. Although comparatively small, the H atom yield is essential to understand the fundamentals of the radiolytic decomposition of water.

## 1.2 Objectives

The main objective of the project is to gain an understanding of the early steps in the radiolysis of water, in particular to determine the main source of H atom and its yield depending on the system and energy applied. Additionally, the reliability of the methods used to measure the H atom yields has been tested under different conditions [11].

To achieve these aims, radiation chemical experiments combined with stochastic track chemistry calculations have been used to investigate the formation of H atom in the irradiation of water and aqueous solutions of formate and deuterated formate.

The experimental work was carried out in the Radiation Laboratory and the Nuclear Structure Laboratory at The University of Notre Dame in Indiana, USA. Gamma and heavy ion irradiations were performed using a  $^{60}\text{Co}$  source and FN Tandem Van de Graaff. Gaseous products produced by irradiation were collected and characterized using a gas chromatograph and a mass spectrometer.

Monte Carlo track simulations were performed using the same general techniques and parameters, as in the previous studies [11-13]. Each calculation

simulates a realistic track structure for the transfer of energy from the ionizing radiation to the medium, determines the physical consequences of each energy transfer event, and models the kinetics of the competition between the relaxation of the spatially non-homogeneous distribution of radiation-induced reactants and their reactions either within the track or with the scavengers.

Overall the aim was to gain a better understanding of the H atom production in the radiolysis of aqueous organic solutions considering different radiation types and concentrations of the species in solution. This study of simple organic in aqueous solution can be easily related to more complicated organic compounds, such as polymers in contact with water.

### 1.3 References

1. Russell, T.W.F., and Colton, C. K., *14 Energy and Environmental Concerns*, in *Advances in Chemical Engineering*. 1991, Academic Press. p. 293-301.
2. Martínez, P., Eliceche, A. M., Marquardt, W., and Pantelides, C. , *Environmental life cycle impact and cost minimization in the steam and power generation plant*, in *Computer Aided Chemical Engineering*. 2006, Elsevier. p. 1791-1796.
3. Christensen, T., Fuglestedt, J., Benestad, C., Ehdwall, H., Hansen, H., Mustonen, R., and Stranden, E. , *Chemical and radiological risk factors associated with waste from energy production*. *Science of The Total Environment*, 1992. **114**: p. 87-97.
4. Mahlman, H.A., *Radiolysis of nitrous oxide saturated solutions: Effect of sodium nitrate, 2-propanol, and sodium formate*. *The Journal of Physical Chemistry*, 1966. **70**: p. 3983-3987
5. Draganic, Z.D., and Draganic, I. G, *Studies on the Formation of Primary Hydrogen Atom Yield G(H) in the Gamma Radiolysis of Water*. *The Journal of Physical Chemistry*, 1972. **76**: p. 2733-2737.
6. Scholes, G., and Simic, M. , *Reactivity of the Hydrogen Atoms Produced in the Radiolysis of Aqueous Systems*. *The Journal of Physical Chemistry*, 1964. **68**: p. 1738-1743.
7. Scholes, G., and M. Simic *Action of gamma-rays on Aqueous Solutions of Nitrous Oxide and the Effects of Added Solutes*. *The Journal of Physical Chemistry* 1964. **68**: p. 1731-1737.
8. Appleby, A., and Schwarz, H. A., *Radical and molecular yields in water irradiated by .gamma.-rays and heavy ions*. *The Journal of Physical Chemistry*, 1969. **73**: p. 1937-1941.
9. Elliot, A.J., Chenier, M. P., Ouellette, D. C., and Koslowsky, V. T., *Temperature Dependence of g Values for Aqueous Solutions Irradiated with 23 MeV  $^2\text{H}^+$  and 157 MeV  $^7\text{Li}^{3+}$  Ion Beams*. *The Journal of Physical Chemistry*, 1996. **100**: p. 9014-9020.
10. Elliot, A.J., Chenier, M. P., and Ouellette, D. C. , *Temperature Dependence of g Values for  $\text{H}_2\text{O}$  and  $\text{D}_2\text{O}$  irradiated with Low Linear Energy Transfer*

- Radiation*. Journal of the Chemical Society, Faraday Trans., 1993. **89**: p. 1193 - 1197.
11. Huerta Parajon, M., Rajesh, P., Mu, T., Pimblott, S.M., and LaVerne, J.A., *H atom yields in the radiolysis of water*. Radiation Physics and Chemistry, 2008. **77**: p. 1203-1207.
  12. LaVerne, J.A., Stefanic, I., and Pimblott, S. M., *Hydrated Electron Yields in the Heavy Ion Radiolysis of Water*. The Journal of Physical Chemistry A, 2005. **109**: p. 9393-9401.
  13. Pimblott, S.M., and LaVerne, J. A., *Effects of Track Structure on the Ion Radiolysis of the Fricke Dosimeter*. The Journal of Physical Chemistry A, 2002. **106**: p. 9420-9427.

## Chapter 2

# An introduction to radiation chemistry and water radiolysis

2.1	Introduction.....	30
2.2	Definition.....	30
2.3	Radiation from radioactive nuclei.....	30
2.4	Interaction of radiation with matter.....	32
2.5	Ionization and excitation produced by radiation.....	34
2.6	Reactions due to excited molecules, ions and free radicals.....	36
	2.6.1 Reactions of excited molecules.....	36
	2.6.2 Reactions of ions.....	36
	2.6.3 Reactions of free radicals.....	37
2.7	Primary radiation processes in water.....	37
2.8	Summary.....	40
2.9	References.....	41

## 2.1 Introduction

This chapter aims to set the background to the thesis, introducing the basis of the radiation chemistry, outlining the processes occurring after the radiolysis of water and explaining their relevance to the scientific community. The discussion begins with the definition of radiation chemistry and the classification of ionizing radiation. This is followed by a section on the interaction of radiation with matter, which is essential to understand the chemistry involved. Finally, an overview of the primary radiation processes is introduced.

## 2.2 Definition

Radiation chemistry is the study of the chemical effects produced in a system by the absorption of ionizing radiation [1]. This includes the chemical effects produced by alpha ( $\alpha$ ), beta ( $\beta$ ) and gamma ( $\gamma$ ) radiation, high-energy charged particles (electrons, protons, deuterons...) and electromagnetic radiation of short wavelength ( $\gamma$ -rays or X-rays with  $\lambda \ll 250 \text{ \AA}$  and  $E \gg 50 \text{ eV}$ ). Radiations are often classified using a parameter called the linear energy transfer. Linear energy transfer (LET) is defined as the linear rate of loss of energy (locally absorbed) by an ionizing particle traversing a material/medium [2]. It is a measure of the kinetic energy transferred per distance travelled when a high energy particle travels through matter, i.e.

$$LET = -\frac{dE}{dx}.$$

LET is generally expressed in  $\text{keV } \mu^{-1}$  or  $\text{eV } \text{nm}^{-1}$ .

## 2.3 Radiation from radioactive nuclei

Different ionizing radiation is produced depending on the radioactive nuclei disintegrating.

**Alpha particles** ( $\alpha$ ) emitted in alpha decays are helium atoms which have lost both electrons and consist of one nucleus with 2 neutrons and 2 protons expressed as  ${}^4_2\text{He}^{2+}$ . Alpha particles show discrete energies characteristic of the radioactive nuclei decaying. Therefore, all particles emitted by the same radioisotope have a similar range in a given material.

Alpha particles interact with matter through inelastic collisions with electrons found in their path. Due to their high charge and large mass, alpha particles are the

least penetrating radiation that radioisotopes produce. Alpha particles trajectories do not change significantly after a collision, so  $\alpha$  particles travel in straight lines and their range is equivalent to their path length and vector penetration, see figure 2.1 below

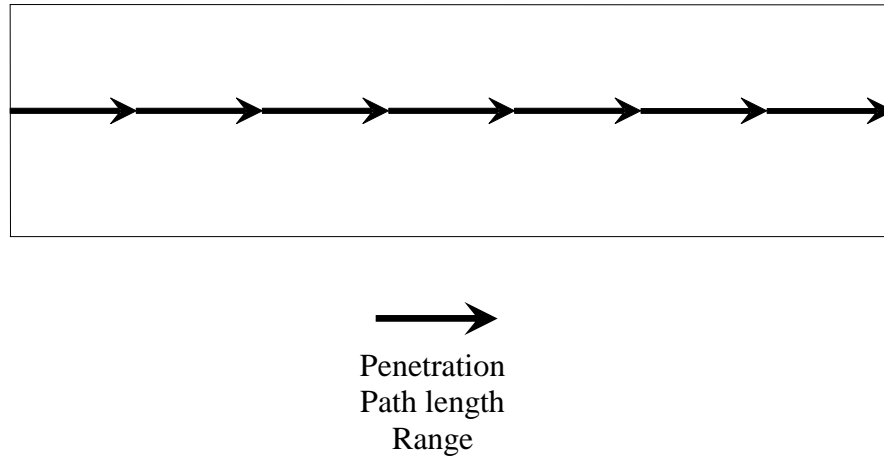


**Figure 2.1** The penetration, path length and range are equivalent for alpha particles.

The average kinetic energy transferred per collision when passing through matter is quite similar for alpha and beta radiation [3]. Alpha particles are the least penetrating radiation; they have the smallest distance travelled between collisions and consequently have the highest LET values.

**Beta particles** ( $\beta$ ) are energetic electrons or positrons emitted by radioactive nuclei with energies varying from zero up to  $E_\beta$ , which is the highest energy value depending on the radioisotope disintegrating. This maximum energy value  $E_\beta$  determines the maximum range that beta particles will have in matter.

When passing through matter beta particles predominantly lose their energy by inelastic collisions. Since beta particles and molecular electrons have the same mass, they can be widely deflected in a single collision losing most of their energy. The term “range” is used in connection to alpha particles to denote the penetration and path length. Due to the large deflections experienced by beta particles after a collision, the path length and penetration are not equivalent and the term range is used to denote the penetration.

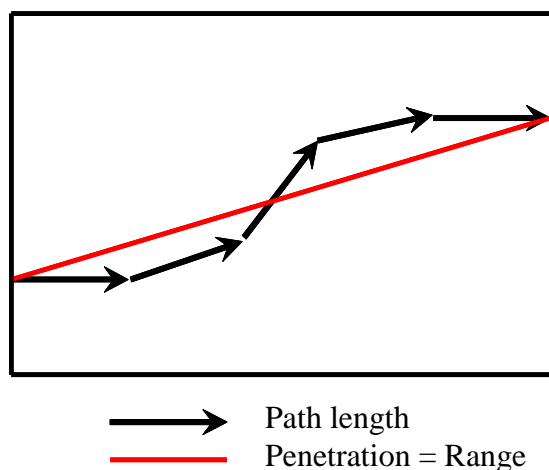


**Figure 2.2** The penetration, path length and range are not equivalent for beta particles.

**Gamma rays** ( $\gamma$ ) are electromagnetic radiation of high energy and short wavelength. Gamma rays produced from radioactive nuclei can have either a number of discrete energies characteristic of the radioactive element or all the same energy (monoenergetic). Whereas alpha and beta particles are gradually decelerated on passing through matter and lose energy through a number of collisions, gamma rays produce a series of particle-like collisions to give secondary electrons. They lose most of their energy in a single collision and a secondary electron of considerable energy is produced. This electron then transports the energy away from the primary event site. The track of this electron is equivalent to a beta particle track. As the photon transfers most of its energy to the ejected secondary electron in the primary ionization, the LET for gamma radiation is usually considered to be that of the electrons ejected after the inelastic collision of the gamma ray with matter.

#### 2.4 Interaction of radiation with matter

The way radiation interacts with matter depends predominantly on the nature of the absorbing material. On passing through matter **electrons** lose energy through electromagnetic radiation emission and inelastic collisions. At high energies, energy is mainly lost by emission of electromagnetic radiation or *bremsstrahlung* where electrons are decelerated and deflected as they pass in the vicinity of another charged particle, such as an atomic nucleus. At lower energies than those at which *bremsstrahlung* emission occurs energy is lost through inelastic collisions, due to the



Coulomb interactions with molecular electrons producing ionization and excitation in the stopping material.

**Heavy charged particles** lose energy mainly by inelastic collisions with electrons in their path. Other types of interactions are comparatively unimportant except at low energies where nuclear collisions and nuclear stopping are the dominant processes. A nuclear collision occurs when heavy charged particles interact with atomic nuclei.

**Electromagnetic radiation** interacts with matter via three main processes; the photoelectric effect, Compton scattering and pair production.

- a) In the *photoelectric effect*, one electron from an inner shell is ejected when it collides with a photon. The vacancy created is filled by an electron from an outer shell and emission of X-ray radiation occurs.
- b) The *Compton effect* occurs when an incident photon is deflected and reduces its energy after interaction with an atomic electron.
- c) In *pair production*, an incident photon is absorbed when passing close to an atomic nucleus and a positron-electron pair is produced. Pair production occurs at very high energies and is unimportant compared with the two former processes in radiation chemistry.

The sum of these processes defines the linear attenuation coefficient, which is the fraction of the incident photons absorbed from the incident beam per unit thickness of absorber [1]. This is represented by the expression:

$$\mu = \tau + \sigma + \kappa$$

where  $\tau$ ,  $\sigma$ ,  $\kappa$  are the contributions of the photoelectric, Compton effect and pair production, respectively.

In addition to these processes, there are two less probable processes whose contributions may be neglected; coherent scattering and photonuclear reactions.

d) In the *coherent scattering*, a photon is scattered with little loss of energy. The main process is Rayleigh scattering where interaction with an atomic e- occurs. This takes place in an energy range where the photoelectric cross section is large, so it can be neglected without introducing a very large error.

e) In *photonuclear reaction*, either a proton or neutron from an atomic nucleus is ejected by collision with a photon of sufficient energy. Photonuclear cross sections are generally small compared with the Compton and pair-production cross sections at the same energy, so its contribution can also be neglected.

**Neutrons** are not generally considered as ionizing radiation, as they do not cause direct ionization on passing through matter. However, they are able to interact with atomic nuclei by four different processes. The most probable interaction is *elastic scattering*, where the energy of the neutron is shared between the colliding neutron and the nucleus. *Inelastic scattering* can also occur if a neutron is absorbed by a nucleus, re-emitting a neutron with less energy. The nucleus will remain in an excited state and returns to the ground state by gamma ray emission. *Nuclear reactions*, where a neutron is included into the nucleus and a proton or alpha particle is emitted, occur at high energies. Finally, interaction by *capture* is the most probable way of interaction at thermal temperatures. In this case, one neutron is captured into a nucleus giving heavier isotope of the target molecule.

## 2.5 Ionization and excitation produced by radiation

Heavy charged particles and electrons give rise to a series of excited and ionized atoms in their path as they lose energy when passing through matter. Excitation is produced when atomic electrons of the stopping material gain energy and are promoted to a higher energy level. Ionization events occur when the energy gained is high enough to eject the atomic electron. Something similar occurs when electromagnetic radiation passes through matter. Atomic electrons absorb the energy transferred by the electromagnetic radiation and dissipate it along their path. In conclusion, the passage of any type of ionizing radiation through matter leads to the formation of tracks of excited and ionized particles. Each type of radiation dissipates the energy at different rates which means that tracks of different local energy (and reactants) density are obtained. Further excitation and ionization is produced by sufficiently energetic expelled electrons.

Secondary electrons produce clusters of ionization and excitation events close to the location of the parent primary ionization. These clusters are known as spurs. In heavy ion tracks the primary events are close together, however, in energetic electron tracks the primary events are well separated. Consequently, the distribution of ionizations and electrons is very different.

**Heavy charged particles** tracks are densely populated with primary energy loss events situated close to each other giving a central core of excited and ionized species surrounded by spurs from the tracks of ejected electrons, see figure 2.3.

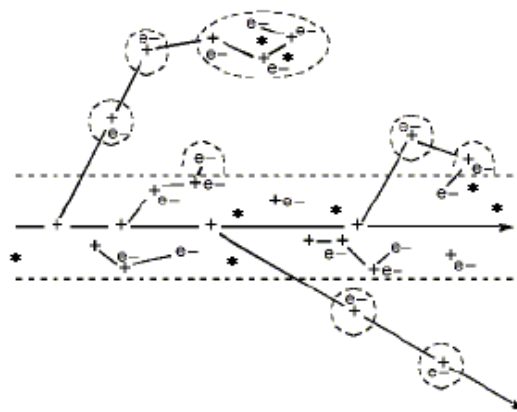


**Figure 2.3** Schematic representation of heavy ion track structure. Stars represent the excited water molecule [4].

Different types of energy deposition are found in **fast electron** track structures depending on how energetic the secondary electrons are. A schematic representation is shown in figure 2.4. Secondary electrons have a short range and are situated close to the primary ionizations for small energies of about 100 eV. However, some electrons are ejected with enough energy to travel further and generate their own highly energetic spurs known as blobs (from 100 up to 500 eV), short tracks (from 500 up to 5000 eV) and branch tracks (from 5000 eV) [5].

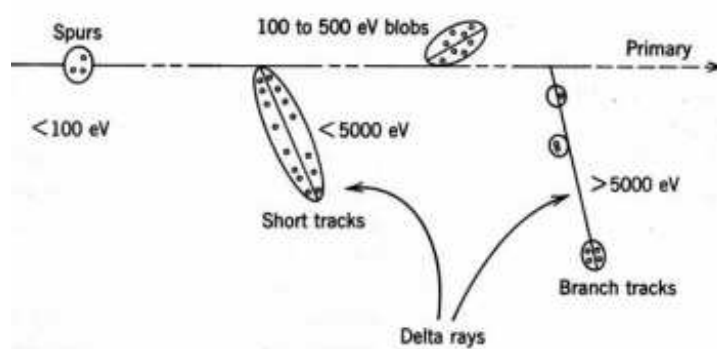


**Figure 2.4** Fast electrons track structure (• Positive ions) [1]

The consequences of energetic electrons and gamma or X rays are similar as electromagnetic radiation produces high energy secondary electrons. The only distinction being that in gamma radiolysis the fast electron track begins well within the irradiated medium.

## 2.6 Reactions due to excited molecules, ions and free radicals

Excited molecules, ions and free radicals are produced along the track as a result of the transfer of energy from the ionizing radiation to the medium. Some of the possible reactions involving excited molecules, ions and free radicals are listed below [1].

## 2.6.1 Reactions of excited molecules

- Excitation to singlet and triplet excited states:  $A \rightarrow A^*$
- Radiative or non-radiative conversion to the ground state (no chemical reaction)  $A^* \rightarrow A$
- Non-radiative energy transfer:  $A^* + B \rightarrow A + B^*$
- Dissociation into free radicals:  $A^* \rightarrow R\cdot + S\cdot$
- Dissociation into molecular products:  $A^* \rightarrow M + N$
- Electron transfer:  $A^* + B \rightarrow A^+ + B^-$  (or  $A^- + B^+$ )
- Hydrogen abstraction:  $A^* + RH \rightarrow R\cdot + AH\cdot$
- Addition:  $A^* + B \rightarrow AB$
- Stern-Volmer reaction:  $A^* + B \rightarrow A + B$

## 2.6.2 Reactions of ions

- Radiation induced ionization:  $A \rightarrow A^+ + e^-$  [or  $(A^+)^* + e^-$ ]
- Neutralization producing singlet or triplet excited states:  $A^+ + e^- \rightarrow A^{**}$  ( $A^*$ )
- Dissociation into molecular products following neutralization:  $A^+ + e^- \rightarrow A^* (A^{**}) \rightarrow M^* + N$
- Neutralization by a negative ion:  $A^+ + A^- \rightarrow A^* + A$
- Dissociation into free radicals following neutralization:  $A^+ + e^- \rightarrow A^* (A^{**}) \rightarrow R\cdot + S\cdot$
- Neutralization of complex by reaction:  $A\cdot B^+ + e^- \rightarrow C + D$
- Dissociation of an excited ion into an ion and a molecule:  $(A^+)^* \rightarrow M^+ + N$
- Dissociation of an excited ion into a positive ion and a radical:  $(A^+)^* \rightarrow R^+ + S\cdot$
- Charge transfer:  $A^+ + B \rightarrow A + B^+$
- Ion-molecule reaction:  $A^+ + B \rightarrow C^+ + D$

## 2.6.3 Reactions of free radicals

**Reactions:**

- Rearrangement:  $AB\cdot \rightarrow BA\cdot$
- Dissociation:  $AB\cdot \rightarrow A\cdot + B$
- Addition:  $R\cdot + C=C \rightarrow R-C=C\cdot$
- Abstraction:  $A\cdot + BC \rightarrow AB + C\cdot$
- Oxygen addition:  $R\cdot + O_2 \rightarrow R-O-O\cdot$

**Destruction:**

- Combination:  $R\cdot + S\cdot \rightarrow RS$
- Disproportionation:  $2RH\cdot \rightarrow RH_2 + R$
- Electron transfer:  $M^{z+} + R\cdot \rightarrow M^{(z+1)+} + R^-$

The abstraction reaction listed is important in the experimental section which focuses on the abstraction of hydrogen from selected solutes.

## 2.7 Primary radiation processes in water

Reactions in the picosecond domain of the radiolysis of water are usually described in terms of a reaction scheme like [6], as seen in Figure 2.5.

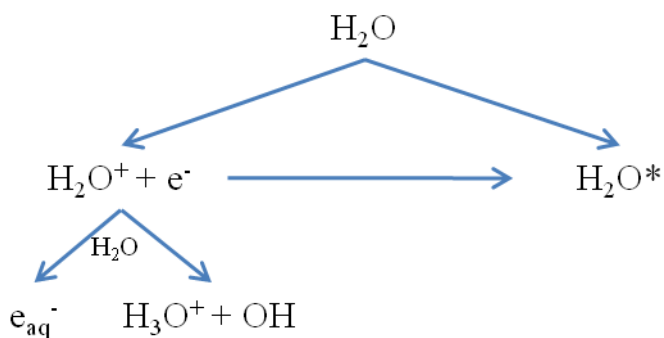


**Figure 2.5** Early processes in the radiolysis of water

Ionized water molecules and water excited states are produced in the range of the femtoseconds due to the ionizing radiation traversing (i.e. gamma rays or energetic particles). Subsequently,  $\text{H}_2\text{O}^+$  reacts with a neighbouring water molecule to form OH radicals and hydronium. The water excited state decays as seen in Figure 2.6,

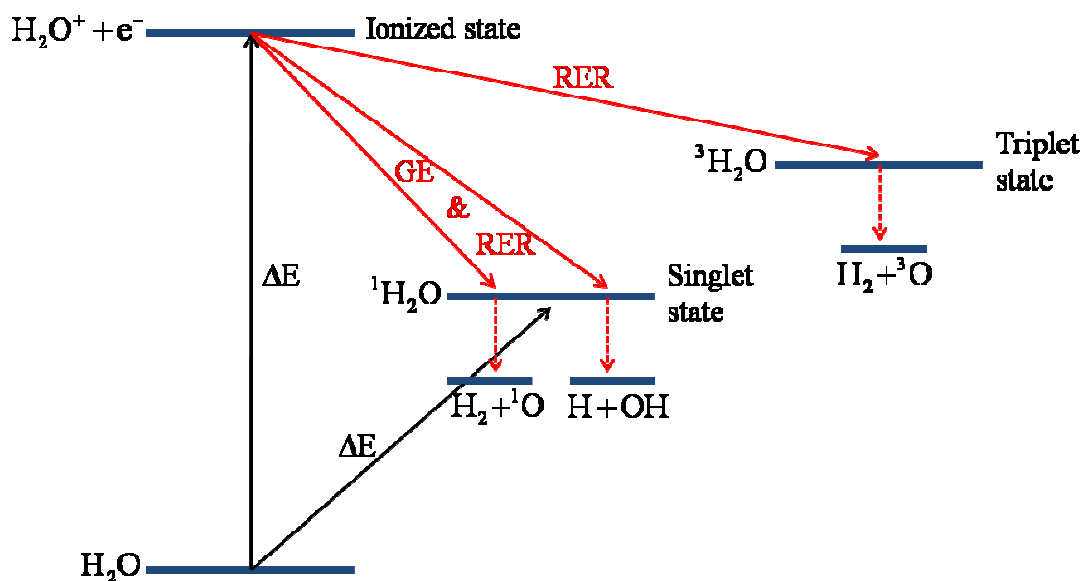


**Figure 2.6** Decay of the water excited states

where GE and RER refer to the geminate and the random encounter reaction respectively. In the absence of spin relaxation, geminate reactions lead to the formation of a singlet state since there is just one possible encounter  $\uparrow\downarrow$ , whereas, a random encounter reaction between unrelated ions may lead to the formation of either a singlet or a triplet state. An example can be formulated considering a two pairs spur, as explained by Pimblott et al. [7]. In order to identify the possible states of the system it is necessary to consider not only the number and type of particles, but also the ways in which their spins are correlated. The two pair spur has an initial singlet state configuration. The resulting eight possible states are shown in figure 2.7. The states 1-4 represent the four possible initial states. In states 1 and 2 the correlated pairs are singlets and the encounters between uncorrelated radicals have probability 1/4 of being singlet and 3/4 of being triplet. On the contrary, in states 3 and 4 the correlated pairs are triplets and the singlet and triplet probabilities of the uncorrelated pairs have reversed probabilities (3/4 and 1/4, respectively). The states 5-8 represent the four possible states in the evolution of the spur. In state 5 the pair B-B had a singlet reaction while in state 7 the pair A-A had a singlet reaction. This forces the remaining pair to have a singlet interaction. In state 6 an A-B pair has had a singlet reaction leaving a singlet A-B pair and state 8 represents the state after two singlet reactions. In our model, state 2 is always considered to be the initial state the spur: geminate partners are treated as a singlet pair.

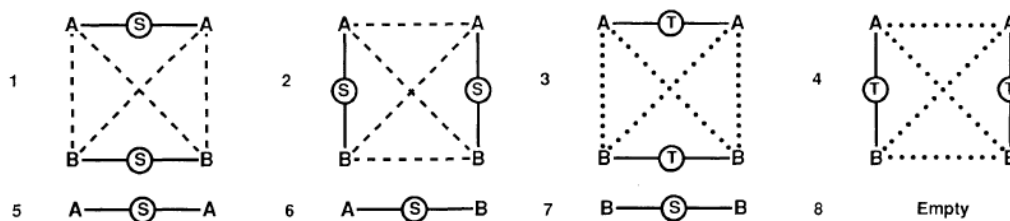


**Figure 2.7** Spin states of a two pair spurs accessible; (— $\text{S}$ —) singlet probability = 1.0; (...) singlet probability = 0.75; (---) singlet probability = 0.25; (— $\text{T}$ —) singlet probability = 0.0 [7].

Secondary electrons are attenuated to thermal energy (about 0.025 eV) in the range of the 100 femtoseconds; some are captured by positive ions while others become hydrated,  $e_{\text{aq}}^-$ . While the energy attenuation is initially due to electronic transfer events, at low energies degradation is due to vibrational and rotational events.

As a result of the primary processes, water molecules are decomposed into free radicals and ions which become solvated at times smaller than 2 picoseconds. Diffusion limited chemistry is considered from this point; radicals diffuse randomly reacting with either whatever solutes they find in their path or one another before diffusing far from the vicinity. The evolution of the OH,  $e_{\text{aq}}^-$ , H,  $\text{H}_2$  and  $\text{H}_2\text{O}_2$  yields in the gamma or fast electron radiolysis of neat water with time has been modeled using the techniques described later in this chapter and shown in figure 2.8.

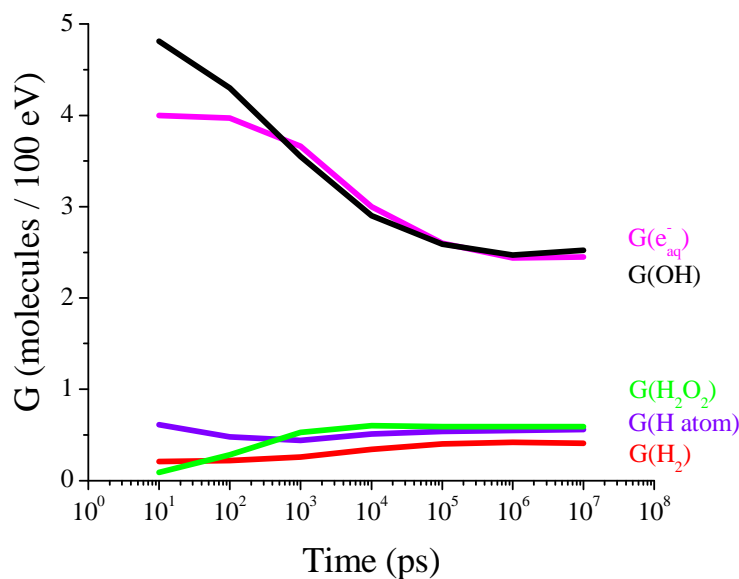


**Figure 2.8** Evolution of  $e_{\text{aq}}^-$ , OH, H,  $\text{H}_2\text{O}_2$  and  $\text{H}_2$  yields with time following  $\gamma$  or fast  $e^-$  radiolysis of water.

Radicals, molecular products and subsequent reactions are then controlled by diffusion in the bulk of the liquid. A schematic representation of this process is presented below

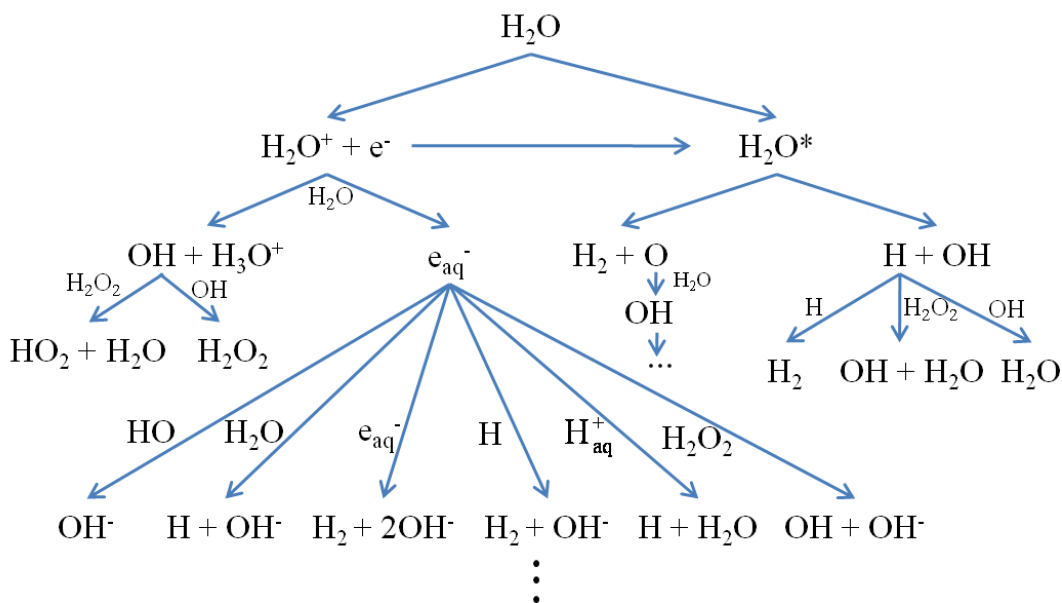


**Figure 2.9** Main primary products in the radiolysis of water

Spurs are formed close together along the tracks due to heavy particle radiation which means that radicals are produced in larger groups. Consequently, as the LET of the radiation increases, the molecular product yields increase, whereas the amounts of radicals which diffuse into the solution decrease. The addition of selected solutes is frequently used to interfere with free radical yields since they may react before the radicals have time to diffuse and combine with one another. The effect of these solutes, named as scavengers, increases with their concentration.

## 2.8 Summary

Knowledge of the principles of the radiation chemistry and the primary radiation processes in water allows the elucidation of complex experimental radiation chemistry. A general overview of the radiation types and the interaction of radiation with matter has been presented as well as the processes and reactions occurring after collision. Finally, the early steps in the radiolysis of water have been introduced in terms of their time scale. Radicals and ions are on a sub-nanosecond



timescale and allowed to diffuse randomly reacting with whatever solutes they find in their path to be finally involved in bulk chemistry.

## 2.9 References

1. Spins, J.W.T., and Woods, R. J., *An Introduction to Radiation Chemistry*. second ed. 1976: Wiley-Interscience.
2. *Report of the International Commission on Radiological Units and Measurements (ICRU) (1959)*. National Bureau of Standards (U.S), 1961(Handbook 78).
3. Pimblott, S.M., and LaVerne, J. A., *Production of low-energy electrons by ionizing radiation*. Radiation Physics and Chemistry, 2007. **76**: p. 1244-1247.
4. Pimblott, S.M. *Heavy Ion Track Structure*. [cited 09/12/2010]; Available from:  
<http://personalpages.manchester.ac.uk/staff/Simon.Pimblott/RCHomePage/default.html>.
5. Mozumder, A., and Magee, J. L., *Model of Tracks of Ionizing Radiations for Radical Reaction Mechanisms*. Radiation Research, 1966. **28**: p. 203-214.
6. Allen, A.O., *The radiation chemistry of water and aqueous solutions*. 1961, New York: D. Van Nostrand Company, INC.
7. Pimblott, S.M., Green, N. J. B., and Brocklehurst, B., *Spin effects on spur kinetics: independent pairs modelling of two-species spurs*. Journal of the Chemical Society, Faraday Trans., 1991. **87**: p. 3601 - 3612.

## Chapter 3

# Facilities, Equipment & Techniques

3.1	Introduction.....	43
3.2	Chemicals.....	43
3.3	Radiation sources.....	43
	3.3.1 The FN Tandem Van de Graaff accelerator.....	44
	3.3.2 The Shepherd 109 <sup>60</sup> Co source.....	53
3.4	Analytical techniques.....	55
	3.4.1 The SRI 8610C gas chromatograph.....	55
	3.4.2 The Balzers Mass Spectrometer.....	57
3.5	Set up and Data Collection.....	58
3.6	Summary.....	61
3.7	References.....	61

### 3.1 Introduction.

The chemicals, radiation sources and analytical techniques employed in this project are described in this chapter. Water-soluble organic compounds, as well as electron and OH radical scavengers used in the hydrogen atom determination process are listed and described in the chemicals section. The heavy ion accelerator and the cobalt-60 source used to irradiate the aqueous samples with alpha and gamma rays respectively are of vital importance, and therefore they are explained in detail. In addition, the in-line set up used to collect gaseous products and the analytical techniques used to characterize the products are described finally.

### 3.2 Chemicals.

The solutions were made with various concentrations of sodium formate,  $\text{NaHCO}_2$  (ACS reagent grade), or deuterated sodium formate,  $\text{NaDCO}_2$  (98 atom %), with 1 mM potassium bromide,  $\text{KBr}$  (ACS reagent grade) and a range of concentrations of sodium nitrate,  $\text{NaNO}_3$  (ACS reagent grade), or sodium selenate,  $\text{Na}_2\text{SeO}_4$  (ACS reagent grade). All the chemicals were from Aldrich and they were used without further purification. The bromide was added to suppress OH radical back reactions with  $\text{H}_2$  and has no other effect on the system. Products from this reaction such as  $\text{Br}_2^-$  will be at sufficiently low concentrations that the hydrated electron will be scavenged by the nitrate before the possibility of reaction. Nanopure water (resistivity 18.7 M $\Omega$ cm) from an in-house H2Only system (consisting of a UV lamp and several microporous ultrafilters) was used to prepare all solutions [1].

### 3.3 Radiation sources.

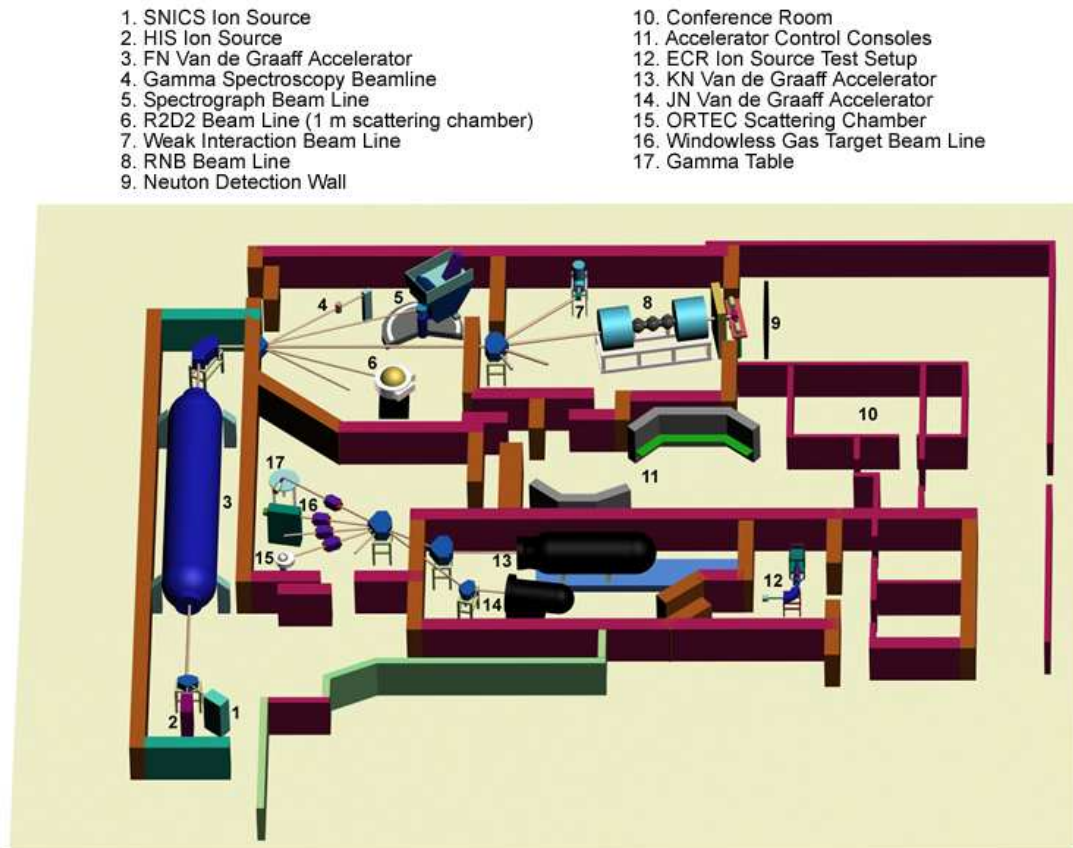
Accelerated heavy ions ( $^4\text{He}$ ,  $^1\text{H}$ ) and gamma rays have been used to investigate hydrogen atom and molecular hydrogen yields at different LET values. Heavy ions were generated in the FN tandem Van de Graaff accelerator, whereas gamma rays were delivered from the Shepherd 109  $^{60}\text{Co}$  source.

Due to their large mass and high charge,  $^4\text{He}$  is the least penetrating radiation of the three studied and in consequence has the highest LET value. Cobalt-60 undergoes radioactive decay with emission of beta particles and energetic gamma rays, which have the highest penetration in matter and therefore, the lowest LET value. Finally,  $^1\text{H}$  has a LET intermediate between  $^4\text{He}$  ions and  $^{60}\text{Co}$  gamma rays.

### 3.3.1 The FN Tandem Van de Graaff accelerator.

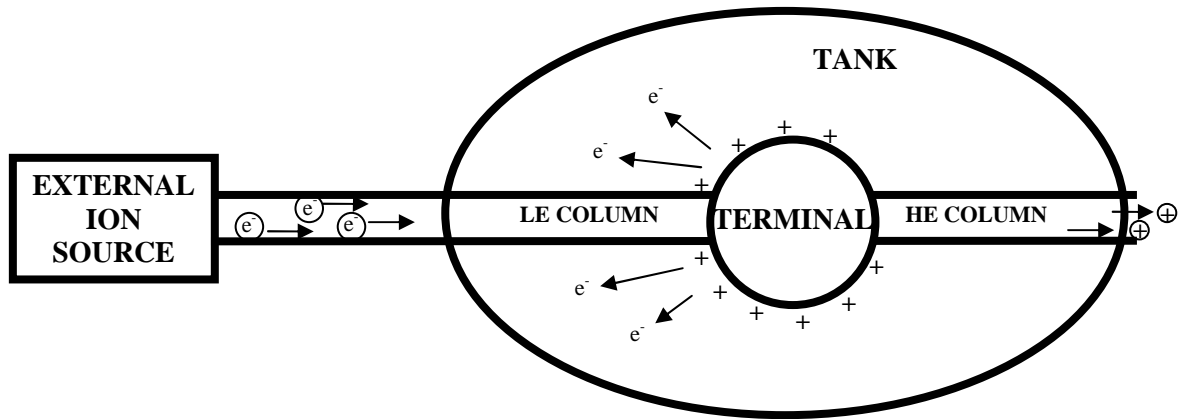
The FN Tandem Van de Graaff Accelerator of the Nuclear Structure Laboratory at The University of Notre Dame has been in service from late 1960's and upgraded several times over the years [2].

Figure 3.1 shows the plan of the facility where the control room is number 11, ion sources are numbers 1 and 2, the acceleration tank is number 3 and beam line number 4 was used for sample irradiation.



**Figure 3.1** Layout of the FN Tandem Van de Graaff accelerator [3].

The FN Tandem Van de Graaff Accelerator has an external ion source producing a negatively charged ion beam travelling in vacuum towards a positively charged terminal. Electrons are stripped from the ions in the terminal as they pass through a thin carbon foil, leaving the ion beam positively charged. The name “Tandem” comes from the beam being accelerated twice, as the negatively and positively charged beam approaches and travels away respectively from the positively charged terminal.



**Figure 3.2** Beam trajectory within the accelerator.

There are two different ion sources at the facilities in Notre Dame, the SNICS and the HIS Ion Sources. The SNICS (Source of Negative Ions by Cesium Sputtering) ion source produces all the negatively charged ions with the exception of the helium beam. Its principles are quite straightforward and represented in the diagram below.

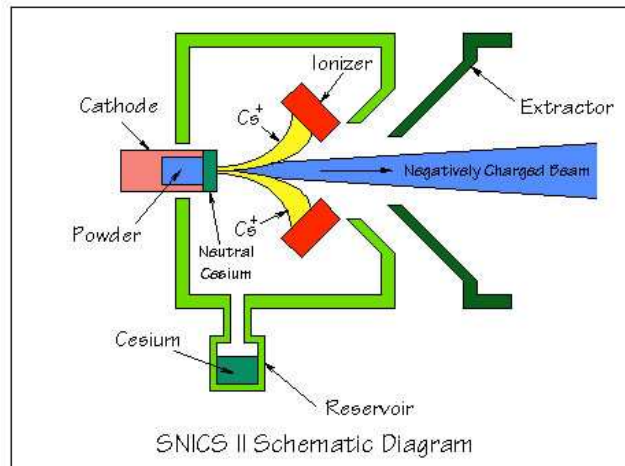


**Figure 3.3** SNICS II Ion Source [4].

The cesium in the reservoir is heated to  $120^\circ\text{C}$ , so some vapour is formed and rises through the vacuum to the cathode and ionizer area. The cathode is cooled while the ionizer remains hot. Some of the cesium vapour condenses on the cathode surface while some of the vapour deposits on the ionizer to be immediately ionized and then ejected towards the cathode. The positively charged cesium ions impact onto the cathode with great energy and some material is sputtered and gains electrons when

passing through the cesium coating. As the source operates at about 80 kV, the negative beam is accelerated out of the source towards the accelerator. A large variety of ion beams can be produced by choosing the appropriate cathode. A basic cathode is a small cylindrical section of copper with a cavity filled with the desired element to be sputtered.

The Helium Ion Source (HIS) employs a complicated procedure but a simple description can be given, as seen in figure 3.4. The source consists of a filament made of tungsten housed within a cavity filled with helium gas. The filament is heated by passing a high current through it and results in the production of electrons by thermionic emission. These electrons then ionize the helium gas, so singly charged positive helium ions move forward through a narrow aperture known as “button”. The positive ion beam passes next through the “extraction” electrode maintained at -20 kV, and the einzel lens, which focus the beam into the lithium charge exchange chamber, where the beam goes through a narrow passage filled with lithium vapour from the heated lithium reservoir. Some of the positive helium ions gain electrons when colliding with the lithium atoms which leads to the formation of singly negatively charged helium ions ready for injection into the accelerator. The lithium charge exchange is maintained at -20 kV, which means that the singly charged negative helium beam is ejected out of the charge exchange region at 40 keV due to the 20 keV gained as they accelerate into the region plus the 20 keV as they accelerate away from the region. This lithium charge exchange chamber is therefore acting as a small tandem accelerator because of the charge exchange process.

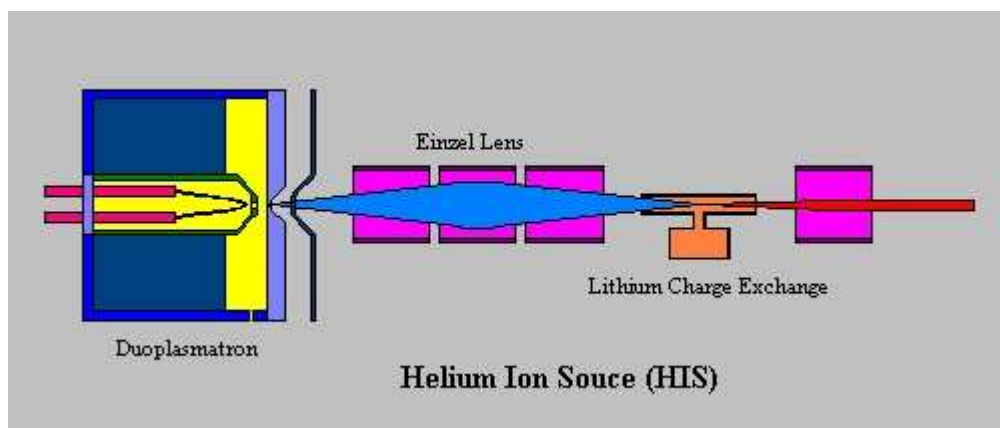


**Figure 3.4** Helium Ion Source (HIS) [5].

The FN Tandem Accelerator is housed into a tank, showed below, made of steel and with approximate dimensions: 12.2 m long x 3.7 m diameter. Its function is to isolate the high voltage electrodes from the outside and avoid electrical discharges. The latter is achieved by filling the tank to high pressure with an insulating gas, typically SF<sub>6</sub> or a SF<sub>6</sub>-N<sub>2</sub> mixture.



**Figure 3.5** Acceleration tank of the FN Van de Graaff accelerator at the Univ. of Notre Dame [6].

The terminal electrode is supported within the tank by two columns. The low energy column (LE) refers to the column in the tank base nearest to the ion source, whereas, the high energy column (HE) extends from the terminal to the opposite tank base. Each column is made of approximately 200 aluminium planes. Each one of these planes is glued to four glass blocks in order to electrically isolate them. These columns are suspended and held on the terminal electrode by compression supplied by a large spring located in the HE tank base. Resistors are connected between each metal electrode at the top of the column, creating a voltage divider circuit. Charge is continually flowing from the terminal to ground through these resistors, and therefore the charge in the terminal must be continually replenished.

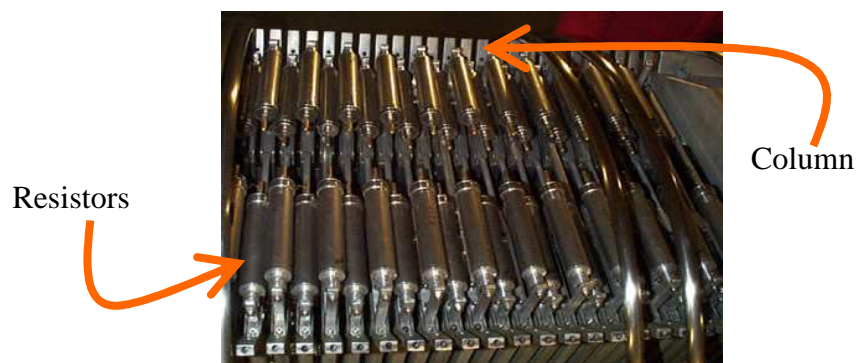


**Figure 3.6** Resistors connected between each metal electrode of the column [6].

Resistors are shown in the Figure 3.6, which is a view from the top of the column. Each resistor is about the size of a pencil and is made of a small ceramic core with a thin film coating and housed in an aluminium tube in order to shield them.

The evacuated beam tubes are mounted along the side of the column. There are four acceleration tubes, two before the terminal and two after, each measuring 2.4 metres long, 20.3 centimetres in diameter and approximately a hundred kilograms weight. Each tube is composed of about 100 pairs of hollow cylindrical glass spacers glued to aluminium “dish shape” electrodes with an aperture in the center to allow the passage of the beam. The tubes are connected to the columns by metal springs which link each plane of the column with the corresponding plane in the tube.

Figure 3.7 shows a close up of a section of the column and a beam tube. The column is the set of aluminium vertical bars in the background while the tube is the round set of metal electrodes and glass spacers in the foreground. The “acorn nuts” between the electrodes on the tube are spark gaps. They are designed to dissipate any spark to ground so the energy does not pass through the glass spacers and potentially shatter them. The metallic triangles at the bottom of the column are used to run strings through their slots in order to communicate with the terminal from ground, setting voltages, etc. The dark colour on the glass spacers is due to the radiation exposure.

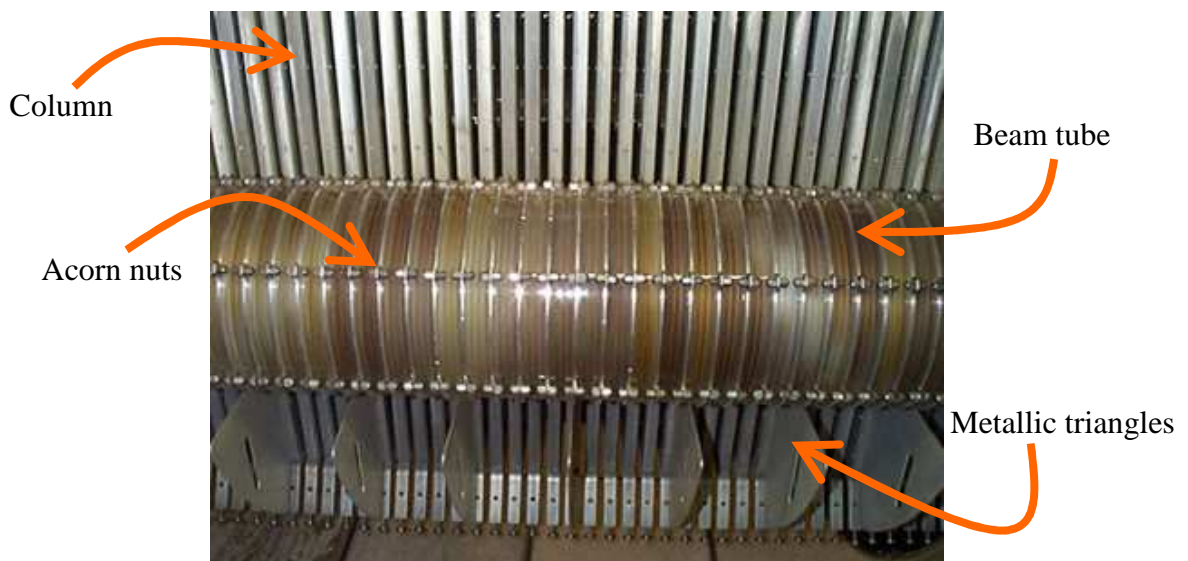


**Figure 3.7** Acceleration tube and column within the acceleration tank [6].



The system used to charge the terminal is known as a ‘‘Pelletron chain’’ (see Figure 3.8). It consists of a chain formed by charged metal pellets connected by nylon links, which isolate electronically two consecutive pellets. In the FN Tandem accelerator there are two different Pelletron chains, one in the LE column and one in the HE column. A motor and a pulley are used to drive the chain at approximately 40 mph through the accelerator.

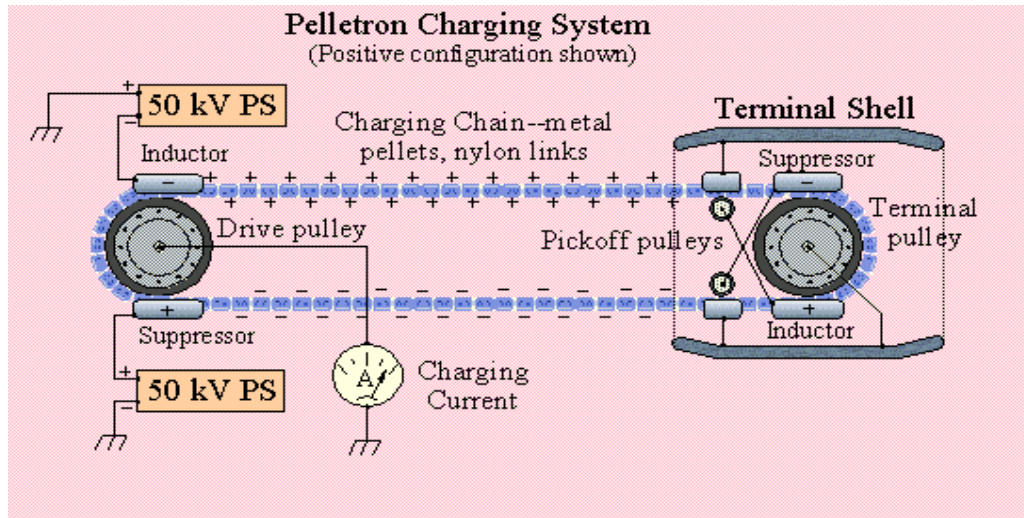


**Figure 3.8** Pelletron charging system [7].

To understand how the terminal is charged, consider the travel of a single pellet in Figure 3.8. The single pellet passes through the drive pulley close to the inductor charged to a negative potential by the external source, the electrons in the pellet flow to ground through the pulley due to this negative potential, and therefore the pellet leaves with a net positive charge when moving towards the terminal. When approaching the terminal shell, the pellet slightly contacts with a ‘‘pickoff wheel’’ to produce a small amount of positive charge that flows to the inductor at the bottom of the terminal. This inductor remains at large positive potential due to the small contributions of the numerous pellets within the chain. The pellet continues towards the negatively charged suppressor which makes the positive charge on the pellet flow to the upper surface. The contact between the positively charged pellet and the terminal pulley helps the positive charge to flow first to the terminal pulley and then to the terminal shell through a carbon brush arrangement. As the pellet keeps on moving through the terminal pulley, it enters to the positive charged inductor region, which makes the negative charge from the terminal flow to the lower surface of the

pellet leaving a positive net potential in the terminal. The terminal is therefore charged by the upper and lower sections of the chain. The upper section charges the terminal positively while the lower takes negative charge away from the terminal.

The terminal voltage is measured by a device known as a Generating Volt Meter (GVM) which is mounted in the wall of the tank. The GVM has alternated rotor and stator blades. As the rotor blades spin, the stators are alternately exposed to the electric field of the terminal. Therefore, an electric signal is produced that is proportional to the terminal voltage [8].

The charge provided to the terminal by the Pelletron chain must be in equilibrium with the charge flowing to ground through the resistors. The corona feedback is a system of very sharp needles on a moveable arm. As the corona system is moved towards the terminal, a discharge begins at the tips of the needles causing charge to flow from the terminal through the needles and then to ground. In addition, a variable resistor is attached to the corona needles in order to help control the charge extracted from the terminal. The signal used to adjust this variable resistor is provided by the Stabilizer, which is a feedback circuit used to control and stabilize the terminal voltage. It has two operative modes, known as the Generating Voltmeter (GV) Control and the Slit Control (see Figure 3.10). In the GV control, the terminal voltage provided by the GVM is compared to the voltage desired by the experimenter using a setting on the front panel. If any difference occurs, the Stabilizer automatically adjusts the variable resistor, which allows the terminal voltage to change until both voltage values agree. In Slit Control, an error signal is generated by a set of metal slits, which are symmetrically placed at both sides of the beam at the exit of the analyzing magnet (see Figure 3.9). This magnet is used to select the ion momentum of interest by controlling the current in the magnet and therefore the magnetic field,  $B$ , which fixes the radius of curvature,  $r$ , of the ions entering the field according to their momentum,  $p$ , and charge,  $Q$ , ( $rB = p/Q$ ), all other beams collide with the walls and never reach the target.

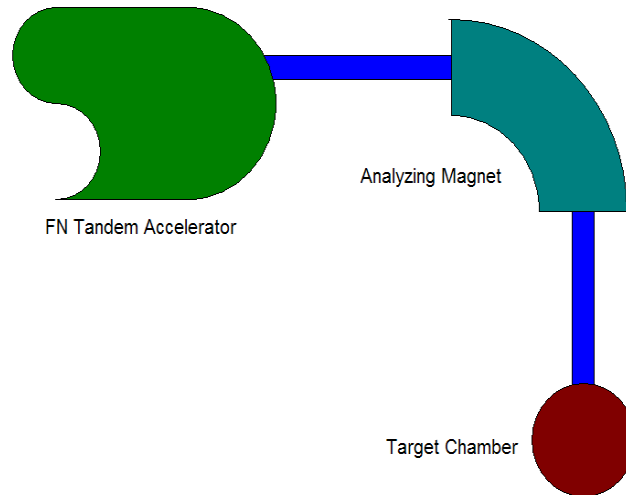


**Figure 3.9** The analyzing Magnet of The FN Van de Graaff [8].

For example, if the terminal voltage decreases slightly, the charged ions entering the magnet will collide with the left slit. Therefore, the difference between the amount of particles colliding in the left and right slits is an indication of whether the voltage on the terminal is too high, too low or just right. This signal is then sent to the Stabilizer to control the variable resistor in a similar way as with the GV control.

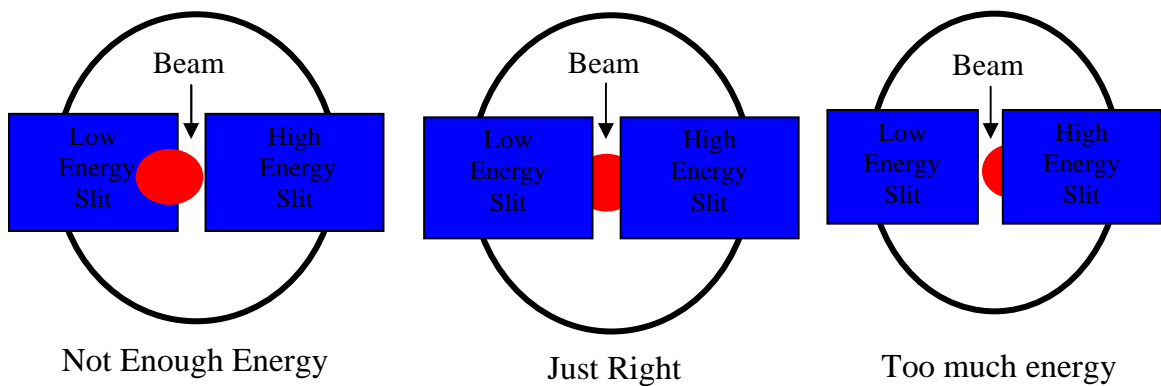


**Figure 3.10** Metal slits within the analyzing Magnet used in the Slit control mode[8].

The ion beam then leaves the magnet with the right energy and trajectory to irradiate our sample placed in the target room.

In this project, energetic beams of 5 MeV  $^1\text{H}^+$  and 5 MeV  $^4\text{He}^{2+}$  inside the sample cell, were produced by respective voltages of 2.75 MV at 1.5 nA and 3.43 MV at 1.5 nA in the accelerator. These voltages and the energy required to produce the energetic beams were determined by using the SRIM (Stopping and Range of

Ions in Matter) and TRIM (Transport of Ions in Matter) software packages as shown in table 3.1. The voltage is first calculated by setting the ion type and energy inside the sample cell. The energy beam is then given by the expression,

$$E = V(Q_{\text{out}} + 1) \quad (3.1)$$

where  $V$  is the voltage and  $Q_{\text{out}}$  is the ion charge. The difference between the energy beam and the energy inside the sample cell is the attenuated energy when passing through the metal cap of the beam line and the mica window of the sample cell.

<b>Ion type</b>	<b>Voltage (MV)</b>	<b>Energy beam (MeV)</b>	<b>Energy inside the cell (MeV)</b>	<b>Attenuated energy (MeV)</b>	<b>Stopping power (at 5 MeV) (MeV cm<sup>2</sup> g<sup>-1</sup>)</b>	<b>Stopping power (track average) (MeV cm<sup>2</sup> g<sup>-1</sup>)</b>
<sup>1</sup> H <sup>+</sup>	2.75	5.5	5	0.5	78.5	180
<sup>4</sup> He <sup>2+</sup>	3.43	10.29	5	5.29	886	1530

**Table 3.1** Parameters of the energy beam.

The sample receives between 50 and 100 beam counts which means that the energy received can be calculated by using the appropriate conversion factors as shown in Figure 3.11.

$$\frac{\text{Beam counts (coulombs)} \times \text{Conv. factor} \left( \frac{\text{elem. charges}}{\text{coulombs}} \right)}{\text{n}^\circ \text{ of elementary charges} \times \text{Instrument calibration}} \times \text{Beam Energy (eV)} = E(\text{eV})$$

**Figure 3.11** Calculation of the energy received by a sample irradiated with heavy ions.

The beam counts are given in  $10^{-8}$  coulombs which by definition is equal to  $6.242 \times 10^{18}$  elementary charges. This value is then divided by the number of elementary charges of the beam times the instrument calibration, and finally multiplied by the energy of the beam. The final result is the energy received by the sample. Calculations for <sup>4</sup>He and <sup>1</sup>H are shown next,

${}^4\text{He}$

Number of beam counts  
(50 – 100)  $\uparrow$

$$\frac{V \times 10^{-8} \text{ coulomb} \times 6,242 \times 10^{18} \frac{\text{elem. charges}}{\text{coulombs}}}{2 \text{ elem. charges} \times 0.975} \times 5 \times 10^6 \text{ eV} = 8 \times 10^{18} - 1.6 \times 10^{19} \text{ eV}$$

He beam energy

Instrument calibration  $\rightarrow$

${}^1\text{H}$

Number of beam counts  
(50 – 100)  $\uparrow$

$$\frac{V \times 10^{-8} \text{ coulomb} \times 6,242 \times 10^{18} \frac{\text{elem. charges}}{\text{coulombs}}}{1 \text{ elem. charges} \times 0.975} \times 5 \times 10^6 \text{ eV} = 1.6 \times 10^{19} - 3.2 \times 10^{19} \text{ eV}$$

H beam energy

Instrument calibration  $\rightarrow$

### 3.3.2 The Shepherd ${}^{60}\text{Co}$ source.

Cobalt is a hard but fragile, bluish-grey metal. Cobalt-60 is a radioisotope of cobalt that is not found in nature due to its short radioactive half life of about 5.27 years. However, it is produced artificially in nuclear reactors by exposing cobalt-59 to neutron radiation.

The decay scheme of cobalt-60 is shown in Figure 3.12. Cobalt-60 undergoes radioactive decay to the stable isotope nickel-60 with emission of beta particles and energetic gamma rays. There are two possible beta transitions; however, one is much more probable than the other one [9].

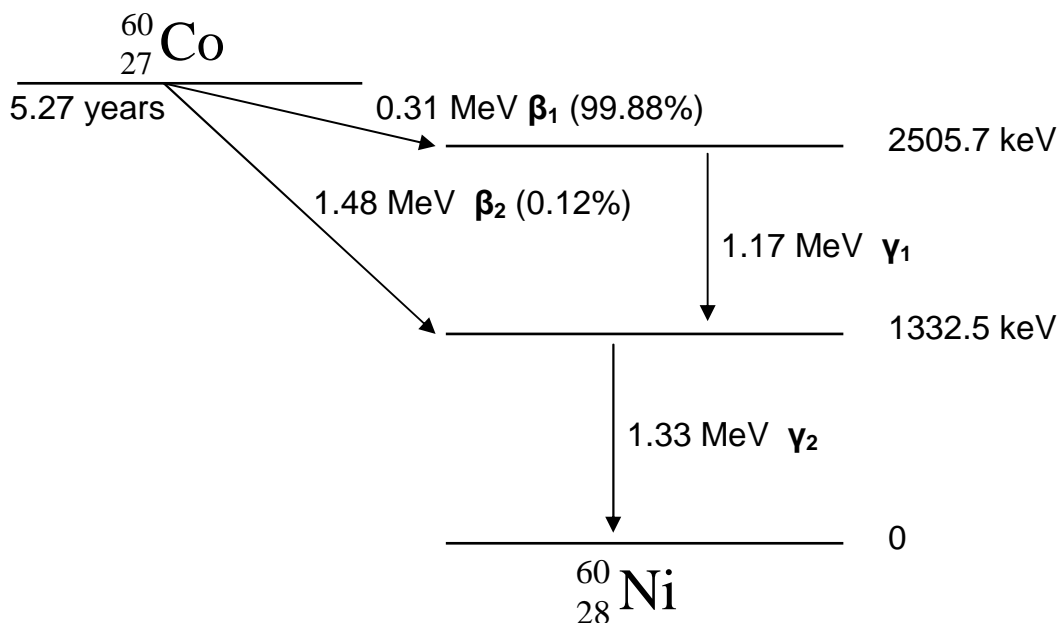


**Figure 3.12** Decay scheme of  ${}^{60}\text{Co}$

The cobalt-60 is commonly housed in shielded metal containers for industrial or medical purposes; these are referred to as radiation “sources”. The Shepherd 109 cobalt-60 source (see Figure 3.13) has been in service in the Radiation Laboratory at the University of Notre Dame (USA) since 21<sup>st</sup> November 1997 with an initial activity of 24,000 curies (1 curie =  $3.7 \times 10^{10}$  disintegrations per second) and current activity of about 4,500 curies.



**Figure 3.13** The Shepherd 109 cobalt-60 source in the Radiation Laboratory at the University of Notre Dame (own photo).

The metallic door on the upper side of the source is opened to place the sample and closed to isolate it. The monitor on the left hand side is used to control the radiation time and to operate the motor which drives the sample down to the lower chamber of the source. In the lower chamber of the source there are 12 rods of cobalt and the sample lowers to the middle (see Figure 3.14).

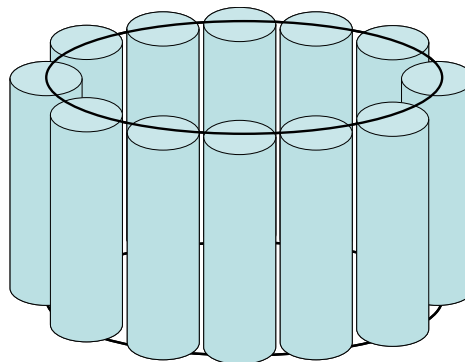


**Figure 3.14** Cobalt-60 rods layout within the Shepherd 109 cobalt-60 source.

In this project, radiation doses ranged from approximately 24 to 78 krad or from  $3.0 \times 10^{21}$  to  $4.1 \times 10^{21}$  eV kg<sup>-1</sup>, with four millilitres samples loaded into the sample cell.

### 3.4 Analytical techniques.

Gaseous samples were analysed using two different techniques to determine their chemical composition. Gas chromatography is a technique used for the separation of gaseous mixtures. A chromatograph essentially consists of a stationary phase within a column and a detector. A chemically inert carrier gas is used to transport the sample through the column and to the detector. Mass spectrometry is a commonly used technique for the determination of the elemental composition of a sample. A spectrometer essentially consists of an ion source, a mass analyser and a detector. The gaseous samples are ionized in the ion source, separated in the mass analyser and transport to the detector.

#### 3.4.1 The SRI 8610C gas chromatograph.

In the current experiments, a SRI 8610C gas chromatograph has been employed for the determination of molecular hydrogen. A simplified layout is shown in figure 3.15. Ultra high-purity argon was used as the carrier gas with a flow rate of about 50 ml/min. The argon passed through a flow regulator, an injector port, a four-way valve and into a 3 m 5x molecular sieve column with a thermal conductivity detector.

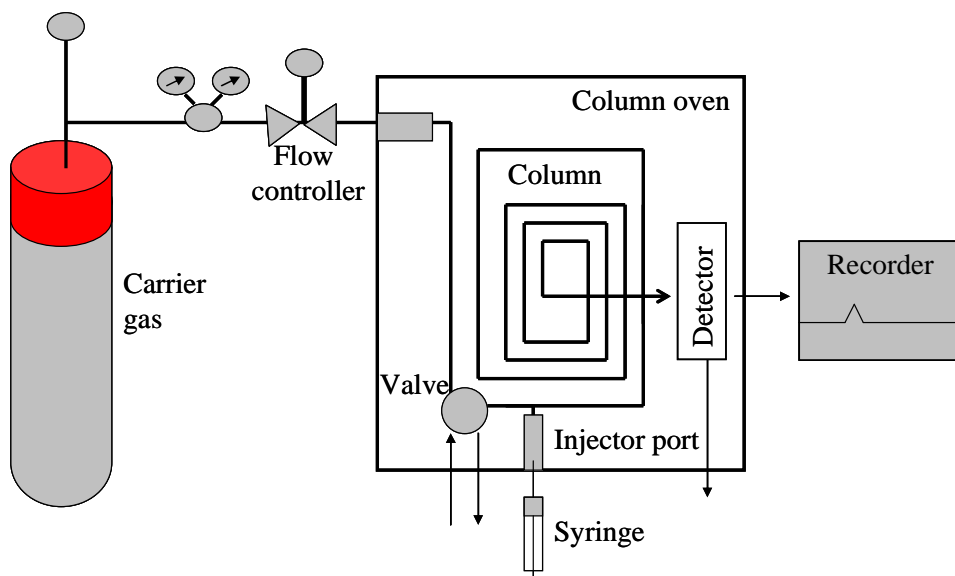


**Figure 3.15** SRI 8610C Gas chromatograph layout.

Argon was used as the carrier gas in the molecular hydrogen determination, since they have very different thermal conductivities.

A four-way valve is included for sample injection as shown in figure 3.16. It has two different positions, when the valve is opened the carrier gas flows straight through the column to the detector. However, in the closed position, the carrier gas flows through the sample pushing the gases in the cell towards the column.

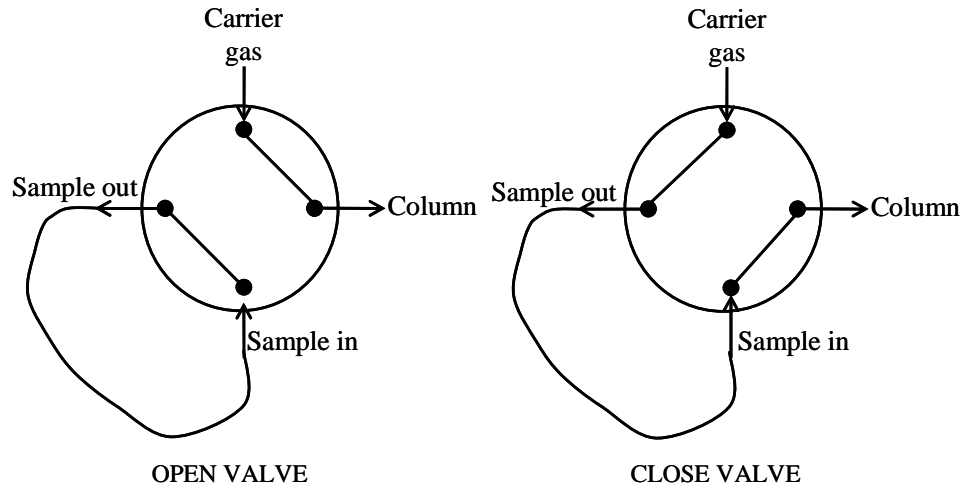


**Figure 3.16** Four-way valve within the SRI 8610C gas chromatograph.

The molecular sieve column is made of aluminosilicate zeolite which contains tiny pores of a well defined size and it is commonly used as an absorbent for air and humidity. Molecules small enough, such as nitrogen or water, pass through the pores and are then absorbed, while larger molecules are not. A molecular sieve can adsorb water molecules up to 22% of its own weight. Gases are separated due to their different rates of adsorbance on the column and then are observed by the detector [10].

The thermal conductivity detector consists of a typical *Wheatstone bridge* circuit (see Figure 3.17). The thermal conductivity of the carrier gas is monitored by the R4 resistor; however, when an analyte elutes from the column and flows across resistor R3, a measurable potential change is produced and registered as a signal [11].



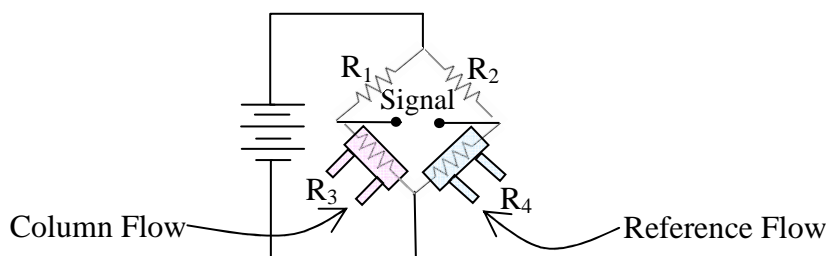


**Figure 3.17** Thermal conductivity detector.

### 3.4.2 The Balzers Mass Spectrometer.

The basic steps of an ordinary mass spectrometer are shown in figure 3.18.

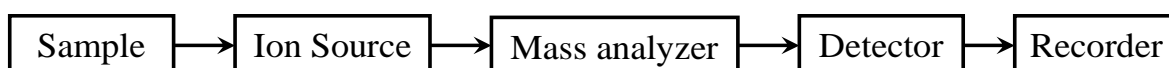


**Figure 3.18** Schematic design of an ordinary Mass Spectrometer.

The Balzers Mass Spectrometer [12] used in the present experiments ionizes the gas samples with a hot filament. It is based on a heated wire filament with an electric current running through it and emits electrons by thermionic emission. These energetic electrons interact with gas phase molecules in the ion source to produce ions. The ionized gas passes through a small electric field on its way to the quadrupole mass analyzer [13].

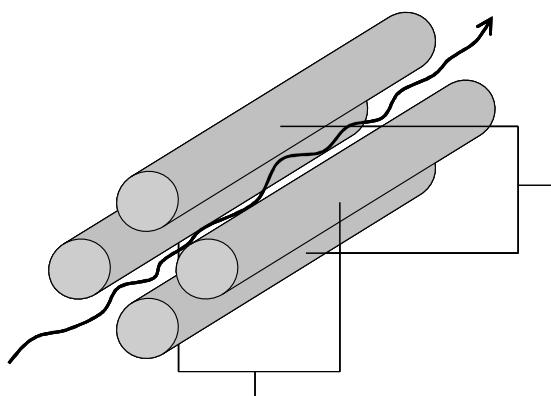


**Figure 3.19** Titanium rods within the quadrupole mass analyzer of The Balzers Mass Spectrometer.

The quadrupole is made of four titanium rods of about 1 cm diameter and 10 cm long. Opposite rod pairs are electrically connected and a radio frequency voltage is applied between each pair of rods. A direct current voltage is then superimposed

on the R.F. voltage. The ions are separated as they travel in between the rods of the quadrapole based on their mass to charge ratio. By setting the appropriate voltage and frequency, selected ions reach the detector while the rest collide with the rods.

A secondary electron multiplier is used to detect the presence of ions emerging from the quadrapole mass analyzer [14]. As the ions collide with the surface of an electrode, secondary electrons from the outer layers are released. The number of secondary electrons released depends on the type of incident primary ion, its angle, energy and nature of the incident surface. These parameters are ultimately related to the abundance of an ion, the intensity of the ion beam, and the area of the peak.

### 3.5 Set up and Data Collection.

Two very similar inline set ups were used for the collection and characterization of products in the heavy ion and gamma ray irradiation of aqueous systems.

#### 3.5.1 Heavy ion radiolysis of aqueous formate solutions.

Twenty millilitres samples were loaded into a Pyrex cell (see Figure 3.20) with a thin mica window ( $\sim 6 \text{ mg/cm}^2$ ). The sample cell contained a magnetic stirrer operating continuously and inlet and outlet ports to purge the sample before irradiation with ultra high purity argon. The set up is shown in Figure 3.20.



**Figure 3.20** Pyrex cell filled with 20 milliliters of the sample (own photo).

The sample receives between 50 and 100 beam counts on the heavy ions accelerator. Once the sample has been irradiated, the carrier gas is allowed to pass through the cell carrying the molecular hydrogen formed into the gas chromatograph. The carrier gas was ultra high purity argon with a flow rate of ~50 ml/min. The gas passes through a constant flow regulator, an injection septum, a four way valve and into a 3 meter 5x molecular sieve column. Total molecular hydrogen was determined from the gas chromatograph signal of a thermal conductivity detector (TCD). The sample leaves the gas chromatograph and enters the mass spectrometer connected inline, as seen in Figure 3.21. The mass spectrometer (Balzers) has a QMA 140 analyzer with axially mounted secondary electron multiplier. The capillary tube has a 25  $\mu\text{m}$  diameter and is 20 cm in length. The hydrogen isotopes were monitored at masses 2 ( $\text{H}_2$ ), 3 (HD) and 4 ( $\text{D}_2$ ).

Calibration was carried out by injecting different volumes of pure  $\text{H}_2$  and  $\text{D}_2$  with a gas-tight microliter syringe. The estimated error in gas measurement is expected to be ~5%. Radiation chemical yields are expressed as G values (molecules/100eV), which is equivalent to  $\sim 0.1 \mu\text{mol J}^{-1}$ .

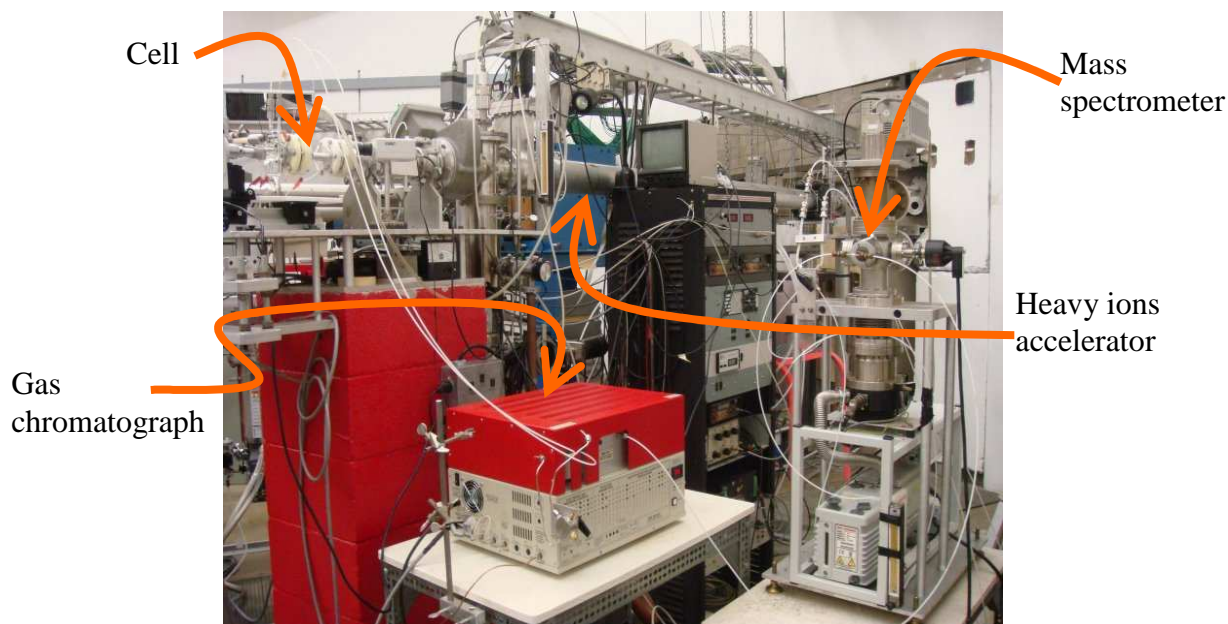


**Figure 3.21** The gas chromatograph and the mass spectrometer are connected inline with the sample cell placed on the heavy ions accelerator (own photo).

## 3.5.2 Gamma radiolysis of aqueous formate solutions.

Four millilitres samples were loaded into a sample cell that consists of a 1 cm cuvette with inlet and outlet ports to purge the sample before irradiation, as seen in Figure 3.22.

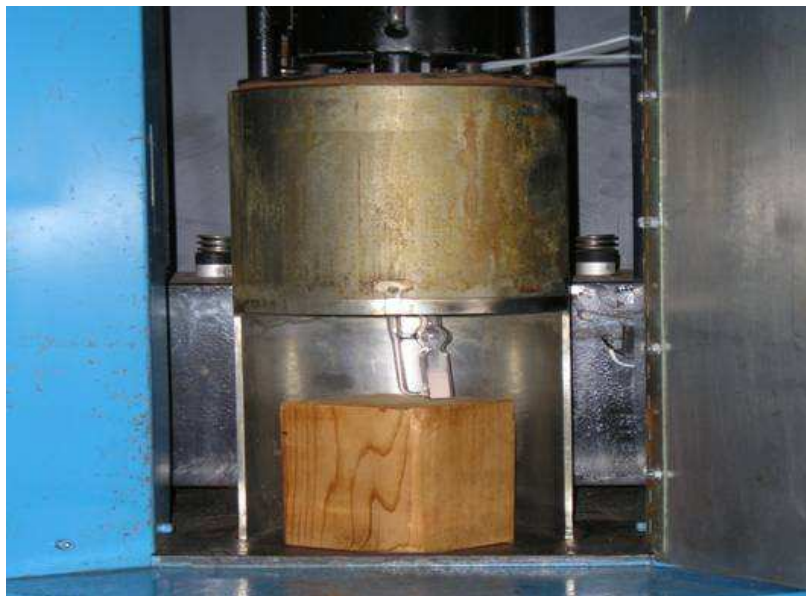


**Figure 3.22** Cuvette filled with four milliliters of the sample placed in the gamma source (own photo).

Ultra high purity argon with a flow rate of ~50 ml/min was used to deaerate the solutions and as a carrier gas. The sample was then irradiated for a given time between 3 and 30 minutes.

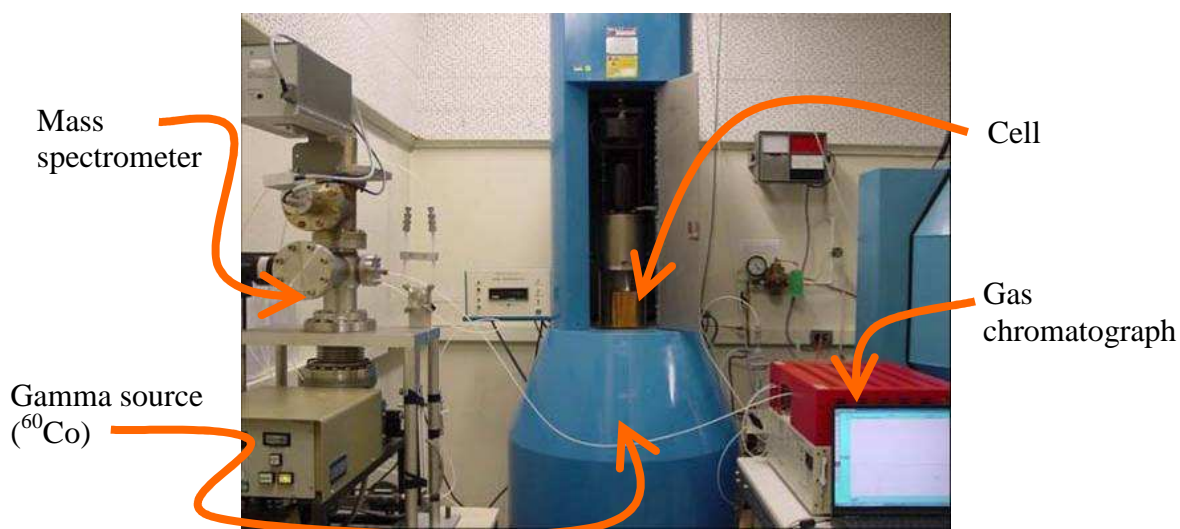


**Figure 3.23** Gas chromatograph and mass spectrometer connected in line with the sample cell placed in the gamma source (own photo).

Once the sample has been irradiated, the carrier gas is allowed to pass through the cell carrying the molecular hydrogen formed into the gas chromatograph. Total molecular hydrogen was determined from the gas chromatograph signal after passing through a constant flow regulator, an injection septum, a four way valve and into a 3 meter 5x molecular sieve column. The sample leaves the gas chromatograph and enters the mass spectrometer connected inline, as seen in Figure 3.23. The mass spectrometer (Balzers) has a QMA 140 analyzer with axially mounted secondary electron multiplier. The capillary tube has a 25  $\mu\text{m}$  diameter and is 20 cm in length. The hydrogen isotopes were monitored at masses 2 ( $\text{H}_2$ ), 3 (HD) and 4 ( $\text{D}_2$ ).

### 3.6 Summary

The chemicals and experimental techniques used in this project have been described in this chapter. A variety of radiation sources have been used for studying the H atom formation in the radiolysis of aqueous systems with added electron scavengers. The analytical techniques used to characterise the hydrogen atom and molecular hydrogen have been described and theoretical basis of the techniques has been explained.

### 3.7 References

1. Huerta Parajon, M., Rajesh, P., Mu, T., Pimblott, S.M., and LaVerne, J.A., *H atom yields in the radiolysis of water*. Radiation Physics and Chemistry, 2008. **77**: p. 1203-1207.
2. Schuler, R.H., *Radiation chemistry at Notre Dame 1943-1994*. Radiation Physics and Chemistry, 1996. **47**: p. 9-17.
3. *Layout of the FN Tandem Van de Graaff Accelerator*. Institute for Structure and Nuclear Astrophysics 2009 [cited 20 January 2010]; Available from: [http://www.nd.edu/~nsl/Research\\_Facilities/Layout/1.jpg](http://www.nd.edu/~nsl/Research_Facilities/Layout/1.jpg).
4. *SNICS II Sputter Ion Source*. Institute for Structure and Nuclear Astrophysics 2009 [cited 20 January 2010]; Available from: [http://www.nd.edu/~nsl/Research\\_Facilities/Snics/nsl\\_snics.html](http://www.nd.edu/~nsl/Research_Facilities/Snics/nsl_snics.html).
5. *HIS Helium Ion Source*. Institute for Structure and Nuclear Astrophysics 2009 [cited 20 January 2010]; Available from: [http://www.nd.edu/~nsl/Research\\_Facilities/HIS\\_source/his.html](http://www.nd.edu/~nsl/Research_Facilities/HIS_source/his.html).
6. *FN Tandem Van de Graaff Accelerator*. Institute for Structure and Nuclear Astrophysics 2009 [cited 20 January 2010]; Available from: [http://www.nd.edu/~nsl/html/research\\_FN.html](http://www.nd.edu/~nsl/html/research_FN.html).
7. *Charging system*. National Electrostatics Corporation 2001 [cited 20 January 2010]; Available from: <http://www.pelletron.com/charging.htm>.
8. *Accelerator operator's school March 2009.ppt*. Institute for Structure and Nuclear Astrophysics 2009 [cited 20 January 2010]; Available from:

- [http://www.nd.edu/~nsl/nsl\\_docs/General\\_Lab/Accelerator%20School/School%202009/](http://www.nd.edu/~nsl/nsl_docs/General_Lab/Accelerator%20School/School%202009/).
9. Ojovan, M.I., and Lee, W. E., *Nuclear Decay*, in *An Introduction to Nuclear Waste Immobilisation*. 2005, Elsevier: Oxford. p. 9-21.
  10. Poole, C.F., Worsfold, P., Townshend, A., and Poole, C., *GAS CHROMATOGRAPHY | Column Technology*, in *Encyclopedia of Analytical Science*. 2005, Elsevier: Oxford. p. 18-34.
  11. Cruz, D., Chang, J. P., Showalter, S. K., Gelbard, F., Manginell, R. P., and Blain, M. G., *Microfabricated thermal conductivity detector for the micro-ChemLab(TM)*. *Sensors and Actuators B: Chemical*, 2007. **121**: p. 415.
  12. Balzers High Vacuum, L., *The new Balzers quadrupole mass spectrometer QMG511-- an instrument speaking the computer language*. *Vacuum*, 1973. **23**: p. 374-374.
  13. Hoffmann, E., *Mass Spectrometry: Principles and Applications*. Fourth ed. 2003, Toronto: John Wiley & Sons.
  14. Alan, D.M., and A. Wilkinson, *IUPAC Compendium of Chemical Terminology*. 2nd Edition ed. 1997, Cambridge: Blackwell Science.

# Chapter 4

## Stochastic Models

4.1	Introduction.....	64
4.2	Radiation processes.....	64
4.3	Monte Carlo simulation of track structure.....	65
	4.3.1 Monte Carlo simulation of electron track structure.....	65
	4.3.1.1 Cross sections.....	68
	4.3.2 Monte Carlo simulation of heavy ion track structure.....	72
4.4	Monte Carlo simulation of chemical evolution of the track.....	73
4.5	Summary.....	78
4.6	References.....	78

#### 4.1 Introduction

The radiation induced processes occurring after water radiolysis have been studied in order to be able to understand and model the chemistry involved. A variety of different models have been developed in the literature, which take into account the nature of the irradiated matter and the ionizing radiation. In this chapter, the stochastic models used to simulate the track structure and the chemical evolution of the track are described. Command scripts used to run the simulations are enclosed in Appendix C.

#### 4.2 Radiation process

Many different physical and chemical processes are expected after irradiation. By modelling these processes, the chemical effects of radiation on matter can be studied. The different processes are listed in figure 4.1.

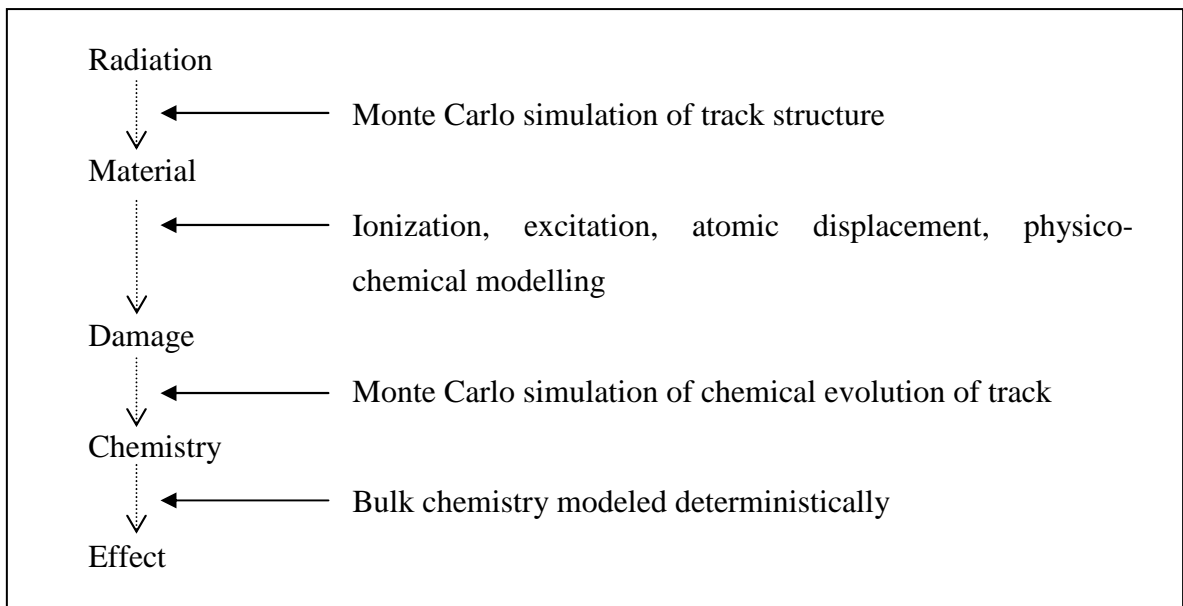


**Figure 4.1** Physical and chemical processes in the evolution of radiation tracks

Energy loss by energetic ions is a stochastic phenomenon. There is more than one way in which a particular track can evolve with time, however, some of the outcomes are more probable than others. An interaction between the radiation particle and matter may result in elastic or inelastic collisions and in the latter case in an ionization or excitation event. From these primary physical events, the chemical evolution of the track can be followed with time by using an appropriate model specific to the irradiated medium.



### 4.3 Monte Carlo simulation of track structure

The Monte Carlo methods used to simulate the fast electron and heavy ion track structures in gaseous and liquid water have been described previously in detail [1-3]. The modelling follows the flow diagram, figure 4.2, which has been developed on the basis of the real radiation processes observed after collisions occur. Excitation and ionization events may occur as a result of energy transfer due to inelastic collisions. Each ionization event generates a new electron which may result in further excitation or ionization events.

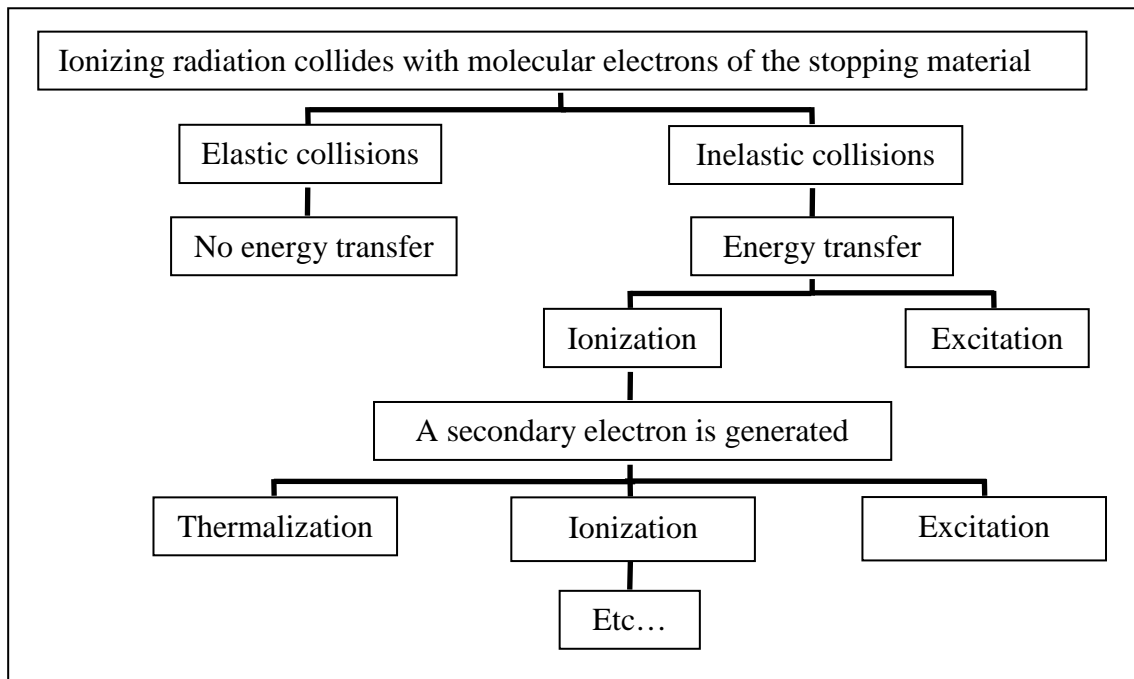


**Figure 4.2** Physico-chemical processes in a radiation track

While only slight differences are found between methodologies employed to simulate the energetic electron and heavy ion track structures, the cross sections employed within these simulation methodologies may be very different.

#### 4.3.1 Monte Carlo simulation of electron track structure

The Monte Carlo methodology for simulating the structure of electron tracks starts from one high energy electron ( $E$ ) travelling in a defined direction. This electron is initially at point  $z$ , and the distance travelled before a collision will be defined as  $\Delta z$ . The electron trajectory has a Poisson distribution with a mean free path,  $\lambda_{\text{total}}$ , which is the average distance travelled between consecutive collisions

and is dependent on the total cross section  $\sigma_{\text{total}}$  ( $\text{m}^2/\text{molecule}$ ) for inelastic and elastic collisions as well as the number density of molecules,  $N$  ( $\text{molecules}/\text{m}^3$ ).

$$A_{\text{total}} = (N\sigma_{\text{total}})^{-1} = [\rho(\sigma_{\text{elastic}} + \sigma_{\text{inelastic}})]^{-1} \quad (4.1)$$

The distance travelled between two consecutive collisions is calculated by using the inversion method [4] and sampling from the probability distribution function

$$P(A_{\text{total}}, \Delta z) = 1 - \exp\left(\frac{-\Delta z}{A_{\text{total}}}\right) \quad (4.2)$$

with a uniformly distributed random number  $U_1$  in the range  $0 - 1$ . Now, knowing the direction of the trajectory and calculating the distance travelled between collisions, the initial electron position  $z$  can be replaced by the new one  $z_{\text{new}}$ .

A second random number,  $U_2$ , is now compared with the probability of an inelastic or elastic collision to determine whether the collision results in an energy transfer and if an energy transfer results in an ionization, an excitation or a vibration event:

$$0 < U_2 < \frac{\sigma_{\text{ionization}}}{\sigma_{\text{inelastic}} + \sigma_{\text{elastic}}} \quad \text{IONIZATION} \quad (4.3)$$

$$\frac{\sigma_{\text{ionization}}}{\sigma_{\text{inelastic}} + \sigma_{\text{elastic}}} < U_2 < \frac{\sigma_{\text{ionization}} + \sigma_{\text{excitation}}}{\sigma_{\text{inelastic}} + \sigma_{\text{elastic}}} \quad \text{EXCITATION} \quad (4.4)$$

$$\frac{\sigma_{\text{ionization}} + \sigma_{\text{excitation}}}{\sigma_{\text{inelastic}} + \sigma_{\text{elastic}}} < U_2 < \frac{\sigma_{\text{inelastic}}}{\sigma_{\text{inelastic}} + \sigma_{\text{elastic}}} \quad \text{VIBRATION} \quad (4.5)$$

$$\frac{\sigma_{\text{inelastic}}}{\sigma_{\text{inelastic}} + \sigma_{\text{elastic}}} < U_2 < 1 \quad \text{ELASTIC} \quad (4.6)$$

With  $\sigma_{\text{inelastic}}$ ,  $\sigma_{\text{elastic}}$ ,  $\sigma_{\text{ionization}}$  and  $\sigma_{\text{excitation}}$  being the inelastic, elastic, ionization and excitation cross sections respectively,  $\sigma_{\text{inelastic}} = \sigma_{\text{electronic}} + \sigma_{\text{vibrational}} + \sigma_{\text{rotational}}$  and  $\sigma_{\text{electronic}} = \sigma_{\text{ionization}} + \sigma_{\text{excitation}}$ .

An illustrative representation of the probability distribution of elastic and inelastic events can be found in figure 4.3.

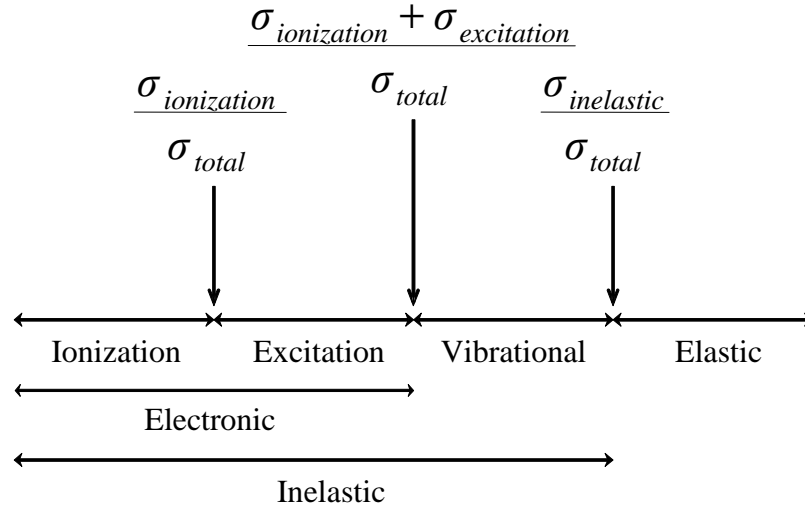


**Figure 4.3** Diagrammatic representation of the probability distribution of elastic and inelastic events

At this point the energy remaining is calculated from the difference between the initial energy ( $E$ ) and the energy transferred as a result of the collision ( $\Delta E$ ):

$$E_{\text{new}} = E - \Delta E \quad (4.7)$$

The energy transferred is generated by a third random number  $U_3$ . If a vibrational event occurs, the energy transferred is defined by the vibrational excitation. If an electronic excitation or ionization takes place, the energy loss is obtained from the cumulative cross section for these processes and the ionization efficiency.

The simulation continues depending on the event occurring. When inelastic collisions result in ionization events, two electrons have to be considered; the parent or primary electron and the daughter or secondary electron generated by the ionization event. The directions of the primary and secondary electrons are determined from the conservation of energy and momentum equalities. If the energy of the secondary electron is smaller than a previously defined limit energy ( $E_{\text{daughter}} < E_{\text{stop}}$ ), the primary electron simulation proceeds in the same manner until the defined final energy  $E_{\text{final}}$  is reached. Otherwise, when the daughter energy is greater ( $E_{\text{daughter}} > E_{\text{stop}}$ ), its energy should be reduced below  $E_{\text{stop}}$  before continuing the simulation of the primary electron. If there is an excitation the direction of travel is not modified. New primary electron trajectories are determined if there is an elastic

collision from the differential elastic cross section or from kinematics if there is a vibrational energy loss.

#### 4.3.1.1 Cross sections

The methodology described above needs a series of energy-dependent cross sections for liquid water [5-8]. In this section, expressions used to calculate cross sections for liquid water are introduced.

The cross section concept is used to express the probability of an interaction between atomic particles. This requires an encounter parameter with units of area per molecule. Cross sections can be measured for many processes. In track structure simulations, the cross section is usually divided into elastic and inelastic collisions with the latter separated further into the various “inferior” processes of electronic (ionization and excitation), vibrational and rotational excitations.

$$\sigma_{\text{inelastic}} = \sigma_{\text{electronic}} + \sigma_{\text{vibrational}} + \sigma_{\text{rotational}} \quad (4.8)$$

Rotational cross sections are ignored since their contribution is very small compared to the electronic and vibrational cross sections. Frequently in experimental determinations, rotational processes are included in the elastic cross sections since their effects are not distinguishable from elastic collisions. In the calculations reported, vibrational cross sections and elastic cross sections employed to simulate liquid water are assumed to be the same as those for the gas phase. The electronic cross sections for ionization and excitation events are calculated from the experimental dipole oscillator strength distribution as described below and then partitioned into the two contributions using experimental data for the ratio of  $\sigma_{\text{ionization}}/\sigma_{\text{elastic}}$ .

$$\left\{ \begin{array}{l} \text{Modeled value:} \\ \text{Experimental value:} \end{array} \right. \quad \begin{array}{l} \sigma_{\text{electronic}} = \sigma_{\text{ionization}} + \sigma_{\text{excitation}} \\ \sigma_{\text{ionization}} / \sigma_{\text{electronic}} \end{array} \quad \begin{array}{l} (4.9) \\ (4.10) \end{array}$$

The sum of all the cross sections estimated gives the total cross section.

In the following discussion, atomic units are assumed, i.e.  $m = 1$ ,  $\hbar = 1$ .

**Electronic:** The probability of an energy loss,  $\Delta E$ , per unit distance traveled by a non relativistic electron with incident energy  $E = v^2/2$  is given by the expression

$$\tau(E, \Delta E) = \int \text{Im} \left[ \frac{-1}{\varepsilon(q, \Delta E)} \right] \frac{dq}{q} \quad (4.11)$$

With Im symbolizing the “imaginary part of” and where  $\text{Im}[-1/\varepsilon(q, \Delta E)]$  is known as the energy loss function. The complex dielectric response function,  $\varepsilon(q, \Delta E)$ , defines

the response of a homogeneous medium to an energy transfer  $\Delta E$  and a momentum transfer  $q$ , which is the amount of momentum that one particle transfers to another particle when they collide.

For most materials, the only available dielectric data are the dipole oscillator strength distribution,  $f(\Delta E)$ , which are related to the “ $q = 0$ ” value of the energy loss function [9]

$$\text{Im}\left[-1/\varepsilon(0, \Delta E)\right] = (10h^2 e^2 N / 2m) f(\Delta E) / \Delta E. \quad (4.12)$$

The “binding energy”,  $\Delta E'$ , is the energy released or lost to the medium after collision occurs. Ashley proposed an approximation to quadratically extend the optical data into the energy-momentum plane [10], thereby giving

$$\text{Im}\left[-1/\varepsilon(q, \Delta E)\right] = \int \frac{\Delta E'}{\Delta E} \text{Im}\left[-\frac{1}{\varepsilon(0, \Delta E')}\right] \delta\left(\Delta E - \left(\Delta E' + \frac{q^2}{2}\right)\right) d\Delta E' \quad (4.13)$$

The probability  $\tau(E, \Delta E)$  is easily related to the density normalized differential cross section by

$$N d\sigma = \tau(E, \Delta E) d\Delta E \quad (4.14)$$

where  $N$  is the number density of molecules in the medium. The integration gives the inelastic cross section dependent on the initial electron energy  $E$  and the energy lost  $\Delta E$  calculated as:

$$\sigma_{\text{inelastic}}(\Delta E, E) = \frac{1}{N} \int \tau(E, \Delta E) d\Delta E \quad (4.15)$$

To formulate the electronic cross-sections, conservation of energy and momentum of a resting electron and an electron with incident energy  $v^2/2$  are considered. After collision with a molecular electron, the primary particle departs with energy  $v_1^2/2$ , an energy  $v_2^2/2$  is given to the secondary electron and a binding energy  $\Delta E'$  is released to the system. Energy conservation gives the expression

$$v^2/2 = v_1^2/2 + v_2^2/2 + \Delta E' \quad (4.16)$$

Whereas the energy loss can be expressed as

$$\Delta E = v^2/2 - v_1^2/2 = v_2^2/2 + \Delta E' > \Delta E' \quad (4.17)$$

As electrons are indistinguishable, the highest energy electron is always assumed to be the primary so

$$v_1^2/2 > v_2^2/2 > 0 \quad (4.18)$$

In addition, considering the equalities

$$\Delta E = \Delta E' + q^2/2 \quad (4.19)$$

$$v_1 = (v^2 - 2\Delta E)^{1/2} \quad (4.20)$$

Momentum conservation gives the inequalities

$$v - v_1 < q < v + v_1 \quad (4.21)$$

$$-(v^2 - 2\Delta E) + v(v^2 - 2\Delta E)^{1/2} > \Delta E' > 0 > -(v^2 - 2\Delta E) - v(v^2 - 2\Delta E)^{1/2} \quad (4.22)$$

which reduces to

$$0 < \Delta E' < -(v^2 - 2\Delta E) + v(v^2 - 2\Delta E)^{1/2} = \Delta E'_{\max} \quad \text{for } 0 < \Delta E < v^2/4 \quad (4.23)$$

$$\begin{aligned} \Delta E_- &= 1/4v^2(1 + 2\Delta E'/v^2 - v(1 - 4\Delta E'/v^2)^{1/2}) < \Delta E \\ \Delta E &< 1/4v^2(1 + 2\Delta E'/v^2 + v(1 - 4\Delta E'/v^2)^{1/2}) = \Delta E_+ \end{aligned} \quad (4.24)$$

Using the optical approximation and the momentum and energy conservation expressions listed above, the collision probability is

$$\tau(E, \Delta E) = \frac{1}{2\pi E} \int_{\Delta E'_{\min}}^{\Delta E'_{\max}} \text{Im}[-1/\varepsilon(0, \Delta E)] G(\Delta E, \Delta E') \Delta E' d\Delta E' \quad (4.25)$$

where allowing for exchange

$$\begin{aligned} G(\Delta E, \Delta E') &= \frac{1}{\Delta E(\Delta E - \Delta E')} + \frac{1}{(v^2/2 - \Delta E)(v^2/2 - \Delta E + \Delta E')} - \\ &\quad - \frac{1}{\sqrt{\Delta E(\Delta E - \Delta E')(v^2/2 - \Delta E)(v^2/2 - \Delta E + \Delta E')}} \end{aligned} \quad (4.26)$$

with  $\Delta E'_{\min} = 0$  when  $0 < \Delta E < v^2/4$  or  $\Delta E'_{\min} = 2\Delta E - v^2/2$  when  $v^2/4 < \Delta E < 3v^2/8$  [9].

This probability is used to determine the inelastic cross section, according to equation 4.15

$$\begin{aligned} \sigma(E, E'_{\max}) &= \frac{1}{2} \frac{1}{N} \chi \bullet \\ &\bullet \int_0^{E/2} \text{Im}[-1/\varepsilon(0, \Delta E^{\Delta E})] \bullet \left[ \frac{1}{a} \ln \left[ \frac{(1-a+s)(1+a-s)}{(1-a-s)(1+a+s)} \right] - \frac{2}{1+a} F(\arcsin(s/(1-a)), \frac{1-a}{1+a}) \right] \frac{\Delta E}{E} d\Delta E' \end{aligned} \quad (4.27)$$

where  $a = \Delta E'/E$  and  $s = (1 - 2a)^{1/2}$ . The function  $F(x, y)$  is the incomplete elliptic integral of the first kind and the parameter  $\chi = 1/(\pi E)$ .

In addition, the mean free path is defined as

$$\Lambda^{-1}(E) = \int \tau(E, \Delta E) d\Delta E \quad (4.28)$$

Therefore, the total inelastic cross section can be expressed in terms of the inverse inelastic mean free path becoming

$$\sigma(E, E'_{\max}) = \frac{1}{N} \Lambda^{-1}(E) \quad (4.29)$$

Many track structure simulations used a parameter known as the Y function, which describes the probability of an energy loss smaller than a value  $\Delta E$  and therefore, is the ratio of the cumulative inelastic cross section,  $\sigma(E, \Delta E)$ , to the total inelastic cross section,  $\sigma(E, \Delta E_{\max})$ . Further consideration of the bounds is needed when determining the cumulative inelastic cross section since the energy loss  $\Delta E$  must be lower than  $\Delta E_{\max}$  [9]. The bounds are giving by  $0 < \Delta E' < -(v^2 - 2\Delta E) + v(v^2 - 2\Delta E)^{1/2}$  and  $\Delta E' > 2\Delta E - v^2/2$  and the maximum permissible energy loss  $\Delta E = 3E/4$  when  $\Delta E' = E/2$ .

The cumulative inelastic cross section in the range  $0 < \Delta E < E/2$  follows the expression

$$\sigma(E, \Delta E) = \frac{1}{2} \frac{\chi}{N} \int_0^{\Delta E'_{\max}} d\Delta E' \text{Im}[-1/\epsilon(0, \Delta E')] [\Sigma_2] \Delta E' / E \quad (4.30)$$

with

$$[\Sigma_2] = \frac{1}{a} \ln \left[ \frac{(b-a)(1-b+a)(1+a-s)(1-a+s)}{b(1-b)(1-a-s)(1+a+s)} \right] + \frac{2}{1+a} \text{F} \left( \arcsin \left( \frac{1+a-2b}{1-a} \right), \frac{1-a}{1+a} \right) - \frac{2}{1+a} \text{F} \left( \arcsin \left( \frac{s}{1-a} \right), \frac{1-a}{1+a} \right) \quad (4.31)$$

while for the interval  $E/2 < \Delta E < 3E/4$

$$\sigma(E, E') = \frac{A^{-1}(E)}{N} - \frac{1}{2} \frac{\chi}{N} \int_{\Delta E'}^{2E'-E} dE' \text{Im}[-1/\epsilon(0, \Delta E')] [\Sigma_3] \Delta E' / E \quad (4.32)$$

where

$$[\Sigma_3] = \frac{1}{a} \ln \left[ \frac{(b-a)(1-b+a)}{b(1-b)} \right] + \frac{2}{1+a} \text{F} \left( \arcsin \left( \frac{1+a-2b}{1-a} \right), \frac{1-a}{1+a} \right). \quad (4.33)$$

**Elastic:** Elastic cross sections are expected not to vary significantly due to condensation since these interactions are collisions between electrons and charged particles. Parameterization of experimental data has been done before [2]. The elastic cross sections used in the simulations reported were derived from experimental data for the gas phase. Differential cross sections at an energy,  $E$ , were fitted to a polynomial function.

$$\sigma'(\theta, E) = a_0 + a_1\theta + a_2\theta^2 + a_3\theta^3 + a_4\theta^4 \quad (4.34)$$

The energy dependence of the coefficients,  $a_i$ , was then fitted to a second polynomial.

$$a_i(E) = \sum_{i=0}^4 b_i E^i \quad (4.35)$$

The total elastic cross section is then easily obtained at a given electron energy from.

$$\sigma_{\text{elastic}} = 2\pi \int_0^\pi \sigma'(\theta, E) \sin \theta d\theta \quad (4.36)$$

## 4.3.2 Monte Carlo simulation of heavy ion track structure

The modelling of heavy ion track structure uses similar methods to those employed for fast electron tracks. The simulation proceeds by following the ionizing particle collision by collision through the medium using an energy dependent inelastic cross section obtained from the dipole oscillator strength distribution of liquid water. The nature of the energy event (ionization or excitation) is obtained from the energy dependent ionization efficiency for liquid water [5]. If an ionization event occurs, the trajectory of the ejected electron is followed using the methods outlined earlier until its energy is smaller than a defined cut-off energy, usually 25 eV since the possibility of further ionization below that energy is quite small. According to the fast electron description, the attenuation of these low energy electrons is included by using spatial distributions either obtained from simulations using experimental ice phase cross sections [11, 12] or optimized to reproduce the kinetics of  $e_{\text{aq}}^-$  measured in fast  $e^-$  pulse radiolysis.

The trajectory of the energetic ions is followed until its initial energy drops by 10-100 keV. This procedure produces an ion track representative of an ion at a given energy, not for the ions complete attenuation. Unlike the electron track structure simulation, the chemistry of an entire heavy ion track is obtained by integrating the chemistry of consecutive track segments [1].

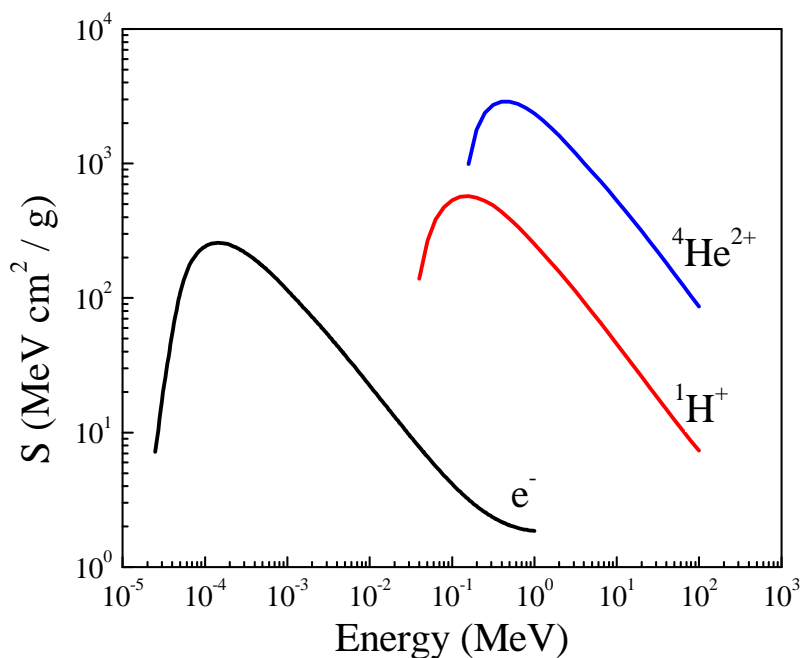


**Figure 4.4** Stopping power for electrons, hydrogen and helium in terms of the particle energy.



From a chemical point of view, there is no appreciable change in the stopping power (see Figure 4.4) from 50 keV to 1 MeV when simulating the electron track structure since the Bragg peak for electrons occurs at low energy. Since the LET value does not change substantially, a 10 – 20 keV energy segment in this range is a good approximation of the whole track in a chemistry study. However, this approximation is not applicable to the heavy ions. Small energy intervals are considered at different ion energy and LET, so their appropriately averaged results are a good approximation of the whole track.

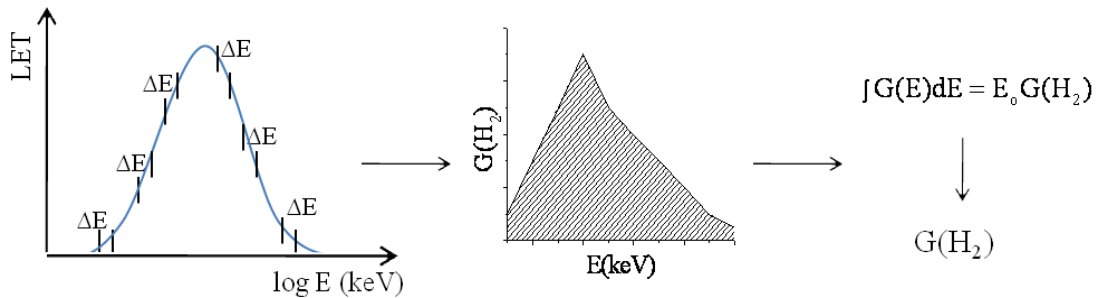


**Figure 4.5** Heavy ion track structure is calculated at consecutive track segments.

As shown in figure 4.5, independent  $G(H_2)$  are calculated for each track segment. Hence, a curve of  $G(H_2)$  is plotted at a given energy,  $E$ , and LET as a function of  $E$  and the area under the curve is calculated. The track average yield is obtained by dividing the result of the integral by the initial energy  $E_0$ ,

$$G_{track} = \frac{1}{E_0} \int_0^E G_{segment} dE. \quad (4.37)$$

#### 4.4 Monte Carlo simulation of chemical evolution of the track

Traditionally, deterministic kinetics methods have been used to model the chemical evolution of a radiation track. These models considered a typical radiation spur or track segment and modelled evolution using conventional “macroscopic” diffusion and rate laws [13, 14]. Recently, stochastic radiation chemistry models have been developed in which reactant trajectories are simulated by random flights methods [15]. Particle positions are generated at initial time using a track structure simulation. Every interparticle distance is calculated and compared with the reaction distance. When a pair is close enough to react, the encounter is considered and the particles are removed from further consideration. After every possible pair has been

considered at initial time, particles are allowed to move and react further by diffusion controlled encounter.

Random flights are assigned for each particle during a carefully chosen time step  $\delta t$ . The random flights simulation determines the final particle position after time step  $\delta t$  checking whether the new interparticle distances  $r_m$  are smaller than the reaction distance  $R_m$ . However, an important problem may arise if during the time step,  $\delta t$  a specific pair of particles reach a separation  $r_m$  lower than  $R_m$  before moving apart during the same time step. In this case the reaction would not be counted.

This problem is solved by using the Brownian bridge which defines the probability for a conditional encounter during the time step  $\delta t$  [16]

$$W_{\text{Br}} = \exp\left[-\frac{(r'_m - R_m)(r_m - R_m)}{D'_m \delta t}\right] \quad (4.38)$$

where  $r'_m$  and  $r_m$  are the initial and final inter-particles distances,  $R_m$  the encounter distance and  $D'_m$  the relative diffusion coefficient. The Brownian Bridge methodology is only valid if the radial drift does not change appreciably throughout the time step  $\delta t$ . Consequently the Brownian Bridge is used when particles are close and the probability of an encounter during the time step is significant. Random flights simulation is applicable to high and low permittivity solvents, however, this approach is computationally expensive and prohibitively so for systems with large number of reactants.

An alternative stochastic simulation method known as the independent reaction times (IRT) model has been developed to model the diffusion-reaction kinetics of radiation-induced reactive species in water, where intermolecular Coulombic forces are weak. The IRT model is based on an independent pairs approximation, in which the interparticle distances are allowed to evolve independently so the triangle relationship of three particles, see figure 4.6, is not maintained.

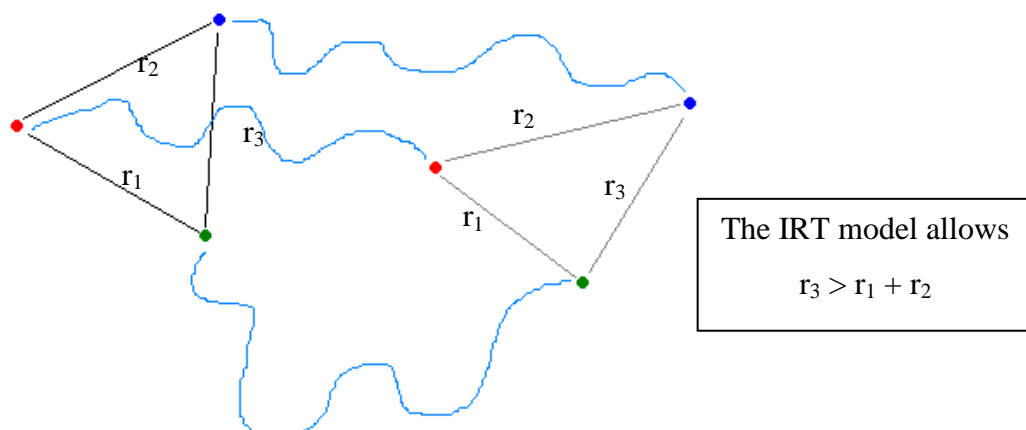


**Figure 4.6** The triangle relationship of three particles

This approximation is the same approximation used in the conventional treatment of diffusion limited bulk chemistry [17].

IRT simulation has been shown to reproduce kinetics simulated using random flights methods for neutrals and ions in high permittivity solvents. The basic simulation steps in the IRT approach are shown in figure 4.7.

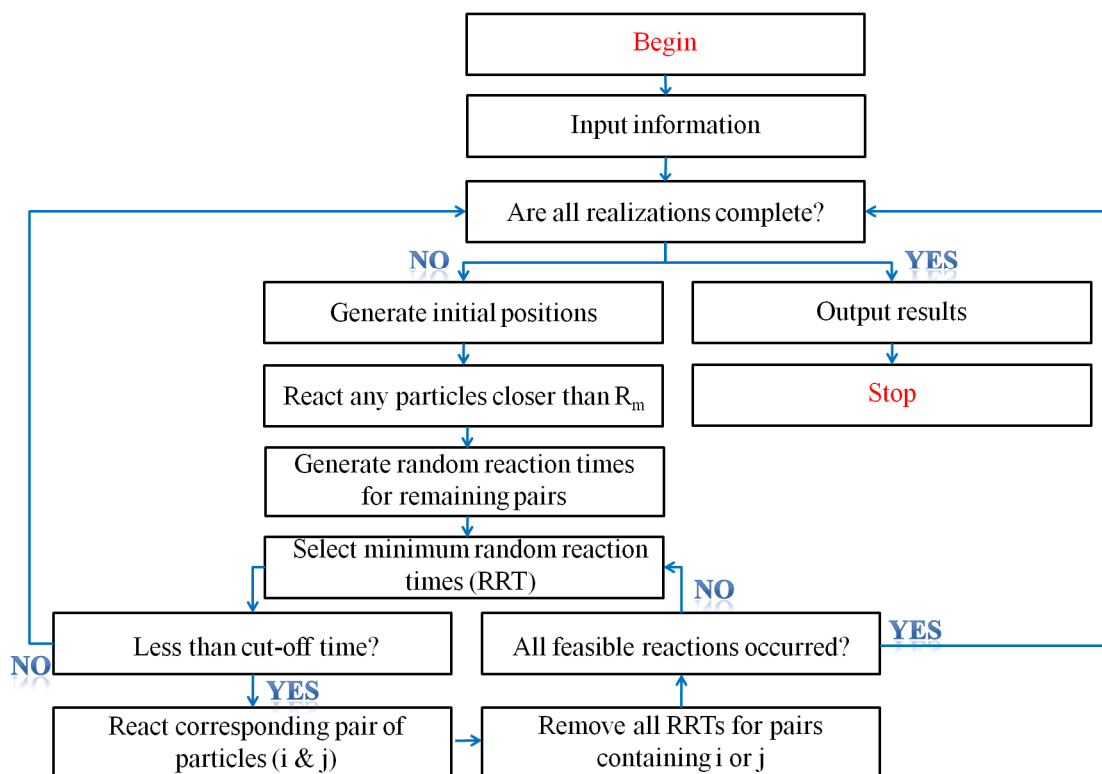
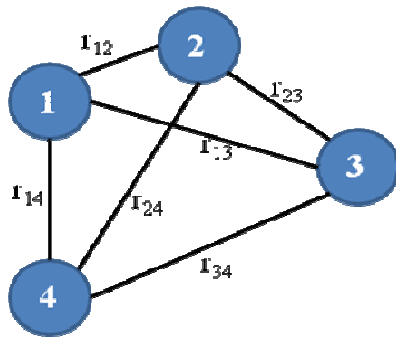


**Figure 4.7** Independent Reaction Times simulation method

This collection of steps can be easily outlined by using a simple example which considers the encounter of 4 particles [18], see figure 4.8.



Pair	$r_{ij}$	$t_{ij}$	Reaction
1 + 2	1.3	12	X
1 + 3	2.1	27	X
1 + 4	1.0	40	2
2 + 3	1.1	8	1
2 + 4	1.7	125	X
3 + 4	1.8	$\infty$	X

**Figure 4.8** Example of the IRT model

Random reaction times are generated for every pair by using random numbers uniformly distributed on the interval (0 - 1) and the appropriate random reaction time distribution functions. In the example, the shortest reaction time is found for encounter between particles 2 and 3. Therefore, these two particles “react” and are removed for any further consideration. The next pair to encounter would be particles 1 and 4 as all the other pairs have been removed.

As in the random flights treatment the initial positions are determined by a track structure simulation. Interparticle distances are calculated and checked for time  $t = 0$  encounter. Random reaction times are then generated from the pair distances of the remaining particles and the distribution function,  $W(t)$ . In the absence of any intermolecular force, the expression for  $W(t)$  is [19]

$$W(t) = \frac{R}{r} \operatorname{erfc}\left(\frac{r-R}{\sqrt{4D't}}\right) \quad (4.39)$$

where  $r$  is the interparticle distance,  $R$  is the reaction distance,  $D'$  is the relative diffusion coefficient and  $\operatorname{erfc}(x)$  is the complementary error function defined as

$$\operatorname{erfc}(x) = 1 - \operatorname{erf}(x) = \frac{2}{\sqrt{\pi}} \int_x^{\infty} e^{-t^2} dt. \quad (4.40)$$

Simulations using the IRT method are much faster than random flights simulation as the trajectories of the diffusing particles are not modeled, only the encounter times are calculated.

A number of enhancements to the basic formalism are necessary to model real radiation chemical kinetics, which include (i) reactions between ionic reactants where an inter-ion Coulombic force modifies the diffusion, and (ii) reactions which produce potentially reactive products.

*Ionic reactants.* In the radiation chemistry of water and aqueous systems many of the reactants are ions. In solvents of high relative permittivity such as water, where the Coulomb forces between ions are weak [20], the reaction time distribution function used in the IRT method is reformulated from the recombination probability for neutrals in the form,

$$W(r,t) \approx \frac{R_{eff}}{r_{eff}} \operatorname{erfc} \left[ \frac{r_{eff} - R_{eff}}{\sqrt{4D't}} \right] \quad (4.41)$$

which employs an effective distance scale for the separation  $r$

$$r_{eff} = \frac{r_c}{\exp\left(\frac{r_c}{r}\right) - 1} \quad (4.42)$$

and for the reaction distance  $R$

$$R_{eff} = \frac{r_c}{\exp\left(\frac{r_c}{R}\right) - 1} \quad (4.43)$$

The constant  $r_c$  is the Onsager distance and is the distance at which the Coulomb potential energy is  $k_B T$ . In the limit of large separations, the expression for ions asymptotically approaches the one for neutrals.

*Reactive products.* Reactive products are species generated during the evolution of the system capable of further reactions. As random flights simulation calculates every new position after collision, the position of the new reactive product is known. This is not the case in the IRT model since the diffusive motion of the particles is not followed. If the reactive product is generated at zero time, their random reaction times can be generated in a straightforward way. A new approximation must be included to consider the effect of these new particles. A number of different approximations have been investigated [16]. In the simulations reported here, new particle positions are not generated, but the evolution of interparticle distances is considered and these distances are allowed to evolve independently. Hence, when a pair reacts, the separation from all the other species

can be evaluated. This process then allows the generation of random reaction times for the reactive products of the pair reaction.

Because of the high efficiency shown in recent studies with high permittivity solvents [20], the IRT method has been used in this project to model the chemistry involved in the radiolysis of aqueous systems.

#### 4.5 Summary

The stochastic models used to simulate the track structure and the chemical evolution of the track have been described in this chapter. Slightly different methods are used to model the electron and the heavy ion track structures based on their different LET values. Our model of choice, method known as the independent reaction times (IRT) model, has showed high reliability in high permittivity solvents, such as water, with a more simple methodology which reduces computing time.

#### 4.6 References

1. Pimblott, S.M., and LaVerne, J. A., *Effects of Track Structure on the Ion Radiolysis of the Fricke Dosimeter*. The Journal of Physical Chemistry A, 2002. **106**: p. 9420-9427.
2. Pimblott, S.M., LaVerne, J. A., and Mozumder, A., *Monte Carlo Simulation of Range and Energy Deposition by Electrons in Gaseous and Liquid Water*. The Journal of Physical Chemistry, 1996. **100**: p. 8595-8606.
3. Pimblott, S.M., and Siebbeles, L. D. A., *Energy loss by non-relativistic electrons and positrons in liquid water*. Nuclear Instruments and Methods in Physics Research Section B: Beam Interactions with Materials and Atoms, 2002. **194**: p. 237-250.
4. Luc, D., ed. *Non-uniform random variate generation*. 1986, Springer-Verlag: New York.
5. Goodhead, D.T., Leenhouts, H. P., Paretzke, H. G., Terrissol, M., Nikjoo, H., and Blaauboer, R., *Track Structure Approaches to the Interpretation of Radiation Effects on DNA*. Radiation Protection Dosimetry, 1994. **52**: p. 217-223.
6. Goodhead, D.T., and Nikjoo, H., *Track Structure Analysis of Ultrasoft X-rays Compared to High- and Low-LET Radiations*. International Journal of Radiation Biology, 1989. **55**: p. 513 - 529.
7. Nikjoo, H., Goodhead, D. T., Charlton, D. E., and Paretzke, H. G., *Energy Deposition in Small Cylindrical Targets by Monoenergetic Electrons*. International Journal of Radiation Biology, 1991. **60**: p. 739 - 756.
8. Nikjoo, H., Goodhead, D. T., Charlton, D. E., and Paretzke, H. G. , *Energy deposition in small cylindrical targets by ultrasoft X-rays*. Physics in Medicine and Biology, 1989. **34**: p. 691-705.
9. Green, N.J.B., LaVerne, J. A., and Mozumder, A., *Differential track structure of electrons in liquid water*. Radiation Physics and Chemistry, 1988. **32**: p. 99.

10. Ashley, J.C., *Interaction of low-energy electrons with condensed matter: stopping powers and inelastic mean free paths from optical data*. Journal of Electron Spectroscopy and Related Phenomena, 1988. **46**: p. 199-214.
11. Michaud, M., and Sanche, L., *Total cross sections for slow-electron (1–18 eV) scattering in solid H<sub>2</sub>O*. Physical Review A, 1987. **36**: p. 4672.
12. Michaud, M., and Sanche, L., *Absolute vibrational excitation cross sections for slow-electron (1–18 eV) scattering in solid H<sub>2</sub>O*. Physical Review A, 1987. **36**: p. 4684.
13. Burns, W.G., Sims H. E., and Goodall, J. A. B., *Radiation chemical diffusion kinetic calculations with prescribed and non-prescribed diffusion - I. Spherical and cylindrical cases* Radiation Physics and Chemistry, 1984. **23**: p. 143-80.
14. Schwarz, H.A., *Applications of the spur diffusion model to the radiation chemistry of aqueous solutions*. The Journal of Physical Chemistry, 1969. **73**: p. 1928-1937.
15. Turner, J.E., Hamm, R. N., Wright, H. A., Ritchie, R. H., Magee, J. L., Chatterjee, A., and Bolch, W. E., *Studies to link the basic radiation physics and chemistry of liquid water*. International Journal of Radiation Applications and Instrumentation. Part C. Radiation Physics and Chemistry, 1988. **32**: p. 503-510.
16. Clifford, P., Green, N. J. B., Oldfield, M. J., Pilling M. J., and Pimblott S. M., *Stochastic models of multi-species kinetics in radiation-induced spurs*. Journal of the Chemical Society, Faraday Transactions 1, 1986. **86**: p. 2673 - 2689.
17. Rice, S.A., *Diffusion limited-reactions*. Vol. 25. 1985, Amsterdam: Elsevier. 404.
18. Pimblott, S.M., *Application of Stochastic Models to Radiation Chemistry*. 1988, St. Peter's College: Oxford.
19. Chandrasekhar, S., *Stochastic Problems in Physics and Astronomy*. Reviews of Modern Physics, 1943. **15**: p. 1.
20. Clifford, P., Green, N. J. B., Pilling, M. J., and Pimblott, S. M., *Stochastic models of diffusion-controlled ionic reactions in radiation-induced spurs. I. High-permittivity solvents*. The Journal of Physical Chemistry, 1987. **91**: p. 4417-4422.

# Chapter 5

## H atom determination in the gamma radiolysis of water

5.1	Introduction.....	81
5.2	Introduction to the H atom determination in the radiolysis of water.....	81
5.3	Experimental work.....	83
5.4	Supporting calculations.....	84
5.5	Results and discussion.....	84
5.5.1	Formate & nitrate addition.....	85
5.5.2	Deuterated formate & nitrate addition.....	91
5.5.3	Formate & selenate addition.....	93
5.5.4	Methanol & nitrate addition.....	95
5.5.5	Deuterated methanol & nitrate addition.....	96
5.6	Summary.....	97
5.7	References.....	100



### 5.1 Introduction

The objective of this chapter is to determine the H atom yield in the radiolysis of water and its variation with the concentration of the hydrogen atom scavenger. To achieve this goal, two different methods to determine H atom yields have been developed and tested. Experimental results in conjunction with stochastic simulations are presented in this chapter.

### 5.2 Introduction to the H atom determination in the radiolysis of water

The processes involved in H atom production in the radiolysis of water have been widely studied and discussed in the literature [1-5]. In general terms, they can be outlined in the mechanism shown in Figure 5.1.

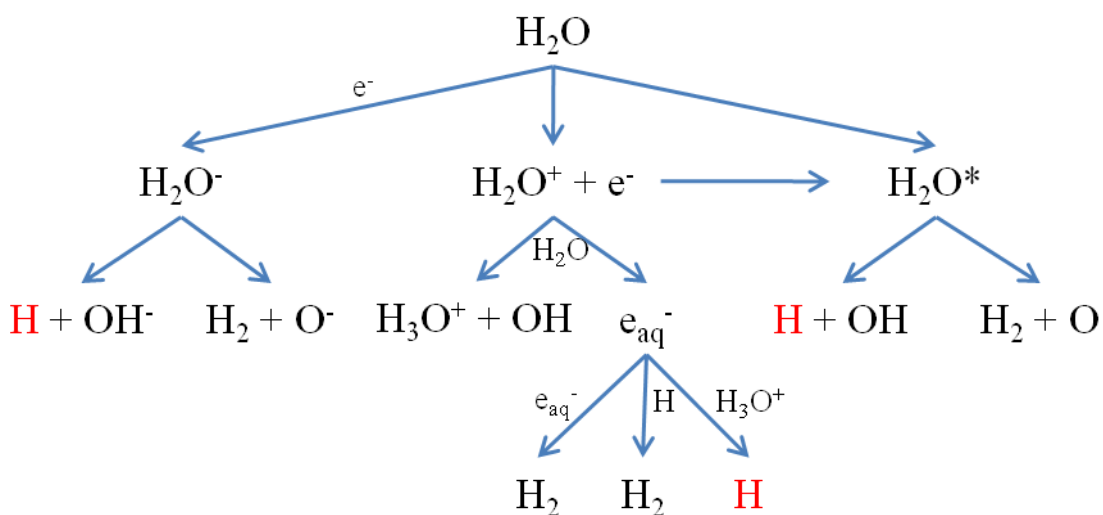
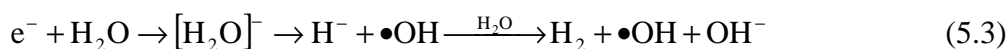


**Figure 5.1** Atomic and molecular hydrogen production in the radiolysis of water.

The hydrogen atom is one of the most important species in the fragmentation of the water excited state and in the radiolysis of water. An accurate examination of the H atom yields after radiolysis will make possible a better understanding of the initial radiolytic decomposition of water. H atom yields have been partially studied in gas phase water [6, 7], but only limited data have been obtained for liquid water. The measurement of H atom yields is difficult since the H atom can behave as a reductant or an oxidant, i.e. like hydrated electrons or OH radicals, depending on the system considered. H atom yields are usually determined by difference measurements of  $H_2$  yields [8-11]: H atoms produced in water irradiation are allowed to abstract H atoms from selected solutes to generate molecular hydrogen. Hydrogen

atom yields are then calculated by taking the difference between the H<sub>2</sub> yield obtained in the presence of the solute and in the absence of the solute. An alternative method uses isotopically labelled solutes where HD is formed quantitatively by direct abstraction of D atoms from the deuterated solute.

It is currently believed that the dominant pathways to the formation of molecular hydrogen, H<sub>2</sub>, in neat water occur due to reactions of the hydrated electron and its precursors [12],



as well as the combination of H atoms



and the decay of directly produced excited states. It is also produced through abstraction reactions between H atoms and solutes containing H atoms. In this project, formate and methanol were used as H atom scavengers,



The rate coefficients for these reactions are  $k_7 = 2.1 \times 10^8 \text{ M}^{-1} \text{ s}^{-1}$  and  $k_8 = 2.6 \times 10^6 \text{ M}^{-1} \text{ s}^{-1}$ , respectively [13]. The H atom yields can be estimated just calculating the difference between H<sub>2</sub> yields obtained when the solute is added and when the solute is not present.

Deuterated solutes may also be used as H atom scavengers. In this case, there are two ways in which H atom yields can be determined; either by the directly measured HD yields or by the subtraction method calculating the difference between the total H<sub>2</sub> yield (H<sub>2</sub> + HD + D<sub>2</sub>) and the H<sub>2</sub> yield in the absence of the deuterated solute. In the present studies, deuterated formate (DCO<sub>2</sub><sup>-</sup>) and tri-deuterated methanol (CD<sub>3</sub>OH) have been used as hydrogen atoms scavengers:

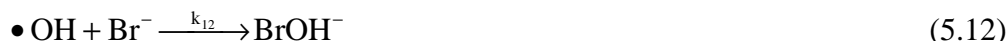


Rate constants for these two reactions are  $k_9 = 2.9 \times 10^7 \text{ M}^{-1} \text{ s}^{-1}$  and  $k_{10} = 1.0 \times 10^5 \text{ M}^{-1} \text{ s}^{-1}$  [13].

The measured  $\text{H}_2$  yield may be affected by slow homogeneous reactions. Water decomposition generates OH radicals which react with  $\text{H}_2$  decreasing the observed yield.



To prevent this reaction, bromide is added as a OH radical scavenger,



where  $k_{12} = 1.1 \times 10^{10} \text{ M}^{-1} \text{ s}^{-1}$  [13]. The concentration of  $\text{Br}^-$  must be kept low as depending on the H atom scavenger added and its concentration, the following reaction may also take place



due to its non-negligible rate coefficient  $k_{13} = 1.76 \times 10^6 \text{ M}^{-1} \text{ s}^{-1}$  [14].

In addition to the direct formation of  $\bullet\text{H}$ , hydrated electrons can generate H atoms by reaction with hydronium within the radiation track,



with  $k_{14} = 2.3 \times 10^{10} \text{ M}^{-1} \text{ s}^{-1}$  [13]. Nitrate or selenate may be added to act as a hydrated electron scavenger.



where the rate constants are  $k_{15} = 9.7 \times 10^9 \text{ M}^{-1} \text{ s}^{-1}$  [13] and  $k_{16} = 1.1 \times 10^9 \text{ M}^{-1} \text{ s}^{-1}$  [15] respectively.

### 5.3 Experimental work

The experimental work was carried out in the Radiation Laboratory at the University of Notre Dame (USA). The Shepherd 109  $^{60}\text{Co}$  source described in chapter 3 was used to irradiate the samples.

Solutions with different concentrations of sodium formate ( $\text{NaHCO}_2$ ), deuterated sodium formate ( $\text{NaDCO}_2$ ), methanol ( $\text{CH}_3\text{OH}$ ) or deuterated methanol ( $\text{CD}_3\text{OH}$ ) were made adding concentrations of 1 mM potassium bromide (KBr) and 1 to 24 mM sodium nitrate ( $\text{NaNO}_3$ ) or 1 to 100 mM sodium selenate ( $\text{Na}_2\text{SeO}_4$ ). All solutions were prepared with nano pure water (resistivity  $18.7 \text{ M}\Omega \text{ cm}^{-1}$ ) from an in-

house H<sub>2</sub>Only system. Four millilitres samples were loaded into a sample cell that consists of a 1 cm cuvette with inlet and outlet ports to purge the sample before irradiation. A gas chromatograph and a mass spectrometer were used inline to determine molecular hydrogen, as previously described in chapter 3.

Calibration of the gas chromatograph was carried out by injecting different volumes of pure H<sub>2</sub> and D<sub>2</sub> gases with a gas-tight microliter syringe. The estimated error in gas measurement is expected to be ~5%. Radiation chemical yields are expressed as G values (molecules/100 eV), which is equivalent to ~ 0.1 μmol/J.

#### 5.4 Supporting calculations

The methodology used in the simulation has been introduced in chapter 4 and in previous studies [16-18]. The method simulates the track structure due to the transfer of energy from the radiation particle to the sample, determines what kind of interaction has occurred (inelastic or elastic collisions, ionization or excitations events, vibration or rotation), and models the kinetics based on the competition between the relaxation of the spatially non-homogeneous distribution of radiation-induced reactants and their reactions either within the track or with the scavengers.

Each simulation of a track structure determines the trajectory of the electron and the daughter electrons as well as their initial and final positions. The nature of the event produced after interaction is modelled by calculating the difference between the initial and the transferred energy and relating this with the cross sections for each one of the possible events using a random number.

The chemical evolution of the track is modelled using the independent reaction times methodology (IRT) based on the independent pairs approximation, as described before.

#### 5.5 Results and discussion

Results have been plotted in terms of G values and scavenging capacities. The G value was established by Burton and Magee in 1952 [3] and is described as the number of molecules produced for each 100 eV absorbed by a substance from ionizing radiation. The scavenging capacity is defined as the pseudo-first order rate that is the product of the scavenger concentration and the scavenging rate coefficient.

Three measurements were made for each experimental point. The associated errors to the experimental values are smaller than the symbol used to represent each

point. The error associated with the scatter of the experimental measurements is expected to be significantly larger than errors introduced by other parameters such as change in humidity (as measurements were made in different seasons and laboratories) or change of nylon cords used to connect the sample cell with the GC and MS (which may cause better isolation). Every measurement with their respective averages and standard deviations are presented in Appendix B.

### 5.5.1 Formate and nitrate addition

Initially, H atom yields were obtained by different measurements of molecular hydrogen obtained in the gamma radiolysis of aqueous formate solutions with concentrations varying from 1 mM to 1 M and containing 1 mM concentrations of sodium nitrate and potassium bromide. In the same graph, modeled results are shown for formate concentrations from 0.1 mM to 10 M.

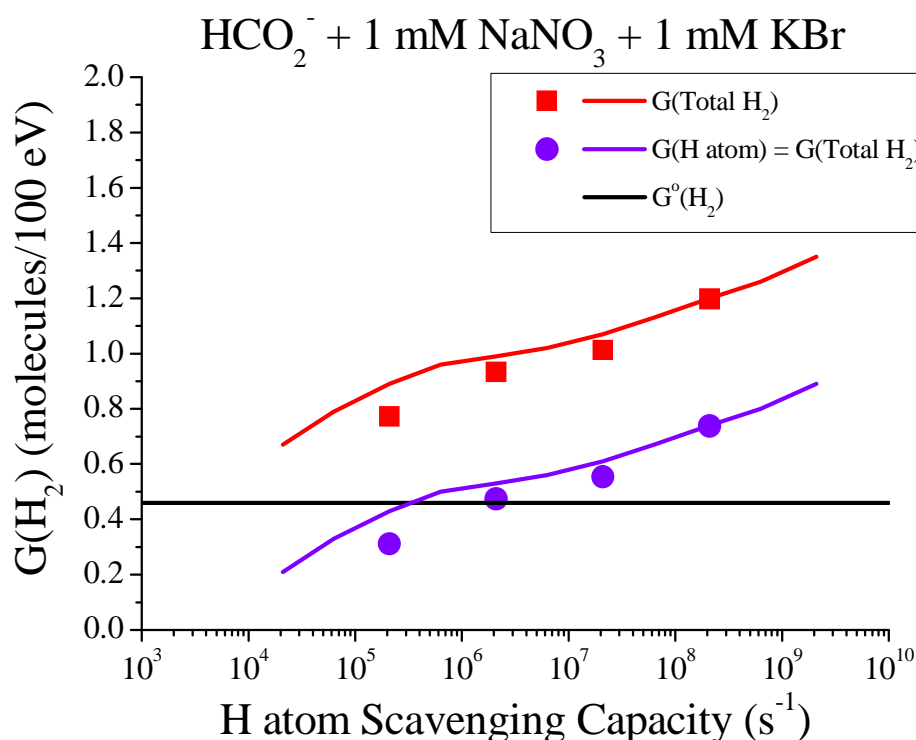


**Figure 5.2** Production of  $\text{H}_2$  and H atom in the  $\gamma$ -radiolysis of aqueous formate solutions with 1 mM  $\text{NaNO}_3$  and 1 mM KBr as a function of the formate scavenging capacity for H atoms.  $G^o(\text{H}_2)$  is the yield of  $\text{H}_2$  from a 1 mM  $\text{NaNO}_3$  / 1 mM KBr solution in the absence of  $\text{HCO}_2^-$ . Lines represent modeled results.

H atom yields obtained by the difference between the total molecular hydrogen yield and the molecular hydrogen yield in neat water vary from 0.31 up to 0.74 molecules/100eV for scavenging capacities from  $2.1 \times 10^5 \text{ s}^{-1}$  up to  $2.1 \times 10^8 \text{ s}^{-1}$ . A detailed report of the errors associated with the experimental values has been included in Appendix B.

Higher total molecular hydrogen values are observed when increasing formate concentrations due to more efficient scavenging of the H atom which prevents intra track reaction leading to other products. Total molecular hydrogen and estimated hydrogen atom yields obtained from the simulation are slightly higher than the experimental values, however, the overall agreement is good.

It would be expected that an increase in the concentration of  $\text{NO}_3^-$  would lead to a decrease in hydrogen atom yields due to the occurrence of reaction 5.15 at the expense of reaction 5.14. In order to test this assertion, the experiments were repeated by changing the sodium nitrate concentration from 1 mM to 24 mM.

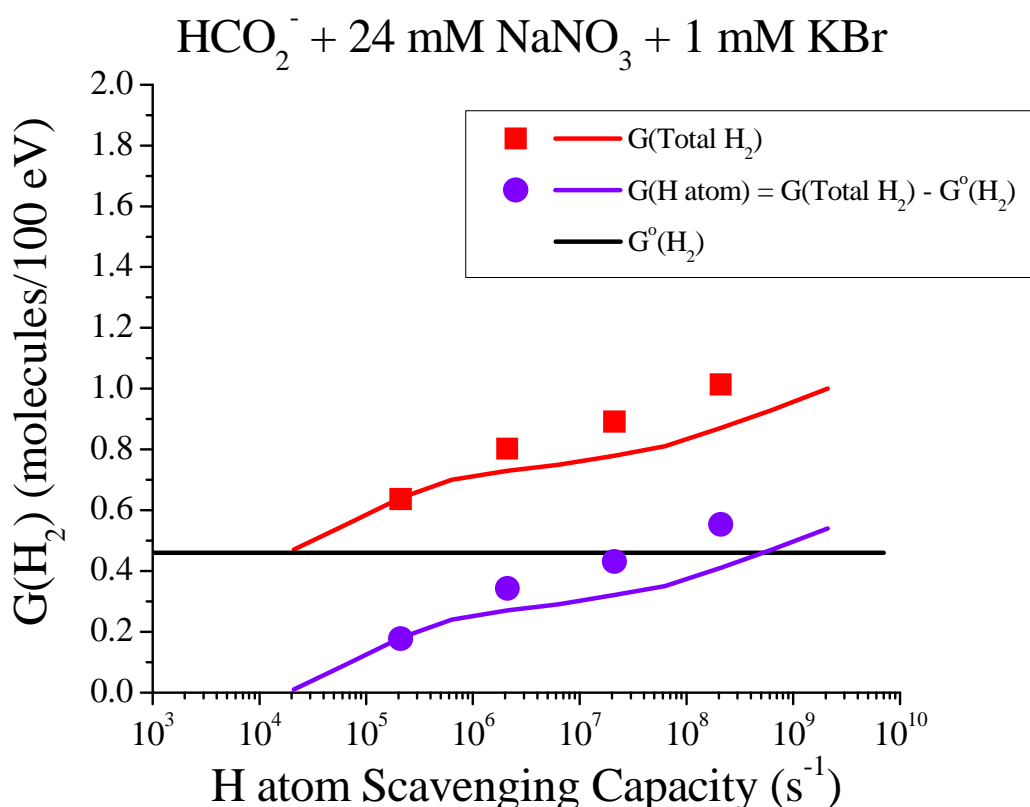


**Figure 5.3** Production of  $\text{H}_2$  and H atom in the  $\gamma$ -radiolysis of aqueous formate solutions with 24 mM  $\text{NaNO}_3$  as a function of the formate scavenging capacity for H atoms. Lines represent modeled results.

In this case the difference observed between  $G(\text{Total H}_2)$  and  $G^0(\text{H}_2)$  in neat water varies from 0.18 up to 0.55 molecules/100eV for scavenging capacities ranging from  $2.1 \times 10^5 \text{ s}^{-1}$  to  $2.1 \times 10^8 \text{ s}^{-1}$ . Higher sodium nitrate concentrations have the expected effect on the observed yield of  $\text{H}_2$ . The increased concentration of the hydrated electron scavenger decreases the production of hydrogen atoms due to reaction 5.14 and consequently the production of molecular hydrogen due to reactions 5.4, 5.5 and 5.6. H atom yields obtained by the difference method with added 1 or 24 mM sodium nitrate are compared in figure 5.4.

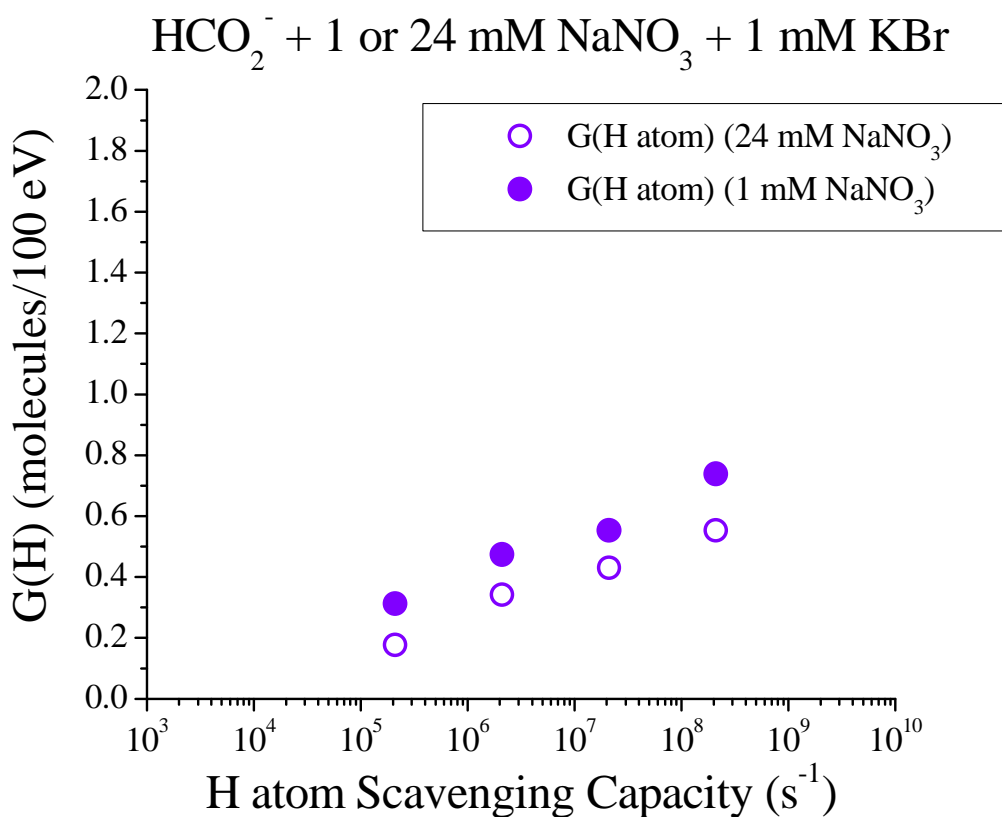


**Figure 5.4** Production of and H atom in the  $\gamma$ -radiolysis of aqueous formate solutions with 1 or 24 mM  $\text{NaNO}_3$  as a function of the formate scavenging capacity for H atoms.

The hydrogen atom yield clearly decreases as the concentration of the electron scavenger decreases. The higher the concentration of nitrate, the more efficient the scavenging of the hydrated electrons and, therefore, the lower the amount of hydrogen atoms produced through reaction 5.14.

The scavenging of H atoms by nitrate has a rate constant of  $1.4 \times 10^6 \text{ M}^{-1} \text{ s}^{-1}$  [13]. Therefore, considering the rate constants previously presented for scavenging of H atoms by formate, methanol, deuterated formate and deuterated methanol, reaction of H with nitrate is not expected to compete with reaction 5.7 due to formate. However, it should be noted that reactions 5.8, 5.9 and 5.10 have rate coefficients for the scavenging of H atoms by  $\text{CH}_3\text{OH}$ ,  $\text{DCO}_2^-$  and  $\text{CD}_3\text{OH}$  low enough to be affected at low concentrations by the presence of  $\text{NO}_3^-$ .

The total molecular hydrogen yields obtained from the addition of 1 or 24 mM sodium formate are shown in Figure 5.5 along with previous results found in the literature when using formate as a hydrogen atom scavenger [9, 19, 20].

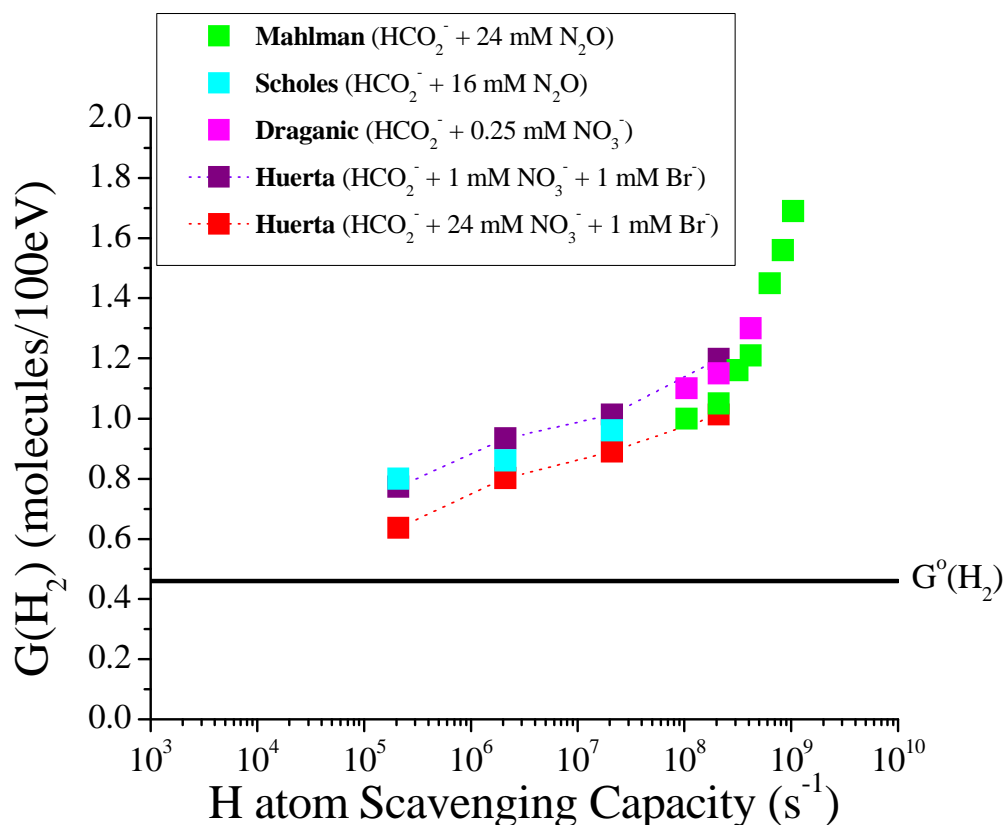


**Figure 5.5** Production of  $\text{H}_2$  in the  $\gamma$ -radiolysis of aqueous formate solutions with different concentrations of  $\text{NaNO}_3$  or  $\text{N}_2\text{O}$  as a function of the formate scavenging capacity for H atoms. (Results from Mahlman [9], Scholes [11], Draganic [8] and Huerta [21]).



Nitrous oxide, used by Scholes [11], reacts with hydrated electrons in a similar manner to nitrate,

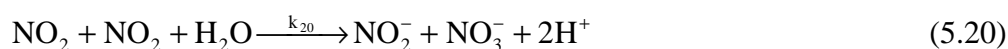


with  $k_{17} = 9.1 \times 10^9 \text{ M}^{-1} \text{ s}^{-1}$  [22]. Table 5.1 compares the scavenging capacities of the experimental systems considered in figure 5.4 with respect to the  $e_{aq}^-$ . There are clearly two distinct groups of data, with scavenging capacities in the range  $1.0 - 2.5 \times 10^8 \text{ s}^{-1}$  (1, 2 and 5) and a group with scavenging capacities in the interval  $2.4 - 10.0 \times 10^6 \text{ s}^{-1}$  (3 and 4).

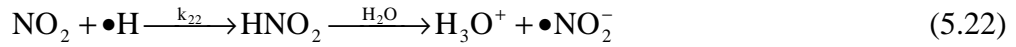
Set	Authors	$k(\text{NO}_3^- + e_{aq}^-)$ ( $\text{M}^{-1} \text{ s}^{-1}$ )	$k(\text{N}_2\text{O} + e_{aq}^-)$ ( $\text{M}^{-1} \text{ s}^{-1}$ )	[scavenger] (mM)	$e_{aq}^-$ scavenging capacity ( $\text{s}^{-1}$ )
1	Mahlman		$9.1 \times 10^9$	24.00	$2.2 \times 10^8$ (2)
2	Scholes		$9.1 \times 10^9$	16.00	$1.5 \times 10^8$ (3)
3	Draganic	$9.7 \times 10^9$		0.25	$2.4 \times 10^6$ (5)
4	Huerta	$9.7 \times 10^9$		1.00	$9.7 \times 10^6$ (4)
5	Huerta	$9.7 \times 10^9$		24.00	$2.3 \times 10^8$ (1)

**Table 5.1**  $e_{aq}^-$  Scavenger capacities in terms of the scavenger and its concentration. The decline in  $e_{aq}^-$  Scavenger capacities is shown in red numbers.

At this point it is worthwhile considering the chemistry occurring after scavenging of the hydrated electron. The radical anion,  $\text{NO}_3^{2-}$ , is obtained due to reaction 5.15 as a result of the hydrated electron scavenging reaction by nitrate. Subsequently, this product reacts with other species in solution to generate nitrogen dioxide and ultimately nitrite

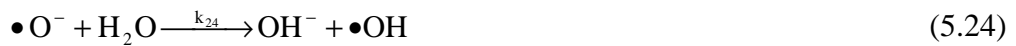


with  $k_{18} = 8.9 \times 10^4 \text{ M}^{-1} \text{ s}^{-1}$  [23],  $k_{19} \sim 2.0 \times 10^{10} \text{ M}^{-1} \text{ s}^{-1}$  [24],  $k_{20} = 1.5 \times 10^8 \text{ M}^{-1} \text{ s}^{-1}$  [25] and  $k_{21} = 1.0 \times 10^9 \text{ M}^{-1} \text{ s}^{-1}$ . Both  $\text{NO}_2^-$  and  $\text{NO}_2$  may react with the H atom decreasing its total yield,



with  $k_{22} = 1.0 \times 10^{10} \text{ M}^{-1} \text{ s}^{-1}$  [26] and  $k_{23} = 7.1 \times 10^8 \text{ M}^{-1} \text{ s}^{-1}$  [27].

In nitrous oxide solution,  $\text{O}^-$  is obtained as the product of the  $e_{\text{aq}}^-$  scavenging reaction. Under neutral and acidic conditions  $\text{O}^-$  reacts with  $\text{H}_2\text{O}$  and  $\text{H}_{\text{aq}}^+$  to give the OH radical



with  $k_{24} = 1.7 \times 10^6 \text{ M}^{-1} \text{ s}^{-1}$  [22] and  $k_{25} = 4.8 \times 10^{10} \text{ M}^{-1} \text{ s}^{-1}$  [28]. It may also react with several other species within the solution



where  $k_{26} = 2.2 \times 10^{10} \text{ M}^{-1} \text{ s}^{-1}$  [29],  $k_{27} = 2.2 \times 10^8 \text{ M}^{-1} \text{ s}^{-1}$  [30] and  $k_{28} = 1.1 \times 10^8 \text{ M}^{-1} \text{ s}^{-1}$  [31] and  $k_{29} = 1.4 \times 10^9 \text{ M}^{-1} \text{ s}^{-1}$  [32]. It would be expected that  $e_{\text{aq}}^-$  would have reacted with  $\text{N}_2\text{O}$  before it has the chance to react with  $\text{O}^-$ . Reaction 5.27 should occur before reaction 5.28 and therefore, no decrease on  $G(\text{H}_2)$  would be expected. Finally, formate would react with most of the hydrogen atom formed within the track before it has the opportunity to react with  $\text{O}^-$  and therefore, it would not reduce  $G(\text{H}_2)$  any more than the scavenging of the hydrated electron does. Consequently,  $\text{O}^-$  would be much more likely to react with either  $\text{H}_2\text{O}$  or  $\text{H}_{\text{aq}}^+$ . In conclusion, it would be expected to obtain lower  $G(\text{H}_2)$  values at the same  $e_{\text{aq}}^-$  scavenging capacity when using nitrate rather than nitrous oxide as an electron scavenger.

It is worthwhile to consider the chemistry of the OH radical as it is the primary product obtained in the reactions of  $\text{O}^-$ . The hydroxyl radical may react with the molecular hydrogen decreasing its total yield,



with  $k_{30} = 4.2 \times 10^7 \text{ M}^{-1} \text{ s}^{-1}$  [22]. Bromide was then added to avoid the action of the OH radical on decreasing the molecular hydrogen yield



where  $k_{31} = 1.1 \times 10^{10} \text{ M}^{-1} \text{ s}^{-1}$  [22].

In addition, it may react with hydrated electrons or with formate,



where  $k_{32} = 3 \times 10^{10} \text{ M}^{-1} \text{ s}^{-1}$  [22] and  $k_{33} = 3.2 \times 10^9 \text{ M}^{-1} \text{ s}^{-1}$  [22]. It might be expected that at high concentrations of formate, reaction 5.32 would prevent the reaction of the hydrated electron with the OH radical. This would produce an increase in the concentration of  $e_{\text{aq}}^-$  and therefore, an increase of the hydrogen atom and molecular hydrogen yields due to reactions 5.4, 5.5 and 5.6.

### 5.5.2 Deuterated formate and nitrate addition

H atom yields are determined from deuterated solutes by direct measurements of HD yields and from the difference measurements of molecular hydrogen yields as shown in Figure 5.6.

H atom yields obtained from the difference between  $G(\text{Total H}_2)$  and  $G^0(\text{H}_2)$  vary from 0.14 to 0.55 molecules/100eV for scavenging capacities ranging from  $2.9 \times 10^4 \text{ s}^{-1}$  to  $2.9 \times 10^7 \text{ s}^{-1}$ . Whereas H atom yields obtained by direct measurement of HD yields are shown to vary from 0.12 to 0.44 molecules/100eV for the same scavenging capacities. There is a good agreement between the two techniques, particularly at low deuterated formate concentrations. The disagreement showed at higher concentrations may be explained by considering the following reaction



with  $k_{34} = 3.2 \times 10^9 \text{ M}^{-1} \text{ s}^{-1}$  [22]. Increasing the concentration of formate will increase the amount of reaction 5.34 decreasing the concentration of hydroxyl radical, which will cause a reduction in the reactions 5.35 and 5.36.



The former will increase the concentration of  $e_{\text{aq}}^-$  and therefore, the molecular hydrogen yield due to reaction 5.4 while, the latter will increase the

concentration of hydrogen atoms and consequently, the concentration of molecular hydrogen. This analysis suggests that hydrogen atom yields obtained by the difference method at high concentrations of formate may be not reliable since the yield of molecular hydrogen formed by the intra track chemistry would increase as the concentration of  $\text{HCO}_2^-$  increases.

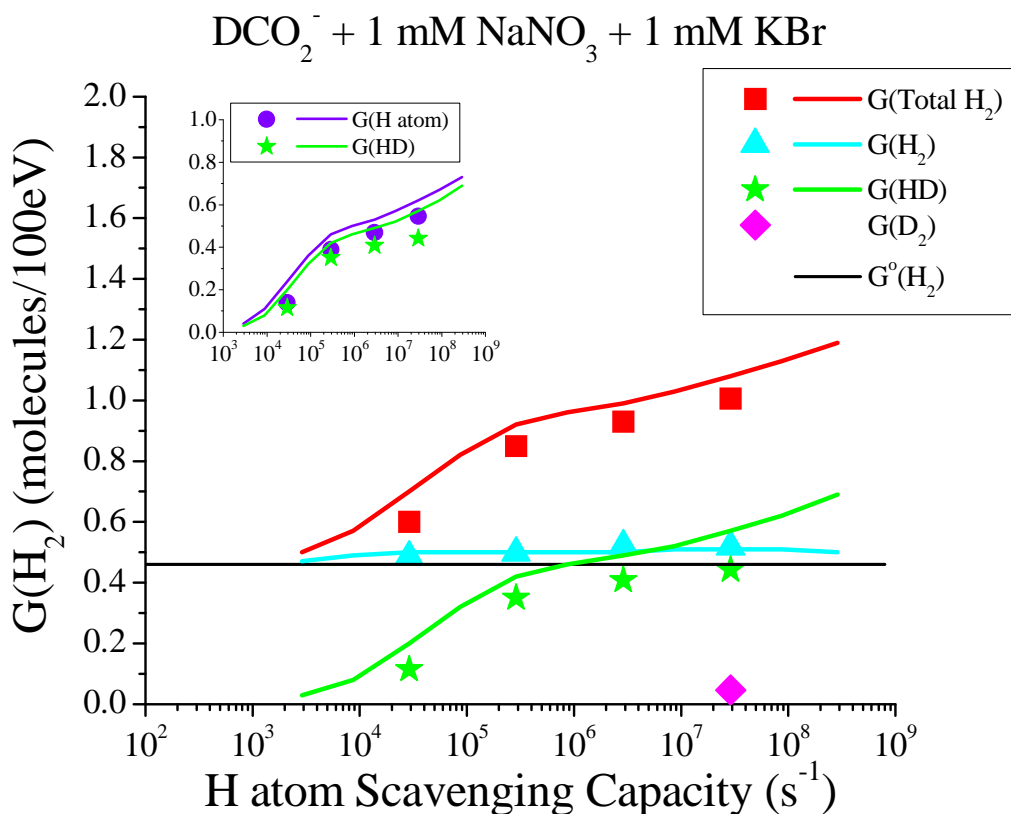


**Figure 5.6** Production of  $\text{H}_2$  in the  $\gamma$ -radiolysis of aqueous deuterated formate solutions with 1 mM  $\text{NaNO}_3$  as a function of the formate scavenging capacity for H atoms. Lines represent modeled results.

Modeled results slightly overestimate the yield of H atom but in general show good agreement, as shown in table 5.2.

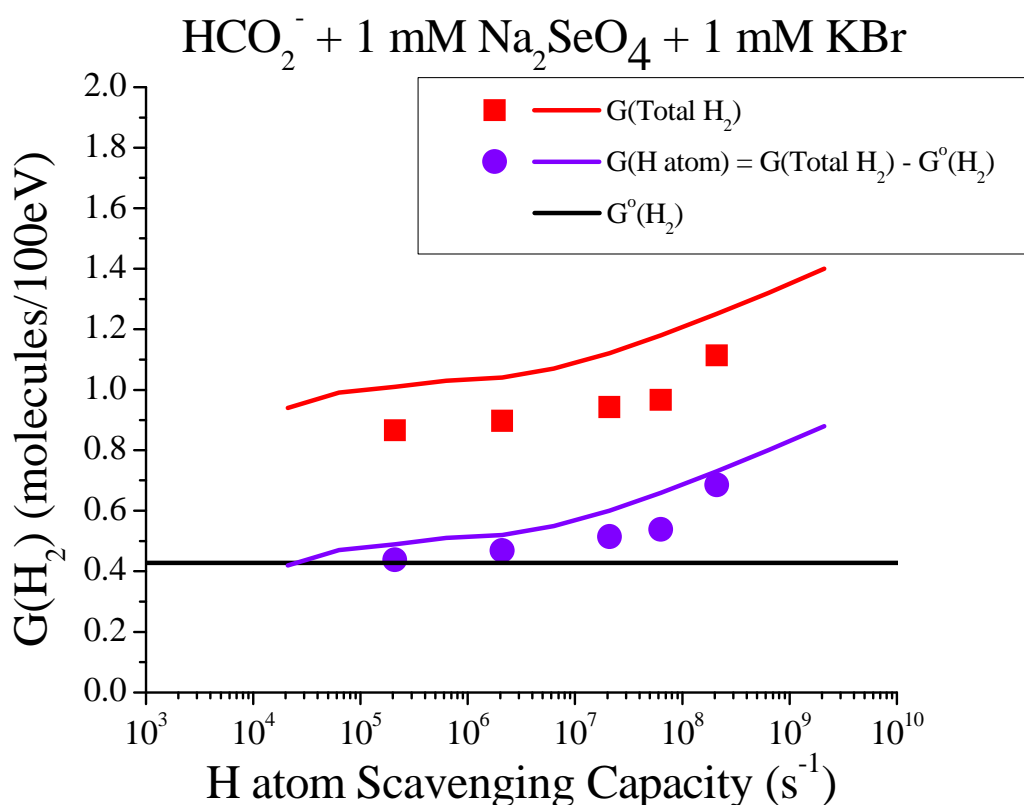
$[\text{HCO}_2^-]$	1 mM	10 mM	100 mM	1 M	Average $\pm$ stnd error
$[\text{G(Hatom)}/\text{G(HD)}]_{\text{exp}}$	1.22	1.11	1.15	1.24	$1.18 \pm 0.06$
$[\text{G(Hatom)}/\text{G(HD)}]_{\text{sim}}$	1.20	1.10	1.08	1.09	$1.12 \pm 0.06$

Table 5.2 Accuracy of the difference method for estimating  $\text{G(H)}$  at each concentration of nitrate.

The determination of the H atom yield through the difference method is reasonably accurate as errors of less than 20 % are obtained both in experimental and modelled results.

### 5.5.3 Formate and selenate addition

Similar results to those shown should be expected when nitrate is replaced by selenate as electron scavenger. Results for 1 mM  $\text{SeO}_4^{2-}$  solution are shown in figure 5.7.



**Figure 5.7** Production of H<sub>2</sub> and H atom in the  $\gamma$ -radiolysis of aqueous formate solutions with 1 mM  $\text{Na}_2\text{SeO}_4$  as a function of the formate scavenging capacity for H atoms.  $G^o(\text{H}_2)$  is the yield of H<sub>2</sub> from a 1 mM  $\text{Na}_2\text{SeO}_4$  solution in the absence of  $\text{HCO}_2^-$ . Lines represent modeled results.

Hydrogen atom yields obtain by the difference method are observed to increase as the hydrogen atom scavenging capacity increases. Experimental values are ranging from 0.44 up to 0.69 molecules/100eV for scavenging capacities varying from 2.1 x

$10^5$  to  $2.1 \times 10^8 \text{ s}^{-1}$ . Whereas, hydrogen atom yields varying from 0.31 up to 0.74 for the same scavenging capacities had been obtained when using nitrate.

The discrepancies between the experimental and the simulated results may be due to some complication with the chemistry of the selenate. This is discussed in detail in the next chapter.

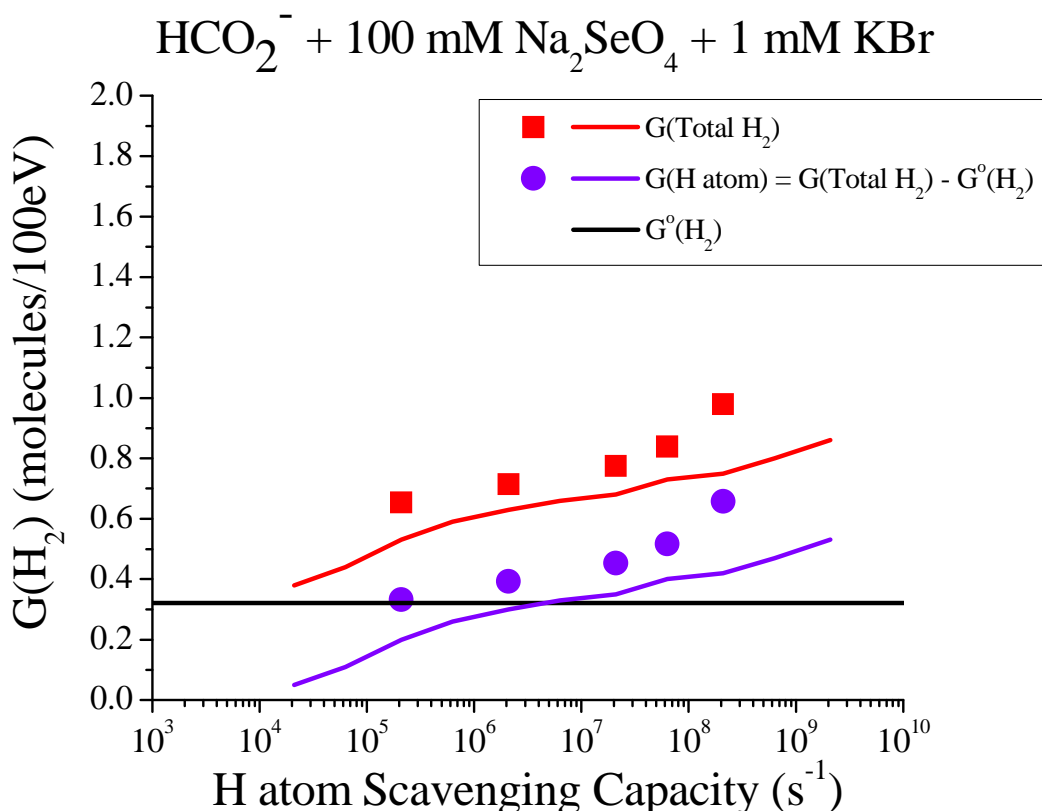


**Figure 5.8** Production of  $\text{H}_2$  in the  $\gamma$ -radiolysis of aqueous formate solutions with 100 mM  $\text{Na}_2\text{SeO}_4$  as a function of the formate scavenging capacity for H atoms.  $G^o(\text{H}_2)$  is the yield of  $\text{H}_2$  from a 1 mM  $\text{NaNO}_3$  solution in the absence of  $\text{HCO}_2^-$ . Lines represent modeled results.

Hydrogen atom yields decrease from the range 0.44 - 0.69 to the range 0.33 - 0.66 molecules/100eV for scavenging capacities varying from  $2.1 \times 10^5$  to  $2.1 \times 10^8 \text{ s}^{-1}$  when the concentration of selenate is increased from 1 to 100 mM (see Figure 5.8). A higher concentration of  $\text{e}_{\text{aq}}^-$  scavenger results in a decrease of  $G(\text{Total H}_2)$  and  $G(\text{H atom})$  due to reactions 5.4, 5.5 and 5.14.

## 5.5.4 Methanol and nitrate addition

In addition to previous studies performed with formate, complementary experiments were made with methanol as a hydrogen atom scavenger with a rate constant of  $2.6 \times 10^6 \text{ M}^{-1} \text{ s}^{-1}$  [13]. This has the same order of magnitude as the rate constants for the reaction of hydrogen with nitrate ( $\sim 1.4 \times 10^6 \text{ M}^{-1} \text{ s}^{-1}$  [13]) or bromide ( $\sim 1.76 \times 10^6 \text{ M}^{-1} \text{ s}^{-1}$  [14]), which may result in competition between these three reactions to scavenge the hydrogen atom. Consequently, methanol should be viewed as an unreliable scavenger for the H atom yield determination in aqueous radiolysis. Experimental evidence is shown in figure 5.9 and discussion follows.

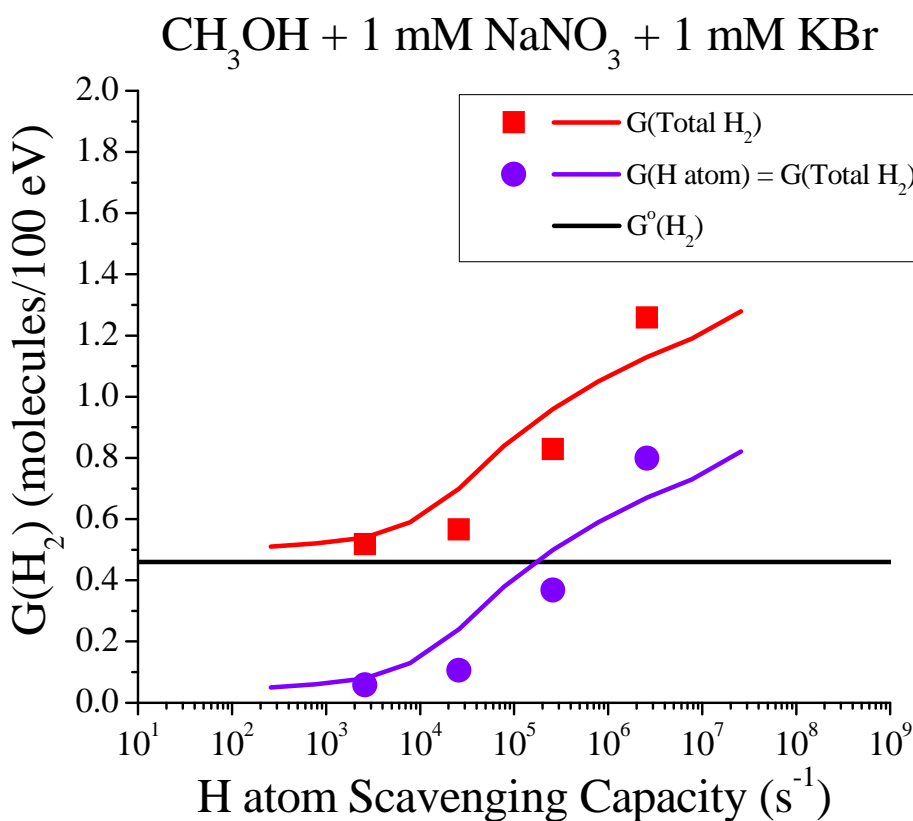


**Figure 5.9** Production of  $\text{H}_2$  and H atom in the  $\gamma$ -radiolysis of aqueous methanol solutions with 1 mM  $\text{NaNO}_3$  as a function of the formate scavenging capacity for H atoms. Lines represent modeled results.

The hydrogen atom values obtained were found to vary from 0.06 to 0.80 molecules/100eV for scavenging capacities ranging from  $2.6 \times 10^3 \text{ s}^{-1}$  to  $2.6 \times 10^6 \text{ s}^{-1}$ . The experimental value obtained at 1 M  $\text{CH}_3\text{OH}$  seems to have been overestimated

according to the simulated results. The low H atom yields registered at the lowest concentrations of methanol may be explained by considering that the rate constant for scavenging of hydrogen atoms by formate is  $2.1 \times 10^8 \text{ M}^{-1} \text{ s}^{-1}$  [13] and for methanol is  $2.6 \times 10^6 \text{ M}^{-1} \text{ s}^{-1}$  [13] therefore, it is reasonable to hypothesise that, at low concentrations of methanol, scavenging of hydrogen atoms by nitrate or bromide, with rate constants of  $\sim 1.4 \times 10^6 \text{ M}^{-1} \text{ s}^{-1}$  [13] and  $\sim 1.76 \times 10^6 \text{ M}^{-1} \text{ s}^{-1}$  [14] respectively, can compete with methanol for H atoms resulting in a considerable drop in total  $\text{H}_2$  yields. To test this hypothesis, the probability of hydrogen atom scavenging by nitrate, bromide, methanol and formate are compared in the ratios shown in Table 5.3,

$$\frac{k_{\text{H}+\text{NO}_3^-}[\text{NO}_3^-]}{R} : \frac{k_{\text{H}+\text{X}}[\text{X}]}{R} : \frac{k_{\text{Br}^-+\text{H}}[\text{Br}^-]}{R} \quad (5.37)$$

where  $R = k_{\text{H}+\text{NO}_3^-}[\text{NO}_3^-] + k_{\text{H}+\text{X}}[\text{X}] + k_{\text{Br}^-+\text{H}}[\text{Br}^-]$  and X represents the H atom scavenger (i.e.  $\text{CH}_3\text{OH}$  or  $\text{HCO}_2^-$ )

$[\text{Br}^-] \text{ M}$	$[\text{NO}_3^-] \text{ M}$	$[\text{CH}_3\text{OH}] \text{ M}$	$\text{Br}^-$	$\text{NO}_3^-$	$\text{CH}_3\text{OH}$
1E-3	1E-3	1E-3	1	1	2
		1E-2	1	1	16
		1E-1	1	1	163
		1E+0	1	1	1625
$[\text{Br}^-] \text{ M}$	$[\text{NO}_3^-] \text{ M}$	$[\text{HCO}_2^-] \text{ M}$	$\text{Br}^-$	$\text{NO}_3^-$	$\text{HCO}_2^-$
1E-3	1E-3	1E-3	1	1	131
		1E-2	1	1	1313
		1E-1	1	1	13125
		1E+0	1	1	131250

**Table 5.3** H atom scavenging kinetic ratios among  $\text{Br}^-$ ,  $\text{NO}_3^-$ ,  $\text{CH}_3\text{OH}$  and  $\text{HCO}_2^-$ .

### 5.5.5 Deuterated methanol and nitrate addition

This complication becomes worse when tri-deuterated methanol is considered. The rate constant for scavenging of H atoms by deuterated methanol is  $1.0 \times 10^5 \text{ M}^{-1} \text{ s}^{-1}$  [13]) and therefore, reaction of H with nitrate or bromide is expected to successfully compete with reaction 5.10 even at higher deuterated methanol concentrations as seen in figure 5.10.



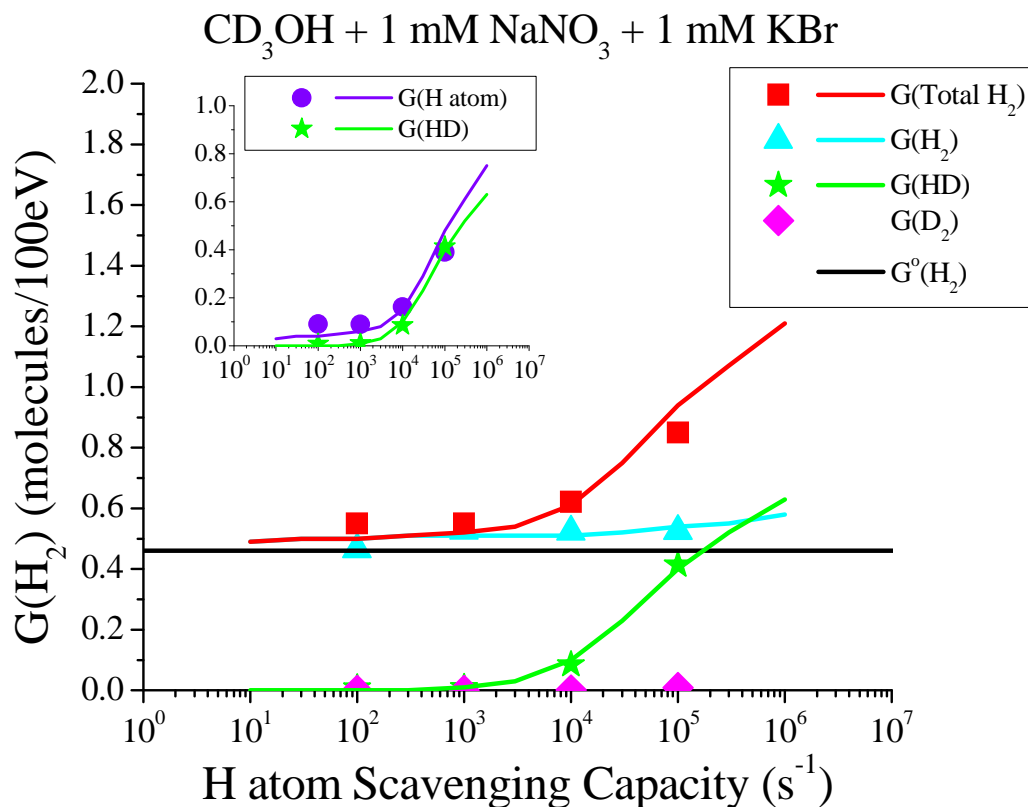


**Figure 5.10** Production of  $\text{H}_2$  and H atom in the  $\gamma$ -radiolysis of aqueous deuterated methanol solutions with 1 mM  $\text{NaNO}_3$  as a function of the formate scavenging capacity for H atoms. Lines represent modeled results.

H atom yields obtained by direct measurement of HD yields are shown to vary from 0.01 to 0.41 molecules/100eV for scavenging capacities ranging from  $2.9 \times 10^4 \text{ s}^{-1}$  to  $2.9 \times 10^7 \text{ s}^{-1}$ . Whereas, H atom yields obtained from  $G(\text{Total H}_2)$  and  $G^o(\text{H}_2)$  difference vary from 0.09 to 0.49 molecules/100eV for the same scavenging capacities. The agreement of the Monte Carlo simulations with experimental values is good, as seen in figure 5.10.

## 5.6 Summary

Hydrogen atom yields have been calculated by difference measurements of  $\text{H}_2$  yields and by direct measurements of HD yields when using deuterated H atom scavengers. Higher yields are observed when increasing the concentration of the hydrogen atom scavenger due to more efficient scavenging of the H atom, as shown in figure 5.11.

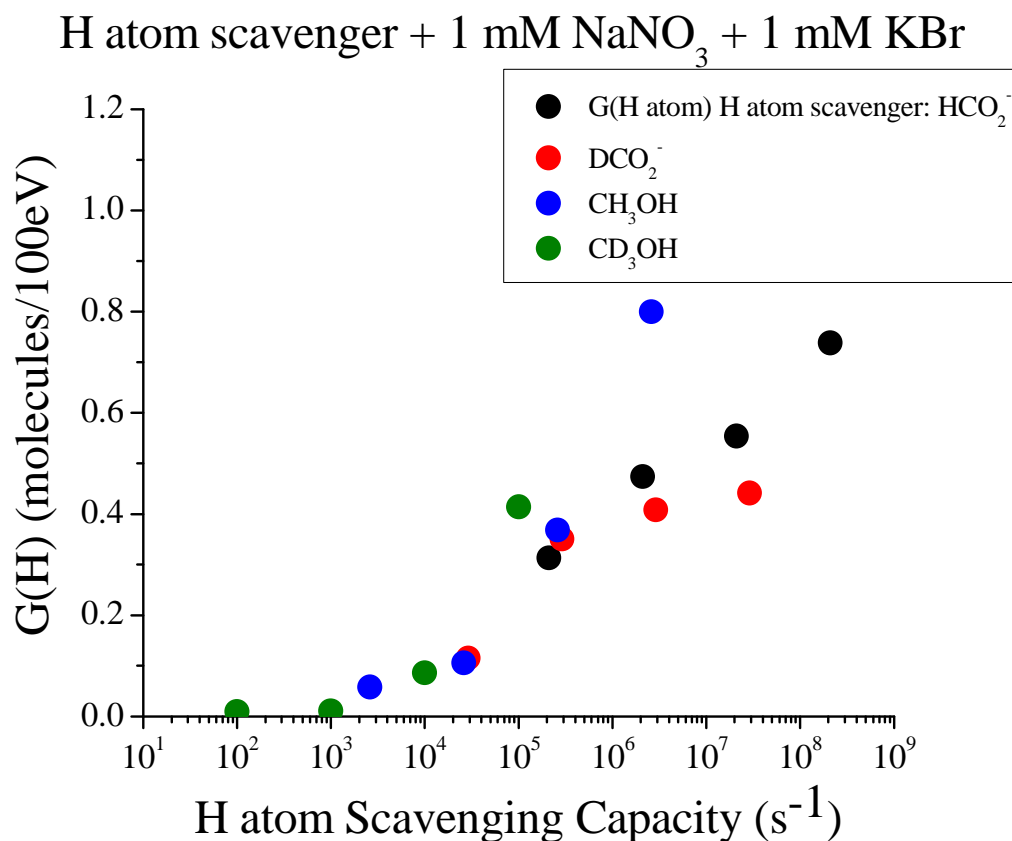


**Figure 5.11** Production of H atom in the  $\gamma$ -radiolysis of aqueous HCO<sub>2</sub><sup>-</sup>, DCO<sub>2</sub><sup>-</sup>, CH<sub>3</sub>OH or CD<sub>3</sub>OH with 1 mM NaNO<sub>3</sub> and 1 mM KBr as a function of the H atom scavenging capacity for H atoms.

The accuracy of the difference method has been questioned at high concentrations of the H atom scavenger since the yield of molecular hydrogen formed by intra track chemistry would increase as the concentration of the H atom scavenger increases which would cause the G(H atom) not to be reliable enough. Nitrate and selenate were both used as electron scavengers showing similar efficiencies, however, some discrepancies with modeled results were found. This will be studied in detail in the next chapter. Finally, methanol and deuterated methanol do not seem appropriate to estimate H atom yields as nitrate or bromide can compete with them for the hydrogen atom due to their similar rate constants.

The scavenging capacity has units inversely proportional to time and therefore, the hydrogen atom production can be studied in terms of time as shown in figure 5.12.

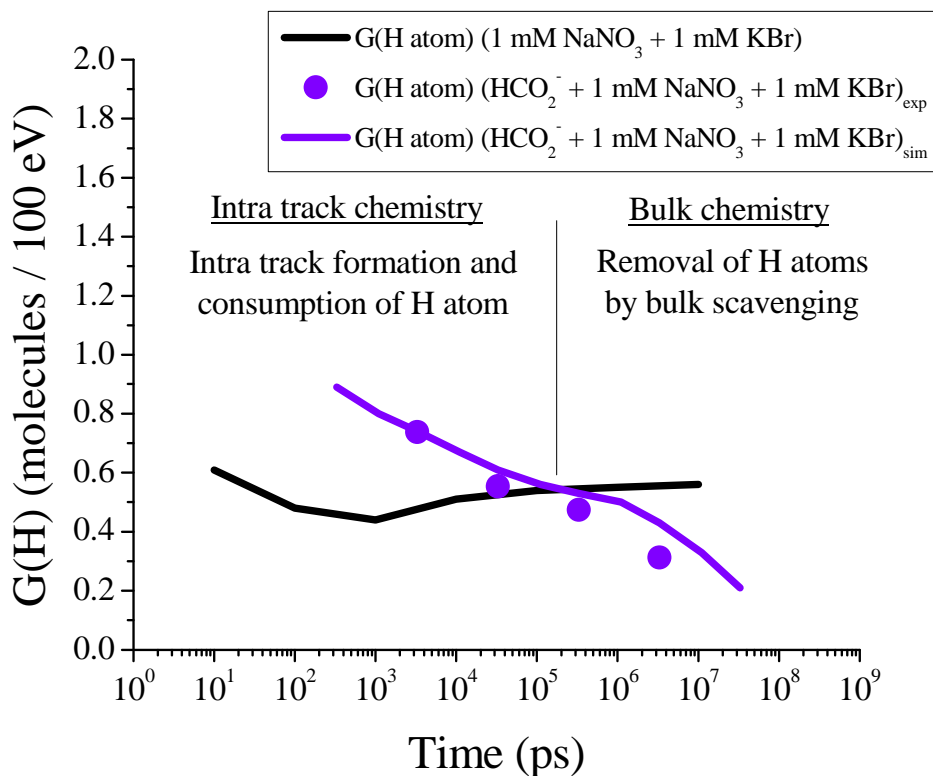


**Figure 5.12** Hydrogen atom production as a function of time.

The black line represents the simulation of the hydrogen atom yield in the gamma radiolysis of water with 1 mM  $\text{NaNO}_3$  and 1 mM  $\text{KBr}$  as a function of time. The blue dots and line represent the experimental and modeled H atom production in the  $\gamma$ -radiolysis of aqueous formate solutions with 1 mM  $\text{NaNO}_3$  and 1 mM  $\text{KBr}$  as a function of time. At times shorter than  $2 \times 10^5$  ps, i.e. to the left of the intersection of the black and violet line, there is a competition among the reactions governed by diffusion where H atom is being formed and destroyed,



From the intersection to the right (i.e. at longer times), the H atom always reacts with the added scavengers decreasing its total yield.



(nitrite,  $\text{NO}_2^-$ , formed due to the chemistry of the nitrate, this will be studied in detail and reported in chapter 6)



The exact intersection point represents the G(H atom) formed in the track.

## 5.7 References

1. Sukhonosov, V.Y., *Geminate recombination of quasi-free electrons in liquid water*. High Energy Chemistry, 1995. **29**: p. 5-10.
2. Gauduel, Y., Pommeret, S., Migus, A., and Antonetti A. , *Some evidence of ultrafast H<sub>2</sub>O<sup>+</sup>-water molecule reaction in femtosecond photoionization of pure liquid water: influence on geminate pair recombination dynamics* Chemical Physics, 1990. **149**: p. 1-10.
3. Burton, M., and Magee, J. L., *Advances in Radiation Chemistry*. Vol. 5. 1976, New York: Wiley, John & Sons, Incorporated. 337.
4. Pimblott, S.M., and LaVerne, J. A., *On the Radiation Chemical Kinetics of the Precursor to the Hydrated Electron*. The Journal of Physical Chemistry A, 1998. **102**: p. 2967-2975.
5. Hamill, W.H., and Sawai, T., *Evidence for very early effects in the radiolysis of water*. The Journal of Physical Chemistry, 1970. **74**: p. 3914-3924.
6. Armstrong, D.A., *The radiation chemistry of gases*. Radiation Chemistry: Principles and Applications (VCH Publisher), 1987: p. 263-319.
7. Johnson, G.R.A., and Simic, M., *Primary processes in the formation of hydrogen atoms in the radiolysis of water vapor*. The Journal of Physical Chemistry, 1967. **71**: p. 1118-1123.
8. Draganic, Z.D., and Draganic, I. G., *Studies on the Formation of Primary Hydrogen Atom Yield G(H) in the Gamma Radiolysis of Water*. The Journal of Physical Chemistry, 1972. **76**: p. 2733-2737.
9. Mahlman, H.A., *Radiolysis of nitrous oxide saturated solutions: Effect of sodium nitrate, 2-propanol, and sodium formate*. The Journal of Physical Chemistry, 1966. **70**: p. 3983-3987
10. Scholes, G., Simic, M., and Weiss, J., *Nature and Reactivity of the Primary Reducing Species in the Radiolysis of Aqueous Solutions*. Discussions Faraday Society, 1963. **36**: p. 214-222.
11. Scholes, G., and M. Simic *Action of gamma-rays on Aqueous Solutions of Nitrous Oxide and the Effects of Added Solutes*. The Journal of Physical Chemistry 1964. **68**: p. 1731-1737.
12. Pastina, B., LaVerne, J. A., and Pimblott, S. M., *Dependence of Molecular Hydrogen Formation in Water on Scavengers of the Precursor to the Hydrated Electron*. The Journal of Physical Chemistry A, 1999. **103**: p. 5841-5846.
13. Buxton, G.V., Greenstock, C. L., Helman, W. P., and Ross, A. B., *Critical Review of Rate Constants for Reactions of Hydrated Electrons, Hydrogen Atoms and Hydroxyl Radicals (OH/O<sup>•</sup>) in Aqueous Solution*. The Journal of Physical Chemistry, 1988: p. 513-886.
14. Bartels, D.M., and Mezyk, S. P., *EPR measurement of the reaction of atomic hydrogen with bromide and iodide in aqueous solution*. The Journal of Physical Chemistry, 1993. **97**: p. 4101-4105.
15. Anbar, M., and Hart, E. J., *Reactivity of hydrated electrons toward inorganic compounds*. Advances in chemistry series 1968: p. 79-94.

16. Pimblott, S.M., and LaVerne, J. A, *Effects of Track Structure on the Ion Radiolysis of the Fricke Dosimeter*. The Journal of Physical Chemistry A, 2002. **106**: p. 9420-9427.
17. LaVerne, J.A., Stefanic, I., and Pimblott, S. M., *Hydrated Electron Yields in the Heavy Ion Radiolysis of Water*. The Journal of Physical Chemistry A, 2005. **109**: p. 9393-9401.
18. Pimblott, S.M., LaVerne, J. A., and Mozumder, A., *Monte Carlo Simulation of Range and Energy Deposition by Electrons in Gaseous and Liquid Water*. The Journal of Physical Chemistry, 1996. **100**: p. 8595-8606.
19. Draganic, Z.D., and Draganic, I. G., *Studies on the Formation of Primary Hydrogen Atom Yield (GH) in the g Radiolysis of Water*. The Journal of Physical Chemistry, 1972. **76**: p. 2733-2737.
20. Scholes G., S., M., and Weiss, J., *Nature and Reactivity of the Primary Reducing Species in the Radiolysis of Aqueous Solutions*. Discussions Faraday Society, 1963. **36**: p. 214-222.
21. Huerta Parajon, M., Rajesh, P., Mu, T., Pimblott, S. M., and LaVerne, J. A., *H atom yields in the radiolysis of water*. Radiation Physics and Chemistry, 2008. **77**: p. 1203-1207.
22. Buxton, G.V., Greenstock, C. L., Helman, W. P., and Ross, A. B., *Critical Review of Rate Constants for Reactions of Hydrated Electrons, Hydrogen Atoms and Hydroxyl Radicals (OH/O<sup>-</sup>) in Aqueous Solution*. The Journal of Physical Chemistry Ref. Data 1988. **17**: p. 513-886.
23. Broszkiewicz, R.K., *The pulse radiolysis study of NaNO<sub>2</sub> and NaNO<sub>3</sub> solutions*. Bull. Polish Academy of Sciences, Ser. Sci. Chim., 1976. **24**: p. 221 - 229.
24. Benderskii, V.A., Krivenko, A. G., Ponomarev, E. A., and Fedorovich, N. V., *Rate constants of protonation of the ion radical NO<sub>3</sub><sup>2-</sup>*. Elektrokimiya, 1987. **23**: p. 1435 - 1439.
25. Park, J.Y., and Lee, Y. N., *Solubility and decomposition kinetics of nitrous acid in aqueous solution*. The Journal of Physical Chemistry, 1988. **92**: p. 6294 - 6302.
26. Logager, T., and Sehested, K., *Formation and decay of peroxyxynitrous acid: A pulse radiolysis study*. The Journal of Physical Chemistry, 1993. **97**: p. 6664 - 6669.
27. Smaller, B., Avery, E. C., and Remko, J. R. , *EPR Pulse Radiolysis Studies of the Hydrogen Atom in Aqueous Solution. I. Reactivity of the Hydrogen Atom*. The Journal of Chemical Physics, 1971. **55**: p. 2414-2418.
28. Elliot, A.J., *Rate Constants and G-Values for the Simulation of the Radiolysis of Light Water over the Range 0-300°C*. 1994, AECL -11073, COG-94-167
29. Matheson, M.S., and Rabani, J., *Pulse Radiolysis of Aqueous Hydrogen Solutions. I. Rate Constants for Reaction of e<sub>aq</sub><sup>-</sup> with Itself and Other Transients. II. The Interconvertibility of e<sub>aq</sub><sup>-</sup> and H*. The Journal of Physical Chemistry, 1965. **69**: p. 1324-1335.
30. Zehavi, D., and Rabani, J., *Pulse radiolytic investigation of Oaq<sup>-</sup> radical ions*. The Journal of Physical Chemistry, 1971. **75**: p. 1738 - 1744.
31. Hickel, B., and Sehested, K., *Activation energies for the reactions O<sup>-</sup> + H<sub>2</sub> and O<sup>-</sup> + D<sub>2</sub> in aqueous solution*. The Journal of Physical Chemistry, 1991. **95**: p. 744 - 747.
32. Buxton, G.V., *Pulse Radiolysis of Aqueous Solutions*. Transactions of the Faraday Society, 1969. **65**: p. 2150 - 2158.

## Chapter 6

# Influence of scavengers of the $e_{aq}^-$ and its precursors on the H atom yield.

6.1	Introduction.....	103
6.2	Introduction to the H atom determination in the radiolysis of water.....	103
6.3	Experimental work.....	106
6.4	Supporting calculations.....	107
6.5	Results and discussion.....	107
6.5.1	Total molecular hydrogen production.....	108
6.5.1.1	Gamma radiolysis.....	108
6.5.1.2	$^1\text{H}$ radiolysis.....	117
6.5.1.3	$^4\text{He}$ radiolysis.....	120
6.5.1.4	Conclusions.....	125
6.5.2	H atom production.....	126
6.5.2.1	Gamma radiolysis.....	126
6.5.2.2	$^1\text{H}$ radiolysis.....	135
6.5.2.3	$^4\text{He}$ radiolysis.....	139
6.5.3.4	Conclusions.....	147
6.5.3	Experimental and stochastic modeled yields.....	148
6.5.3.1	Gamma radiolysis.....	149
6.5.3.2	$^1\text{H}$ radiolysis.....	152
6.5.3.3	$^4\text{He}$ radiolysis.....	154
6.5.3.4	Discussion.....	159
6.6	Summary.....	161
6.7	References.....	161

### 6.1 Introduction

In the radiolysis of water, H atom is not only produced by the fragmentation of the water excited state, but also by intra-track reactions due to the hydrated electron. In this chapter, gamma and heavy ion irradiations were performed in the presence of selected electron scavengers to determine the dependence of the H atom yield on the scavenging of the hydrated electron and its precursor.

### 6.2 Introduction

H atom is produced directly by the fragmentation of water excited states and during the diffusion-kinetic evolution of the radiation track by the intra-track reaction of  $e_{aq}^-$  with  $H_{aq}^+$ ,

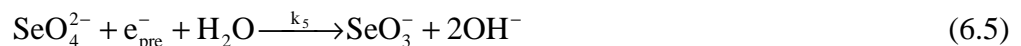


with  $k_1 = 2.3 \times 10^{10} \text{ M}^{-1} \text{ s}^{-1}$  [1]. The yield of this reaction can be reduced by the addition of selected electron scavengers (S).



The influence of electron scavengers on the molecular hydrogen yield has been already studied [2, 3]. A steady decrease in molecular hydrogen yields was found with increased scavenging capacity for the hydrated electron. However, a faster decrease in molecular hydrogen yields was shown for scavengers with higher rate constants for reaction with the precursor to the hydrated electron compared to the hydrated electron. The molecular hydrogen yield more accurately correlates with the scavenging capacity of a precursor to the hydrated electron than the hydrated electron.

Gamma and heavy ion irradiations were performed in the presence of  $NaNO_3$ , and  $Na_2SO_4$  as electron scavengers to determine the dependence of the H atom yield on the scavenging reaction of the hydrated electron and its precursor. Both added scavengers are known to scavenge precursors to the hydrated electron efficiently while selenate is a poor scavenger of the hydrated electron. The reactions of selenate with  $e_{aq}^-$  and  $e_{pre}^-$  are



where the rate constants are respectively  $k_4 = 1.1 \times 10^9 \text{ M}^{-1} \text{ s}^{-1}$  [4] and  $k_5 = 1.0 \times 10^{13} \text{ M}^{-1} \text{ s}^{-1}$  [5]. Subsequently, the  $SeO_3^-$  radical disproportionates to give selenite and selenate

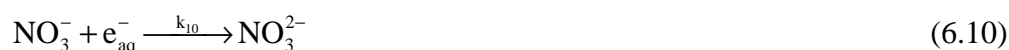


with  $k_6 \sim 1.04 \times 10^9 \text{ M}^{-1} \text{ s}^{-1}$  [6]. The selenite(IV) ion, obtained from the disproportionation, can additionally react with the hydrated electron, hydroxyl radical and hydrogen atom

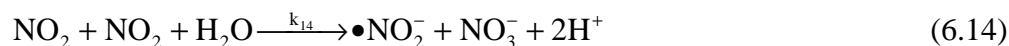
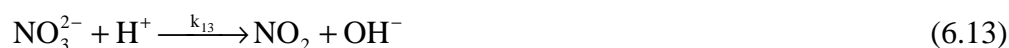


where  $k_7 = 2.3 \times 10^6 \text{ M}^{-1} \text{ s}^{-1}$  [4]  $k_8 = 1.6 \times 10^9 \text{ M}^{-1} \text{ s}^{-1}$  [7] and  $k_9 < 1.0 \times 10^6 \text{ M}^{-1} \text{ s}^{-1}$  [6].

Nitrate efficiently scavenges the precursor to the hydrated electron, but it is also a good scavenger of the hydrated electron



with  $k_{10} = 9.7 \times 10^9 \text{ M}^{-1} \text{ s}^{-1}$  [8] and  $k_{11} = 1.0 \times 10^{13} \text{ M}^{-1} \text{ s}^{-1}$  [5]. Afterwards, the  $NO_3^{2-}$  intermediate reacts with other species in solution to generate nitrogen dioxide and nitrite



with  $k_{12} = 8.9 \times 10^4 \text{ M}^{-1} \text{ s}^{-1}$  [9],  $k_{13} \sim 2.0 \times 10^{10} \text{ M}^{-1} \text{ s}^{-1}$  [10],  $k_{14} = 1.5 \times 10^8 \text{ M}^{-1} \text{ s}^{-1}$  [11] and  $k_{15} = 1.0 \times 10^9 \text{ M}^{-1} \text{ s}^{-1}$ .

In dilute solutions, it is important to consider the relative probabilities of H atom reacting with all the solutes present, i.e. in addition to reactions with formate or deuterated formate, it is necessary to consider reactions with nitrate or selenate,



where  $k_{16} = 1.6 \times 10^6 \text{ M}^{-1} \text{ s}^{-1}$  [12] and  $k_{17} < 1.0 \times 10^6 \text{ M}^{-1} \text{ s}^{-1}$  [6], and bromide,





where  $k_{18} = 1.7 \times 10^6 \text{ M}^{-1} \text{ s}^{-1}$  [6]. The relative contributions of the scavenging reactions are compared in the ratios shown in Tables 6.1 and 6.2 (nitrate and selenate are considered interchangeable in these ratios as their affinity for the H atom is very similar and therefore, no appreciable differences would be expected).

$$\frac{k_{X+H}[X]}{k_{\text{HCO}_2^-+H}[\text{HCO}_2^-] + k_{\text{NO}_3^-+H}[\text{NO}_3^-] + k_{\text{Br}^-+H}[\text{Br}^-]} \quad X = \text{HCO}_2^-, \text{NO}_3^-, \text{Br}^-$$

$$\frac{k_{X+H}[X]}{k_{\text{DCO}_2^-+H}[\text{HCO}_2^-] + k_{\text{NO}_3^-+H}[\text{NO}_3^-] + k_{\text{Br}^-+H}[\text{Br}^-]} \quad X = \text{DCO}_2^-, \text{NO}_3^-, \text{Br}^-$$

[HCO <sub>2</sub> <sup>-</sup> ](M)	[NO <sub>3</sub> <sup>-</sup> ](M)	[Br <sup>-</sup> ](M)	HCO <sub>2</sub> <sup>-</sup>	NO <sub>3</sub> <sup>-</sup>	Br <sup>-</sup>
1.E-02	1.E-03	1.E-03	1235	1	1
	1.E-02		1235	9	1
	1.E-01		1235	94	1
	1.E+00		1235	941	1

1.E+00	1.E-03	1.E-03	123529	1	1
	1.E-02		123529	9	1
	1.E-01		123529	94	1
	1.E+00		123529	941	1

**Table 6.1** Formate, nitrate and bromide reaction ratios with the hydrogen atom.

[DCO <sub>2</sub> <sup>-</sup> ](M)	[NO <sub>3</sub> <sup>-</sup> ](M)	[Br <sup>-</sup> ](M)	DCO <sub>2</sub> <sup>-</sup>	NO <sub>3</sub> <sup>-</sup>	Br <sup>-</sup>
1.E-02	1.E-03	1.E-03	171	1	1
	1.E-02		171	9	1
	1.E-01		171	94	1
	1.E+00		171	941	1

1.E+00	1.E-03	1.E-03	17059	1	1
	1.E-02		17059	9	1
	1.E-01		17059	94	1
	1.E+00		17059	941	1

**Table 6.2** Deuterated formate, nitrate and bromide reaction ratios with the hydrogen atom.

Formate and deuterated formate have the highest affinity for the H atom with the sole exception of the highest concentration of the electron scavengers and the lowest concentration of the hydrogen scavenger where the H atom yield might be slightly affected by the reaction with nitrate or selenate.

Selenate scavenges the precursors to the hydrated electron efficiently, but is a poor scavenger of the hydrated electron. The ratio  $k_{(epre+S)} / k_{(eaq+S)}$  is significantly higher for selenate ( $9.09 \times 10^3$ ) than nitrate ( $1.03 \times 10^3$ ). This difference suggests that a higher dependence of the  $H_2$  and H atom formation on the  $e_{aq}^-$  would produce similar curves for the comparison of the  $H_2$  yields as a function of the scavenging capacity for the hydrated electron ( $S_{eaq}$ ) for the two scavengers and two different curves in terms of the precursor to the hydrated electron. Otherwise, a higher dependence on the  $e_{pre}^-$  would lead to similar curves as a function of the  $S_{epre}$  and two different curves in terms of the hydrated electron.

### 6.3 Experimental work

Gamma irradiations were performed in the Radiation Laboratory at The University of Notre Dame (USA), using the Shepherd 109  $^{60}Co$  irradiator previously described. Solutions with 10 mM or 1 M sodium formate ( $NaHCO_2$ ) or 10 mM deuterated sodium formate ( $NaDCO_2$ ), 1 mM potassium bromide (KBr) and different concentrations of sodium nitrate ( $NaNO_3$ ) or sodium selenate ( $Na_2SeO_4$ ) were prepared with nano pure water (resistivity  $18.7 M\Omega cm^{-1}$ ) from an in-house  $H_2$ Only system. Four millilitres samples were loaded into a sample cell that consists of a 1 cm cuvette with inlet and outlet ports to purge the sample before irradiation. A gas chromatograph and a mass spectrometer were used inline to determine molecular hydrogen as shown in chapter 3.

Irradiations with heavy ions were conducted in the Nuclear Structure Laboratory at The University of Notre Dame (USA). The FN Tandem Van de Graaff described in chapter 3 was used to irradiate the samples. Solutions with 1 M sodium formate ( $NaHCO_2$ ) or 10 mM deuterated sodium formate ( $NaDCO_2$ ), 1 mM potassium bromide (KBr) and different concentrations of sodium nitrate ( $NaNO_3$ ) or sodium selenate ( $Na_2SeO_4$ ) were prepared with nano pure water (resistivity  $18.7 M\Omega cm^{-1}$ ) from an in-house  $H_2$ Only system. Twenty millilitres samples were loaded into a Pyrex cell with a thin mica window ( $\sim 6 mg cm^{-2}$ ) attached. The sample cell contained a magnetic stirrer operating continuously and inlet and outlet ports to

purge the sample before irradiation. Hydrogen was determined with a gas chromatograph and a mass spectrometer connected inline with the sample cell placed on the heavy ions accelerator.

Calibration was carried out by injecting different volumes of pure  $H_2$  and  $D_2$  gases with a gas-tight microlite syringe. The total molecular hydrogen was monitored from the chromatographic response, while the hydrogen isotopes were determined from the mass spectrometric response. The error in gas measurement is expected to be ~ 5%.

#### 6.4 Supporting calculations

Monte Carlo track simulations were performed using the same techniques already explained in chapter 3 and in previous studies [13-15]. Each simulation calculates the transfer of energy from the radiation particle to the sample to simulate the track structure, determine whether this energy transfer results in an ionization, an excitation or a vibration event and models the kinetics based on the competition between the relaxation of the spatially non-homogeneous distribution of radiation-induced reactants and their reactions either within the track or with the scavengers.

Each simulation determines the trajectory of the primary ion and the daughter electrons as well as their initial and final positions. The nature of the event produced after collision is determined by relating the difference between the initial and the transferred energy with the cross sections for each one of the possible events using a random number.

The independent reaction times methodology (IRT), based on the independent pairs approximation, is used to model the diffusion-reaction kinetics of radio-induced reactive species in water.

#### 6.5 Results and discussion

Total  $H_2$  and H atom yields are presented below for the gamma,  $^1H$  and  $^4He$  radiolysis of 10 mM to 1 M formate and 10 mM to 1 M deuterated formate aqueous solutions with added sodium nitrate or sodium selenate with concentrations varying from 1 mM to 1 M and containing 1 mM potassium bromide.

## 6.5.1 Total molecular hydrogen production

The total molecular hydrogen yield is the addition of the H atom yield and the molecular hydrogen yield in neat water. Its study is essential to gain an understanding of the early steps in the radiolysis of water and in particular to determine the main source of H atom and its yield.

## 6.5.1.1 Gamma radiolysis

Experimental results are presented first for the gamma radiolysis of 10 mM sodium formate as a function of the hydrated electron scavenging capacity and later as the precursor to the hydrated electron scavenging capacity.

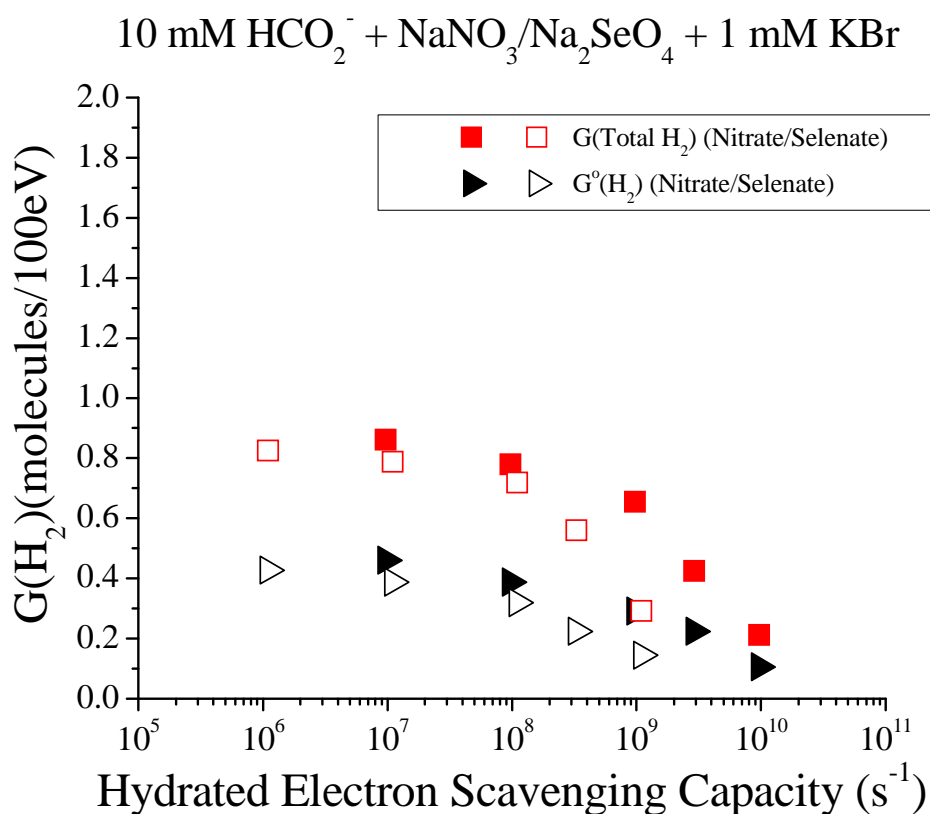


**Figure 6.1** Production of  $\text{H}_2$  in the  $\gamma$ -radiolysis of aqueous 10 mM formate solutions with  $\text{NaNO}_3$  or  $\text{Na}_2\text{SeO}_4$  as a function of the hydrated electron scavenging capacity.  $G^o(\text{H}_2)$  is the yield of  $\text{H}_2$  at different concentrations of the electron scavengers in the absence of any H atom scavenger.

A decrease in the total molecular hydrogen yield is observed as the concentration of the electron scavenger increases. When selenate is added, total

molecular hydrogen yield decreases from 0.83 to 0.30 molecules/100eV for scavenging capacities ranging from  $1.1 \times 10^6 \text{ s}^{-1}$  to  $1,1 \times 10^9 \text{ s}^{-1}$ , while it goes from 0.86 to 0.21 molecules/100eV for scavenging capacities varying from  $9.7 \times 10^6 \text{ s}^{-1}$  to  $9.7 \times 10^9 \text{ s}^{-1}$  when nitrate is added.

Production of  $\text{H}_2$  as a function of the precursor to the hydrated electron scavenging capacity is shown in figure 6.2.

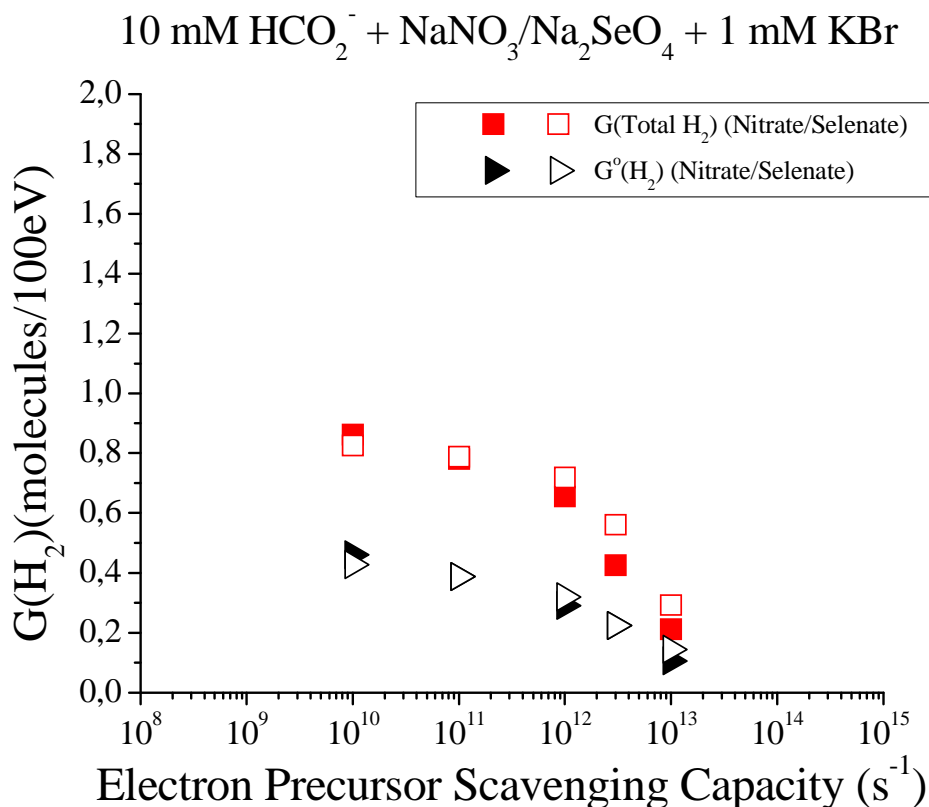


**Figure 6.2** Production of  $\text{H}_2$  in the  $\gamma$ -radiolysis of aqueous 10 mM formate solutions with  $\text{NaNO}_3$  or  $\text{Na}_2\text{SeO}_4$  as a function of the precursor to the hydrated electron scavenging capacity.  $G^o(\text{H}_2)$  is the yield of  $\text{H}_2$  at different concentrations of the electron scavengers in the absence of any H atom scavenger.

Average total molecular hydrogen yields vary from 0.86 to 0.25 molecules/100eV for scavenging capacities ranging from  $\sim 1.0 \times 10^{10} \text{ s}^{-1}$  to  $1.0 \times 10^{13} \text{ s}^{-1}$ .

Complementary experiments were carried out at higher concentrations of sodium formate in order to study its effect on the molecular hydrogen production.

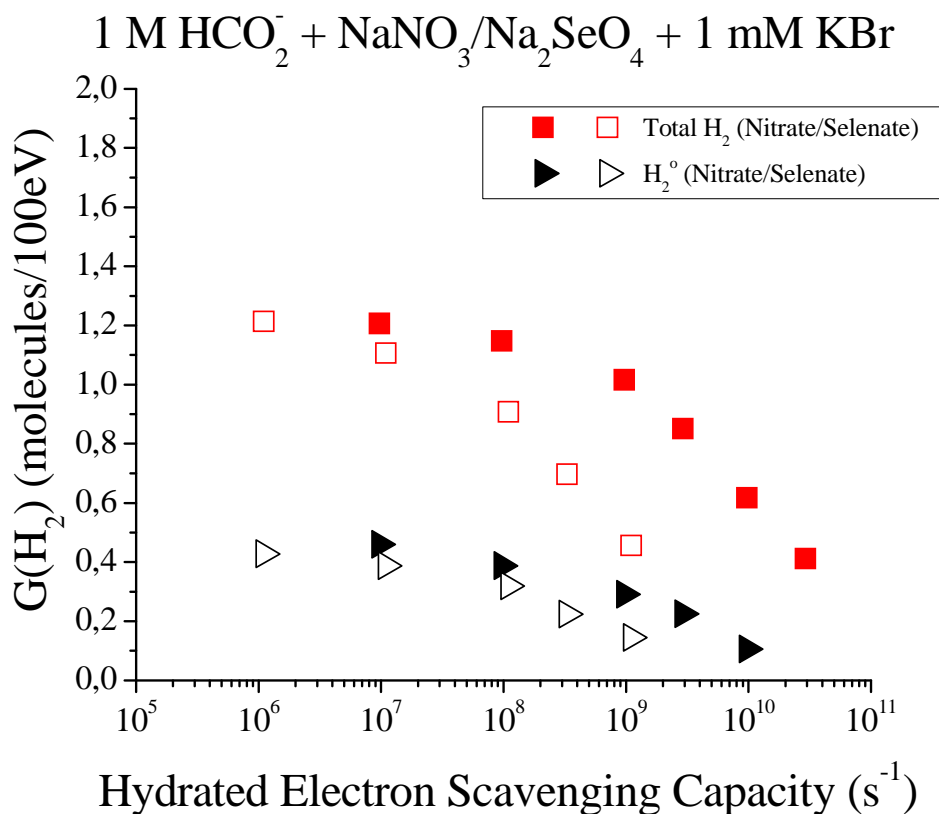


**Figure 6.3** Production of  $\text{H}_2$  in the  $\gamma$ -radiolysis of aqueous 1 M formate solutions with  $\text{NaNO}_3$  or  $\text{Na}_2\text{SeO}_4$  as a function of the hydrated electron scavenging capacity.  $G^\circ(\text{H}_2)$  is the yield of  $\text{H}_2$  at different concentrations of the electron scavengers in the absence of any H atom scavenger.

Higher formate concentrations increase the concentration of molecular hydrogen due to a more efficient scavenging of hydrogen atoms. Therefore, increased  $\text{H}_2$  yields were obtained in the  $\gamma$ -radiolysis of aqueous 1 M formate solutions with  $\text{Na}_2\text{SeO}_4$  or  $\text{NaNO}_3$  with values ranging from 1.21 to 0.46 and 1.20 to 0.41 molecules/100eV respectively. Results are shown in figure 6.4 in terms of the electron precursor scavenging capacity.

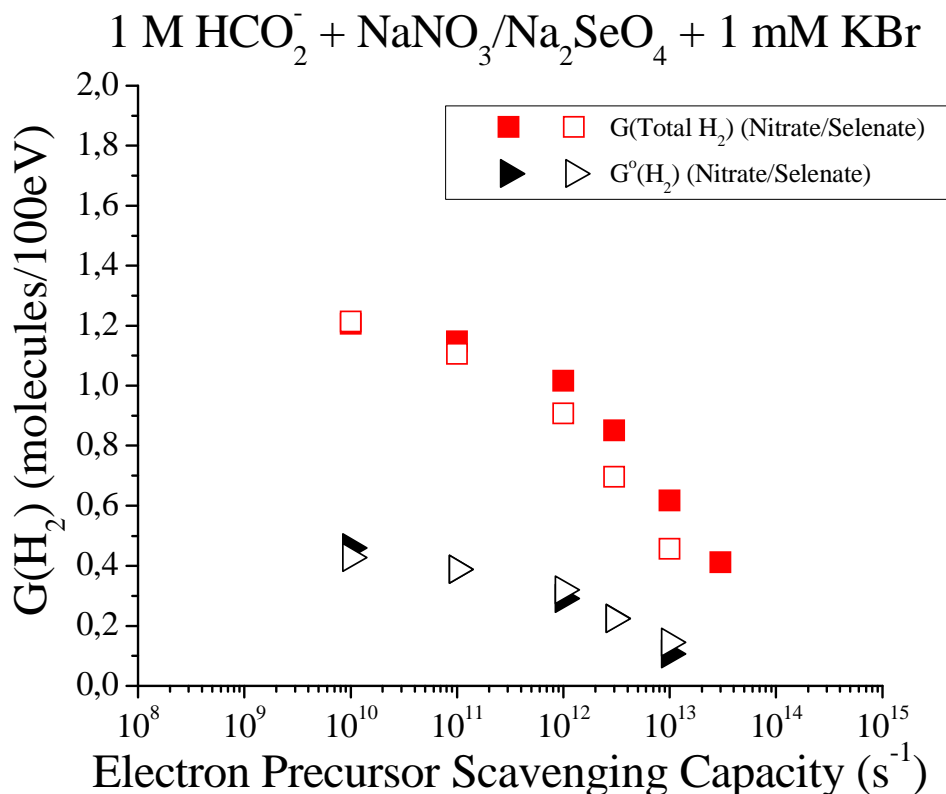
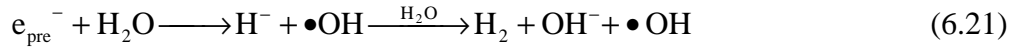


**Figure 6.4** Production of  $\text{H}_2$  in the  $\gamma$ -radiolysis of aqueous 1 M formate solutions with  $\text{NaNO}_3$  or  $\text{Na}_2\text{SeO}_4$  as a function of the precursor to the hydrated electron scavenging capacity.  $G^0(\text{H}_2)$  is the yield of  $\text{H}_2$  at different concentrations of the electron scavengers in the absence of any H atom scavenger.

In figures 6.1 to 6.4, two different curves are observed in terms of the hydrated electron scavenging capacity while one common curve is observed in terms of the scavenging capacity of the precursor to the hydrated electron. This difference suggests a stronger correlation of the molecular hydrogen formation with the scavenging of a precursor to the hydrated electron rather than a hydrated electron. Examination of figure 6.2 shows the yield of the molecular hydrogen is  $\sim 0.7$  molecules/100eV at a scavenger capacity of approximately  $1.0 \times 10^{12} \text{ s}^{-1}$  for the precursors to the hydrated electron. This value is  $\sim 80\%$  of the total molecular hydrogen produced, demonstrating that the precursors to the H atom and  $\text{H}_2$  are formed on a sub-picosecond timescale. Diffusion controlled reaction of the  $e_{aq}^-$  at these short times to produce  $\text{H}_2$  is not feasible since the fastest known reaction of  $e_{aq}^-$  occurs with the hydrated proton at a rate of  $2.4 \times 10^{10} \text{ M}^{-1} \text{ s}^{-1}$  [16], which means that other mechanism have to be involved. Molecular hydrogen is assumed to be largely formed in the primary radiolysis events due to the electron precursor, i.e.



with a smaller amount formed from directly produced excited states and by intra track reactions of  $e_{aq}^-$  and H. From now on, molecular hydrogen yields will be presented in terms of the electron precursor scavenging capacity.

In theory, nitrate is a good scavenger of the hydrated electron and even at low scavenging capacities and prevents H atom formation via reaction 6.1. On the other hand, selenate is a poor scavenger of the hydrated electron and therefore, does not prevent H atom formation via reaction 6.1. This means that, in theory, lower molecular hydrogen and hydrogen atom yields should be obtained due to the addition of nitrate. However, the difference between the  $G(\text{total } H_2)$  due to the addition of nitrate or selenate is small. This suggests that, reaction 6.1 does not occur to a significant extension within the radiation track since, although theoretically a difference between molecular hydrogen yields obtained due to the addition of nitrate or selenate was expected, in practice, there is essentially no difference.

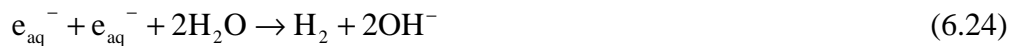
In addition to the more efficient scavenging of H atoms as the concentration of formate is increased, two other factors may increase the yield of  $H_2$ . Sodium formate reacts with the hydroxyl radical



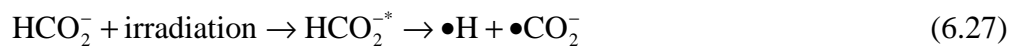
with  $k_{22} = 3.2 \times 10^9 \text{ M}^{-1} \text{ s}^{-1}$  [8]. It is expected that at high concentrations of formate, reaction 6.22 prevents the reaction of the hydrated electron with the OH radical



where  $k_{23} = 3 \times 10^{10} \text{ M}^{-1} \text{ s}^{-1}$  [8]. This would produce an increase in the concentration of  $e_{aq}^-$  and therefore, an increase of the H atom and  $H_2$  yields due to reactions



Additional molecular hydrogen can be obtained due to the direct irradiation of the solute at high concentrations







This direct irradiation will be discussed in detail next in this chapter.

Yields obtained from the irradiation of 10 mM deuterated formate with gamma rays are shown in figure 6.5 as a function of the precursor to the hydrated electron scavenger capacity.

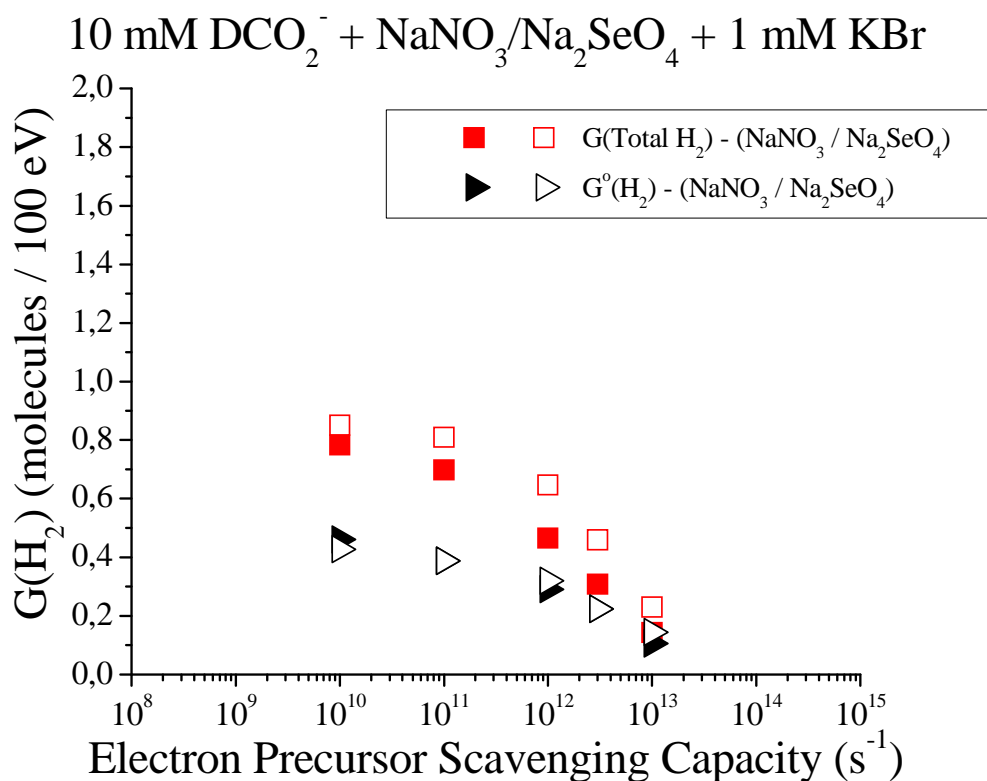
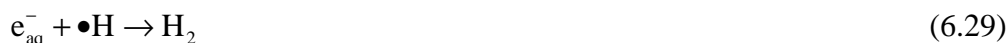


**Figure 6.5** Hydrogen atom and molecular hydrogen production in the  $\gamma$ -radiolysis of aqueous 10 mM deuterated formate solutions with  $NaNO_3$  or  $Na_2SeO_4$  as a function of the precursor to the hydrated electron scavenging capacity.  $G^o(H_2)$  is the yield of  $H_2$  at different concentrations of the electron scavengers in the absence of any H atom scavenger.

On the addition of deuterated formate, the  $G(\text{total } H_2)$  is equal to the sum of  $G(H_2) + G(HD) + G(D_2)$ . Total molecular hydrogen yields show an almost common line in terms of the electron precursor scavenging capacity. It is observed to be slightly higher due to the addition of selenate than nitrate. Selenate is a poor scavenger of the hydrated electron and therefore, the molecular hydrogen yield is expected to be higher due to reactions 6.29 and 6.30.





The formation of molecular hydrogen, at scavenging capacities higher than  $10^{12} \text{ s}^{-1}$ , is governed by the reactions of the electron precursor. The reactions of the hydrated electron to generate molecular hydrogen occurs at times longer than  $10^{-12} \text{ s}$  which means that, at lower scavenging capacities than  $\sim 10^{12} \text{ s}^{-1}$ , additional molecular hydrogen to that obtained due to the reactions of the electron precursor, will be formed due to the reactions of the hydrated electron and the reaction of two hydrogen atoms. Therefore, it is expected that  $\text{H}_2$  yields when selenate rather than nitrate is added are higher at low scavenging capacities of the electron precursor.

Figure 6.6 shows the results of the gamma radiolysis of aqueous 1 M deuterated formate solutions with added  $\text{NaNO}_3$ . No experiments were carried out with addition of selenate at this concentration.

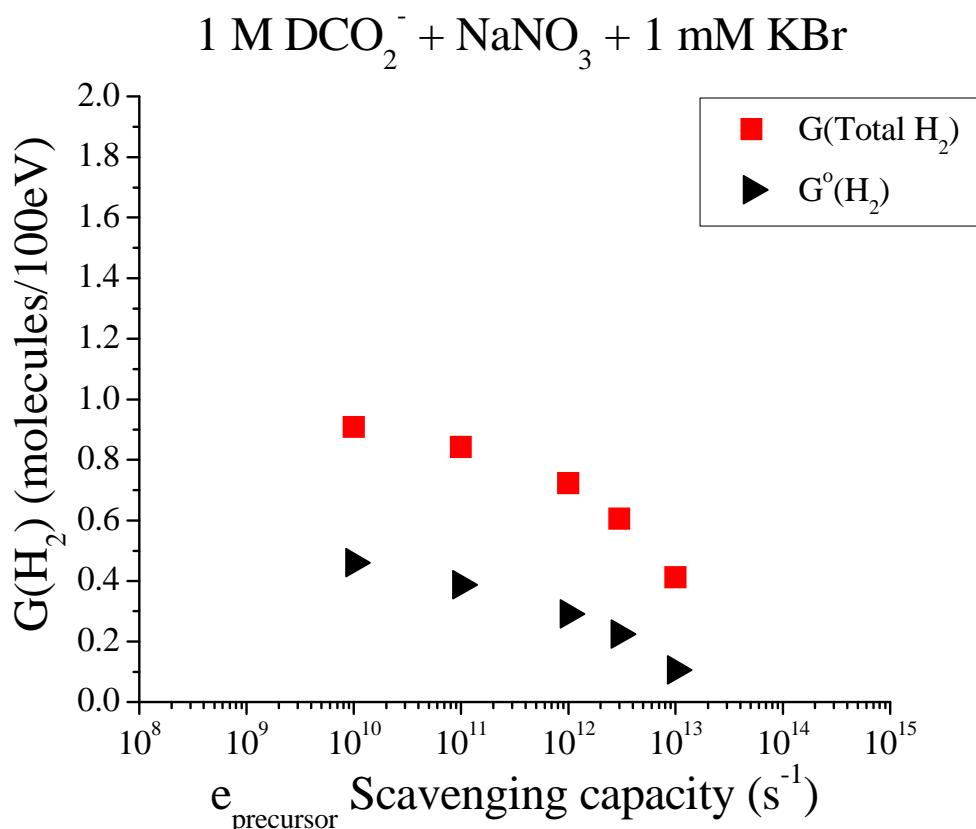


**Figure 6.6** Hydrogen production in the  $\gamma$ -radiolysis of aqueous 1 M deuterated formate solutions with  $\text{NaNO}_3$  as a function of the precursor to the hydrated electron scavenging capacity.  $G^o(\text{H}_2)$  is the yield of  $\text{H}_2$  at different concentrations of the electron scavengers in the absence of any H atom scavenger.

As before, the molecular hydrogen yield decreases as the electron precursor scavenging capacity increases. When the concentration of  $DCO_2^-$  is increased from 10 mM to 1 M, the hydrogen atom yield increases from 0.78 to 0.91 and 0.14 to 0.41 molecules / 100 eV for electron precursor scavenging capacities  $1 \times 10^{10}$  and  $1 \times 10^{13}$   $s^{-1}$  respectively, due to the more efficient scavenging capacity of the hydrogen atom.

A two dimensional grid of results varying scavenging capacities logarithmically for the H atom and for the electron precursor from  $10^5$  to  $10^9$   $s^{-1}$  and  $10^{10}$  to  $10^{13}$   $s^{-1}$  respectively has been obtained in the gamma radiolysis of sodium formate or deuterated formate with added nitrate. Figure 6.7 compares the total molecular hydrogen yields in terms of the hydrogen atom scavenging capacity to investigate the overall set of results when nitrate is added as electron scavenger.

10 mM/1 M  $HCO_2^-$  and 10 mM/1 M  $DCO_2^-$  +  $NaNO_3$  + 1 mM KBr

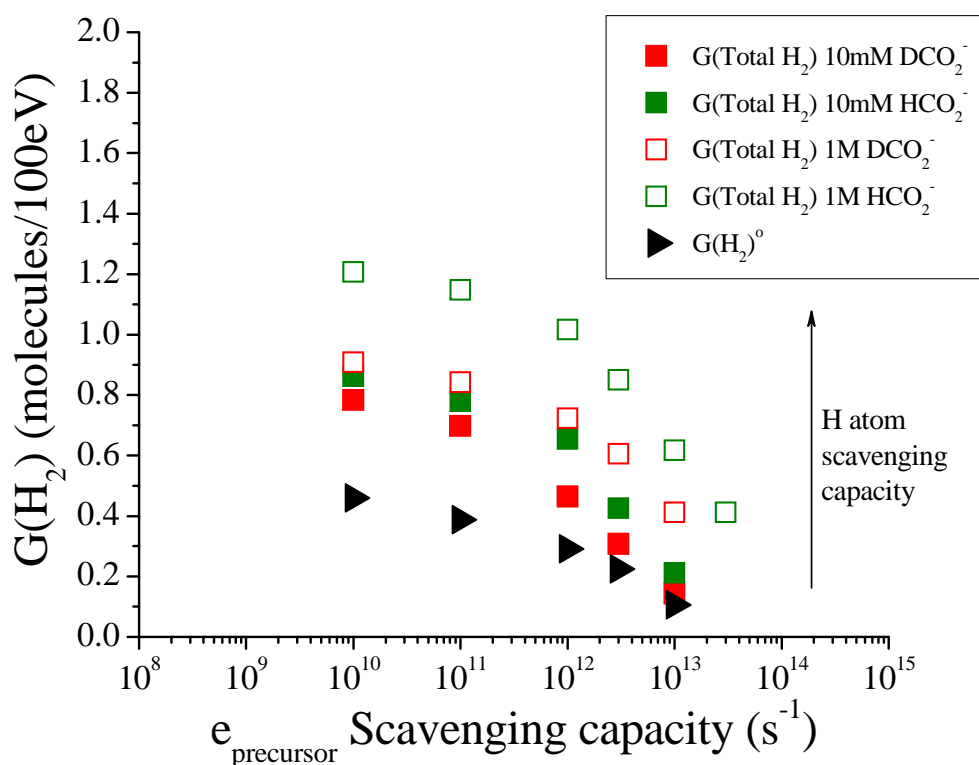


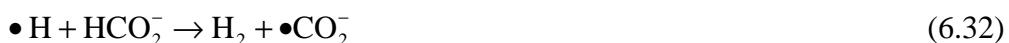
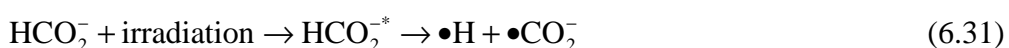
**Figure 6.7**  $H_2$  yields behavior in the gamma radiolysis of aqueous systems in terms of the H atom scavenging capacity and the electron precursor scavenging capacity.  $G^0(H_2)$  is the yield of  $H_2$  at different concentrations of the electron scavengers in the absence of any H atom scavenger.

In figure 6.7, total molecular hydrogen yields are presented for the gamma radiolysis of formate and deuterated formate aqueous solutions at different hydrogen atom scavenging capacities, as shown in table 6.3.

[HCO <sub>2</sub> <sup>-</sup> ] (M)	[DCO <sub>2</sub> <sup>-</sup> ] (M)	$k_{H+HCO_2^-}$ (M <sup>-1</sup> s <sup>-1</sup> )	H atom scavenging capacity (s <sup>-1</sup> )
	0.01	$2.9 \times 10^7$	$2.9 \times 10^5$
0.01		$2.1 \times 10^8$	$2.1 \times 10^6$
	1	$2.9 \times 10^7$	$2.9 \times 10^7$
1		$2.1 \times 10^8$	$2.1 \times 10^8$

**Table 6.3** Variation of the H atom scavenging capacity

The greatest G(Total H<sub>2</sub>) are obtained through the addition of 1 M sodium formate while lowest values are seen when 10 mM sodium deuterated formate is added. These solutions have the highest and the lowest H atom scavenging capacities, respectively. The results follow a logical pattern with the G(Total H<sub>2</sub>) increasing as the H atom scavenging capacity increases. However, much higher G(Total H<sub>2</sub>) is observed in the radiolysis of aqueous 1 M sodium formate solutions compared to the others concentrations considered. This is due to more efficient competition of the scavenging capacity with intra track reactions, as well as, the direct radiolysis of the solute at this high concentration of the solute



and the reaction of the sodium formate with OH radicals



with  $k_{33} = 3.2 \times 10^9 \text{ M}^{-1}\text{s}^{-1}$  [8]. As introduced before in this chapter, it is expected that at high concentrations of formate, reaction 6.33 prevents the reaction of the hydrated electron with the OH radical



where  $k_{34} = 3 \times 10^{10} \text{ M}^{-1}\text{s}^{-1}$  [8]. This would produce an increase in the concentration of  $e_{aq}^-$  and therefore, an increase of the hydrogen atom and molecular hydrogen yields due to reactions



### 6.5.1.2 $^1\text{H}$ radiolysis

$^1\text{H}$  ions have higher LET values than the Compton scattered electrons of gamma rays. The expected consequence is that the local concentration of reactants in the track will be denser. This means that an increase in the intra track reactions should be observed and the  $\text{H}_2$  yields will increase due to an increase in  $G^\circ(\text{H}_2)$ .

The  $^1\text{H}$  irradiation of sodium formate or sodium deuterated formate aqueous solutions with added nitrate and 1 mM bromide was carried out. Firstly, the molecular hydrogen production in the  $^1\text{H}$  radiolysis of aqueous 10 mM formate solutions with added  $\text{NaNO}_3$  is presented in figure 6.8.

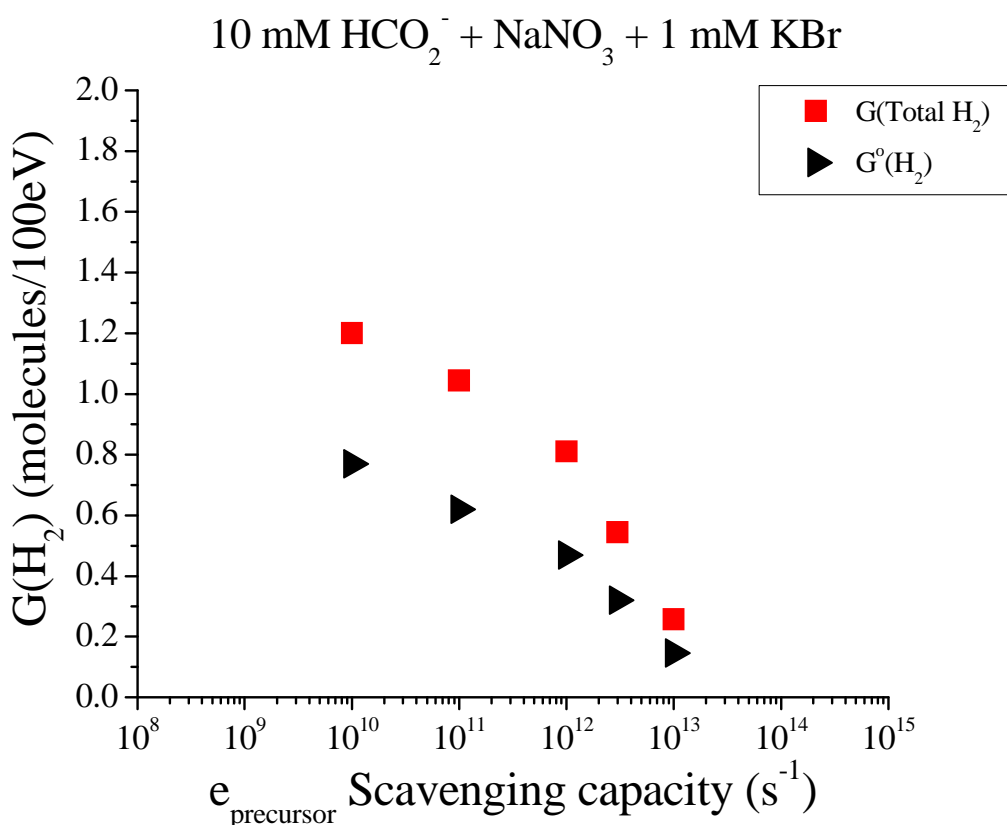


**Figure 6.8** Molecular hydrogen production in the  $^1\text{H}$ -radiolysis of aqueous 10 mM formate solutions with  $\text{NaNO}_3$  as a function of the precursor to the hydrated electron scavenging capacity.  $G^\circ(\text{H}_2)$  is the yield of  $\text{H}_2$  at different concentrations of the electron scavengers in the absence of any H atom scavenger.

The molecular hydrogen yield decreases as the electron precursor scavenging capacity increases as occurred with gamma rays. Comparison with the yields obtained in the gamma radiolysis of 10 mM formate solutions shows the total molecular hydrogen yield increasing from 0.86 to 1.20 and 0.21 to 0.26 molecules / 100 eV for the lowest and highest concentrations of added nitrate respectively.

Solutions containing 1 M deuterated formate were also irradiated as seen in figure 6.9.

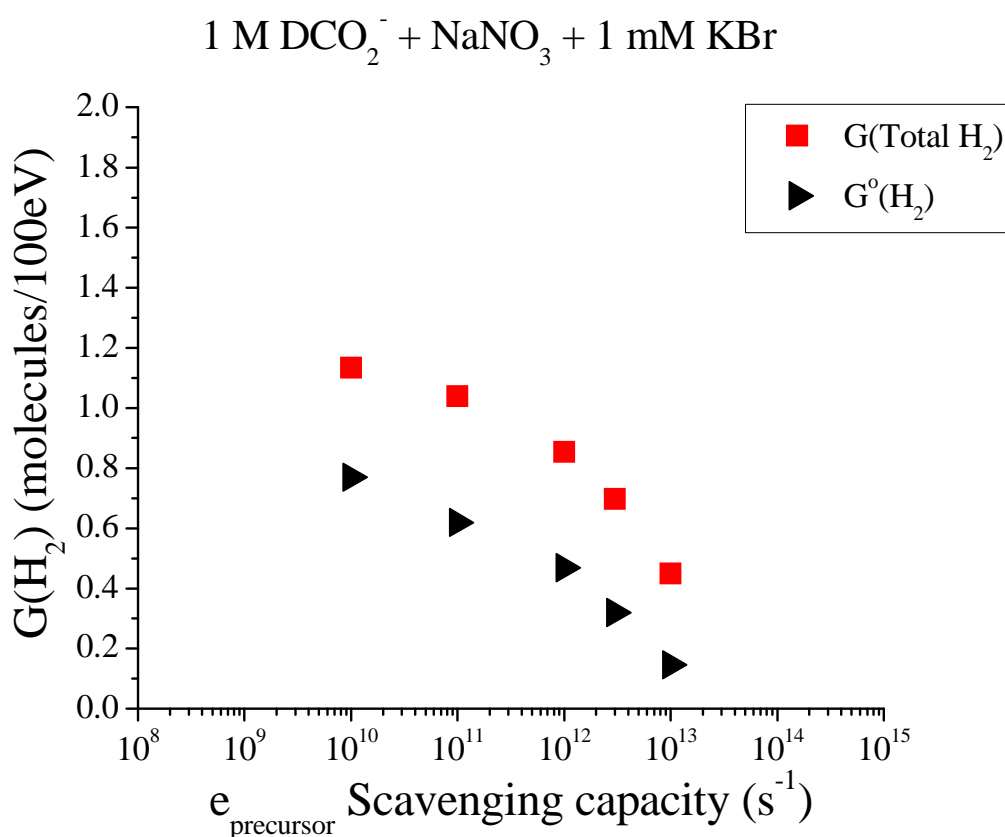


**Figure 6.9** Hydrogen production in the  $^1\text{H}$ -radiolysis of aqueous 1 M deuterated formate solutions with  $\text{NaNO}_3$  as a function of the precursor to the hydrated electron scavenging capacity.  $G^o(\text{H}_2)$  is the yield of  $\text{H}_2$  at different concentrations of the electron scavengers in the absence of any H atom scavenger.

The total molecular hydrogen yield measured in the gamma and  $^1\text{H}$  radiolysis of 1 M  $\text{DCO}_2^-$  increases from 0.91 to 1.13 and 0.41 to 0.45 molecules / 100 eV for the lowest and highest electron precursor scavenging capacity respectively. This is due to the increase in the intra track reactions as the local concentration of reactants

in the track will be more dense and the molecular hydrogen yields will increase due to an increase in  $G^{\circ}(H_2)$

A comparison of molecular hydrogen yields in the  $^1H$  radiolysis of aqueous solutions with different H atom scavenging capacities is shown in figure 6.10.

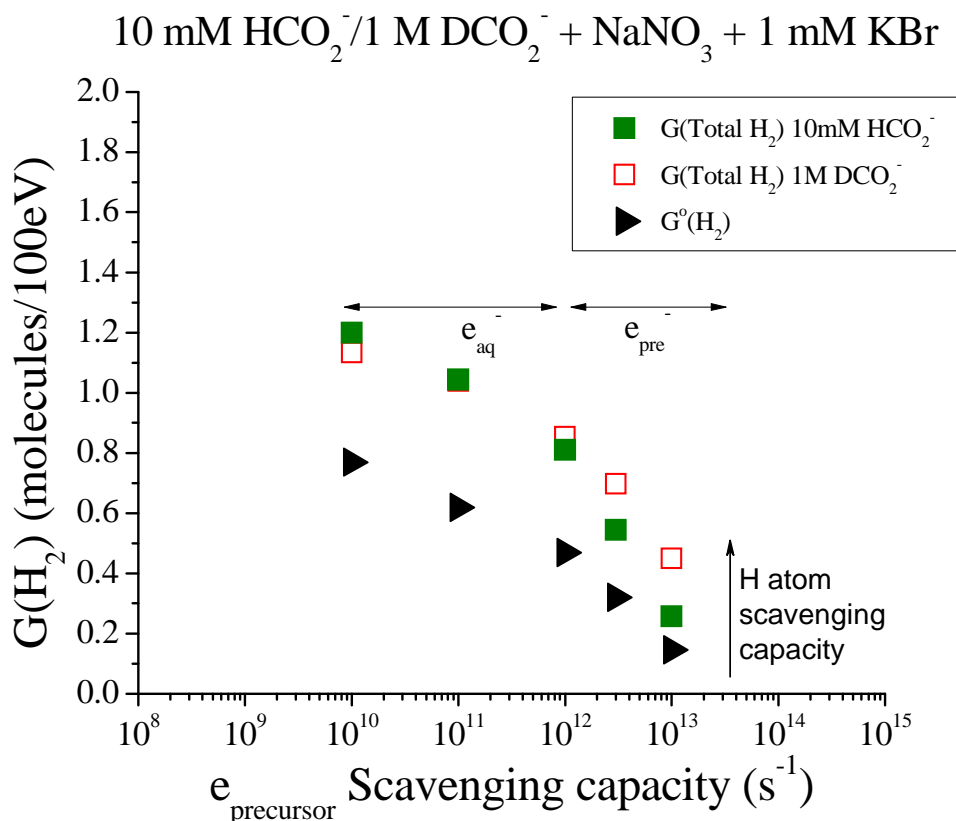


**Figure 6.10**  $H_2$  yields behavior in the  $^1H$  radiolysis of aqueous systems and in terms of the H atom scavenging capacity and the concentration of the electron scavenger.  $G^{\circ}(H_2)$  is the yield of  $H_2$  at different concentrations of the electron scavengers in the absence of any H atom scavenger.

The total molecular hydrogen yield in the  $^1H$  radiolysis of 10 mM  $HCO_2^-$  roughly matches  $G(Total H_2)$  in the  $^1H$  radiolysis of 1 M  $DCO_2^-$  at low electron precursor scavenging capacities, but drops faster at the lowest hydrogen atom scavenging capacity and the higher electron precursor scavenging capacities. This suggests that the  $G(Total H_2)$  is independent of the concentration of the hydrogen atom scavenger over the timescales where molecular hydrogen is mainly formed by the reactions of the hydrated electron and shows dependence on the concentration of

the hydrogen atom scavenger in the region where molecular hydrogen is mainly formed by the reactions of the electron precursor.

### 6.5.3 $^4\text{He}$ radiolysis

Complementary experiments to those with gamma rays and  $^1\text{H}$  ions were performed with  $^4\text{He}$  ions. First, total molecular hydrogen and hydrogen atom yields are determined in the  $^4\text{He}$  radiolysis of aqueous 10 mM formate solutions with  $\text{NaNO}_3$ .

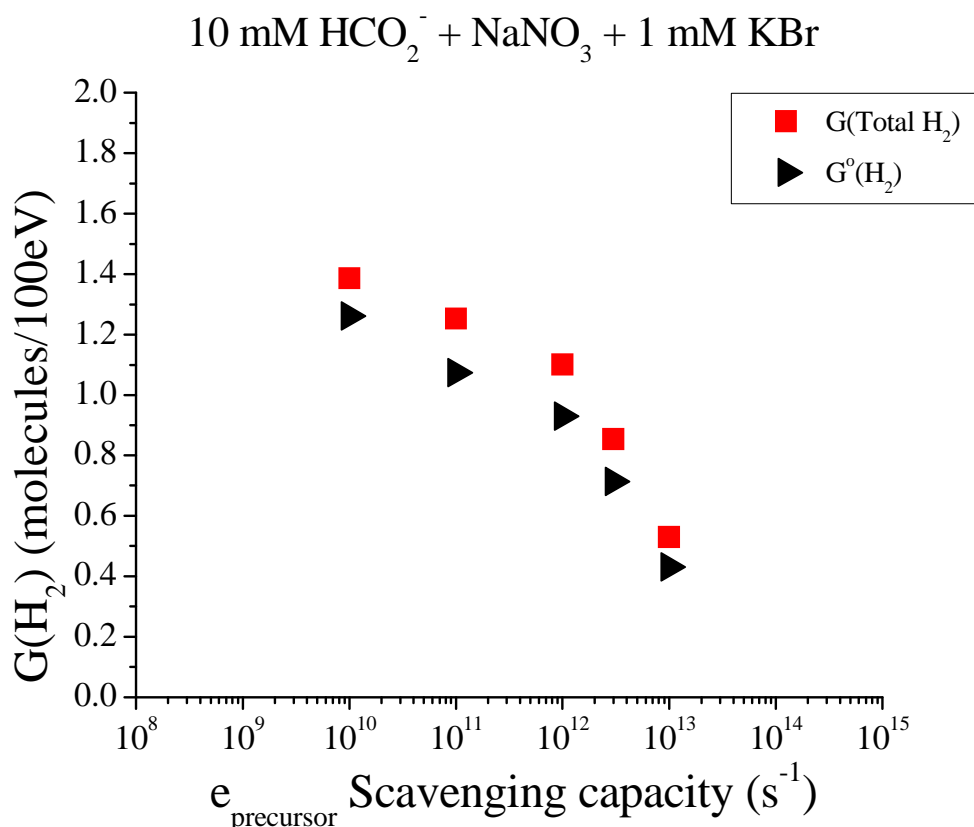


**Figure 6.11** Molecular hydrogen production in the  $^4\text{He}$ -radiolysis of aqueous 10 mM formate solutions with  $\text{NaNO}_3$  as a function of the precursor to the hydrated electron scavenging capacity.  $G^o(\text{H}_2)$  is the yield of  $\text{H}_2$  at different concentrations of the electron scavengers in the absence of any H atom scavenger.

$^4\text{He}$  ions have even higher LET values than  $^1\text{H}$  ions, which means that, an increase in the intra track reactions should be observed and, therefore, an increase in the molecular hydrogen yields. Results are compared with those obtained in the irradiation with gamma rays and  $^1\text{H}$  ions in Table 6.4.



	Gamma rays	$^1\text{H}$ Ions	$^4\text{He}$ Ions
<b>G(Total H<sub>2</sub>)</b> Molecules / 100 eV	0.86 $\xrightarrow{+}$	1.20 $\xrightarrow{+}$	1.39

**Table 6.4** Molecular hydrogen yields variation in the gamma,  $^1\text{H}$  and  $^4\text{He}$  radiolysis of 10 mM  $\text{HCO}_2^-$  with  $\text{NaNO}_3$  at the lowest considered electron precursor scavenging capacity. Arrows show the increment of G(Total H<sub>2</sub>) with LET.

Total molecular hydrogen yields have increased as expected.

Figure 6.12 shows the yield of molecular hydrogen when deuterated formate at low concentration was irradiated in the presence of nitrate and selenate.

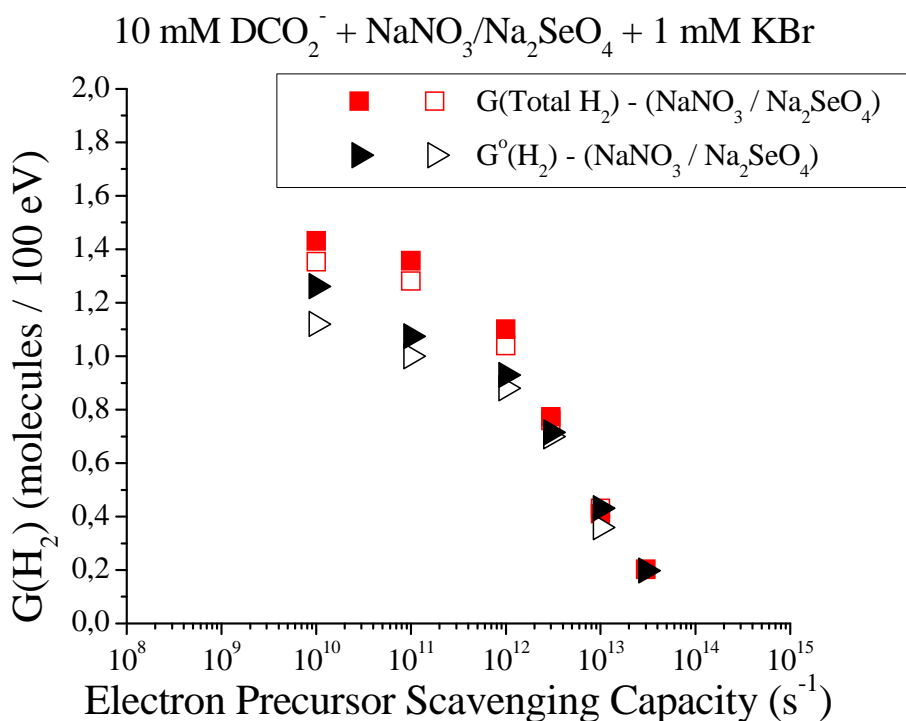


**Figure 6.12** Molecular hydrogen and H atom production in the  $^4\text{He}$ -radiolysis of aqueous 10 mM  $\text{DCO}_2^-$  solutions with  $\text{NaNO}_3$  or  $\text{Na}_2\text{SeO}_4$  as a function of the precursor to the hydrated electron scavenging capacity.  $G^0(\text{H}_2)$  is the yield of  $\text{H}_2$  at different concentrations of the  $e^-$  scavengers in the absence of any H atom scavenger.

Molecular hydrogen yields were observed to vary for the addition of  $\text{NaNO}_3$  or  $\text{Na}_2\text{SeO}_4$  from 1.43 to 0.20 and 1.35 to 0.43 molecules/100eV respectively. A good agreement is found between the two set of results for the different scavengers with only minor disagreements between  $G(\text{H}_2)$  values and  $G^0(\text{H}_2)$  values at low electron precursor scavenging capacities.

When yields are compared with those in the gamma radiolysis with nitrate added as electron scavenger, total molecular hydrogen yields increase from 0.78 to 1.43 and 0.14 to 0.20 molecules / 100 eV for the lowest and highest electron precursor scavenging capacities respectively. In the presence of selenate,  $G(\text{Total H}_2)$  increases from 0.85 to 1.35 and 0.23 to 0.43 molecules / 100 eV for the lowest and highest electron precursor scavenging capacities respectively. The molecular hydrogen yield clearly increases with LET. This emphasizes the correlation of the formation of the  $\text{H}_2$  with a second order reaction of the hydrated electron precursor.

Additional experiments with  $^4\text{He}$  ions were carried out using 1 M formate solutions with  $\text{NaNO}_3$  and  $\text{Na}_2\text{SeO}_4$ , as seen in figure 6.13.

Total  $\text{H}_2$  yields in the  $^4\text{He}$ -radiolysis of aqueous 1 M formate solutions with  $\text{NaNO}_3$ , or  $\text{Na}_2\text{SeO}_4$  are decreasing from 1.37 to 0.65 and 1.39 to 0.65 molecules/100eV respectively. There is a good agreement between the two set of results for the different electron scavengers.

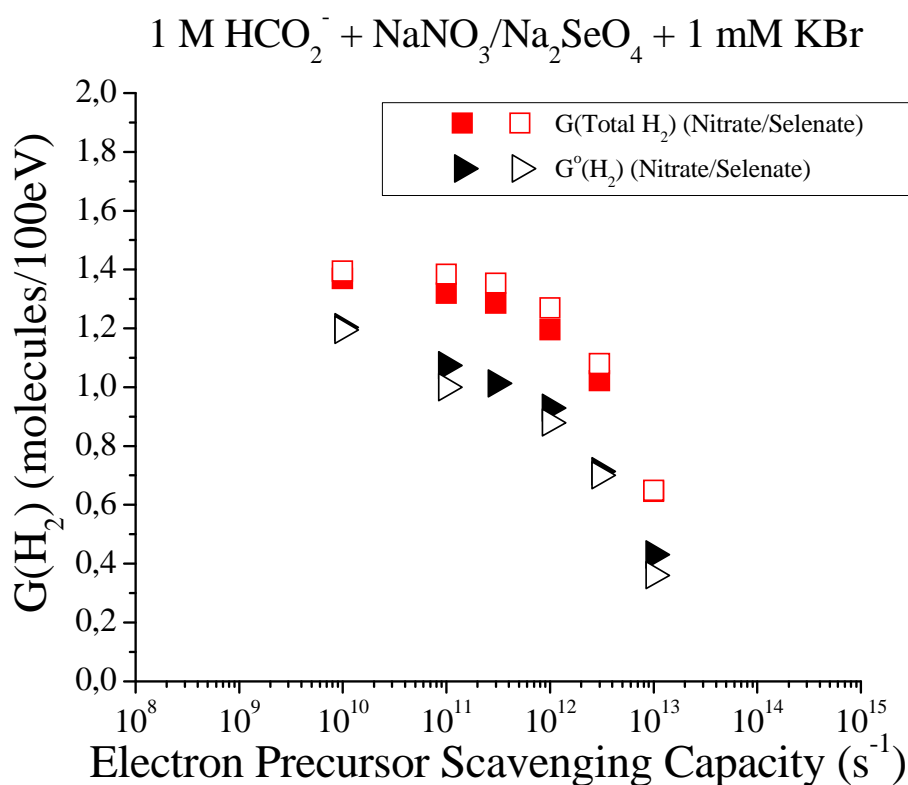


**Figure 6.13** Production of  $\text{H}_2$  in the  $^4\text{He}$ -radiolysis of aqueous 1 M formate solutions with  $\text{NaNO}_3$  or  $\text{Na}_2\text{SeO}_4$  as a function of the precursor to the hydrated electron scavenging capacity.  $G^\circ(\text{H}_2)$  is the yield of  $\text{H}_2$  at different concentrations of the electron scavengers in the absence of any H atom scavenger.

Higher concentrations of  $H_2$  were expected with increasing LET due to the increase of intra track reactions and with increased concentration of formate.

	Gamma rays	$^1H$ Ions	$^4He$ Ions
10 mM $HCO_2^-$	0.86 $\downarrow$ +	1.20 $\leftarrow$ +	1.39 $\leftarrow$
1 M $HCO_2^-$	1.21 $\downarrow$ +	1.37 $\leftarrow$ +	1.37 $\leftarrow$

**Table 6.5** Total molecular hydrogen yields variation in the gamma,  $^1H$  and  $^4He$  radiolysis of 10 mM  $HCO_2^-$  or 1 M  $HCO_2^-$  with  $NaNO_3$  at the lowest considered electron precursor scavenging capacity. Arrows show the increment of  $G(\text{Total } H_2)$  with LET.

Examination of the data in Table 6.5 shows that the molecular hydrogen yield does not increase with the hydrogen atom scavenging capacity:  $G(H_2)$  is independent of the H atom scavenging capacity in  $^4He$  irradiation.

The irradiation of 1 M  $DCO_2^-$  aqueous solutions with  $^4He$  ions is presented in figure 6.14.

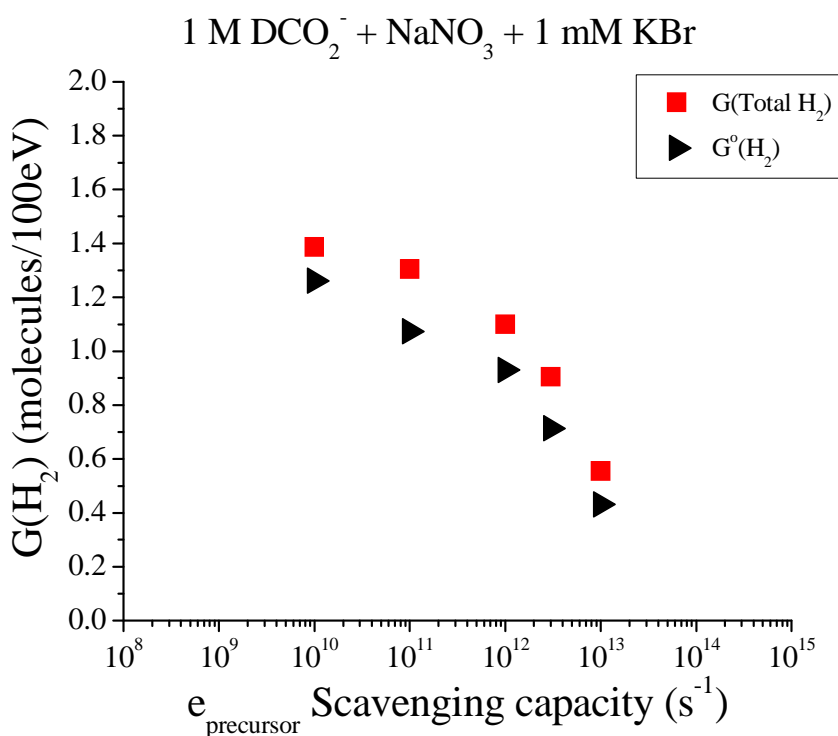


**Figure 6.14** Molecular hydrogen yields in the  $^4He$ -radiolysis of aqueous 1 M formate solutions with  $NaNO_3$  as a function of the precursor to the hydrated electron scavenging capacity.  $G^o(H_2)$  is the yield of  $H_2$  at different concentrations of the electron scavengers in the absence of any H atom scavenger.

A series of results in the gamma,  $^1\text{H}$  and  $^4\text{He}$  radiolysis of aqueous 1 M  $\text{DCO}_2^-$  solutions with nitrate have been obtained and compared in table 6.6.

	[ $\text{DCO}_2^-$ ] (M)	Gamma rays	$^1\text{H}$ Ions	$^4\text{He}$ Ions
<b>G(Total H<sub>2</sub>)</b> Molecules / 100 eV	0.01	0.78	+	1.43
	1	0.91	+	1.39

**Table 6.6** G(Total H<sub>2</sub>) in the  $\gamma$ ,  $^1\text{H}$  and  $^4\text{He}$  radiolysis of 1 M  $\text{DCO}_2^-$  solutions with  $\text{NaNO}_3$  at the lowest considered electron precursor scavenging capacity. Arrows show the increment of G(Total H<sub>2</sub>) with LET.

As it was observed in Table 6.5, G(Total H<sub>2</sub>) remains almost constant when the H atom scavenging capacity increases by two orders of magnitude in the  $^4\text{He}$  irradiation. The G(Total H<sub>2</sub>) increases with LET in both 10 mM and 1 M deuterated formate solutions due to the increase in the intra track reactions.

The behavior of the molecular hydrogen yield over four orders of magnitude of H atom scavenging capacities is considered in figure 6.15.

10 mM/1 M  $\text{HCO}_2^-$  and 10 mM/1 M  $\text{DCO}_2^- + \text{NaNO}_3 + 1 \text{ mM KBr}$

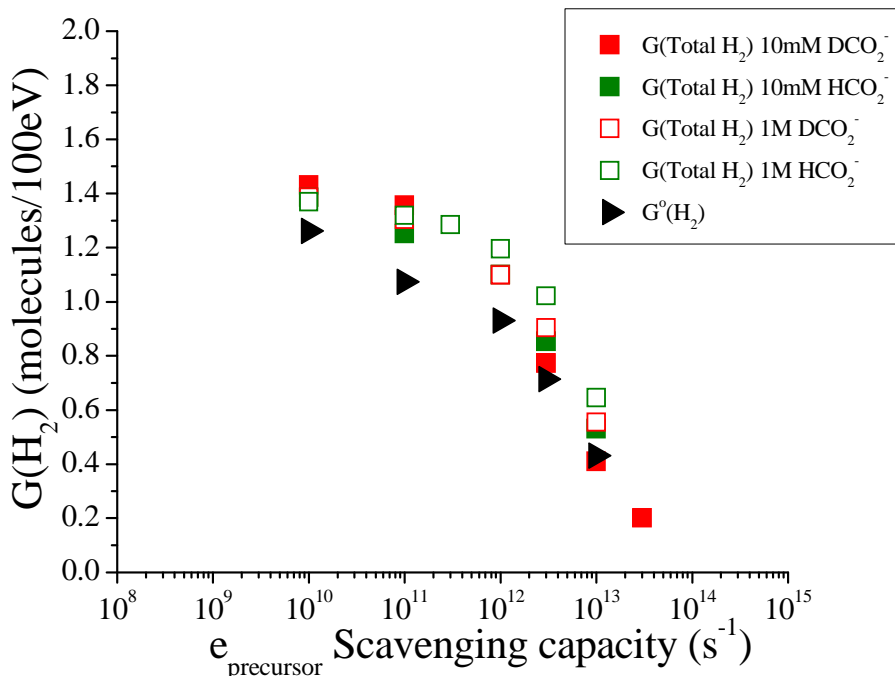


**Figure 6.15** H<sub>2</sub> yields behavior in the  $^4\text{He}$  radiolysis of aqueous systems and in terms of the H atom scavenging capacity and the concentration of the electron scavenger.  $G^0(\text{H}_2)$  is the yield of H<sub>2</sub> at different concentrations of the electron scavengers in the absence of any H atom scavenger.

$G(\text{Total H}_2)$  due to the addition of different concentrations of  $\text{HCO}_2^-$  or  $\text{DCO}_2^-$  are close together at each electron precursor scavenging capacity considered: i.e. the total  $\text{H}_2$  yield is independent of the H atom scavenging capacity. Since the total  $\text{H}_2$  yield is also similar to the  $\text{H}_2$  yield in neat water, the contribution of the H atom yield to the total  $\text{H}_2$  yield must be very small as  $G(\text{Total H}_2) = G^0(\text{H}_2) + G(\text{H atom})$ .

#### 6.5.1.4 Conclusions

Total  $\text{H}_2$  yields have been measured in the  $\gamma$ ,  $^1\text{H}$  and  $^4\text{He}$  radiolysis of aqueous  $\text{HCO}_2^-$  and  $\text{DCO}_2^-$  concentrations. The  $G(\text{Total H}_2)$  has been observed to increase with LET. A graphical representation of this increase is shown in Figure 6.16.

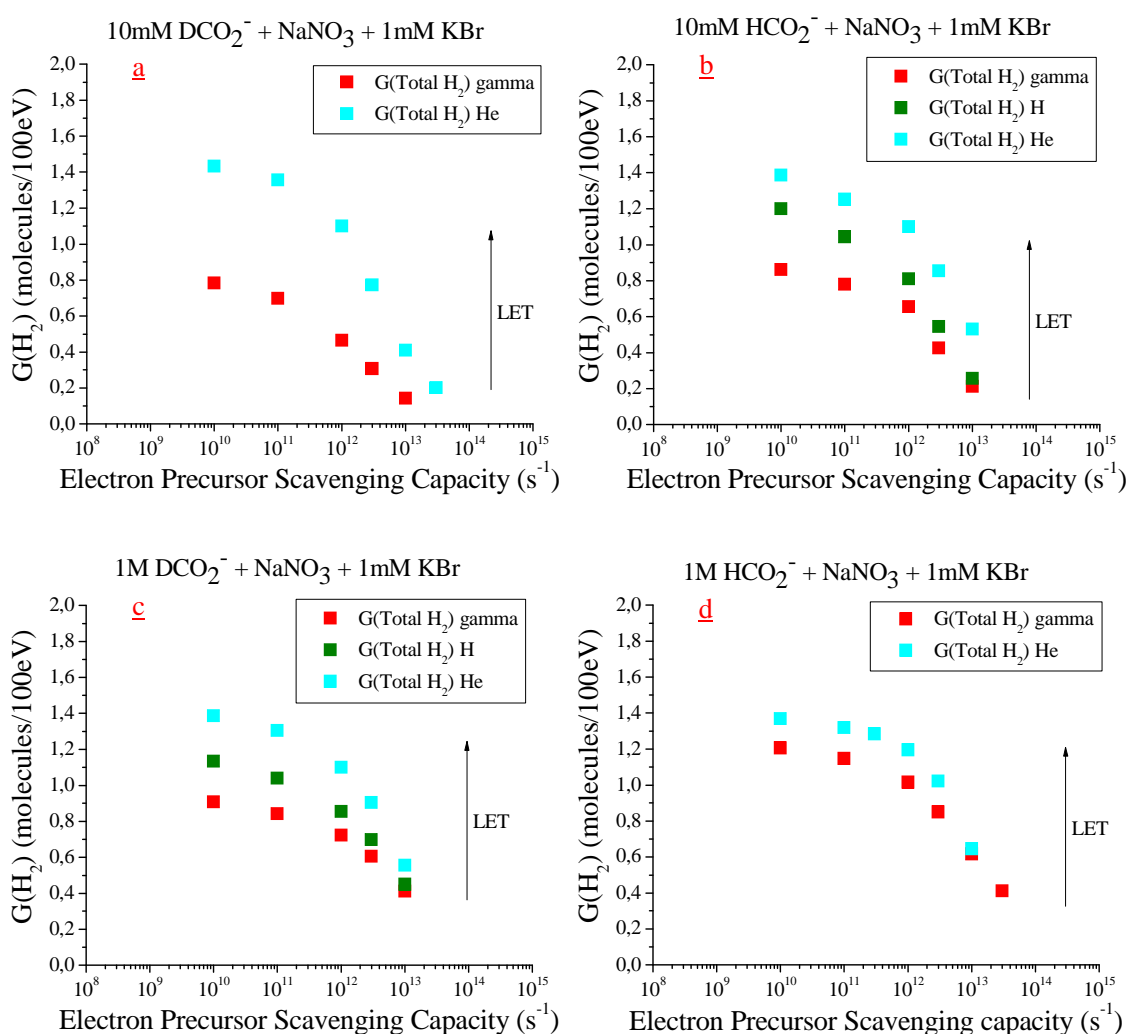


**Figure 6.16** Total molecular hydrogen yields behavior in terms of the LET value of the radiation source and the concentration of the electron scavenger.

The hydrogen atom scavenging capacity increases from a to b to c to d. In these graphs, the  $G(\text{Total H}_2)$  is clearly seen to increase with LET at each of the different H atom scavenging capacities considered.

### 6.5.2 Hydrogen atom production

Under the currently accepted model, the hydrogen atom is formed in the radiolysis of the water through the fragmentation of water excited state and the reactions of the hydrated electron and its precursor. An accurate examination of the H atom yields after radiolysis will make possible a better understanding of the initial radiolytic decomposition of water.

#### 6.5.2.1 Gamma radiolysis

Hydrogen atom yields obtained by the difference measurements of molecular hydrogen yields are presented in figure 6.17 for the gamma radiolysis of aqueous 10 mM sodium formate.

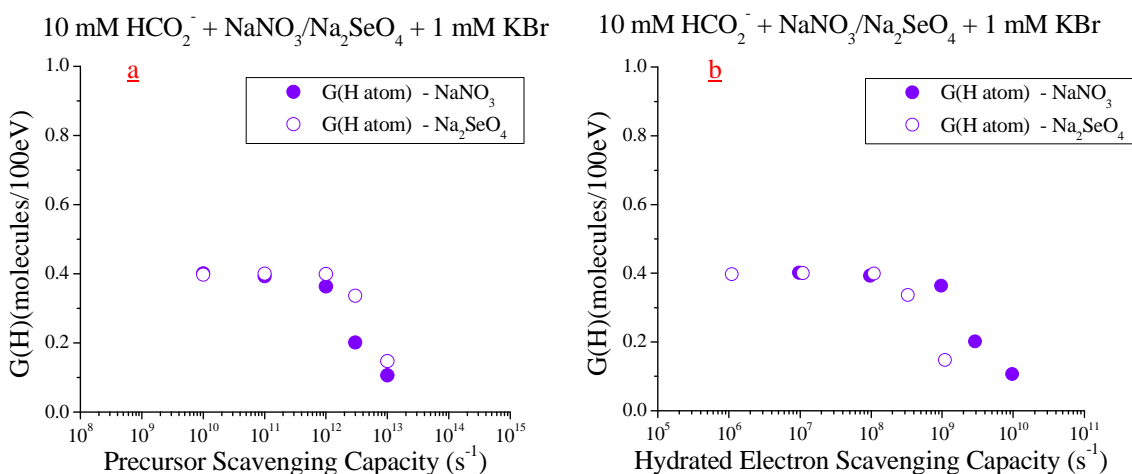


**Figure 6.17** Hydrogen atom predictions in the  $\gamma$ -radiolysis of aqueous 10 mM formate solutions with  $\text{NaNO}_3$  or  $\text{Na}_2\text{SeO}_4$  as a function of the precursor to the hydrated electron scavenging capacity (a) and the hydrated electron scavenging capacity (b).

The hydrogen atom yields vary from 0.43 to 0.10 molecules/100eV. Different curves of H atom yields are obtained in terms of the hydrated electron scavenging capacity, while similar curves of H atom yields are obtained as a function of the electron precursor scavenging capacity. In addition, a hydrogen atom yield of about

0.35 molecules/100eV is implied at about a picosecond. This timescale is too fast for the  $e_{aq}^-$  whose fastest reaction occurs with the hydrated proton at a rate of  $2.4 \times 10^{10} \text{ M}^{-1} \text{ s}^{-1}$ [16]. All this suggests a stronger dependence of the H atom formation on the reactions of the electron precursor, i.e. via



as well as on the decay of directly produced excited states, as shown in reaction 6.40.



Hydrogen atom predictions obtained from the difference measurement of molecular hydrogen yields for the  $\gamma$ -radiolysis of 1 M formate solutions are shown in Figure 6.18

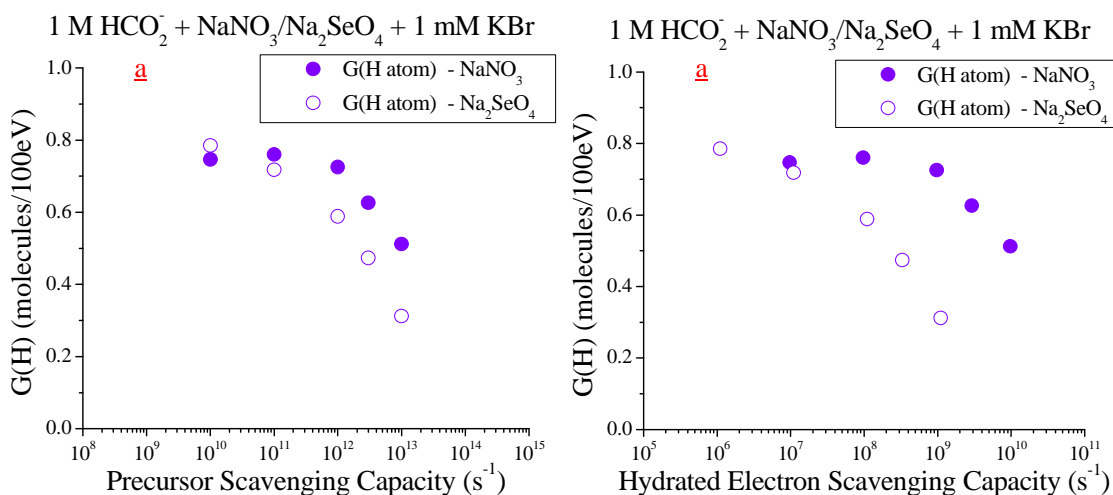


**Figure 6.18** Hydrogen atom predictions in the  $\gamma$ -radiolysis of aqueous 1 M formate solutions with  $\text{NaNO}_3$  or  $\text{Na}_2\text{SeO}_4$  as a function of the precursor to the hydrated electron (a) and the hydrated electron scavenging capacity (b).

Similar hydrogen atom yields were obtained for nitrate and selenate solutions at low concentrations of the electron scavengers, however, slight differences are observed at higher concentrations. The similarity of the curves of H atom yields as a function of the electron precursor scavenging capacity highlights the stronger dependence of the H atom formation on the early events occurring in the radiolysis of water. From now on, hydrogen atom yields will be expressed in terms of the electron precursor scavenging capacity.

Yields obtained from the irradiation of 10 mM deuterated formate with gamma rays are shown in figure 6.19 as a function of the precursor to the hydrated electron scavenger capacity.

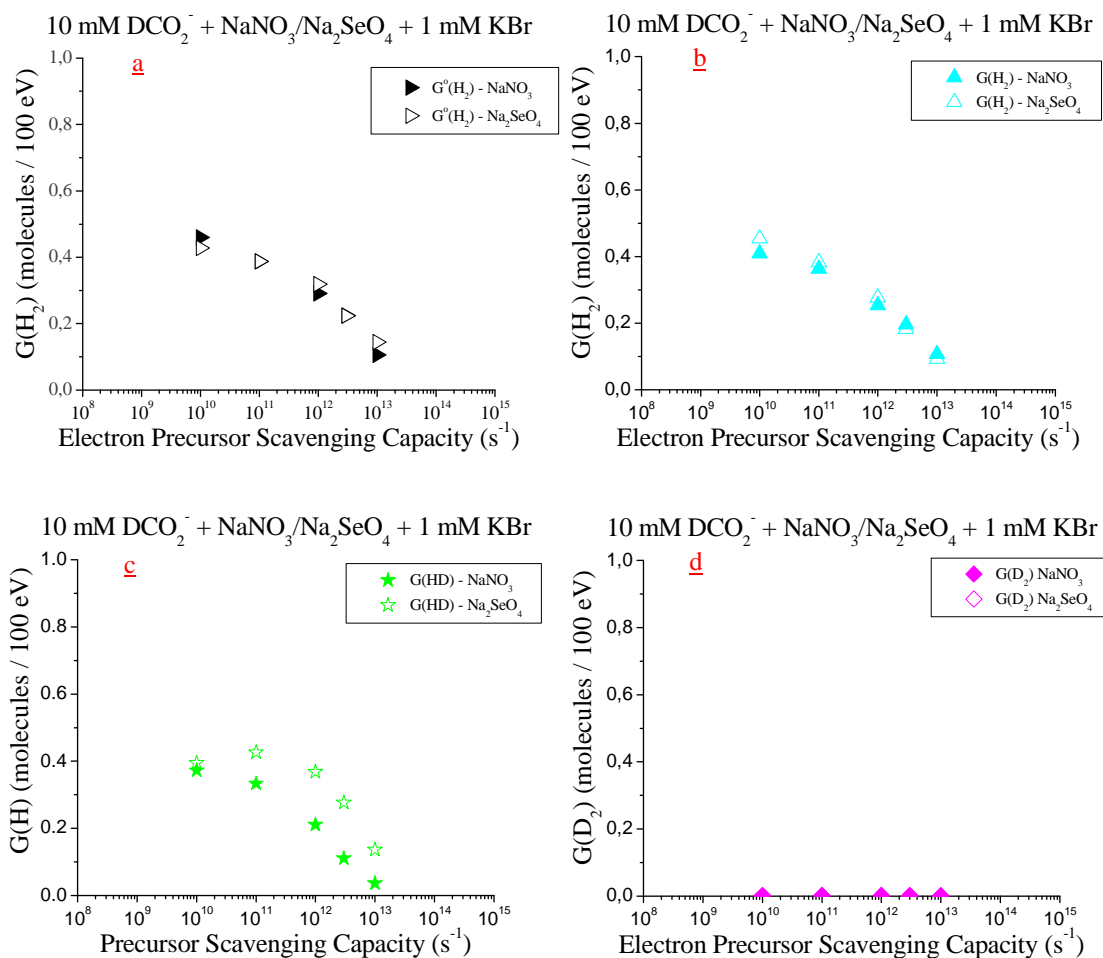


**Figure 6.19** Hydrogen atom and molecular hydrogen production in the  $\gamma$ -radiolysis of aqueous 10 mM deuterated formate solutions with NaNO<sub>3</sub> or Na<sub>2</sub>SeO<sub>4</sub> as a function of the precursor to the hydrated electron scavenging capacity.  $G^0(H_2)$  is the yield of H<sub>2</sub> at different concentrations of the electron scavengers in the absence of any H atom scavenger.

The results have been presented in four different graphs for a better understanding. Good agreement is found between  $G(H_2)$  and  $G^0(H_2)$  obtained from both electron scavengers. Hydrogen atom yields are higher in selenate rather than nitrate solution. HD atom yields determined in the  $\gamma$ -radiolysis of aqueous 10 mM deuterated formate solutions with NaNO<sub>3</sub> or Na<sub>2</sub>SeO<sub>4</sub> are ranging from 0.37 to 0.04 and 0.39 to 0.14 molecules/100eV respectively. No significant yield of D<sub>2</sub> is measured.



Results in terms of the added electron scavenger are presented next in separated graphs for discussion.

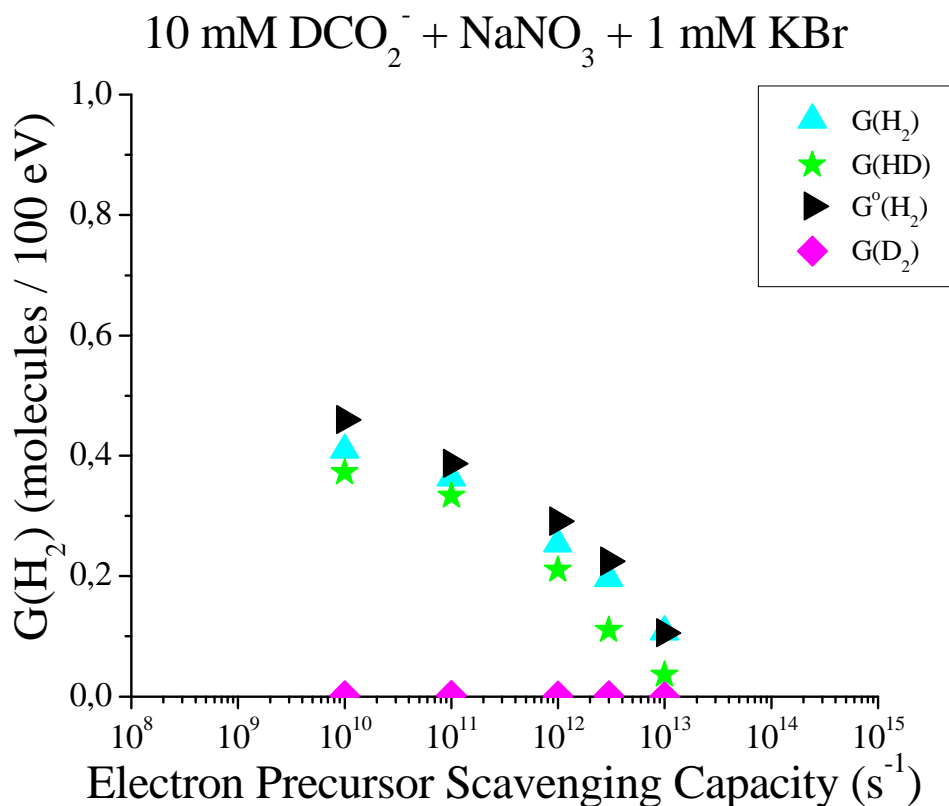
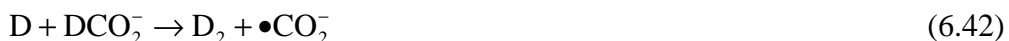


**Figure 6.20** Hydrogen production in the  $\gamma$ -radiolysis of aqueous 10 mM deuterated formate solutions with  $\text{NaNO}_3$  as a function of the precursor to the hydrated electron scavenging capacity.  $G^\circ(\text{H}_2)$  is the yield of  $\text{H}_2$  at different concentrations of the electron scavengers in the absence of any H atom scavenger.

The molecular hydrogen yield decreases as the concentration of the electron scavenger increases. In the presence of deuterated formate, molecular hydrogen should be only formed due to the radiolysis of water, which means that  $G(\text{H}_2)$  should agree with  $G^\circ(\text{H}_2)$  obtained in neat water. Hydrogen atom yields obtained from the direct measurement of HD yields are seen to be lower than  $\text{H}_2$  yields. The yield of  $G(\text{D}_2)$  is nearly zero ( $\sim 0.001$  molecules / 100 eV) as its formation would require either



or



At high concentrations of deuterated formate, production of deuterium atom by direct radiolysis of the solute is possible [17],



but this is not expected to be important in 10 mM solutions.

Something similar is observed when selenate is added as electron scavenger, as seen in figure 6.21.

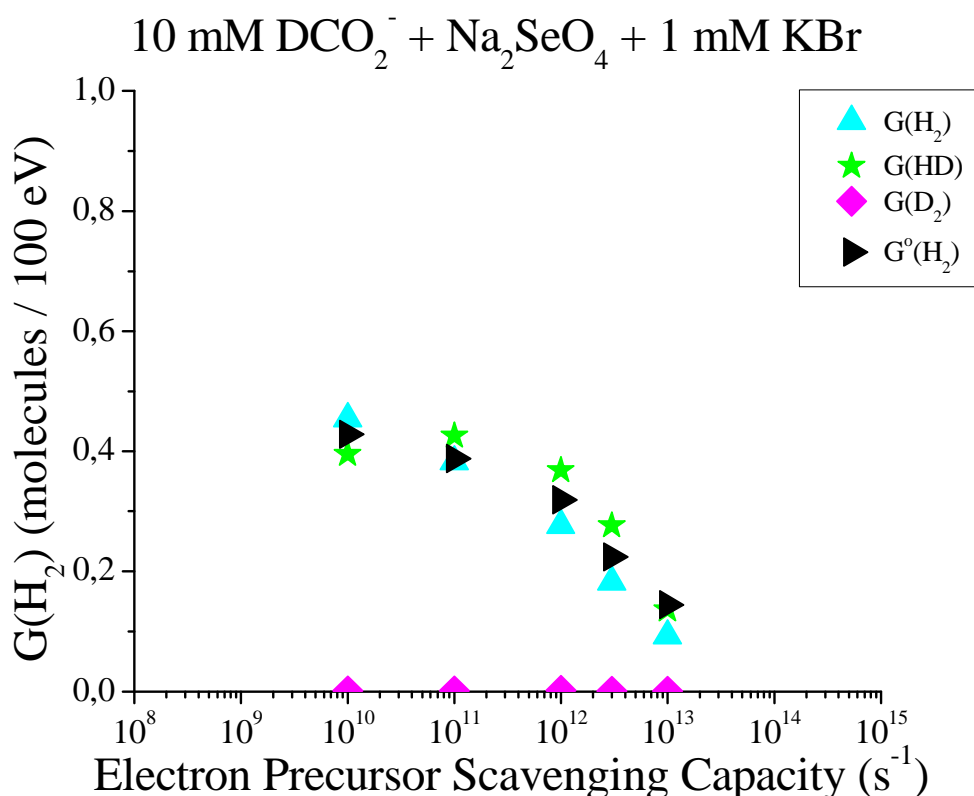


**Figure 6.21** Hydrogen production in the  $\gamma$ -radiolysis of aqueous 10 mM deuterated formate solutions with  $\text{Na}_2\text{SeO}_4$  as a function of the precursor to the hydrated electron scavenging capacity.  $G^0(\text{H}_2)$  is the yield of  $\text{H}_2$  at different concentrations of the electron scavengers in the absence of any H atom scavenger.

Good agreement is shown between  $G(\text{H}_2)$  and  $G^0(\text{H}_2)$  as the only molecular hydrogen formed in the presence of deuterated formate is due to the radiolysis of water. Nearly zero molecular deuterium yields are obtained due to the small concentration of deuterated formate and therefore, the low probability of deuterium

atoms production by direct radiolysis of the solute and subsequent generation of  $D_2$  molecules.

Figure 6.22, as an enlargement of Figure 6.19c presented before, shows the yield of HD in the gamma radiolysis of solutions of nitrate and selenate. There are clear differences between the results. H atom yields in  $SeO_4^{2-}$  solutions are slightly higher than those ones obtained through the addition of nitrate as electron scavenger.

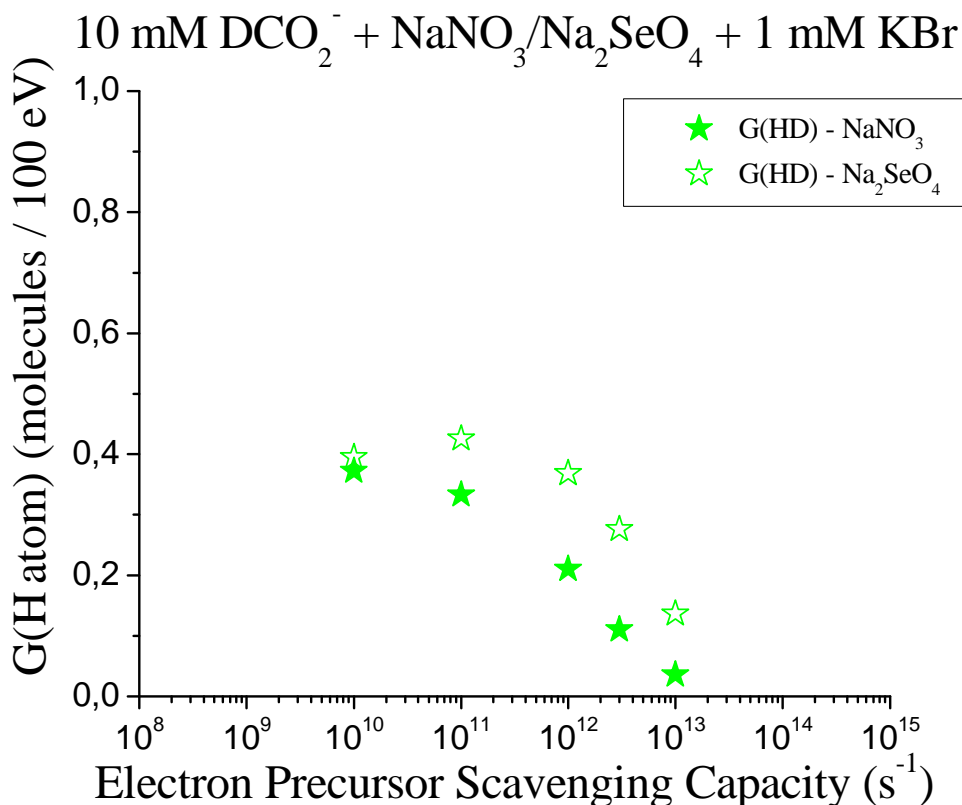


**Figure 6.22** Production of HD in the  $\gamma$ -radiolysis of aqueous 10 mM deuterated formate solutions with  $NaNO_3$  or  $Na_2SeO_4$  as a function of the precursor to the hydrated electron scavenging capacity.

This can be explained by comparing the reactivity of both electron scavengers with the H atom,



with  $k_{45} = 1.6 \times 10^6 \text{ M}^{-1} \text{ s}^{-1}$  [12],  $k_{46} = 1.0 \times 10^{10} \text{ M}^{-1} \text{ s}^{-1}$  [18] and  $k_{47} = 7.1 \times 10^8 \text{ M}^{-1} \text{ s}^{-1}$  [12], and



where  $k_{48} < 1.0 \times 10^6 \text{ M}^{-1} \text{ s}^{-1}$  and  $k_{49} < 1.0 \times 10^6 \text{ M}^{-1} \text{ s}^{-1}$  [6]. Nitrite and nitrogen dioxide may react with the hydrogen atom while selenate and its derivatives do not react significantly. This allows to hypothesize an expected lower  $G(\text{HD})$  when nitrate was considered rather than selenate.

Figure 6.23 shows the results from the  $\gamma$  radiolysis of aqueous 1 M deuterated formate solutions with added  $\text{NaNO}_3$ . No experiments were carried out with addition of selenate at this concentration.

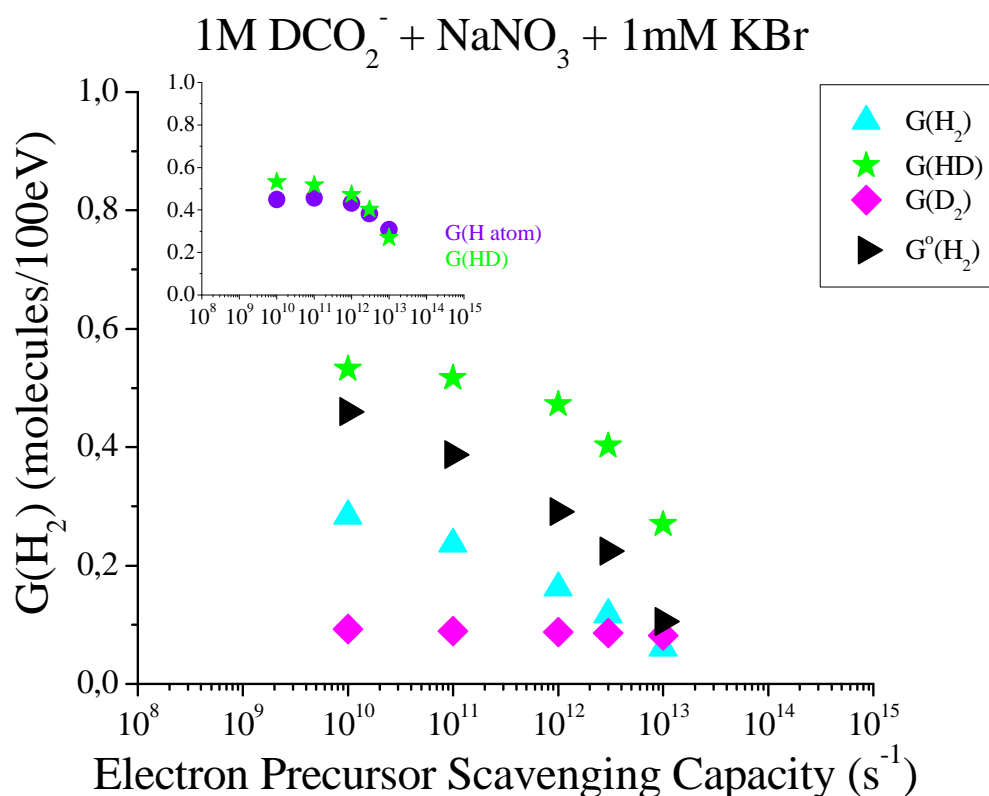


**Figure 6.23** Hydrogen production in the  $\gamma$ -radiolysis of aqueous 1 M deuterated formate solutions with  $\text{NaNO}_3$  as a function of the precursor to the hydrated electron scavenging capacity.  $G(\text{H atom}) = G(\text{Total H}_2) - G^0(\text{H}_2)$ .  $G^0(\text{H}_2)$  is the yield of  $\text{H}_2$  at different concentrations of the electron scavengers in the absence of any H atom scavenger.

Higher HD yields than those obtained at low concentrations of deuterated formate, are obtained. In addition, significant  $G(D_2)$  are observed due to reactions 6.43 and 6.44 at this high concentration of deuterated formate [17]. The expected  $G(D_2)$  can be approximated by determining the energy received by the solute

Solute	Number of electrons	Concentration (M)	% of energy received
H <sub>2</sub> O	10	55	95.65
DCO <sub>2</sub> <sup>-</sup>	25	1	4.35

**Table 6.7** Percentage of energy received by solute depending on the number of electrons and the concentration of the solute.

Considering that  $G(\text{ionization} + \text{excitation}) \sim 5$  molecules / 100 eV [19], it can be approximated that  $G(\text{D atom}) \sim 0.22$  molecules / 100 eV which implies that  $G(D_2) \sim 0.11$  molecules / 100 eV. The experimental values obtained vary from 0.081 to 0.09 molecules / 100 eV which shows a good approximation to the expected value.

A lower  $G(H_2)$  compared to  $G^0(H_2)$  is obtained at this high concentration of the deuterated formate. This is partially due to the reaction of the deuterium atoms, generated in the direct radiolysis of the solute, with the H atom decreasing  $G(H_2)$  but increasing  $G(HD)$ . In fact, the  $G(HD)$  is observed to be slightly higher than the  $G(\text{H atom})$  obtained by the difference method. This discrepancy will be examined more thoroughly when irradiation is performed with <sup>1</sup>H and <sup>4</sup>He ions.

A two dimensional grid of results varying scavenging capacities logarithmically for the H atom and from the electron precursor from  $10^5$  to  $10^9$  s<sup>-1</sup> and  $10^{10}$  to  $10^{13}$  s<sup>-1</sup> respectively, has been obtained in the gamma radiolysis of sodium formate or deuterated formate solutions with added nitrate.

The complete variation of the hydrogen atom yield in the gamma radiolysis is shown in figure 6.24.

10 mM/1 M  $\text{HCO}_2^-$  and 10 mM/1 M  $\text{DCO}_2^- + \text{NaNO}_3 + 1 \text{ mM KBr}$

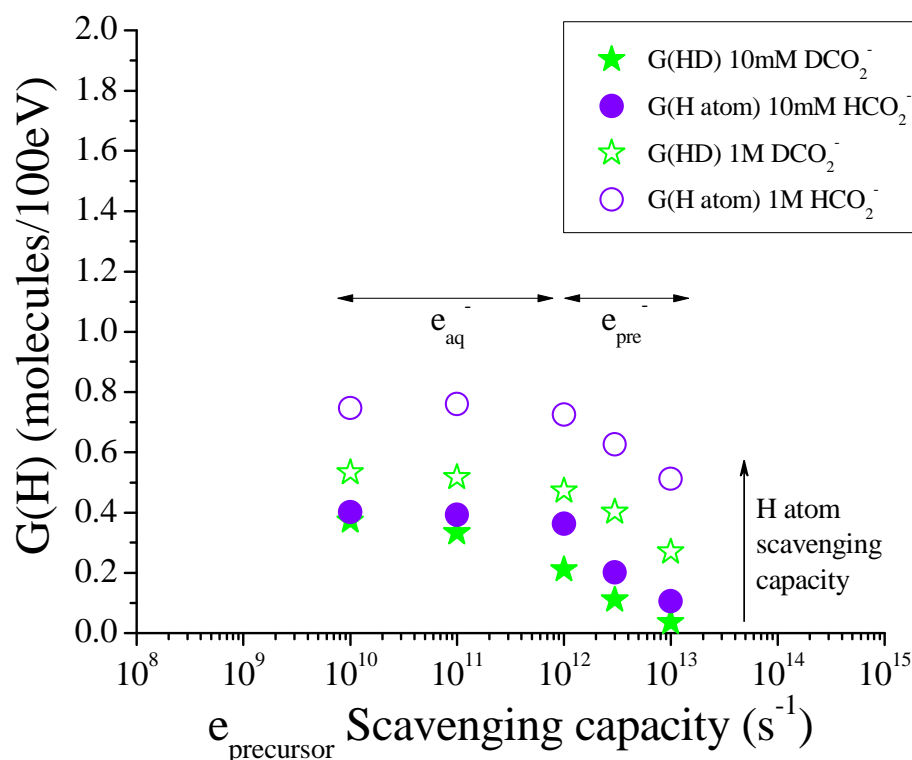


**Figure 6.24** Hydrogen atom yields behavior in the gamma radiolysis of aqueous systems and in terms of the H atom scavenging capacity and the scavenging capacity of the electron scavenger.

$G(\text{H atom})$  shows a similar pattern to that observed for  $G(\text{Total H}_2)$  increasing as the hydrogen atom scavenging capacity increases due to the more effective hydrogen atom scavenging. Hydrogen atom yields are especially high in the radiolysis of aqueous 1 M formate solutions mainly due to the high concentration of the solute and reactions 6.22, 6.23 and 6.26. The hydrogen atom yield remains constant at each H atom scavenging capacity over the range of  $e^-$  precursor scavenging capacity from  $10^{10}$  to  $10^{12} \text{ s}^{-1}$  then decreases at high concentrations of the scavenger of the electron precursor. This variation shows the independence of the hydrogen atom yield on the reactions of the hydrated electron.

The hydrogen atom formation is interpreted as a function of time (assuming  $t \sim (\text{scavenging capacity})^{-1}$ ) in figure 6.25. The H atom starts being formed at around a few hundred femtoseconds ( $\sim 0.1 \text{ ps}$ ) due to the reactions of the electron precursor, reaches its maximum value at around 1 - 2 picoseconds and remain constant until at

least a few hundred picoseconds showing its independence on the reactions of the hydrated electron.

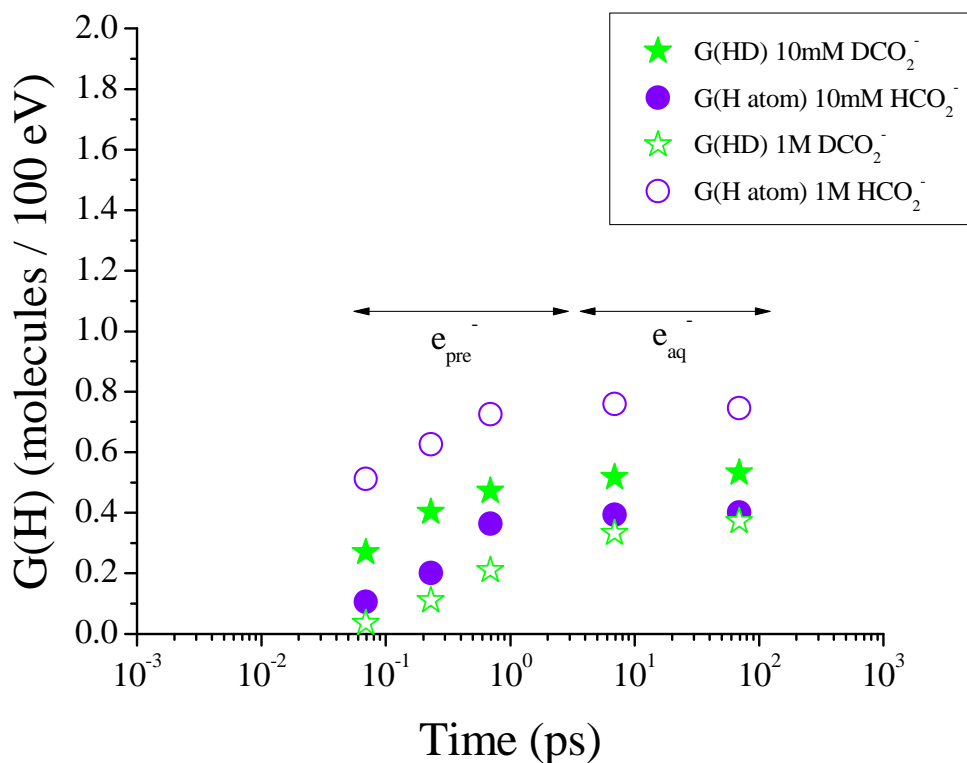


**Figure 6.25** Hydrogen atom production as a function of time in the gamma radiolysis of aqueous systems, where times are estimated as:  $t = \ln 2 / (k_{\text{NaNO}_3 + e_{\text{pre}}} [\text{NaNO}_3])$

#### 6.5.2.2 $^1\text{H}$ radiolysis

$^1\text{H}$  ions have higher LET values than the Compton scattered electrons of gamma rays. This means that an increase in the intra track reactions should be observed. The expected consequence is that the local concentration of reactants in the track will be denser and the molecular hydrogen yields will increase. H atom is formed in the radiolysis of water through the fragmentation of water excited state and the reactions of the hydrated electron and its precursor. It is expected to undergo fast reactions with other species in the track due to the increase in the concentration of reactive radicals, however, the competing effects of these reactions are unclear a priori.

The  $^1\text{H}$  irradiation of sodium formate or sodium deuterated formate aqueous solutions with added nitrate and 1 mM bromide was carried out. Firstly, the

hydrogen production in the  $^1\text{H}$  radiolysis of aqueous 10 mM formate solutions with added  $\text{NaNO}_3$  is presented in figure 6.26.

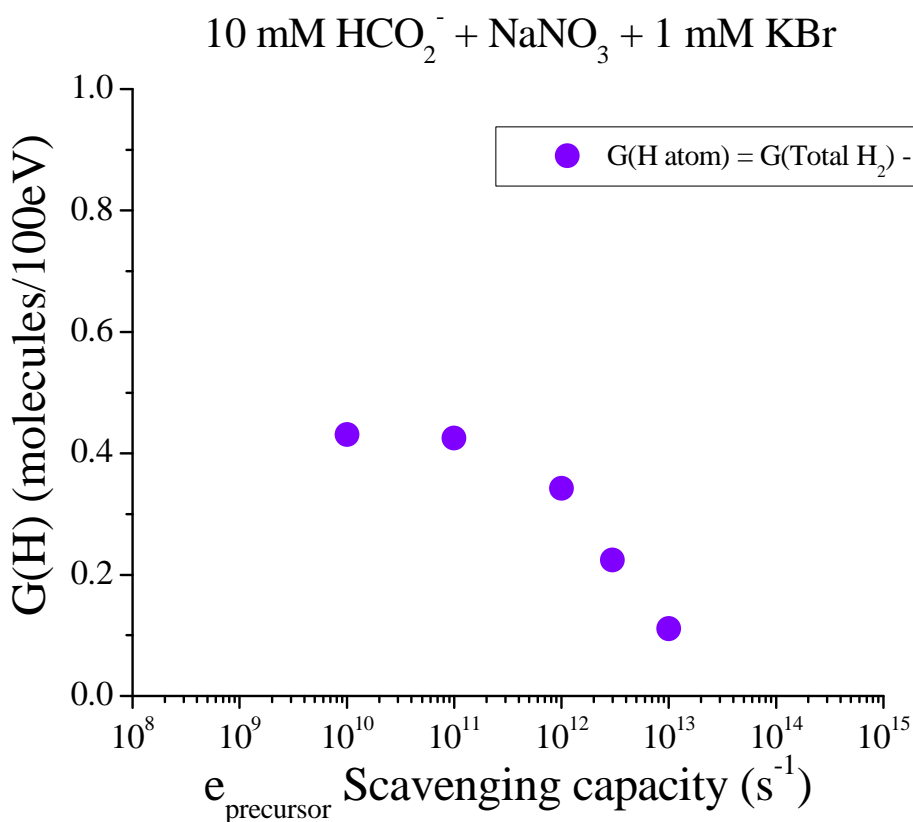


**Figure 6.26** Hydrogen production in the  $^1\text{H}$ -radiolysis of aqueous 10 mM formate solutions with  $\text{NaNO}_3$  as a function of the precursor to the hydrated electron scavenging capacity.

The hydrogen atom yield remains constant up to a scavenging capacity of  $10^{11} \text{ s}^{-1}$  before decreasing. Comparison with the yields obtained in the gamma radiolysis of 10 mM formate solutions shows essentially no change in the H atom yield with values 0.40 and 0.43, and 0.11 and 0.11 molecules / 100 eV at electron precursor scavenging capacities of  $10^{10}$  and  $10^{13} \text{ s}^{-1}$  respectively.

The yields of  $\text{H}_2$ , HD and  $\text{D}_2$  from the  $^1\text{H}$  ion irradiation of solutions containing 1 M deuterated formate are as shown in figure 6.27.



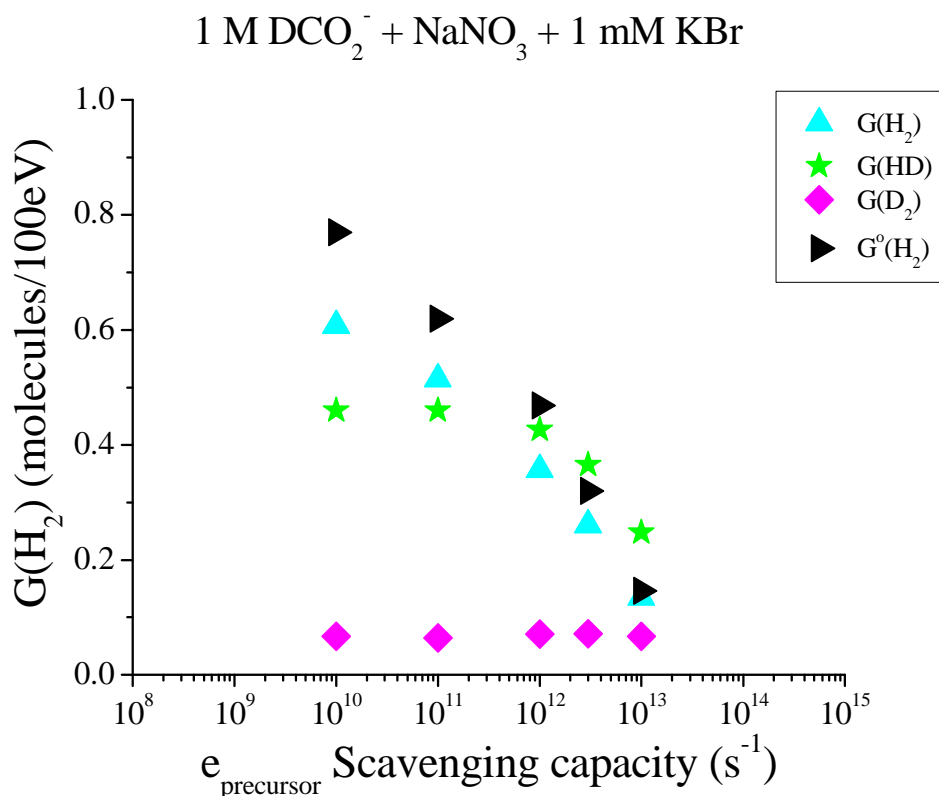


**Figure 6.27** Hydrogen production in the  $^1\text{H}$ -radiolysis of aqueous 1 M deuterated formate solutions with  $\text{NaNO}_3$  as a function of the precursor to the hydrated electron scavenging capacity.  $G^0(\text{H}_2)$  is the yield of  $\text{H}_2$  at different concentrations of the electron scavengers in the absence of any H atom scavenger.

Compared with the yields obtained in the gamma radiolysis of aqueous 1 M deuterated formate solutions, HD yields slightly decrease from 0.53 to 0.46 and 0.27 to 0.25 molecules / 100 eV.

The molecular deuterium yield is measurable due to the high concentration of deuterated formate facilitating reactions 6.43 and 6.44. The yield is independent of the electron scavenging capacity as expected from the mechanism for D production.

The molecular hydrogen yield clearly decreases as the electron scavenging capacity increases while  $G(\text{HD})$  remains almost constant until high electron precursor scavenging capacities ( $\sim 10^{12} \text{ s}^{-1}$ ) in the region where H atom yields are formed due to the reactions of the precursor to the hydrated electron. This underlines the independence of the scavenging of the H atom on the reactions of the hydrated electron in the 5 MeV  $^1\text{H}$  irradiation. Lower  $G(\text{H}_2)$  compared to  $G^0(\text{H}_2)$  are again obtained as was the case in the gamma radiolysis of aqueous 1 M deuterated formate solutions. The direct radiolysis of the solute generates additional atoms of deuterium

which may decrease the formation of molecular hydrogen and increase the formation of HD molecules. In addition,  $G(\text{HD})$  are also observed to be slightly higher than  $G(\text{H atom})$  obtained by the difference method. This supports the assumption of the deuterium atoms, formed through the direct radiolysis of the solute, reacting with H atoms to decrease molecular hydrogen yields and increase HD yields.

Hydrogen atom yields in the  $^1\text{H}$  radiolysis of aqueous solutions with different H atom scavenging capacities are compared in Figure 6.28.

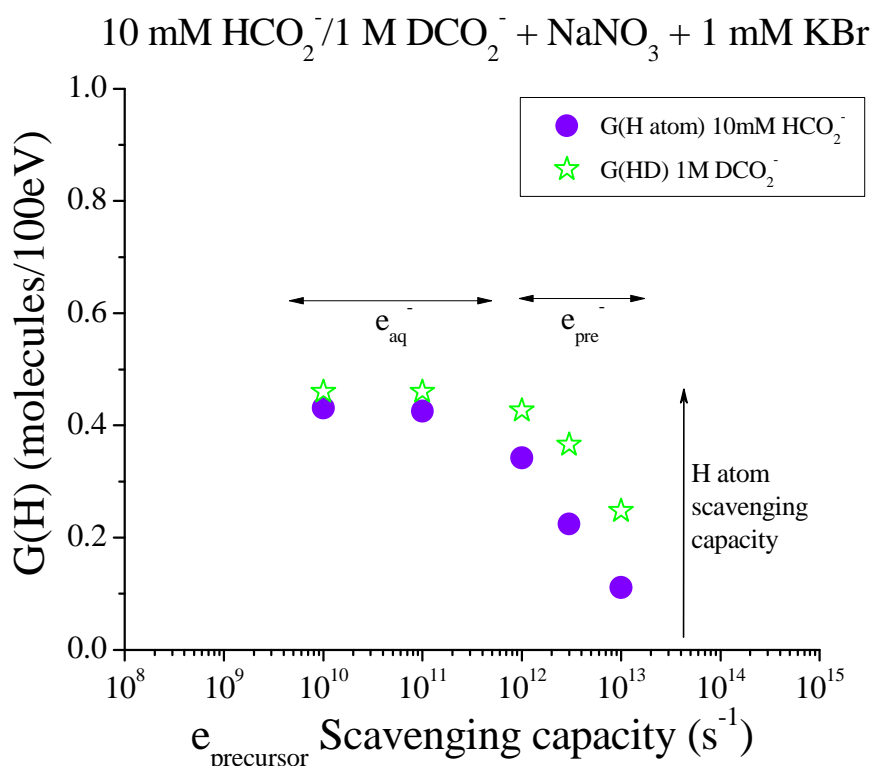


**Figure 6.28** Hydrogen atom yields in the  $^1\text{H}$  radiolysis of aqueous systems in terms of the H atom scavenging capacity and the concentration of the electron scavenger.

Hydrogen atom yields remain constant until high scavenging capacities of the electron scavenger at both concentrations of the H atom scavenger. No substantial differences are found between yields obtained from the two solutions at each electron precursor scavenging capacity despite an order of magnitude difference in the H atom scavenging capacity. This suggests again the independence of the H atom yield on the concentration of the hydrogen atom scavenger and the reactions of the hydrated electron in the 5 MeV  $^1\text{H}$  radiolysis of aqueous solutions containing formate or deuterated formate.

6.5.2.3  $^4\text{He}$  radiolysis

Hydrogen atom yields are determined in the  $^4\text{He}$  radiolysis of aqueous 10 mM formate solutions with  $\text{NaNO}_3$  are presented in Figure 6.29.

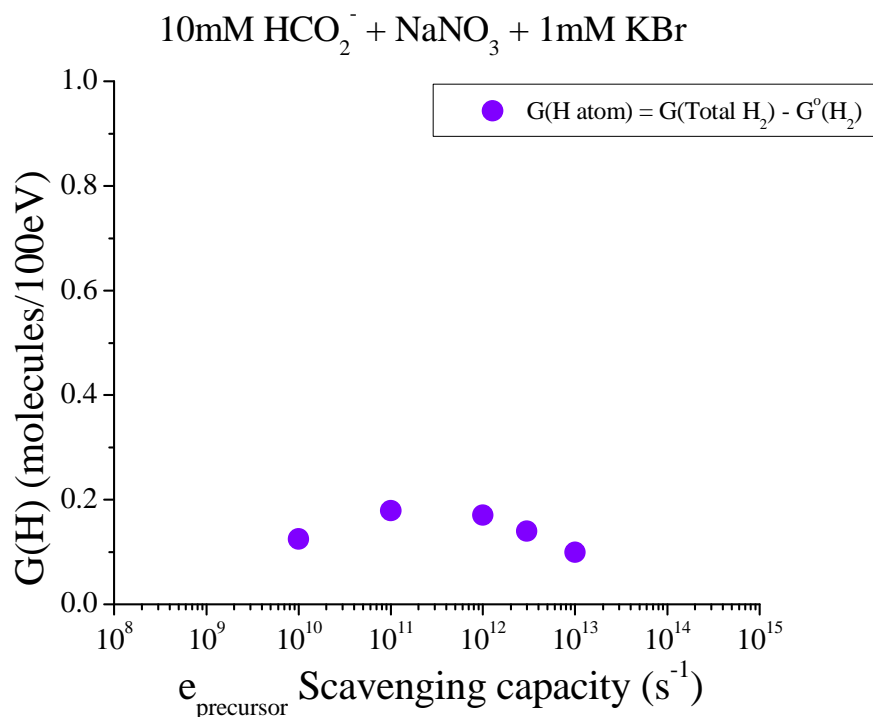


**Figure 6.29** H atom production in the  $^4\text{He}$ -radiolysis of aqueous 10 mM formate solutions with  $\text{NaNO}_3$  as a function of the precursor to the  $e_{aq}^-$  scavenging capacity.

$^4\text{He}$  ions have even higher LET than  $^1\text{H}$  ions of the same energy, which means that, an increase in the intra track reactions should be observed. The expected effect on the hydrogen atom yield is not clear since it might either decrease due to the increase in the intra track reactions of the hydrogen atom with other species in solution or increase due to the increase in the intra track reaction of the precursor to the hydrated electron with  $\text{H}_2\text{O}^+$  or of hydrated electrons with  $\text{H}_{aq}^+$ . Results are compared with those obtained in the irradiation with gamma rays and  $^1\text{H}$  ions in Table 6.8.

	Gamma rays	$^1\text{H}$ Ions	$^4\text{He}$ Ions
<b>G(H atom) Molecules / 100 eV</b>	0.40	0.43	0.13

- - - - ->

**Table 6.8** H atom yield variation in the gamma,  $^1\text{H}$  and  $^4\text{He}$  radiolysis of 10 mM  $\text{HCO}_2^-$  with  $\text{NaNO}_3$  at the lowest considered electron precursor scavenging capacity. The arrows show the behavior of the  $G(\text{H atom})$  with LET.

H atom yields markedly decrease. The increase in the intra track reactions produces the hydrogen atom to react faster with other species in the track decreasing its total yield. However, a slightly lower  $G(H \text{ atom})$  is obtained at the lowest electron scavenger capacity compared with H atom yields at higher concentrations of the electron scavenger. This might be due to either an experimental error or a chemical effect. The observation of this anomalous behaviour at higher concentrations of the hydrogen atom scavenger will elucidate its real nature.

The effect of  $^4\text{He}$  in irradiation of 10 mM  $\text{DCO}_2^-$  is shown in figure 6.30.

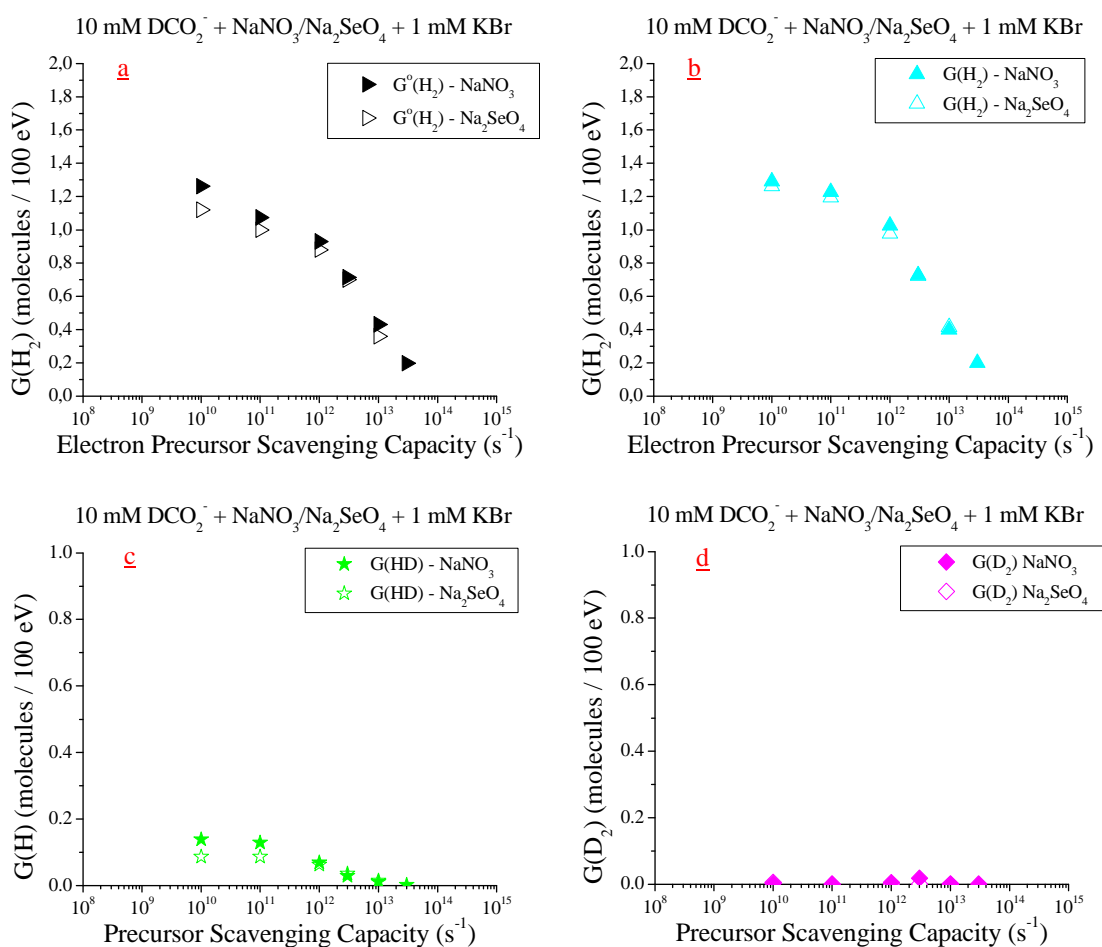


**Figure 6.30**  $\text{H}_2$  and H atom production in the  $^4\text{He}$ -radiolysis of aqueous 10 mM deuterated formate solutions with  $\text{NaNO}_3$  or  $\text{Na}_2\text{SeO}_4$  as a function of the precursor to the hydrated electron scavenging capacity.  $G^\circ(\text{H}_2)$  is the yield of  $\text{H}_2$  at different concentrations of the electron scavengers in the absence of any H atom scavenger.

HD yields range from 0.14 to 0.002 and 0.08 to 0.01 molecules/100eV at scavenging capacities  $10^{10}$  and  $10^{13} \text{ s}^{-1}$  respectively in nitrate and selenate solutions.

Good agreement is found between the two set of results for the different electron scavengers. There is a small difference between  $G(H_2)$  and  $G^0(H_2)$  at low electron precursor scavenging capacities

Comparison of the yields reveals that in the gamma radiolysis when nitrate is added as electron scavenger,  $G(HD)$  decreases from 0.37 to 0.14 and 0.04 to 0.002 molecules / 100 eV at the lowest and highest electron scavenging capacities considered. In selenate addition,  $G(HD)$  decreases from 0.39 to 0.09 and 0.14 to 0.01 molecules / 100 eV. The hydrogen atom yield decreases clearly with LET.

Figure 6.31 compares the yield of the different isotopic forms of molecular hydrogen in the radiolysis of nitrate solutions.

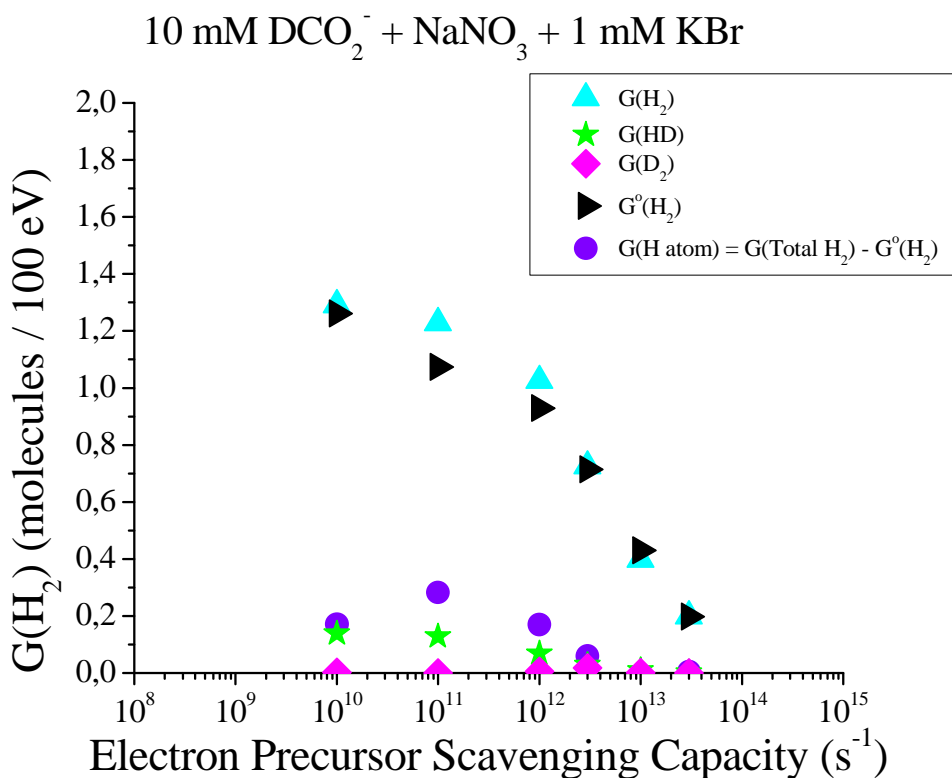


**Figure 6.31** Hydrogen yields in the  $^4He$ -radiolysis of aqueous 10 mM deuterated formate solutions with  $NaNO_3$  as a function of the precursor to the hydrated electron scavenging capacity.  $G^0(H_2)$  is the yield of  $H_2$  at different concentrations of the electron scavengers in the absence of any H atom scavenger.

The figure shows differences between experimental  $G(H_2)$  and  $G^0(H_2)$  as well as  $G(H \text{ atom})$ , as predicted by the difference method, and  $G(HD)$  at electron precursor scavenging capacities of  $10^{11}$  and  $10^{12} s^{-1}$ . Apart from this, results show good agreement.

Comparison of these data with results from gamma radiolysis experiments shows how the  $H_2$  yield increases with LET. The hydrogen atom yield undergoes a significant decrease with LET and remains almost constant with scavenging capacity for  $^4He$  ion radiolysis. Finally, no appreciable  $G(D_2)$  is formed due to the direct irradiation of  $DCO_2^-$  at this low concentration of the deuterated solute.

The yields of the different isotopic forms of molecular hydrogen in the  $^4He$  ion radiolysis of selenate solutions are shown in Figure 6.32. Similar results to those seen for nitrate are observed.

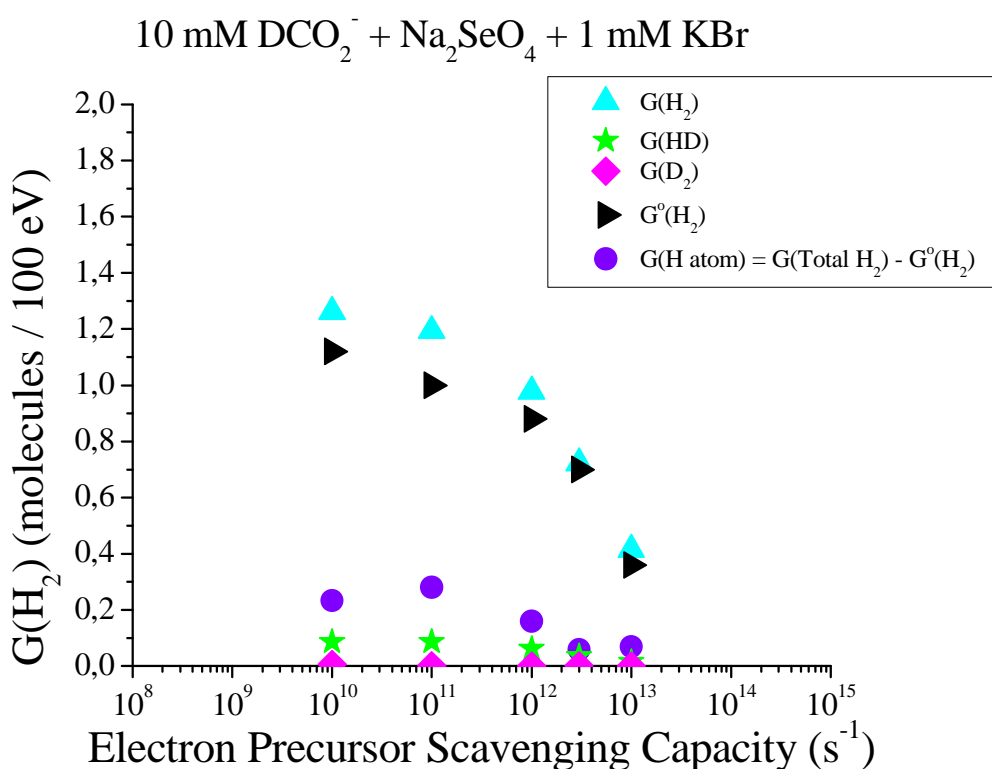


**Figure 6.32** Hydrogen yields in the  $^4He$ -radiolysis of aqueous 10 mM deuterated formate solutions with  $Na_2SeO_4$  as a function of the precursor to the hydrated electron scavenging capacity.  $G^o(H_2)$  is the yield of  $H_2$  at different concentrations of the electron scavengers in the absence of any H atom scavenger.

A discrepancy is observed between the two estimates of  $G(H \text{ atom})$  at the lowest electron scavenging capacities. This suggests that the determination of  $G(H \text{ atom})$  through the difference measurement of molecular hydrogen yields might not be reliable when using radiation sources of high LET values, similarly as it was found in the  $\gamma$ -radiolysis of aqueous formate solutions of high concentration. The disagreement may be explained by considering the reaction



with  $k_{50} = 3.2 \times 10^9 \text{ M}^{-1} \text{ s}^{-1}$  [8]. Increasing the concentration of  $\text{HCO}_2^-$  causes a fractionally large increase in the amount of OH scavenged at high LET than at low LET. Subsequently, this will produce a fractionally bigger decrease of reaction 6.51 which results in an increment of the concentration of hydrated electrons and therefore, an increment on the molecular hydrogen yield due to the reaction of the hydrated electron with either hydrogen atoms or additional hydrated electrons.



This suggests that hydrogen atom yields obtained by the difference method in the heavy ions radiolysis of aqueous formate or deuterated formate solutions could be overestimated since  $G(\text{H}_2)$  would be higher than  $G^0(\text{H}_2)$ , as seen experimentally.

Hydrogen atom yields are shown in figure 6.33 in the  $^4\text{He}$ -radiolysis of aqueous 1 M sodium formate with nitrate as electron scavenger.

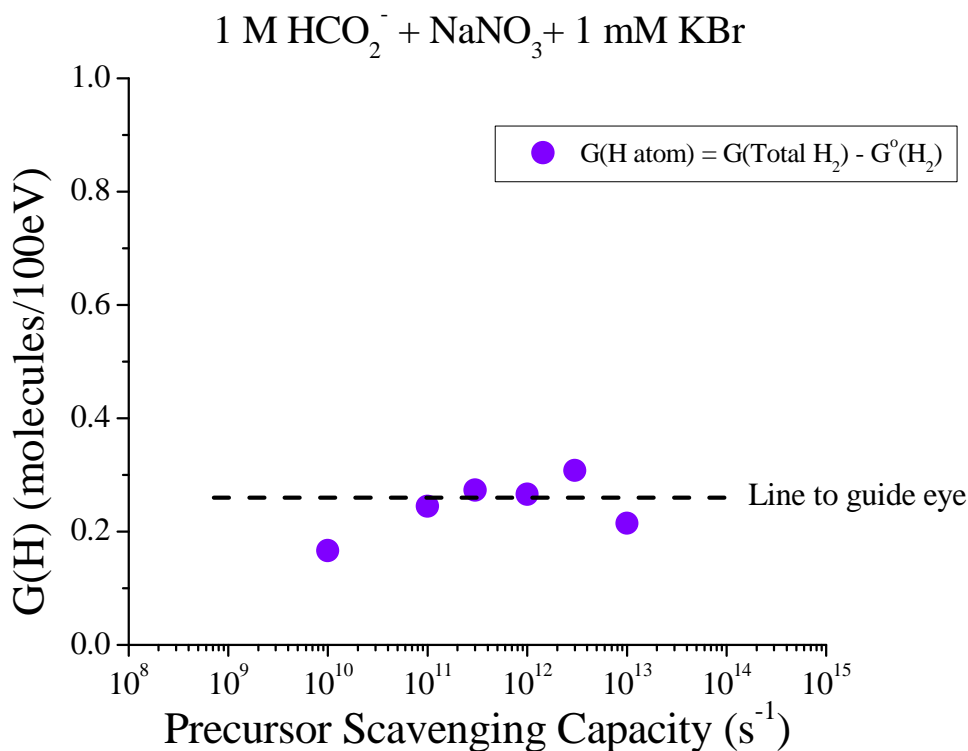


**Figure 6.33** H atom predictions in the  $^4\text{He}$ -radiolysis of aqueous 1 M formate solutions with  $\text{NaNO}_3$  as a function of the precursor to the  $e_{\text{aq}}^-$  scavenging capacity.

H atom yields vary from 0.17 to 0.21 molecules/100eV for scavenging capacities ranging from  $1 \times 10^{10}$  to  $1 \times 10^{13} \text{ M}^{-1} \text{ s}^{-1}$ , showing an almost flat shape or,

in other words, remaining constant as the electron precursor scavenging capacity increases. This underlines the independence of the H atom yield with respect to the scavenging capacity of the  $e^-$  precursor until at least  $1 \times 10^{13} \text{ s}^{-1}$  in the  $^4\text{He}$  irradiation.

	Gamma rays	$^1\text{H}$ Ions	$^4\text{He}$ Ions
10 mM $\text{HCO}_2^-$	0.40 $\downarrow$ $\approx$	0.43 $\rightarrow$ $-$	0.13 $\downarrow$ $\approx$
1 M $\text{HCO}_2^-$	0.75 $\downarrow$ $+$	$-$	0.17 $\downarrow$ $\approx$

**Table 6.9** H atom yields in the  $\gamma$ ,  $^1\text{H}$  and  $^4\text{He}$  radiolysis of 10 mM  $\text{HCO}_2^-$  or 1 M  $\text{HCO}_2^-$  with  $\text{NaNO}_3$  at the lowest considered electron precursor scavenging capacity. The arrows show the behavior of the  $G(\text{H atom})$  with LET.

The H atom yield decreases as the LET value increases. Additionally, the H atom yield increases with the H atom scavenging capacity when irradiated with gamma rays but no appreciable increment is observed with  $^4\text{He}$  ions.

Figure 6.34 shows the H atom yield in the  $^4\text{He}$  ion radiolysis of 1 M formate solutions with selenate as electron scavenger.

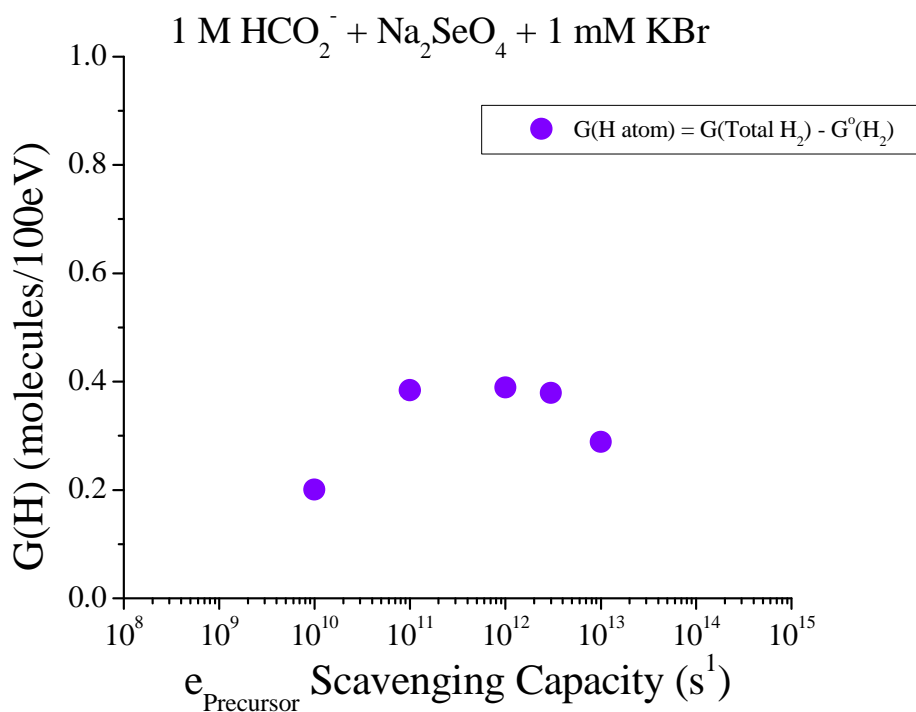


**Figure 6.34** Hydrogen atom predictions in the  $^4\text{He}$ -radiolysis of aqueous 1 M formate solutions with  $\text{Na}_2\text{SeO}_4$  as a function of the precursor to the hydrated electron scavenging capacity.



The H atom yield shows no dependence on the scavenging capacity of the electron scavenger in the interval  $1 \times 10^{11}$  to  $1 \times 10^{13} \text{ s}^{-1}$  where the formation of the H atom is controlled by the reactions of the precursor to the hydrated electron. It decreases at low electron precursor scavenging capacities.

The production of hydrogen in the irradiation of 1 M  $\text{DCO}_2^-$  aqueous solutions with  $^4\text{He}$  ions is presented in Figure 6.35.

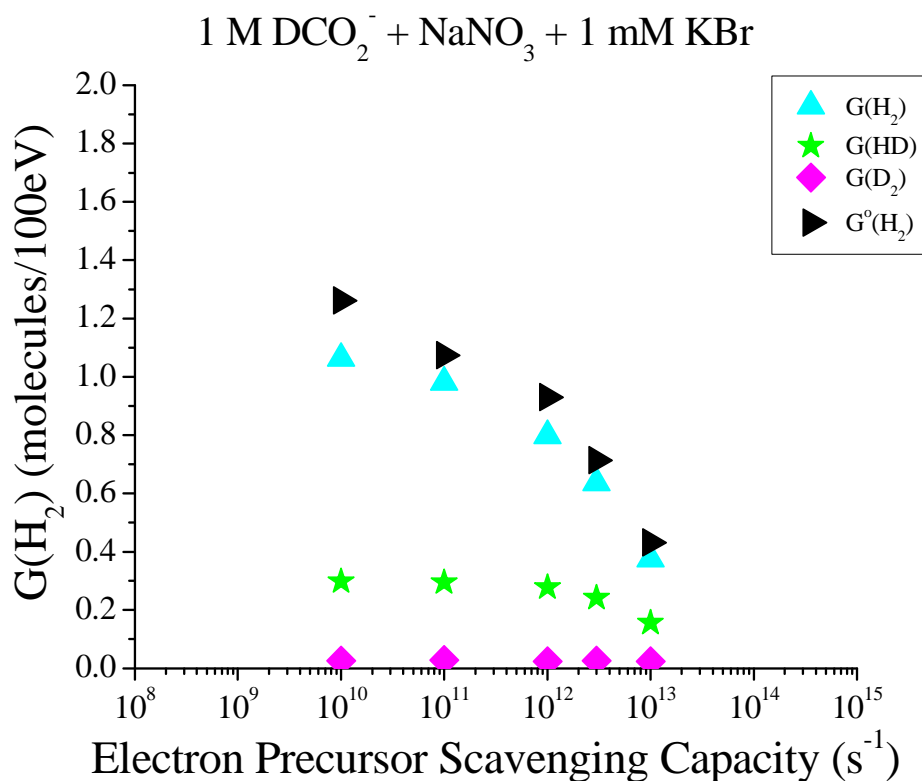


**Figure 6.35** Hydrogen yields in the  $^4\text{He}$ -radiolysis of aqueous 1 M formate solutions with  $\text{NaNO}_3$  as a function of the precursor to the hydrated electron scavenging capacity.  $G^\circ(\text{H}_2)$  is the yield of  $\text{H}_2$  at different concentrations of the electron scavengers in the absence of any H atom scavenger.

A complete series of results in the gamma,  $^1\text{H}$  and  $^4\text{He}$  radiolysis of aqueous 1 M deuterated formate solutions with nitrate have been obtained and compared in table 6.10.

The hydrogen atom yield decreases as the LET value of the radiation source increases. The hydrogen atom is formed at the early stages due to the reactions of the electron precursor and the fragmentation of the water excited state and reacts with

other species in solution. Those reactions are faster as the LET value increases due to the increment in the intra track reactions which produces a faster decrease in the H atom yield.

	Gamma rays	$^1\text{H}$ Ions	$^4\text{He}$ Ions
<b>G(H atom) Molecules / 100 eV</b>	0.53	→ 0.46	→ 0.30

**Table 6.10** Hydrogen atom yields in the gamma,  $^1\text{H}$  and  $^4\text{He}$  radiolysis of 1 M  $\text{DCO}_2^-$  solutions with  $\text{NaNO}_3$  at the lowest considered electron precursor scavenging capacity. The arrows show the behavior of the G(H atom) with LET.

The molecular deuterium yield due to reactions 6.43 and 6.44 is significant at this high concentration of deuterated formate. As in previous cases, the molecular hydrogen yield clearly decreases as the electron precursor scavenging capacity increases while G(H atom) remains constant until high scavenging capacities of the electron precursor. The effect of hydrogen atom scavenging capacity on the behavior of the hydrogen atom yield in terms of the scavenging capacity of the electron precursor, is seen in figure 6.36

The hydrogen atom yield varies from 0.14 to 0.30 and from 0.01 to 0.21 molecules / 100 eV at the lowest and highest electron precursor scavenger capacities respectively. The hydrogen atom yield remains constant for scavenging capacities ranging from  $10^{10}$  to  $10^{12}$   $\text{s}^{-1}$  where the H atom formation is governed by the reactions of the hydrated electron. Then, decreases at higher scavenging capacities where the hydrogen atom formation is governed by the reactions of the electron precursor. This variation shows the dependence of the H atom formation on the reactions of the electron precursor and independence on the reactions of the hydrated electron.

10 mM/1 M  $HCO_2^-$  and 10 mM/1 M  $DCO_2^-$  +  $NaNO_3$  + 1 mM  $KBr$

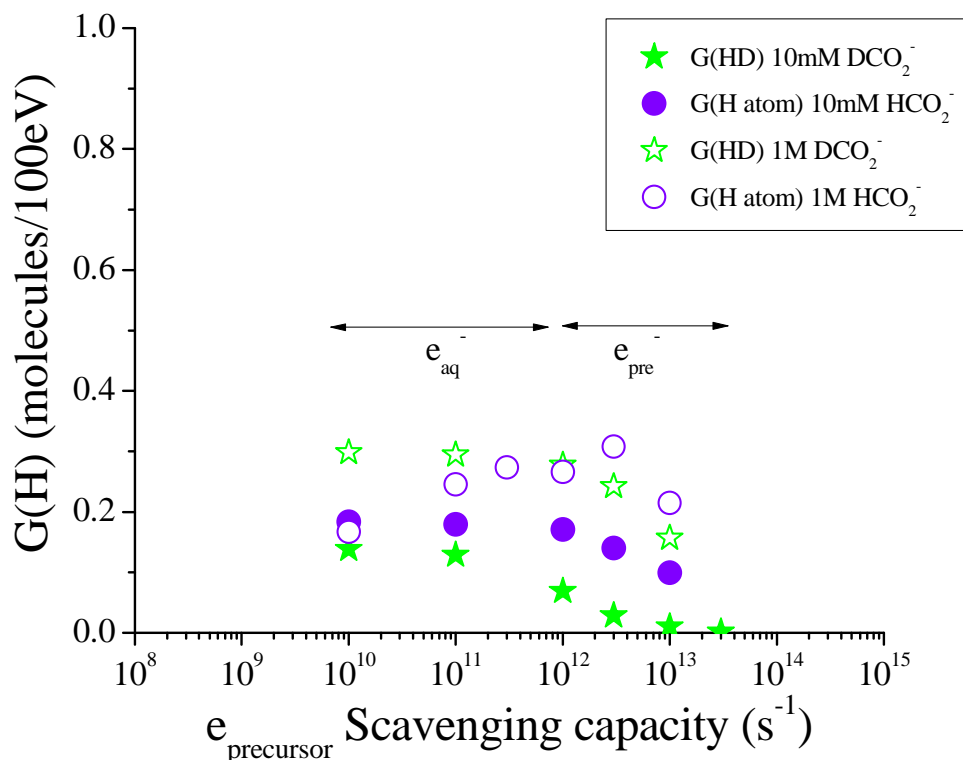


**Figure 6.36** Hydrogen atom yields in the  $^4He$  radiolysis of aqueous systems and in the  $^4He$  radiolysis of aqueous solutions and in terms of the H atom scavenging capacity and the concentration of the electron scavenger.

H atom yields due to the addition of different concentrations of formate or deuterated formate are small and similar at each electron precursor scavenging capacity considered. The H atom yield is independent of the hydrogen atom scavenging capacity as it has already reacted with other species in solution.

#### 6.5.2.4 Conclusions

Hydrogen atom yields have been measured in the gamma,  $^1H$  and  $^4He$  radiolysis of aqueous formate and deuterated formate concentrations. The  $G(H\ atom)$  has been observed to decrease with LET. A graphical representation of this change is shown in figure 6.37.

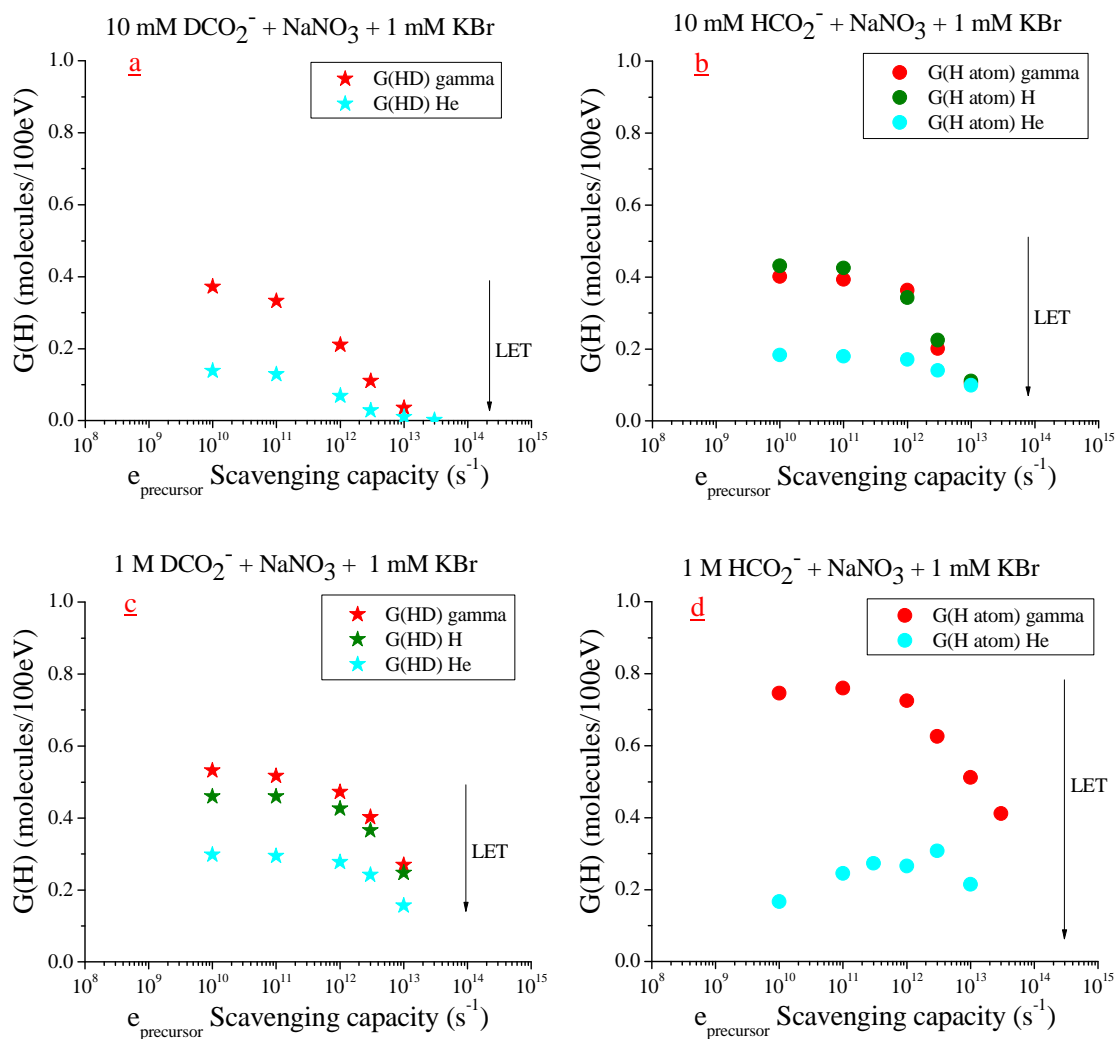


**Figure 6.37** Hydrogen atom yields behavior in terms of the LET value of the radiation source and the concentration of the electron scavenger.

The hydrogen atom scavenging capacity increases from a to b to c to d. In these graphs, the  $G(H)$  atom is clearly seen to decrease with LET at each different H atom scavenging capacity considered, with the sole exception of graph b where  $G(H)$  atom) due to gamma and  $^1H$  radiolysis are very similar. The size of the decrease increases with increasing H atom scavenging capacity.

### 6.5.3 Experimental and stochastic modeled yields

Experimental results are next compared with simulations in order to reach a better understanding of the chemistry occurring in the radiolysis of aqueous systems. In the simulations shown, the reaction pathway for the radiolysis of water is that in Figure 6.38.

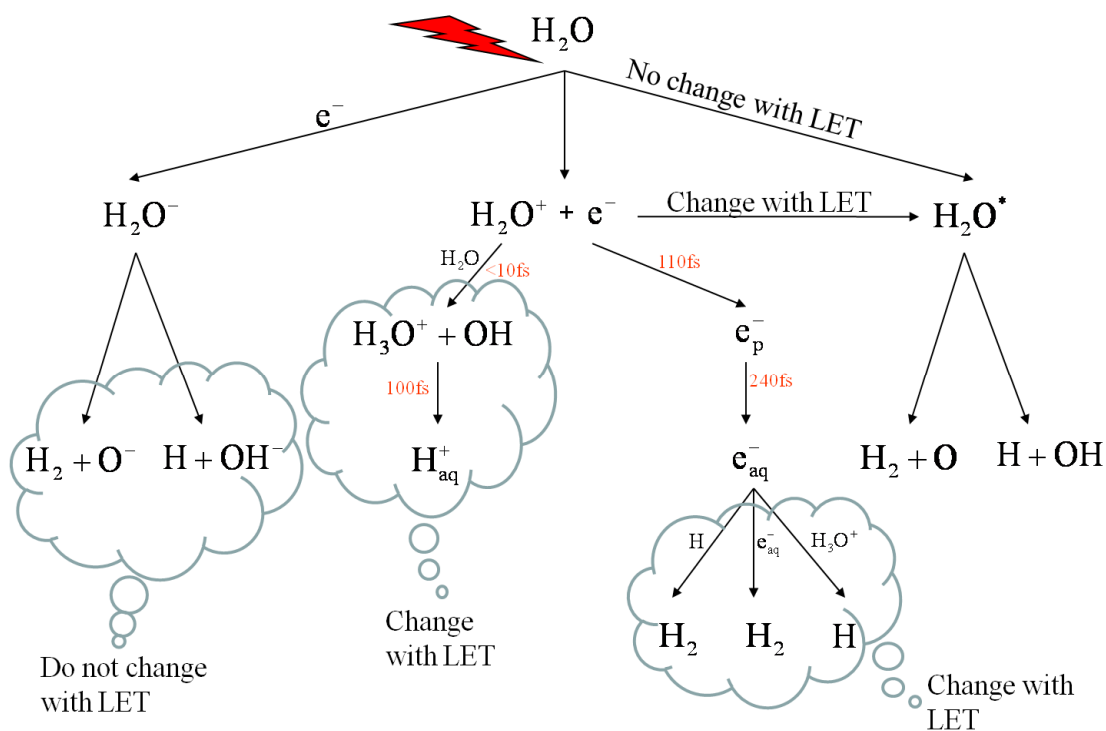


**Figure 6.38** Water radiolysis pathway.

### 6.5.3.1 Gamma radiolysis

Monte Carlo simulations combined with experimental results are shown in Figures 6.39 and 6.40 for the gamma radiolysis of 10 mM and 1 M formate with added  $NaNO_3$  or  $Na_2SO_4$ .

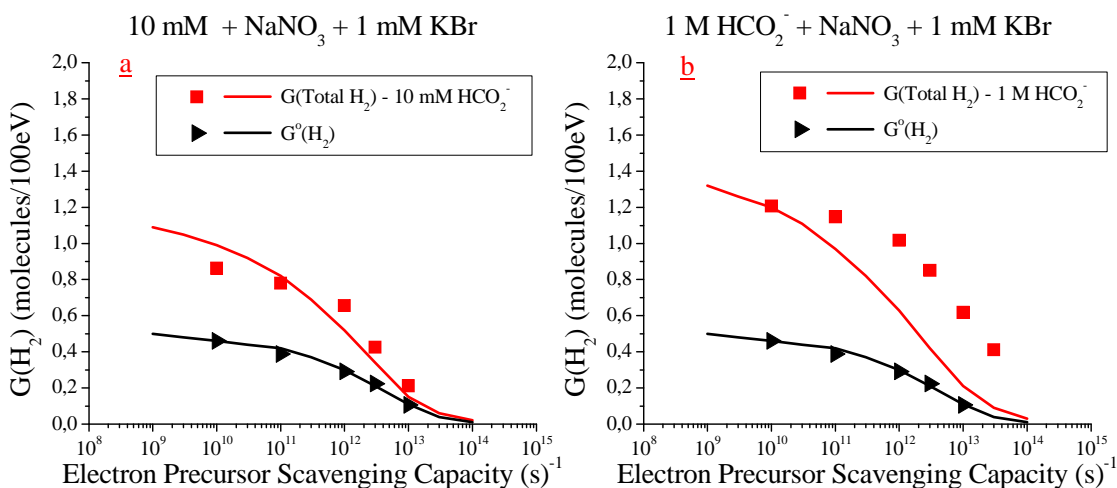


**Figure 6.39** Experimental  $H_2$  yields combined with simulations in the  $\gamma$ -radiolysis of aqueous 10 mM (a) and 1 M (b) formate solutions with added  $NaNO_3$ .  $G^0(H_2)$  is the yield of  $H_2$  at different concentrations of the electron scavengers in the absence of any H atom scavenger. Lines represent the model results.

The agreement between experimental and modeled molecular hydrogen yields is good for water with added nitrate in the absence of formate while differences are seen on the addition of formate. These differences become worse as the concentration of formate increases, as seen on examination of Figure 6.39. Modeled  $G(\text{Total H}_2)$  are observed to drop faster than experimental as the concentration of sodium formate is increased. There is no obvious formate reaction to explain this behavior and, therefore, further simulations with an alternative electron scavenger, hydrogen atom scavenger or radiation source were performed to elucidate an explanation for this behavior. On the addition of sodium formate, experimental and modeled hydrogen atom yields are obtained from the difference measurements of modeled  $G(\text{Total H}_2)$  and  $G^0(\text{H}_2)$ .

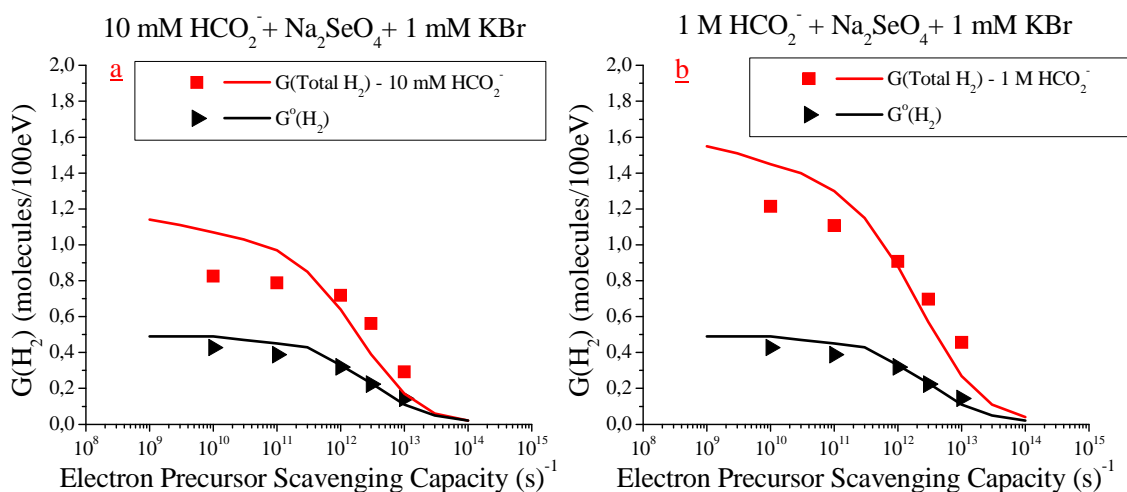


**Figure 6.40** Experimental H<sub>2</sub> yields combined with simulations in the  $\gamma$ -radiolysis of aqueous 10 mM (a) and 1 M (b) formate solutions with added Na<sub>2</sub>SeO<sub>4</sub>.  $G^0(\text{H}_2)$  is the yield of H<sub>2</sub> at different concentrations of the electron scavengers in the absence of any H atom scavenger.

Total H<sub>2</sub> yield calculated by the simulations for selenate containing solutions are clearly overestimated at low scavenging capacities. At first, it may seem that the chemistry of SeO<sub>4</sub><sup>2-</sup> is more complicated than that of nitrate due to the numerous reactions and species derived from it [6, 7]. However, calculations show that at low concentrations of the electron scavenger, those species are barely formed and therefore, something else has to be responsible for those discrepancies.

Experimental results and stochastic calculations are compared in figure 6.41 for the  $\gamma$ -radiolysis of aqueous 10 mM deuterated formate solutions with added

$\text{NaNO}_3$ . Some minor differences are shown at low scavenger capacities, but in general, a good agreement is observed between experiments and Monte Carlo simulations. Slightly overestimation of the experimental results is seen at low electron precursor scavenging capacities, as when sodium formate was considered.

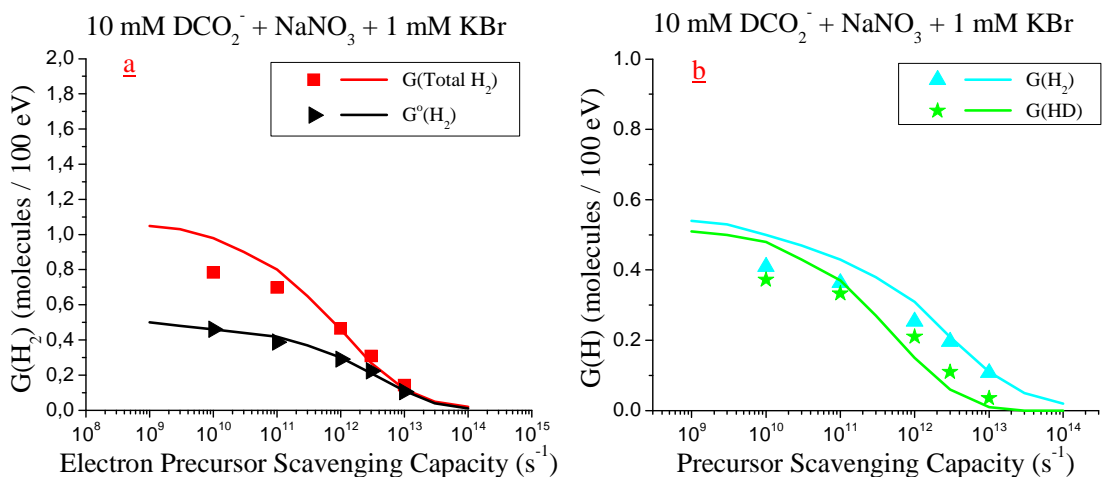


**Figure 6.41** Experimental results combined with simulations in the  $\gamma$ -radiolysis of aqueous 10 mM deuterated formate solutions with  $\text{NaNO}_3$  as a function of the precursor to the hydrated electron scavenging capacity.  $G^0(\text{H}_2)$  is the yield of  $\text{H}_2$  at different concentrations of the electron scavengers in the absence of any H atom scavenger. Lines represent the model results.

Larger discrepancies are found for selenate solutions than for nitrate solutions, as shown in figure 6.42.

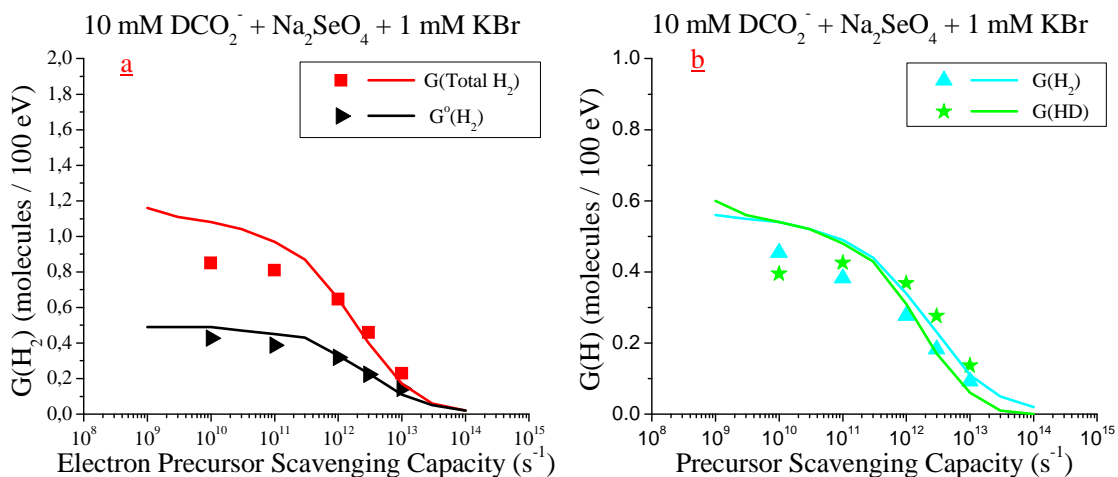


**Figure 6.42** Experimental results combined with simulations in the  $\gamma$ -radiolysis of aqueous 10 mM  $\text{DCO}_2^-$  solutions with  $\text{Na}_2\text{SeO}_4$  as a function of the precursor to the hydrated electron scavenging capacity.  $G^0(\text{H}_2)$  is the yield of  $\text{H}_2$  at different concentrations of the electron scavengers in the absence of any H atom scavenger.

The simulation does not describe the experimental results accurately. Selenite is hardly obtained at low concentration of selenate and therefore its influence over the molecular hydrogen and hydrogen atom yields would be very small.

Experimental results compared with simulations are shown in Figure 6.43 for the gamma radiolysis of aqueous 1 M deuterated formate solutions with added  $\text{NaNO}_3$ .

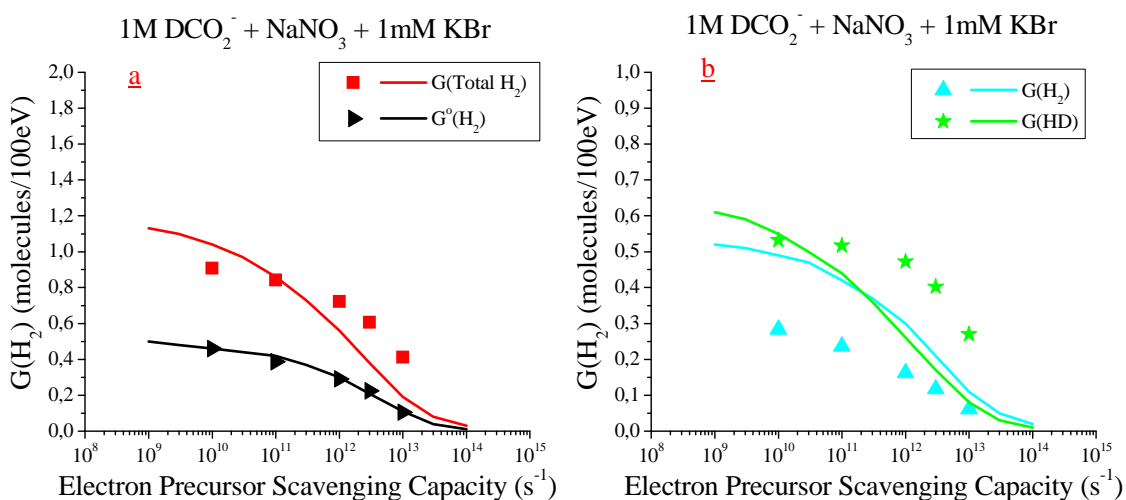


**Figure 6.43** Experimental results combined with simulations in the  $\gamma$ -radiolysis of aqueous 1 M deuterated formate solutions with  $\text{NaNO}_3$  as a function of the precursor to the hydrated electron scavenging capacity.  $G^\circ(\text{H}_2)$  is the yield of  $\text{H}_2$  at different concentrations of the electron scavengers in the absence of any H atom scavenger.

Through the observation of figures 6.41 and 6.43, higher discrepancies between experiments and calculations are found as the scavenging capacity for H atom is increased rather than through the increase in the concentration of the electron scavenger. This increase suggests that radiation chemistry of H atom production is not understood.

### 6.5.2 $^1\text{H}$ radiolysis

An increase in the intra track reactions should be observed in the 5 MeV  $^1\text{H}$  radiolysis of aqueous solutions. The expected consequence is that the local concentration of reactants in the track will be more dense and the molecular hydrogen yields will increase due to an increase in  $G^\circ(\text{H}_2)$ . According to experimental results, H atom will be formed at the early steps due to the reactions of



the electron precursor and the fragmentation of the water excited state, but it would undergo a fast reaction with other species in the track due to the increase in the concentration of reactive radicals decreasing its total yield.

Calculations in the  $^1\text{H}$  irradiation of sodium formate or sodium deuterated formate aqueous solutions with added nitrate and 1 mM bromide were carried out. Firstly, the hydrogen production in the  $^1\text{H}$  radiolysis of aqueous 10 mM formate solutions with added  $\text{NaNO}_3$  is presented in figure 6.44.

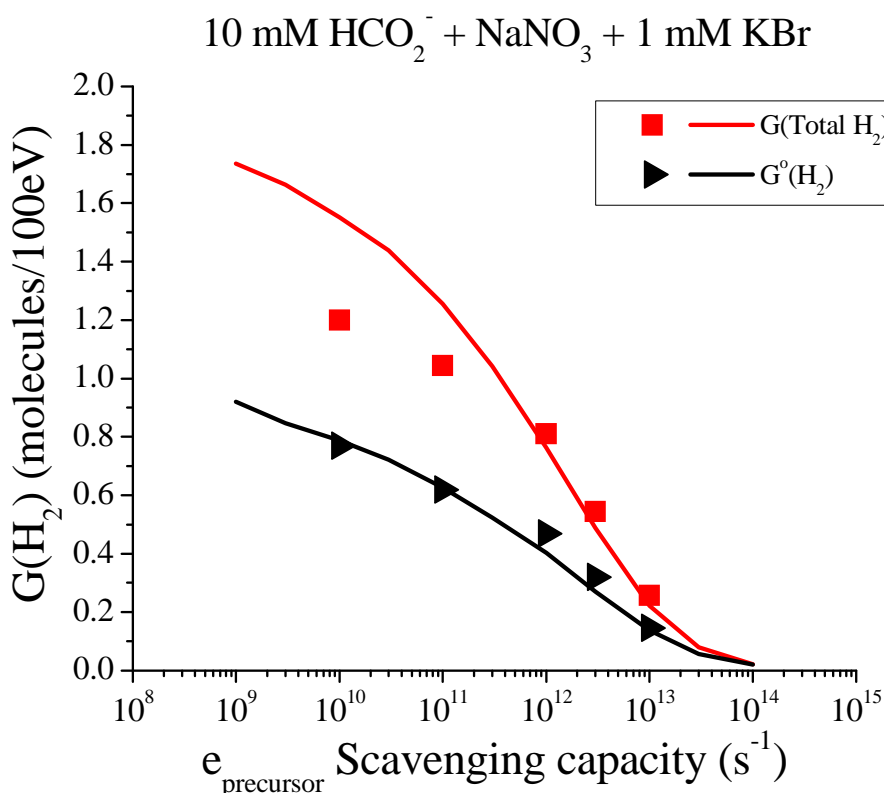


**Figure 6.44** Experimental results combined with simulations in the  $^1\text{H}$ -radiolysis of aqueous 10 mM formate solutions with  $\text{NaNO}_3$  as a function of the precursor to the hydrated electron scavenging capacity.  $G^o(\text{H}_2)$  is the yield of  $\text{H}_2$  at different concentrations of the electron scavengers in the absence of any H atom scavenger.

The figure shows a good agreement between experimental and modeled results in the absence of formate and at high concentrations of the electron scavenger when formate is added. However, the modeled  $G(\text{Total H}_2)$  is significantly overestimated as the concentration of nitrate decreases. Experimental total molecular hydrogen

yields are lower than predicted due to an error in mechanism employed in the calculations.

Figure 6.45 shows calculations for 1 M deuterated formate solutions containing nitrate.

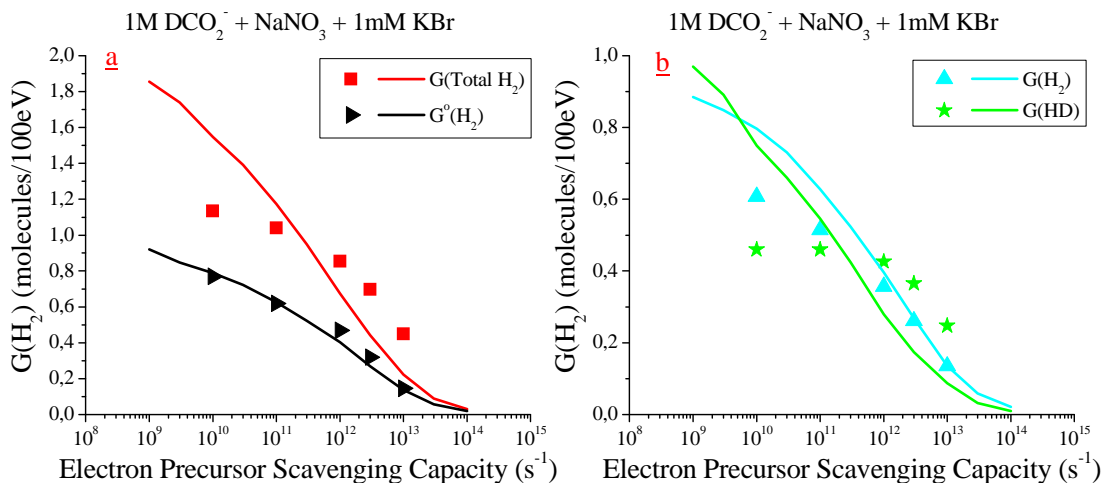


**Figure 6.45** Experimental results combined with simulations in the  $^1H$ -radiolysis of aqueous 1 M deuterated formate solutions with  $NaNO_3$  as a function of the precursor to the hydrated electron scavenging capacity.  $G^0(H_2)$  is the yield of  $H_2$  at different concentrations of the electron scavengers in the absence of any H atom scavenger.

The modeled yield of molecular hydrogen shows correct trend, but overestimates the experimental value at low electron scavenging capacities. In contrast, the prediction for  $HD$  is quite incorrect.

Modeled results are less accurate as the LET of the radiation source is increased.

### 6.5.3 $^4He$ radiolysis

Figure 6.46 shows experimental results compared with simulations of the  $^4He$ -radiolysis of aqueous 10 mM formate solutions.

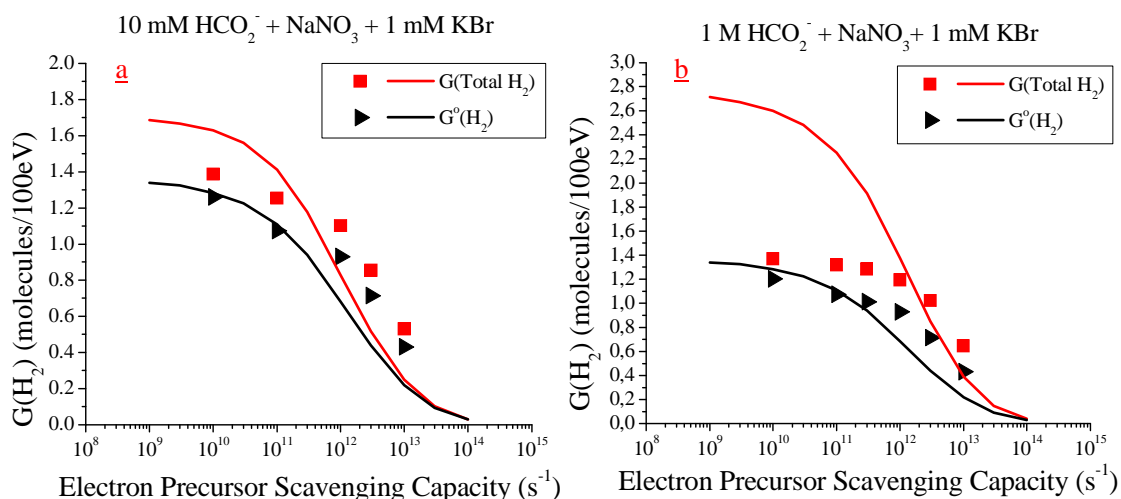


**Figure 6.46** Experimental results combined with simulations in the  $^4\text{He}$ -radiolysis of aqueous 10 mM (a) and 1 M (b) formate solutions with  $\text{NaNO}_3$  as a function of the precursor to the hydrated electron scavenging capacity.  $G^0(H_2)$  is the yield of  $H_2$  at different concentrations of the electron scavengers in the absence of any H atom scavenger. Lines represent the model results.

The simulation of the molecular hydrogen yields shows similar results from those obtained in the  $^1\text{H}$  radiolysis of aqueous solutions. An overestimation of the  $G(\text{Total } H_2)$  at low electron precursor scavenging capacities and a more pronounced decrease in the yields as the scavenging capacity of the electron scavenger increases. However, this is the first time that experimental and modeled  $G^0(H_2)$  do not match. This discrepancy shows the unreliability of the model at high LET.

Experiments and simulations for 10 mM deuterated formate solutions shown in figure 6.47.

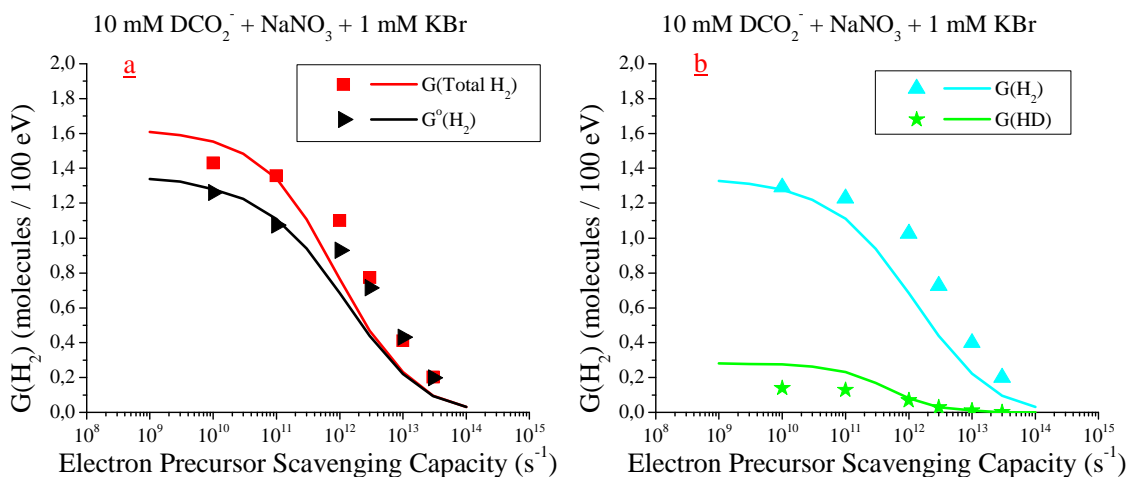


**Figure 6.47** Experimental results combined with simulations in the  $^4He$ -radiolysis of aqueous 10 mM  $DCO_2^-$  solutions with  $NaNO_3$  as a function of the precursor to the hydrated electron scavenging capacity.  $G^0(H_2)$  is the yield of  $H_2$  at different concentrations of the electron scavengers in the absence of any H atom scavenger.

Predictions of the calculations drop faster than experimental results and slightly overestimate the yields at low electron scavenging capacities

Similar discrepancies to those obtained in the simulation of the aqueous system with nitrate are obtained when selenate is added as shown in figure 6.48. Modeled yields drop faster as the concentration of the electron scavenger is increased and differ from experimental results whether the H atom scavenger is present or not.

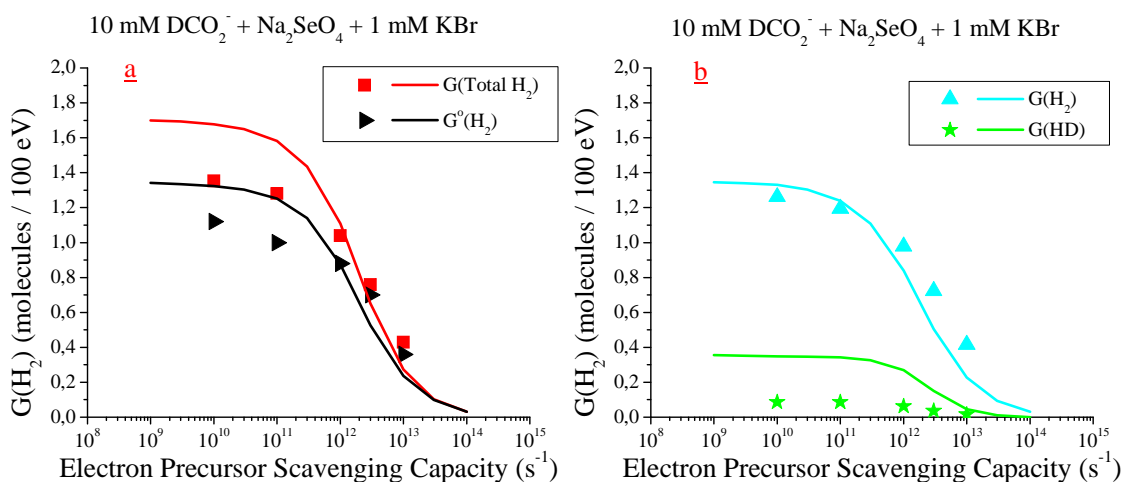


**Figure 6.48** Experimental results combined with simulations in the  $^4He$ -radiolysis of aqueous 10 mM  $DCO_2^-$  solutions with  $Na_2SeO_4$  as a function of the precursor to the hydrated electron scavenging capacity.  $G^0(H_2)$  is the yield of  $H_2$  at different concentrations of the electron scavengers in the absence of any H atom scavenger.

Experiments and Monte Carlo calculations are shown in figure 6.49 for the  $^4\text{He}$ -radiolysis of aqueous 1 M sodium formate. Our calculations clearly overestimate the molecular hydrogen yield from  $^4\text{He}$  ion radiolysis whether  $\text{HCO}_2^-$  is present or not. Molecular hydrogen is generated in excess as the LET increases. The significant excess predicted in the presence of formate is due to an overestimation of the  $G(\text{H atom})$  calculated stochastically which reacts with the formate to generate molecular hydrogen in excess.

Experimentally, H atom yields have been found to decrease with LET, however, our calculations highly overestimate experimental values. Our modeled chemistry does not reproduce the reactions of the H atom and molecular hydrogen as they are both being formed in excess whether formate is added.

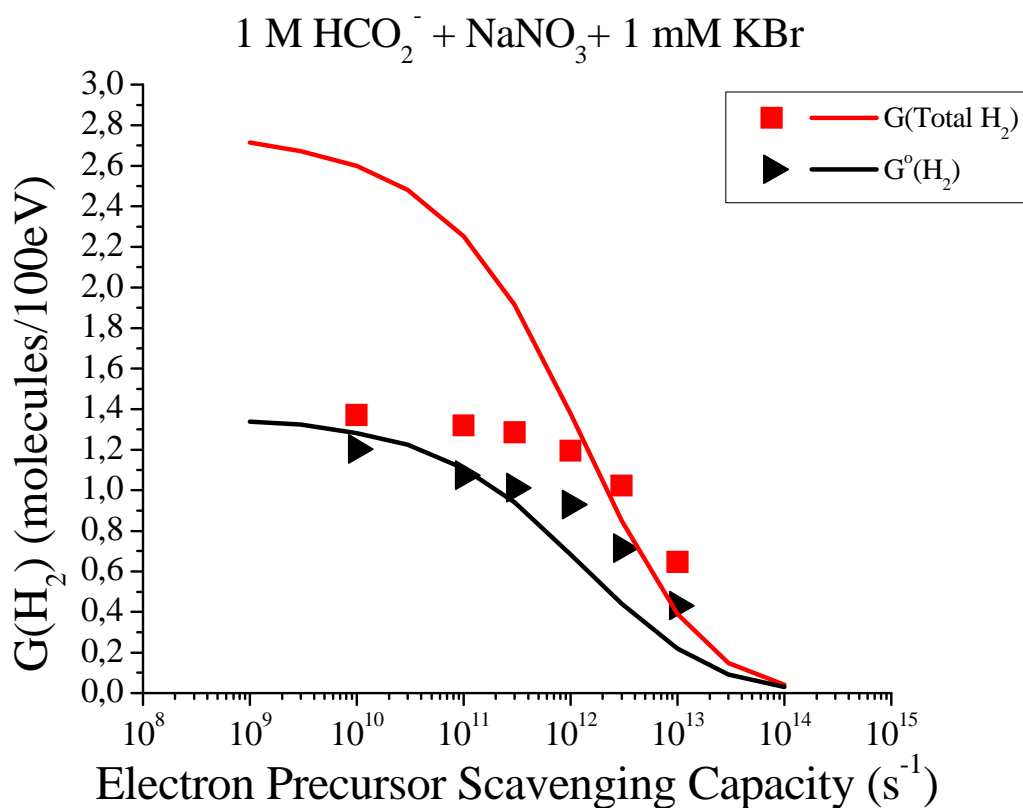


**Figure 6.49** Experimental results combined with simulations in the  $^4\text{He}$ -radiolysis of aqueous 1 M formate solutions with  $\text{NaNO}_3$  as a function of the precursor to the hydrated electron scavenging capacity.  $G^o(\text{H}_2)$  is the yield of  $\text{H}_2$  at different concentrations of the electron scavengers in the absence of any H atom scavenger. Lines represent the model results.

The same discrepancy is observed on the addition of selenate as electron scavenger. Calculations overestimate experimental results with or without added hydrogen atom scavenger.

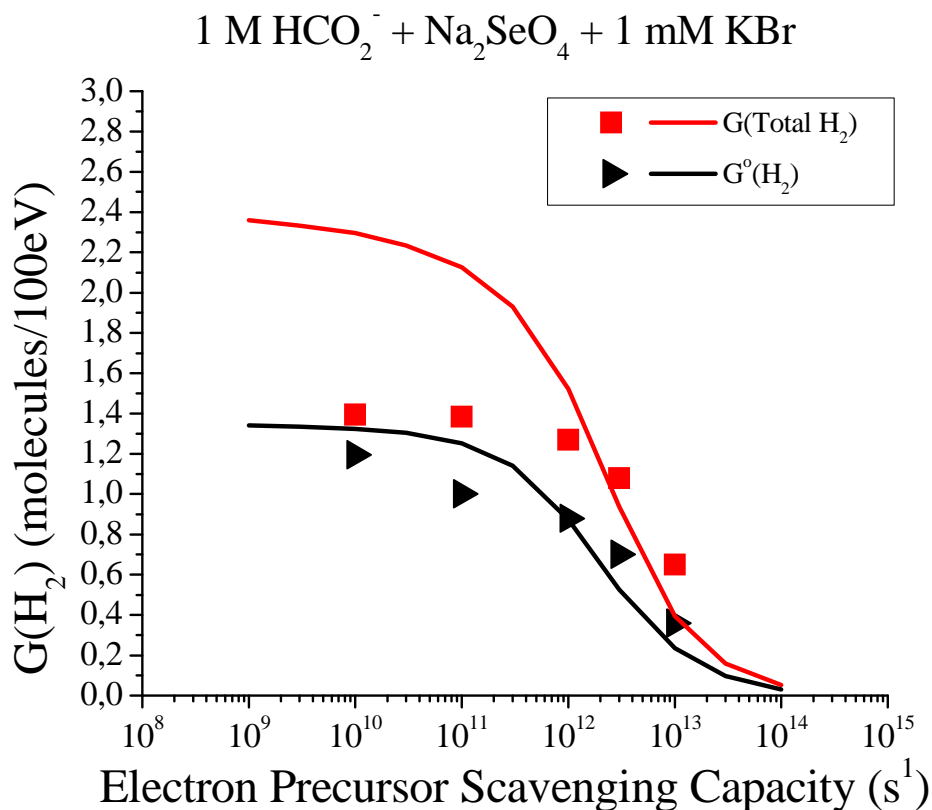


**Figure 6.50** Experimental results combined with simulations in the  $^4\text{He}$ -radiolysis of aqueous 1 M formate solutions with  $\text{Na}_2\text{SeO}_4$  as a function of the precursor to the hydrated electron scavenging capacity.  $G^o(\text{H}_2)$  is the yield of  $\text{H}_2$  at different concentrations of the electron scavengers in the absence of any H atom scavenger. Lines represent the model results.

The result of irradiation of 1 M  $\text{DCO}_2^-$  aqueous solutions with  $^4\text{He}$  ions is presented in figure 6.51. Molecular hydrogen and hydrogen atom yields are overestimated.

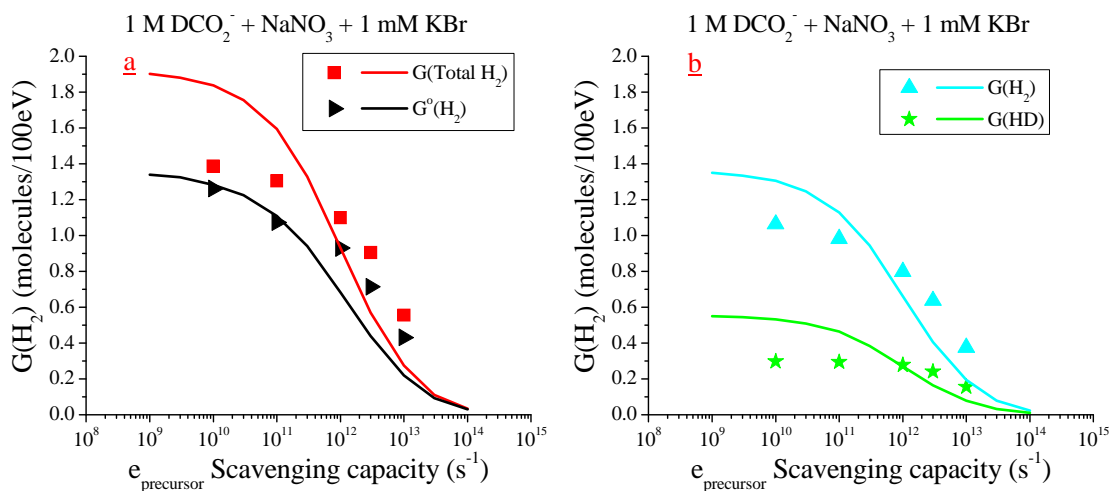


**Figure 6.51** Experimental results combined with simulations in the  $^4\text{He}$ -radiolysis of aqueous 1 M deuterated formate solutions with  $\text{NaNO}_3$  as a function of the precursor to the hydrated electron scavenging capacity.  $G^0(\text{H}_2)$  is the yield of  $\text{H}_2$  at different concentrations of the electron scavengers in the absence of any H atom scavenger.

Our model does not describe the chemistry involved in the radiolysis of aqueous solutions at high H atom scavenging capacities and when irradiating with sources of high LET. The model for water radiolysis needs to be reconsidered. A discussion of the actual model and the improvements that could be applied is developed next.

#### 6.5.3.4 Discussion

A study of the current water radiolysis model must be done in order to elucidate any kind of improvement. The main reactions involved in the generation of hydrogen atom and molecular hydrogen in the radiolysis of water are presented in figure 6.38, showing their respective dependencies on the LET value of the radiation source.

According to the experimental data acquired, the H atom is mainly generated by routes which do vary inversely with LET, as the experimental results have shown a steady decrease of the H atom yield with LET. The H atom might be mainly formed through the fragmentation of the water excited state and the reactions of the electron precursor with water molecules. Then it might undergo intra track reactions

which would decrease its total yield. Those reactions might be faster with sources of high LET and therefore, the  $G(\text{H atom})$  might decrease with LET.

In order to increase with LET, the molecular hydrogen yield should be primarily produced through reactions increasing by LET. In addition, the formation of the molecular hydrogen showed correlation with the reactions of the electron precursor. At this point a new idea has been introduced in order to explain the very different behavior of the hydrogen atom and molecular hydrogen yields. An alternative pathway is presented in Figure 6.52.

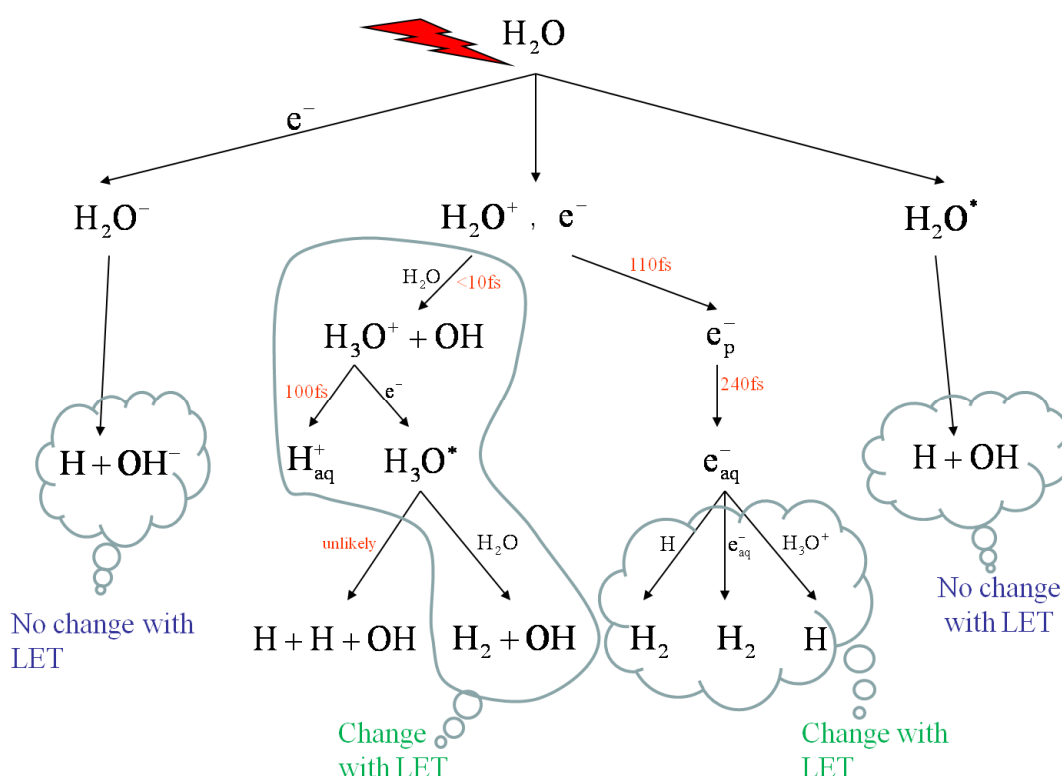


**Figure 6.52** Alternative water radiolysis pathway.

According to this alternative pathway, the hydrogen atom would be mainly formed due to the fragmentation of directly formed water excited state, the reactions of the primary low energy electron with water molecules and, in less extent, due to the reaction of the hydrated electron with hydronium. Molecular hydrogen would be primarily generated in the fragmentation of the  $\text{H}_3\text{O}^*$  excited stated produced by the reaction of the electron precursor with hydronium.



Preliminary simulation studies with this new pathway have not been successful so far, however, it is not an easy task since the rate constants for the fragmentation of the water excites need to be rearranged. Future studies need to be done in this model in order to test and improve it.

## 6.6 Summary

In this chapter the dependence of the H atom formation on the hydrated electron and its precursor has been studied. In addition, its behaviour with respect to the variation of the electron or hydrogen atom scavenger capacities as well as the LET of the radiation source has been considered.

Similar curves of H atom yields were obtained as a function of the electron precursor scavenging capacity, however, different curves of H atom yields were obtained in terms of the hydrated electron scavenging capacity. This led to suggest a stronger dependence of the H atom formation on the reactions of the electron precursor.

In gamma irradiation, it has been proven that the H atom yield increases as the hydrogen atom scavenging capacity increases and decreases as the scavenging capacity of the electron precursor increases, while it is independent of the hydrogen atom scavenging capacity in the 5 MeV  $^1\text{H}$  and 5 MeV  $^4\text{He}$  irradiation. In addition, the hydrogen atom yield decreases as the LET of the radiation source increases.

## 6.7 References

1. Buxton, G.V., Greenstock, C. L., Helman, W. P., and Ross, A. B., *Critical Review of Rate Constants for Reactions of Hydrated Electrons, Hydrogen Atoms and Hydroxyl Radicals (OH/O<sup>•</sup>) in Aqueous Solution*. The Journal of Physical Chemistry, 1988: p. 513-886.
2. LaVerne, J.A., and Pimblott, S. M., *New Mechanism for H<sub>2</sub> Formation in Water*. The Journal of Physical Chemistry A, 2000. **104**: p. 9820-9822.
3. Pastina, B., LaVerne, J. A., and Pimblott, S. M., *Dependence of Molecular Hydrogen Formation in Water on Scavengers of the Precursor to the Hydrated Electron*. The Journal of Physical Chemistry A, 1999. **103**: p. 5841-5846.
4. Anbar, M., and Hart, E. J., *Reactivity of hydrated electrons toward inorganic compounds*. Advances in chemistry series 1968: p. 79-94.
5. Pastina, B., LaVerne, J. A., and Pimblott, S. M., *Dependence of Molecular Hydrogen Formation in Water on Scavengers of the Precursor to the Hydrated Electron*. J. Phys. Chem. A, 1999. **103**: p. 5841-5846.
6. Klaning, U.K., and Sehested, K., *Selenium(V). A pulse radiolysis study*. The Journal of Physical Chemistry, 1986. **90**: p. 5460-5464.

7. Chulkov, V.N., Kartasheva, L. I., and Pikaev, A. K. , *A pulse radiolysis study on the transient products of radiolytic transformations of selenite and selenate ions in aqueous solutions*. High energy chemistry 1995. **29**: p. 11.
8. Buxton, G.V., Greenstock, C. L., Helman, W. P., and Ross, A. B., *Critical Review of Rate Constants for Reactions of Hydrated Electrons, Hydrogen Atoms and Hydroxyl Radicals (OH/O<sup>•</sup>) in Aqueous Solution*. The Journal of Physical Chemistry Ref. Data 1988. **17**: p. 513-886.
9. Broszkiewicz, R.K., *The pulse radiolysis study of NaNO<sub>2</sub> and NaNO<sub>3</sub> solutions*. Bull. Polish Academy of Sciences, Ser. Sci. Chim., 1976. **24**: p. 221 - 229.
10. Benderskii, V.A., Krivenko, A. G., Ponomarev, E. A., and Fedorovich, N. V., *Rate constants of protonation of the ion radical NO<sub>3</sub><sup>2-</sup>*. Elektrokhimiya, 1987. **23**: p. 1435 - 1439.
11. Park, J.Y., and Lee, Y. N., *Solubility and decomposition kinetics of nitrous acid in aqueous solution*. The Journal of Physical Chemistry, 1988. **92**: p. 6294 - 6302.
12. Smaller, B., Avery, E. C., and Remko, J. R., *EPR Pulse Radiolysis Studies of the Hydrogen Atom in Aqueous Solution. I. Reactivity of the Hydrogen Atom*. The Journal of Chemical Physics, 1971. **55**: p. 2414-2418.
13. Pimblott, S.M., and LaVerne, J. A, *Effects of Track Structure on the Ion Radiolysis of the Fricke Dosimeter*. The Journal of Physical Chemistry A, 2002. **106**: p. 9420-9427.
14. LaVerne, J.A., Stefanic, I., and Pimblott, S. M., *Hydrated Electron Yields in the Heavy Ion Radiolysis of Water*. The Journal of Physical Chemistry A, 2005. **109**: p. 9393-9401.
15. Pimblott, S.M., LaVerne, J. A., and Mozumder, A., *Monte Carlo Simulation of Range and Energy Deposition by Electrons in Gaseous and Liquid Water*. The Journal of Physical Chemistry, 1996. **100**: p. 8595-8606.
16. Christensen, T., Fuglestvedt, J., Benestad, C., Ehdwall, H., Hansen, H., Mustonen, R., and Stranden, E. , *Chemical and radiological risk factors associated with waste from energy production*. Science of The Total Environment, 1992. **114**: p. 87-97.
17. Wang, X., Shao, C., Yao, J., and Yu, Z., *Mass and energy deposition effects of implanted ions on solid sodium formate*. Radiation Physics and Chemistry, 2000. **59**: p. 67-70.
18. Logager, T., and Sehested, K., *Formation and decay of peroxyxynitrous acid: A pulse radiolysis study*. The Journal of Physical Chemistry, 1993. **97**: p. 6664 - 6669.
19. Warman, J.M., *The dynamics of electrons and ions in non-polar liquids*. 1981, Interuniversitair Reactor Instituut: Delft.

# Chapter 7

## Conclusions and Further Work

7.1	Conclusions.....	164
7.1.1	H atom determination.....	164
7.1.2	H atom formation.....	164
7.1.3	H atom yield dependence.....	165
7.2	Further work.....	165
7.3	References.....	166

## 7.1 Conclusions

Prior to this work the formation, yields and dependence of the hydrogen atom in the radiolysis of water were poorly understood. Many irradiations with gamma,  $^1\text{H}$  and  $^4\text{He}$  were carried out by addition of different concentrations of formate or deuterated formate as hydrogen atom scavengers, nitrate or selenate as electron scavengers and bromide as hydroxyl radical scavenger.

The H atom has been determined through two different methods, through the difference measurement of molecular hydrogen yields and through the direct measurement of HD yields. The dependence of the hydrogen atom formation in the radiolysis of water has been tested under many different conditions, varying the H atom or the electron scavenger capacities as well as the LET of the radiation source. This effort has led to a broad and complete study of the hydrogen atom formation in the radiolysis of aqueous systems.

### 7.1.1 H atom determination

H atom yields are accurately determined through the difference measurement of molecular hydrogen yields and the direct measurement of HD yields [1]. However, the former method has shown some limitations at high hydrogen atom scavenging capacities and when used in conjunction with radiations of high LET. Therefore, the direct measurement of HD yields has been found to be the most accurate method to determine hydrogen atom yields under any conditions.

### 7.1.2 H atom formation

The addition of two different electron scavengers with different affinity for the hydrated electron and its precursor produced similar curves of H atom yields as a function of the electron precursor scavenging capacity. However, different curves of H atom yields were obtained in terms of the hydrated electron scavenging capacity. This suggests a stronger dependence of the H atom formation on the reactions of the electron precursor to the hydrated electron rather than on the reactions of the hydrated electron.

7.1.3 H atom yield dependence on the hydrogen atom and electron scavenging capacity and LET value.

The H atom yield was observed to increase as the hydrogen atom scavenging capacity increases in gamma radiolysis and to be independent of the hydrogen atom scavenger at high LET. On the other hand, it was observed to decrease as the concentration of the electron scavenger and the LET of the radiation source increases. The former is due to an effective scavenging of hydrated electrons and its precursors which are responsible for the formation of the hydrogen atom while the latter is related to the mechanism of the early formation of the hydrogen atom due to the electron precursor and its subsequent intra track reaction to decrease its yield.

## 7.2 Further work

Much has been learned from the work described in this thesis, however, a greater understanding of the chemistry studied could be gained by carrying out some further calculations. Significant differences between experimental data and the predictions of stochastic simulations have been found in the gamma,  $^1\text{H}$  and  $^4\text{He}$  radiolysis. Further investigations should be made to understand the difference and to improve our modeled results.

The model seems to follow the intra track chemistry in the gamma radiolysis of water but differences appear due to the addition of hydrogen atom scavengers. These differences increase as the LET value of the radiation source increases since the intra track chemistry is not accurately determined. The hydrogen atom is produced in excess in high LET stochastic calculations. This suggests that our model does not reproduce the chemistry occurring after irradiation of water. Further calculations must be undertaken to interpret, investigate and understand the observed experimental data. In addition, experimental molecular hydrogen and hydrogen atom yields in the  $^{12}\text{C}$  radiolysis of aqueous formate and deuterated formate with added nitrate might be done in order to investigate whether  $G(\text{H atom})$  decreases further and to aid in the elucidation of the formation mechanism.

In this project, H atom yields were determined in the radiolysis of aqueous solutions of simple organic molecules. This study might be expanded by considering more complicated organic compounds, including polymers since it is feasible to expect at least traces of water in their vicinity.

7.3 References

1. Huerta Parajon, M., Rajesh, P., Mu, T., Pimblott, S. M., and LaVerne, J. A., *H atom yields in the radiolysis of water*. Radiation Physics and Chemistry, 2008. **77**: p. 1203-1207.

# APPENDIX A

## Publications & Conference Papers

1.1	Publications.....	168
1.2	Conference Papers.....	168

## 1. Publications

Huerta Parajon, M., Rajesh, P., Mu, T., Pimblott, S.M. and LaVerne, J.A., *H atom yields in the radiolysis of water*. Radiation Physics and Chemistry. **77**(10-12): p. 1203-1207.

## 2. Conference Posters

**Gordon Conference in Radiation Driven Processes in Physics, Chemistry and Biology, Proctor Academy, Andover, NH, USA, July 18-23, 2010.**

M. Huerta Parajon, Jay A. LaVerne & Simon M. Pimblott

H atom formation in the gamma and  $^4\text{He}$  ion radiolysis of aqueous formate solutions

**26<sup>th</sup> Miller Conference on Radiation Chemistry, Hotel Helikon, Keszthely, Hungary, August 28 – September 2, 2009.**

M. Huerta Parajon, Jay A. LaVerne & Simon M. Pimblott

H atom formation in the gamma and  $^4\text{He}$  ion radiolysis of aqueous formate solutions

**Association for Radiation Research Annual Meeting, Glasgow, UK, June 22-24, 2009.**

M. Huerta Parajon, Jay A. LaVerne & Simon M. Pimblott

H atom formation in the gamma and  $^4\text{He}$  ion radiolysis of aqueous formate solutions

**3<sup>rd</sup> European Nuclear Young Generation Forum, Córdoba, Spain, May 19–23, 2009.**

M. Huerta Parajon, Jay A. LaVerne & Simon M. Pimblott

H atom formation in the gamma and  $^4\text{He}$  ion radiolysis of aqueous formate solutions

**Gordon Conference in Radiation Driven Processes in Physics, Chemistry and Biology, Waterville Valley Resort Waterville Valley, NH, USA, July 6-11, 2008.**

M. Huerta Parajon, Jay A. LaVerne & Simon M. Pimblott

H atom yields in the radiolysis of water





## H atom yields in the radiolysis of water

M. Huerta Parajon<sup>a,b</sup>, P. Rajesh<sup>a,c</sup>, T. Mu<sup>a</sup>, Simon M. Pimblott<sup>a,b,d</sup>, Jay A. LaVerne<sup>a,e,\*</sup>

<sup>a</sup> Radiation Laboratory, University of Notre Dame, Notre Dame, IN 46556, USA

<sup>b</sup> School of Chemistry, University of Manchester, Manchester M13 9PL, UK

<sup>c</sup> Water and Steam Chemistry Division, BARC Facilities, Kalpakkam 603102, India

<sup>d</sup> Dalton Nuclear Institute, University of Manchester, Manchester M13 9PL, UK

<sup>e</sup> Department of Physics, University of Notre Dame, Notre Dame, IN 46556, USA

### A B S T R A C T

Experimental measurements of molecular hydrogen including the use of isotopic techniques are combined with track model calculations to determine H atom yields in the radiolysis of water. The production of H atoms in the radiolysis of water is relatively small, but is important for fundamental considerations. H atoms are formed by the decay of excited states of water at the sub-picosecond timescale and by hydrated electron reactions during the diffusion-kinetic evolution of the ion track up to microseconds. The competition between H atom loss by combination reactions and its formation by reactions of the hydrated electron makes prediction of the H atom kinetics very difficult. H atom yields determined by subtraction of total molecular hydrogen production in neat water from that observed in the formate solutions is found to agree well with the more direct measurement of HD using deuterated formate as a scavenger. H atom yields are found to decrease with the evolution of the radiation track and decrease with increasing LET. Monte Carlo track model calculations are used to analyze the measured experimental yields and to elucidate the underlying H atom kinetics in the radiolysis of water.

© 2008 Elsevier Ltd. All rights reserved.

### 1. Introduction

The H atom is one of the minor radical species in the radiolysis of water except in a very acidic media and its reducing reactions are generally overshadowed by the more abundant hydrated electron (Buxton, 1987). However, the development of fast time-resolved radiolytic and photolytic techniques have led to a new emphasis on the initial decomposition of water (Garrett et al., 2005). Fragmentation of the water excited state is of special interest and one of the major products of this process is the H atom. H atom yields from initial water decomposition can be estimated in the vapor (Armstrong, 1987; Johnson and Simic, 1967), but the corresponding value for radiolysis of the liquid phase is not known accurately. A complete understanding of the initial radiolytic decomposition of liquid water requires an accurate and systematic investigation of the H atom yield.

The production of H atoms is difficult to measure. They behave like hydrated electrons in some systems and like OH radicals in others, which makes it difficult to find selective scavengers (Buxton, 1987). Yields of H atoms are typically determined by difference measurements of H<sub>2</sub> yields (Appleby, 1967; Appleby

and Schwarz, 1969; Chouraqui and Sutton, 1966; Draganic and Draganic, 1972; Elliot et al., 1996; Mahlman, 1966; Scholes et al., 1963; Scholes and Simic, 1964a,b). Radiolytically produced H atoms are allowed to abstract H atoms from selected solutes to give H<sub>2</sub>, which is easily measured. Subtraction of the H<sub>2</sub> yield in water without the H atom scavenger is assumed to give a good measure of the H atom yield. Typical solutes are acetone, formate, and simple alcohols (methanol, ethanol, and propanol). The technique is expected to give a reasonable value for H atom yields if care is taken to keep the scavenging capacity of the two systems for H<sub>2</sub> precursors comparable. Otherwise, each system is sampling the radiation track at different times during its evolution. Two of the previous studies overcame this problem by using isotopically labeled solutes and measuring HD production (Appleby and Schwarz, 1969; Scholes et al., 1963). HD is expected to be formed quantitatively by a direct D atom abstraction reaction from the solute. The interpretation is straightforward, but a systematic investigation using this type of system has never been performed.

In this work, the formation of H<sub>2</sub> from the radiolysis water with and without added formate was examined in order to determine H atom yields using both direct and indirect scavenging methods. Formate solutions were varied from 1 mM to 1 M to probe the radiation track at various times in its evolution. HD was measured in aqueous solutions of deuterated formate in order to determine the directly scavenged H atom yield. The results obtained using

\* Corresponding author at: Radiation Laboratory, University of Notre Dame, Notre Dame, IN 46556, USA.

E-mail address: [laverne.1@nd.edu](mailto:laverne.1@nd.edu) (J. LaVerne).

the two techniques are compared with each other and with the predictions from Monte Carlo diffusion-kinetic track model calculations. Irradiations were performed with  $\gamma$ -rays and with 5 MeV  $^1\text{H}$  ions and 5 MeV  $^4\text{He}$  ions.

## 2. Experimental section

The solutions were made with various concentrations of sodium formate,  $\text{NaHCO}_2$  (ACS reagent grade), or deuterated sodium formate,  $\text{NaDCO}_2$ , (98 at%), with 1 mM potassium or sodium bromide (ACS reagent grade) and 1 or 24 mM sodium nitrate (ACS reagent grade). All the chemicals were from Aldrich and they were used without further purification. The bromide was added to suppress OH radical back reactions with  $\text{H}_2$  and has no other effect on the system. Products from this reaction such as  $\text{Br}_2^-$  will be at sufficiently low concentrations that the hydrated electron will be scavenged by the nitrate. Nanopure water (resistivity 18.7 M $\Omega$ cm) from an in-house  $\text{H}_2$ Only system (consisting of a UV lamp and several microporous ultrafilters) was used to prepare all solutions.

Radiolysis with  $\gamma$ -rays was performed using a Shepherd 109  $^{60}\text{Co}$  source at the Radiation Laboratory of the University of Notre Dame. The dose rate was about 83 Gy/min as determined using the Fricke dosimeter (Pastina et al., 1999). The sample cell for the  $\gamma$ -irradiations was made from a 1 cm quartz cuvette with inlet and outlet ports for purging the sample before and after irradiation. Sample size was 4 ml and total doses were varied from 240 to 3000 Gy depending on the solute concentration.

The heavy ion irradiations were performed using the FN Tandem Van de Graaff facility of the University of Notre Dame Nuclear Structure Laboratory. The window assembly and irradiation procedure were the same as reported earlier (LaVerne and Schuler, 1987a, b). Energy loss of the ions in passing through all the windows was determined from a standard stopping power compilation (Ziegler et al., 1985). The samples were irradiated with completely stripped ions at a charge beam current of about 1.5 nA. Absolute dosimetry was obtained from the product of the integrated beam current and the ion energy. The radiation chemical yields represent all processes for the complete energy attenuation of the ion, i.e. from the initial ion energy to zero, and are therefore track averaged yields. Total doses were about  $8 \times 10^{18}$  eV in 20 ml of solution (64 Gy). The samples were irradiated in a Pyrex sample cell with a thin mica window ( $\sim 6 \text{ mg/cm}^2$ ) attached. The sample cell contained a magnetic stirrer that was operated continuously during the radiolysis.

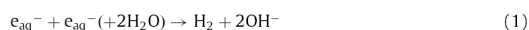
Hydrogen was determined using an in-line technique with a gas chromatograph and a mass spectrometer. Ultra high-purity argon was used as the carrier gas with a flow rate of about 50 ml/min. The argon passed through a constant flow regulator, an injection septum, and a four-way valve and into a 3 m  $5 \times$  molecular sieve column of an SRI 8610C gas chromatograph with a thermal conductivity detector. The samples were purged of air with the argon prior to irradiation. Some of the effluent from the thermal conductivity detector was sampled with a quadrupole mass spectrometer (Balzers, QMA140 analyzer with axially mounted secondary electron multiplier) through a capillary tube ( $\phi = 25 \mu\text{m}$ ,  $L = 20 \text{ cm}$ ). The hydrogen isotopes were monitored at masses 2, 3 and 4. The sample was connected to the gas analysis system using the four-way valve, purged of air, isolated, irradiated, and then injected into the carrier gas stream. Calibration of the detectors was performed by injecting pure  $\text{H}_2$  or  $\text{D}_2$  gases with a gas-tight microliter syringe. Total molecular hydrogen was determined from the chromatographic response, while isotopic ratios were determined from the mass analysis. The error in gas measurement is estimated to be about 5%. Radiation chemical

yields are given in the unit of G values (molecules/100 eV), which is equivalent to 0.1  $\mu\text{mol/l}$ .

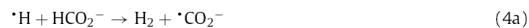
Monte Carlo track simulations were performed using the same general techniques and parameters, as in the previous studies (LaVerne et al., 2005; Pimblott and LaVerne, 2002). Each calculation simulates a realistic track structure for the transfer of energy from the ionizing radiation to the medium, determines the physical consequences of each energy transfer event, i.e. ionization or electronic or vibrational excitation, and models the kinetics of the competition between the relaxation of the spatially nonhomogeneous distribution of radiation-induced reactants and their reactions either within the track or with the scavengers. The track structure methodology uses a collision-by-collision approach employing liquid-phase inelastic collision cross-sections, experimental gas-phase vibrational and elastic collision cross-sections, and incorporates charge cycling using experimentally determined gas-phase cross-sections for protons and an effective charge correction for helium ions. Each track structure simulation determines the relative positions of all the energy loss events along the heavy ion track and for all the secondary electrons ejected. The physicochemical processes, i.e. water ionization and excitation and subsequent fragmentation, are determined from the energy loss in a collision event using experimentally based probabilities for liquid and gaseous water, and the spatial placement of the water fragmentation products is relative to the parent energy-loss event. Diffusion-reaction kinetics of the radiation-induced reactive species is modelled using the independent reaction times (IRT) methodology, which is based upon the independent pairs approximation that is implicit in the Smoluchowski–Noyes treatment of diffusion-limited reaction (Rice, 1985). The chemistry of  $\sim 10^4$  different tracks is modelled to obtain statistically meaningful kinetics. Typically, track segments of 10–100 keV attenuation are considered. A series of track segment yields are calculated at different primary ion energies, and are then integrated to give track average yields for the complete stopping of the  $^1\text{H}$  and  $^4\text{He}$  ions (Pimblott and Mozumder, 2004).

## 3. Results and discussion

Molecular hydrogen formation in neat water,  $\text{H}_2$ , is mainly due to the reactions of precursors to the hydrated electron (Pastina et al., 1999). However, combination reactions of the hydrated electron and H atoms within the radiation track also contribute to  $\text{H}_2$  formation



H atoms can also participate in abstraction reactions with solutes containing H (or D) atoms to give  $\text{H}_2$  (HD). The solute used in the present experiments is the formate anion



with rate coefficients  $k_{4a} = 2.1 \times 10^8 \text{ M}^{-1} \text{ s}^{-1}$  and  $k_{4b} = 2.9 \times 10^7 \text{ M}^{-1} \text{ s}^{-1}$ , respectively (Buxton et al., 1988). The difference in the total yield of  $\text{H}_2$  with formate and  $\text{H}_2^{\bullet}$  determined without formate gives an estimate of the H atom yield.

Few experiments are actually performed in neat water. OH radicals produced by the decomposition of water would react with the  $\text{H}_2$  thereby lowering its yield. Bromide is added at a

concentration of 1 mM to inhibit this reaction. Furthermore, hydrated electrons can be converted to H atoms by reaction with hydronium.



Low concentrations of hydrated electron scavenger are added to limit the occurrence of reaction (5). Typical solutes used for this purpose are nitrous oxide or nitrate ion. The latter was used in these studies,



and reacts with a rate coefficient  $k_6 = 9.7 \times 10^9 \text{ M}^{-1} \text{ s}^{-1}$  (Buxton et al., 1988). The value for  $\text{H}_2^0$  in this work has been determined in solutions of 1 mM bromide and 1 mM nitrate.

The nonhomogeneous spatial distributions of water decomposition species produced by the passage of  $\gamma$ -rays are called spurs and they relax by diffusion and by intraspur combination reactions. H atom yields evolve with time as they react with their siblings in the evolution of the spur. Spur kinetics can be investigated by the use of selective scavengers for the H atom. The scavenging capacity for H atoms is defined as the pseudo-first-order rate coefficient given by the product of the formate concentration and the scavenging rate coefficient,  $k_4$ . Variation of the formate concentration probes the spur chemistry at time scales roughly equivalent to the inverse of the scavenging capacities. Total  $\text{H}_2$  formation yields are shown in Fig. 1 for the  $\gamma$ -radiolysis of 1 mM–1 M formate and deuterated formate solutions containing 1 or 24 mM nitrate. The results agree well with other values in the literature using formate as a scavenger (Draganic and Draganic, 1972; Mahlman, 1966; Scholes and Simic, 1964a,b). The total  $\text{H}_2$  yields are observed to increase with increasing formate concentration due to the scavenging of the H atom in the track at progressively shorter times. The total  $\text{H}_2$  yield is observed to increase from 0.64 to 1.01 molecule/100 eV for scavenging capacities of  $2.1 \times 10^5$ – $2.1 \times 10^8$  or lifetimes of about 5  $\mu\text{s}$ –5 ns, respectively.

Variation of the nitrate concentration has a relatively large effect on hydrogen production. An increase in the scavenging of

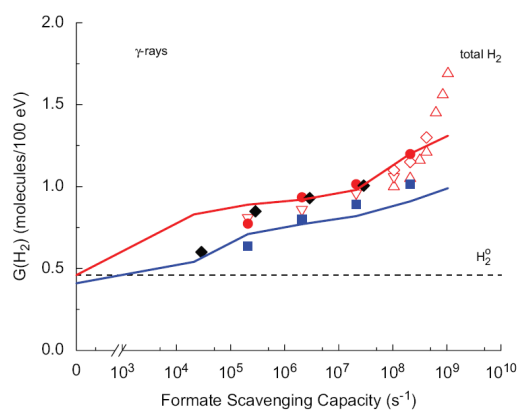


**Fig. 1.** Production of  $\text{H}_2$  in the  $\gamma$ -radiolysis of aqueous formate solutions as a function of the formate scavenging capacity for H atoms: (●)  $\text{HCO}_2^-$ , 1 mM  $\text{NO}_3^-$ , this work; (■)  $\text{HCO}_2^-$ , 24 mM  $\text{NO}_3^-$ , this work; (◆)  $\text{DCO}_2^-$ , 1 mM  $\text{NO}_3^-$ , this work; (◇)  $\text{HCO}_2^-$ , 0.25 mM  $\text{NO}_3^-$  (Draganic and Draganic, 1972); (△)  $\text{HCO}_2^-$ , 24 mM  $\text{N}_2\text{O}$  (Mahlman, 1966); (▽)  $\text{HCO}_2^-$ , 16 mM  $\text{N}_2\text{O}$  (Scholes and Simic, 1964a,b). The dashed line is the  $\text{H}_2^0$  yield determined in water with 1 mM  $\text{NO}_3^-$  and no formate. Solid lines are the results of the Monte Carlo calculations for formate with 1 or 24 mM  $\text{NO}_3^-$ .

hydrated electrons by reaction (6) leads to a decrease in H atom production by reaction (5) and it interferes with  $\text{H}_2^0$  production in reactions 1 and 2. Scavenging of H atoms by nitrate is relatively slow with a rate coefficient of  $1.4 \times 10^6 \text{ M}^{-1} \text{ s}^{-1}$  (Buxton et al., 1988). This reaction does not compete with reaction (4a) in 1 mM  $\text{HCO}_2^-$  solutions. However, the scavenging of H atoms by  $\text{DCO}_2^-$  in reaction (4b) has a rate coefficient of only  $2.9 \times 10^7 \text{ M}^{-1} \text{ s}^{-1}$  and nitrate can effectively compete with the  $\text{DCO}_2^-$  for H atoms at low  $\text{DCO}_2^-$  concentrations (Buxton et al., 1988). The result is a significant drop in total  $\text{H}_2$  yields at low  $\text{DCO}_2^-$  concentration.

Some of the errors associated with the subtraction of  $\text{H}_2$  yields from two different scavenger systems can be avoided by specific scavenging of the H atom. The most common method of H atom scavenging is by D atom abstraction reactions with suitable solutes. The HD product can readily be observed with suitable techniques and differentiated from the yield of  $\text{H}_2$  formed by intra-track reaction. Deuterated formate was chosen in this study, because the rate coefficient is sufficiently fast that intraspur reactions can be probed efficiently and there is only one abstraction site. The results of the isotopic studies with  $\gamma$ -rays are shown in Fig. 2. The total  $\text{H}_2$  yield corresponds to the  $\text{H}_2 + \text{HD} + \text{D}_2$  formed as detected by chromatography. H atom yields can be obtained by the subtraction method, i.e. total  $\text{H}_2 - \text{H}_2^0$ , or by the measured HD yields.  $\text{D}_2$  should be formed only by the direct decomposition of  $\text{DCO}_2^-$ . Agreement between the two techniques is seen to be very good. Measured HD yields decrease from 0.44 to 0.12 molecule/100 eV on the timescale of 34 ns–34  $\mu\text{s}$  representing the evolution of the spur.  $\text{H}_2$  can be produced by direct water radiolysis only and its yield is seen to be invariant with formate concentration and virtually equivalent to the previously determined  $\text{H}_2^0$  value.

The results of the Monte Carlo calculations are slightly higher than the experimental values for total molecular hydrogen production with added formate.  $\text{H}_2$  yields in deuterated formate solutions are equivalent to the molecular hydrogen yield in water without formate,  $\text{H}_2^0$ , and are predicted reasonably well by the calculations. An overestimation of the H atom yields shows up in the comparison of the HD yields and in the total  $\text{H}_2$  yields. This diffusion-kinetic track model gives a good estimate of the hydrated electron yields (LaVerne et al., 2005), but those values

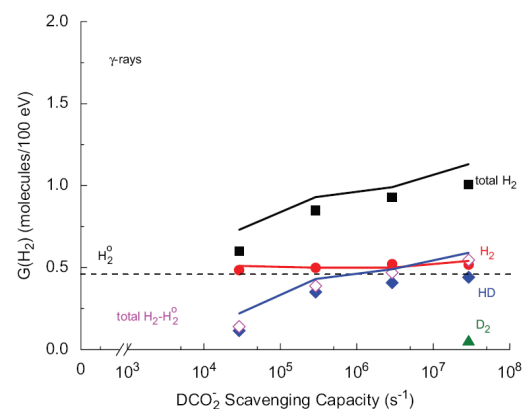


**Fig. 2.** Production of  $\text{H}_2$  in the  $\gamma$ -radiolysis of aqueous deuterated formate solutions with 1 mM  $\text{NO}_3^-$  as a function of the  $\text{DCO}_2^-$  scavenging capacity for H atoms: (■) total molecular hydrogen ( $\text{H}_2 + \text{HD} + \text{D}_2$ ); (●)  $\text{H}_2$ ; (◆) HD; (▲)  $\text{D}_2$ ; (◇) total molecular hydrogen minus the  $\text{H}_2^0$  yield (dashed line) determined in water with 1 mM  $\text{NO}_3^-$  and no formate. Solid lines are the results of the Monte Carlo calculations for total molecular hydrogen ( $\text{H}_2 + \text{HD} + \text{D}_2$ ),  $\text{H}_2$  and HD.

are much larger than the H atom yields and small discrepancies are not as noticeable. A slight overestimation of the water excited state yield or the initial spatial distribution of the H atoms could be responsible for the discrepancies. However, the overall agreement of the Monte Carlo calculations with the experiments is good.

The data of Fig. 1 show a rapid increase in H<sub>2</sub> yields at the highest formate concentrations. Some of these experiments were performed with up to 5 M formate, which corresponds to about 10% by molarity or 90% of the electron density of the solution. Considerable direct absorption of energy by the formate occurs at these high concentrations leading to its decomposition with the resultant formation of additional H<sub>2</sub>. The observed formation of D<sub>2</sub> at the highest formate concentration is an indication of the direct decomposition of formate.

Increasing the linear energy transfer (LET = -dE/dx or the stopping power) of the incident radiation leads to an increase in the local intra-track concentration of reactive species. High concentrations of initial ionization events or of excited states of water may alter the relative significance of the initial water decomposition pathways. Monte Carlo track calculations on the yields of hydrated electrons with high LET ions seem to suggest that these effects can be significant (LaVerne et al., 2005). An increase in LET will also lead to the well-known increase in intra-track radical reactions (LaVerne, 2004). Experiments were performed with 5 MeV <sup>1</sup>H and 5 MeV <sup>4</sup>He ions with track average LETs of 21 and 156 eV/nm, respectively. These LET values are considerably larger than that of 0.2 eV/nm for  $\gamma$ -rays. The increase in total H<sub>2</sub> can be seen in Fig. 3 for each of the types of radiation in the radiolysis of DCO<sub>2</sub> solutions. There is an increase in H<sub>2</sub> yields with increasing LET, which can be attributed mainly to an increase in intra-track reactions.

The results of the radiolysis of DCO<sub>2</sub> solutions with <sup>1</sup>H and with <sup>4</sup>He ions are shown in Figs. 4 and 5, respectively. There is a good match between H atom yields obtained by the subtraction method, i.e. total H<sub>2</sub> - H<sub>2</sub><sup>o</sup>, and the measured HD yields. The H atom yields decrease with increasing LET and for 5 MeV <sup>4</sup>He ions range from 0.23 to 0.05 molecule/100 eV at 34 ns–34  $\mu$ s, respectively. H<sub>2</sub> produced by ultrafast processes in water is independent of formate concentration and virtually equivalent to the H<sub>2</sub><sup>o</sup> values

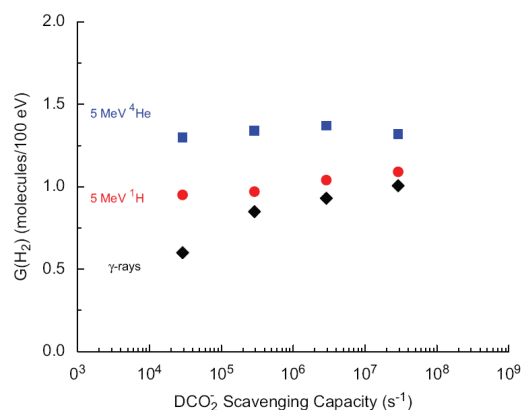


Fig. 3. Total molecular hydrogen production in the radiolysis of aqueous deuterated formate solutions with 1 mM NO<sub>3</sub><sup>-</sup> as a function of the DCO<sub>2</sub> scavenging capacity for H atoms: (■) 5 MeV <sup>4</sup>He ions; (●) 5 MeV <sup>1</sup>H ions; (◆)  $\gamma$ -rays.

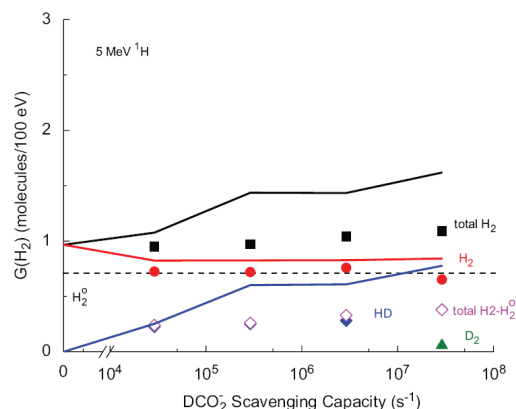


Fig. 4. Production of H<sub>2</sub> in the 5 MeV <sup>1</sup>H radiolysis of aqueous deuterated formate solutions with 1 mM NO<sub>3</sub><sup>-</sup> as a function of the DCO<sub>2</sub> scavenging capacity for H atoms: (■) total molecular hydrogen (H<sub>2</sub>+HD+D<sub>2</sub>); (●) H<sub>2</sub>; (▲) HD; (◆) total molecular hydrogen minus the H<sub>2</sub><sup>o</sup> yield (dashed line) determined in water with 1 mM NO<sub>3</sub><sup>-</sup> and no formate. Solid lines are the results of the Monte Carlo calculations for total molecular hydrogen (H<sub>2</sub>+HD+D<sub>2</sub>), H<sub>2</sub> and HD.

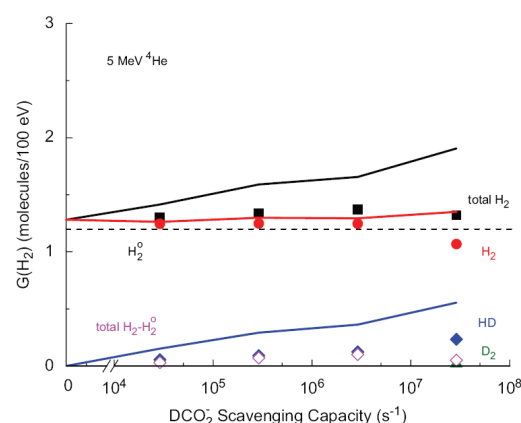


Fig. 5. Production of H<sub>2</sub> in the 5 MeV <sup>4</sup>He radiolysis of aqueous deuterated formate solutions with 1 mM NO<sub>3</sub><sup>-</sup> as a function of the DCO<sub>2</sub> scavenging capacity for H atoms: (■) total molecular hydrogen (H<sub>2</sub>+HD+D<sub>2</sub>); (●) H<sub>2</sub>; (▲) HD; (◆) total molecular hydrogen minus the H<sub>2</sub><sup>o</sup> yield (dashed line) determined in water with 1 mM NO<sub>3</sub><sup>-</sup> and no formate. Solid lines are the results of the Monte Carlo calculations for total molecular hydrogen (H<sub>2</sub>+HD+D<sub>2</sub>), H<sub>2</sub> and HD.

for both ions. Formation of D<sub>2</sub> from direct DCO<sub>2</sub> radiolysis can be observed at the highest concentrations.

#### 4. Conclusions

Experimental measurements of molecular hydrogen including the use of isotopic techniques are combined with track model calculations to determine H atom yields in the radiolysis of water. The production of H atoms in the radiolysis of water is relatively small, but is important from a fundamental viewpoint. H atoms are formed by the decay of excited states of water at the

sub-picosecond time scale and by hydrated electron reactions with hydronium ions during the diffusion-kinetic evolution of the ion track up to microseconds. H atom yields have been determined from the production of HD in the radiolysis of DCO<sub>2</sub> solutions. The results agree well with the H atom yields obtained by the subtraction method, i.e. total H<sub>2</sub> yield in neat water, H<sub>2</sub>, subtracted from that observed in formate solutions. Intra-track reactions cause H atom yields to decrease in time with the evolution of the radiation track and are responsible for lower H atom yield with increasing LET.

#### Acknowledgments


The authors thank Professor Michael Wiescher for making the facilities of the Notre Dame Nuclear Structure Laboratory available. The latter is funded by the National Science Foundation. This contribution is NDRL-4753 from the Notre Dame Radiation Laboratory, which is supported by the Office of Basic Energy Sciences of the US Department of Energy.

#### References

- Appleby, A., 1967. In: *The Chemistry of Ionization and Excitation*. Taylor & Francis, Ltd., London, pp. 269–275.
- Appleby, A., Schwarz, H.A., 1969. Radical and molecular yields in water irradiated by  $\gamma$  rays and heavy ions. *J. Phys. Chem.* 73, 1937–1941.
- Armstrong, D.A., 1987. In: *Radiation Chemistry. Principles and Applications*. VCH Publishers, New York, pp. 263–319.
- Buxton, G.V., 1987. In: *Radiation Chemistry. Principles and Applications*. VCH Publishers, New York, pp. 321–349.
- Buxton, G.V., Greenstock, C.L., Helman, W.P., Ross, A.B., 1988. Critical review of rate constants for reactions of hydrated electrons, hydrogen atoms and hydroxyl radicals (OH/O<sup>-</sup>) in aqueous solution. *J. Phys. Chem. Ref. Data* 17, 513–886.
- Chouraqi, M., Sutton, J., 1966. Origin of primary hydrogen atom yields in the radiolysis of aqueous solutions. *Trans. Faraday Soc.* 62, 2111–2120.
- Draganic, Z.D., Draganic, I.G., 1972. Studies on the formation of primary hydrogen atom yield (GH) in the  $\gamma$  radiolysis of water. *J. Phys. Chem.* 76, 2733–2737.
- Elliot, A.J., Chenier, M.P., Ouellette, D.C., Koslowsky, V.T., 1996. Temperature dependence of  $g$  values for aqueous solutions irradiated with 23 MeV <sup>2</sup>H<sup>+</sup> and 157 MeV <sup>7</sup>Li<sup>3+</sup> ion beams. *J. Phys. Chem.* 100, 9014–9020.
- Garrett, B.C., Dixon, D.A., Camaioni, D.M., et al., 2005. The role of water on electron-initiated processes and radical chemistry: issues and scientific advances. *Chem. Rev.* 105, 355–389.
- Johnson, G.R.A., Simic, M., 1967. Primary processes in the formation of hydrogen atoms in the radiolysis of water vapor. *J. Phys. Chem.* 71, 1118–1123.
- LaVerne, J.A., 2004. In: *Charged Particle and Photon Interactions with Matter*. Marcel Dekker, Inc., New York, pp. 403–429.
- LaVerne, J.A., Schuler, R.H., 1987a. Track effects in radiation-chemistry-production of HO<sub>2</sub> in the radiolysis of water by high-LET Ni<sup>58</sup> ions. *J. Phys. Chem.* 91, 6560–6563.
- LaVerne, J.A., Schuler, R.H., 1987b. Radiation chemical studies with heavy-ions-oxidation of ferrous ion in the fricke dosimeter. *J. Phys. Chem.* 91, 5770–5776.
- LaVerne, J.A., Stefanic, I., Pimblott, S.M., 2005. Hydrated electron yields in the heavy ion radiolysis of water. *J. Phys. Chem. A* 109, 9393–9401.
- Mahlman, H.A., 1966. Radiolysis of nitrous oxide saturated solutions: effect of sodium nitrate, 2-propanol, and sodium formate. *J. Phys. Chem.* 70, 3983–3987.
- Pastina, B., LaVerne, J.A., Pimblott, S.M., 1999. Dependence of molecular hydrogen formation in water on scavengers of the precursor to the hydrated electron. *J. Phys. Chem. A* 103, 5841–5846.
- Pimblott, S.M., LaVerne, J.A., 2002. Effects of track structure on the ion radiolysis of the fricke dosimeter. *J. Phys. Chem. A* 106, 9420–9427.
- Pimblott, S.M., Mozumder, A., 2004. In: *Charged Particle and Photon Interactions with Matter: Chemical, Physicochemical, and Biological Consequences with Applications*. Marcell-Dekker Inc., New York.
- Rice, S.A., 1985. *Diffusion-limited Reactions*. Elsevier, Amsterdam.
- Scholes, G., Simic, M., Weiss, J., 1963. Nature and reactivity of the primary reducing species in the radiolysis of aqueous solutions. *Discuss. Faraday Soc.* 36, 214–222.
- Scholes, G., Simic, M., 1964a. Action of  $g$ -rays on aqueous solutions of nitrous oxide and the effects of added solutes. *J. Phys. Chem.* 68, 1731–1737.
- Scholes, G., Simic, M., 1964b. Reactivity of the hydrogen atoms produced in the radiolysis of aqueous systems. *J. Phys. Chem.* 68, 1738–1743.
- Ziegler, J.F., Biersack, J.P., Littmark, U., 1985. *The Stopping and Range of Ions in Solids*. Pergamon, New York.

Presented at the Gordon Conference in Radiation Driven Processes in Physics, Chemistry and Biology, Proctor Academy, Andover, NH, USA, July 18-23, 2010.


The University of Manchester



## H ATOM FORMATION IN THE GAMMA AND HEAVY ION RADIOLYSIS OF AQUEOUS SYSTEMS

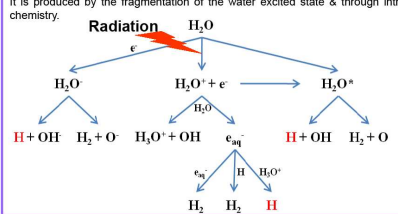
**M. Huerta Parajon<sup>a,b</sup>, Jay A. LaVerne<sup>a</sup> & Simon M. Pimblott<sup>b</sup>**

a University of Notre Dame, Notre Dame, IN 46556, USA  
b University of Manchester, Manchester, M13 9PL, UK  
e-mail: [monica.huerta@postgrad.manchester.ac.uk](mailto:monica.huerta@postgrad.manchester.ac.uk)



---

**The H atom is one of the most important species generated in the radiolysis of water.** It is produced by the fragmentation of the water excited state & through intra-track chemistry.



**Radiation**

$\text{H}_2\text{O} \xrightarrow{\text{Radiation}} \text{H}_2\text{O}^* \rightarrow \text{H} + \text{OH} \quad \text{H}_2 + \text{O}$

$\text{H}_2\text{O} + e^- \rightarrow \text{H}_2\text{O}^{\bullet-} \rightarrow \text{H} + \text{OH} \quad \text{H}_2 + \text{O}$

$\text{H}_2\text{O}^{\bullet-} + \text{H}_2\text{O} \rightarrow \text{H}_3\text{O}^+ + \text{OH}^- \rightarrow \text{H}_3\text{O}^+ + \text{OH}^- \rightarrow \text{H}_2 + \text{O}$

$\text{H}_2\text{O}^{\bullet-} + \text{H}_2\text{O} \rightarrow \text{H}_2 + \text{OH}^- \rightarrow \text{H}_2 + \text{O}$

$\text{H}_2\text{O}^{\bullet-} + \text{H}_2\text{O} \rightarrow \text{H}_2 + \text{OH}^- \rightarrow \text{H}_2 + \text{O}$

$\text{H}_2\text{O}^{\bullet-} + \text{H}_2\text{O} \rightarrow \text{H}_2 + \text{OH}^- \rightarrow \text{H}_2 + \text{O}$

**INTRODUCTION:**

Measurement of hydrogen atom yields is difficult. We have adopted two slightly different methods using GC and MS.

In the first method, H atoms produced by water radiolysis abstract hydrogen atoms from selected solutes to generate  $\text{H}_2$ :

$\bullet\text{H} + \text{HCO}_2^- \rightarrow \text{H}_2 + \text{CO}_2^-$

Then the H atom yield is calculated from the difference between the total  $\text{H}_2$  yield when solute is present and the yield when it is not, named as  $G^*(\text{H}_2)$ .

$G^*(\text{H}) = G(\text{H}_2) - G(\text{Total H}_2) - G^*(\text{H}_2)$

In the second method, HD is formed quantitatively by direct abstraction of D atoms from deuterated solutes.

$\bullet\text{H} + \text{DCO}_2^- \rightarrow \text{HD} + \text{CO}_2^-$

The yield of H atoms is obtained either by the directly measured HD yields or by the first method:

$G(\text{HD}) = G(\text{Total H}_2) - G^*(\text{H}_2)$

Additional H atoms are generated by the intra track reaction:

$\text{H}_2 + e_{aq}^- \rightarrow \bullet\text{H}$

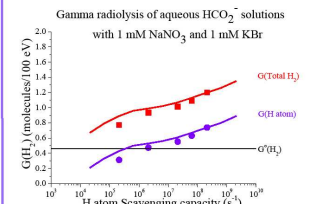
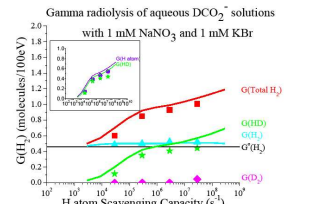
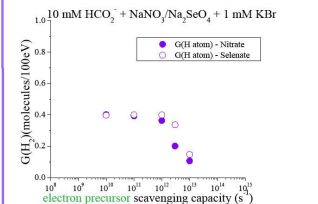
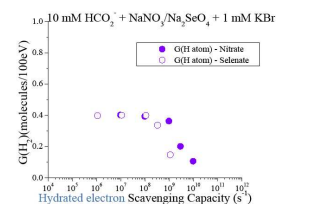
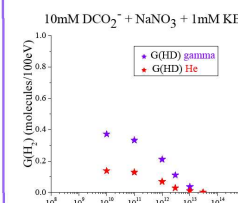
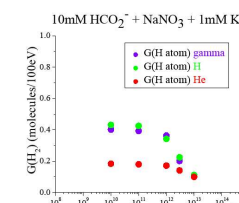
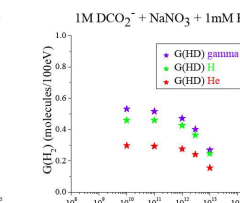
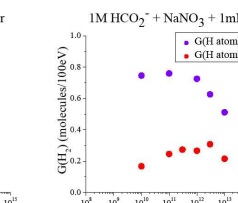
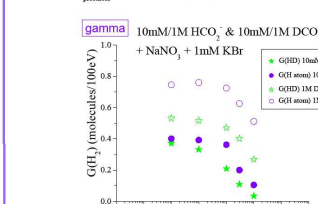
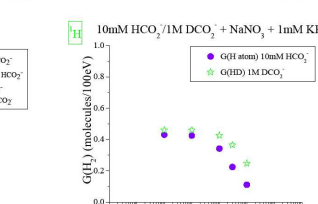
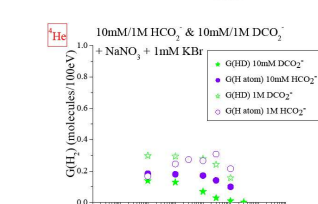
The yield of this reaction can be reduced by the addition of selected electron scavengers:

$\text{S} + e_{aq}^- \rightarrow \text{S}^-$   
 $\text{S} + e_{aq}^- \rightarrow \text{S}^-$

Heavy ions have higher LET values than gamma rays, which means that, an increase in the intra track reactions should be observed and, therefore, an increase on the molecular hydrogen yields.

---

**RESULTS:**

● H atom yields are accurately determined through the direct and indirect methods

● Similar curves of H atom yields are obtained as a function of the electron precursor scavenging capacity



● Different curves of H atom yields are obtained in terms of the hydrated electron scavenging capacity.

● This leads to suggest a stronger dependence of the H atom formation on the reactions of the primary electron.


---

● The H atom yield increases as the hydrogen atom scavenging capacity increases and decreases as the concentration of the electron scavenger and the LET of the radiation source increases.

**ACKNOWLEDGEMENTS:**

Presented at the 26th Miller Conference on Radiation Chemistry, Hotel Helikon, Keszthely, Hungary, August 28 – September 2, 2009.




MANCHESTER  
1824

## H ATOM FORMATION IN THE GAMMA AND <sup>4</sup>HE ION RADIOLYSIS OF AQUEOUS FORMATE SOLUTIONS

M. Huerta Parajon<sup>a,b</sup>, Jay A. LaVerne<sup>a</sup> & Simon M. Pimblott<sup>b</sup>

<sup>a</sup> University of Notre Dame, Notre Dame, IN 46556, USA  
<sup>b</sup> University of Manchester, Manchester, M13 9PL, UK  
e-mail: [monica.huerta@postgrad.manchester.ac.uk](mailto:monica.huerta@postgrad.manchester.ac.uk)



### INTRODUCTION:

The H atom is one of the most important species generated in the radiolysis of water. It is produced by the fragmentation of the water excited state & through intra-track chemistry.

**Radiation**

$$\text{H}_2\text{O} \xrightarrow{\text{e}^-} \text{H}_2\text{O}^{\bullet-} \quad \text{H}_2\text{O}^+ + \text{e}^- \quad \text{H}_2\text{O}^*$$

$$\text{H}_2\text{O}^{\bullet-} \rightarrow \text{H} + \text{OH}^- \quad \text{H}_2\text{O}^+ \xrightarrow{\text{H}_2\text{O}} \text{H}_3\text{O}^+ + \text{OH} \quad \text{H}_2\text{O}^* \rightarrow \text{H} + \text{OH}$$

$$\text{H}_2\text{O}^{\bullet-} \xrightarrow{\text{H}_2\text{O}} \text{H}_2 + \text{OH}^- \quad \text{H}_2\text{O}^+ \xrightarrow{\text{H}_2\text{O}} \text{H}_2 + \text{H}^+$$

Measurement of hydrogen atom yields is difficult. We have adopted two slightly different methods using GC and MS.

In the first method, H atoms produced by water radiolysis abstract hydrogen atoms from selected solutes to generate H<sub>2</sub>.

$$\bullet\text{H} + \text{HCO}_2^- \rightarrow \text{H}_2 + \bullet\text{CO}_2^-$$

Then the H atom yield is calculated from the difference between the total H<sub>2</sub> yield when solute is present and the yield when it is not, named as G<sup>o</sup>(H<sub>2</sub>).

$$G(\bullet\text{H}) = G(\text{Total H}_2) - G^o(\text{H}_2)$$

In the second method, HD is formed quantitatively by direct abstraction of D atoms from deuterated solutes

$$\bullet\text{H} + \text{DCO}_2^- \rightarrow \text{HD} + \bullet\text{CO}_2^-$$

and the yield of H atoms is obtained either by the directly measured HD yields or by the first method:

$$G(\text{HD}) = G(\text{Total H}_2) - G^o(\text{H}_2)$$

Additional H atoms are generated by the intra track reaction:

$$\text{H}_{\text{aq}}^+ + \text{e}_{\text{aq}}^- \rightarrow \bullet\text{H}$$

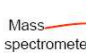
The yield of this reaction can be reduced by the addition of selected electron scavengers:

$$\text{S} + \text{e}_{\text{aq}}^- \rightarrow \text{S}^-$$


$$\text{S} + \text{e}_{\text{pre}}^- \rightarrow \text{S}^-$$

<sup>4</sup>He ions have higher LET values than gamma rays, which means that, an increase in the intra track reactions should be observed and, therefore, an increase on the molecular hydrogen yields.


### EXPERIMENTAL SETUP:



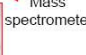
Mass spectrometer




Cell



GC



Mass spectrometer



Heavy ions accelerator

### MODELLING RADIATION PROCESSES:

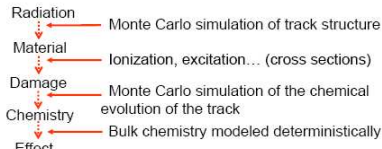
Radiation → Monte Carlo simulation of track structure

Material → Ionization, excitation... (cross sections)

Damage → Monte Carlo simulation of the chemical evolution of the track

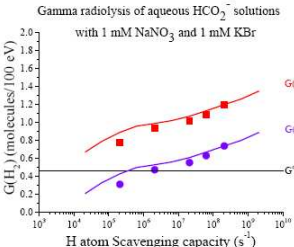
Chemistry → Bulk chemistry modeled deterministically

Effect

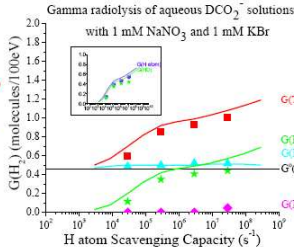


### RESULTS:

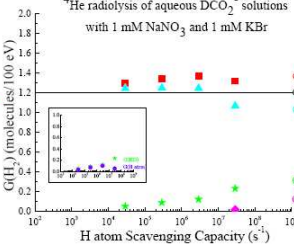
Gamma radiolysis of aqueous HCO<sub>2</sub><sup>-</sup> solutions with 1 mM NaNO<sub>3</sub> and 1 mM KBr



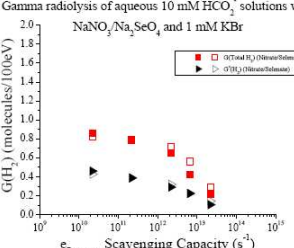
Gamma radiolysis of aqueous DCO<sub>2</sub><sup>-</sup> solutions with 1 mM NaNO<sub>3</sub> and 1 mM KBr



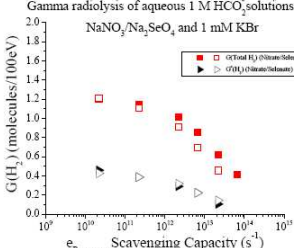
<sup>4</sup>He radiolysis of aqueous DCO<sub>2</sub><sup>-</sup> solutions with 1 mM NaNO<sub>3</sub> and 1 mM KBr



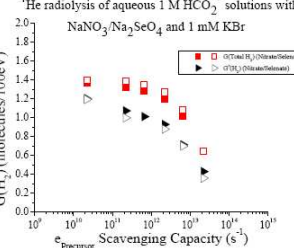
Gamma radiolysis of aqueous 10 mM HCO<sub>2</sub><sup>-</sup> solutions with NaNO<sub>3</sub>/Na<sub>2</sub>SeO<sub>4</sub> and 1 mM KBr



Gamma radiolysis of aqueous 1 M HCO<sub>2</sub><sup>-</sup> solutions with NaNO<sub>3</sub>/Na<sub>2</sub>SeO<sub>4</sub> and 1 mM KBr





<sup>4</sup>He radiolysis of aqueous 1 M HCO<sub>2</sub><sup>-</sup> solutions with NaNO<sub>3</sub>/Na<sub>2</sub>SeO<sub>4</sub> and 1 mM KBr




### REFERENCES:

- Pimblott, S. M. et al., Nucl. Instr. and Meth. B, 2002, **194** (3): p. 237-250.
- Pimblott S. M. & La Verne J. A., J. Phys. Chem. A, 1997, **101**: p. 5828-38.
- Huerta Parajon, M. et al., Rad. Phys. Chem., 2008, **77**, p. 1203-1207.
- Pastina, B. et al., J. Phys. Chem. A, 1999, **103**: p. 5841-46.


### ACKNOWLEDGEMENTS:

Presented at the Association for Radiation Research Annual Meeting, Glasgow, UK, June 22-24, 2009 and the 3rd European Nuclear Young Generation Forum, Córdoba, Spain, May 19–23, 2009.



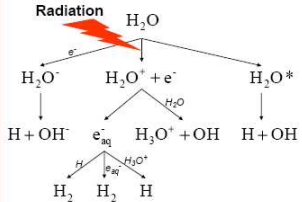
MANCHESTER  
1824



## H ATOM FORMATION IN THE GAMMA AND <sup>4</sup>HE ION RADIOLYSIS OF AQUEOUS FORMATE SOLUTIONS

**M. Huerta Parajon<sup>a,b</sup>, Jay A. LaVerne<sup>a</sup> & Simon M. Pimblott<sup>b</sup>**  
 a University of Notre Dame, Notre Dame, IN 46556, USA  
 b University of Manchester, Manchester, M13 9PL, UK  
 E-mail: [Monica.Huerta@postgrad.manchester.ac.uk](mailto:Monica.Huerta@postgrad.manchester.ac.uk) [Jay.LaVerne@nd.edu](mailto:Jay.LaVerne@nd.edu) [Simon.Pimblott@manchester.ac.uk](mailto:Simon.Pimblott@manchester.ac.uk)

**Radiation**



**Introduction:**

The H atom is one of the most important species generated in the radiolysis of water. It is produced by the fragmentation of the water excited state & through intra-track chemistry.

Measurement of hydrogen atom yields is difficult. We have adopted two slightly different methods using GC and MS.

In the first method, H atoms produced by water radiolysis abstract hydrogen atoms from selected solutes to generate H<sub>2</sub>.

$\bullet\text{H} + \text{HCO}_2^- \rightarrow \text{H}_2 + \bullet\text{CO}_2^-$

Then the H atom yield is calculated from the difference between the total H<sub>2</sub> yield when solute is present and the yield when it is not, named as G<sup>(H)</sup>.

$G^{(\text{H})} = G(\text{H}_2) = G(\text{Total H}_2) - G^{\circ}(\text{H}_2)$

In the second method, HD is formed quantitatively by direct abstraction of D atoms from deuterated solutes.

$\bullet\text{H} + \text{DCO}_2^- \rightarrow \text{HD} + \bullet\text{CO}_2^-$

and the yield of H atoms is obtained either by the directly measured HD yields or by the first method:

$G(\text{HD}) = G(\text{Total H}_2) - G^{\circ}(\text{H}_2)$

Additional H atoms are generated by the intra track reaction:

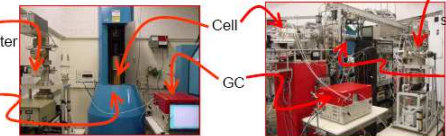
$\text{H}_{30}^+ + e_{30}^- \rightarrow \bullet\text{H}$

The yield of this reaction can be reduced by the addition of selected electron scavengers:

$\text{S} + e_{30}^- \rightarrow \text{S}^-$   
 $\text{S} + e_{\text{pre}}^- \rightarrow \text{S}^-$

<sup>4</sup>He ions have higher LET values than gamma rays, which means that, an increase in the intra track reactions should be observed and, therefore, an increase on the molecular hydrogen yields.

**Experimental setup:**



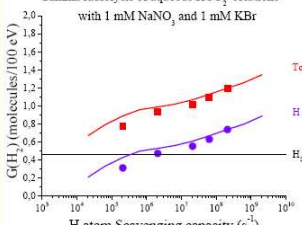
A gas chromatograph and a mass spectrometer are connected inline with the sample cell placed in the gamma source and on the heavy ions accelerator.

**Modelling radiation processes:**

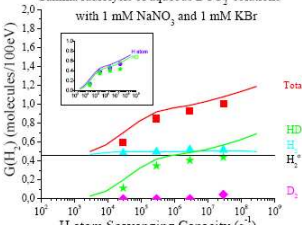
- Radiation → Monte Carlo simulation of track structure
- Material → Ionization, excitation... (cross sections)
- Damage → Monte Carlo simulation of the chemical evolution of the track
- Chemistry → Bulk chemistry modeled deterministically
- Effect

**Results:**

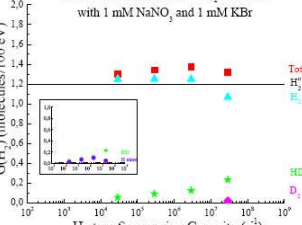
Gamma radiolysis of aqueous HCO<sub>2</sub><sup>-</sup> solutions with 1 mM NaNO<sub>3</sub> and 1 mM KBr



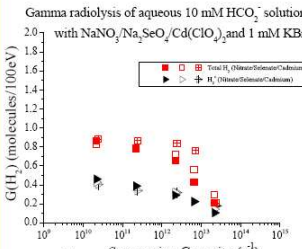
Gamma radiolysis of aqueous DCO<sub>2</sub><sup>-</sup> solutions with 1 mM NaNO<sub>3</sub> and 1 mM KBr



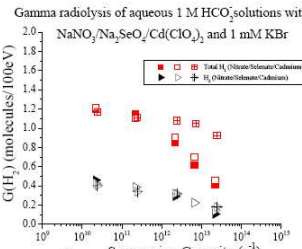
<sup>4</sup>He radiolysis of aqueous DCO<sub>2</sub><sup>-</sup> solutions with 1 mM NaNO<sub>3</sub> and 1 mM KBr



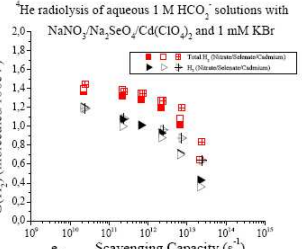
Gamma radiolysis of aqueous 10 mM HCO<sub>2</sub><sup>-</sup> solutions with NaNO<sub>3</sub>/Na<sub>2</sub>SeO<sub>4</sub>/Cd(ClO<sub>4</sub>)<sub>2</sub> and 1 mM KBr



Gamma radiolysis of aqueous 1 M HCO<sub>2</sub><sup>-</sup> solutions with NaNO<sub>3</sub>/Na<sub>2</sub>SeO<sub>4</sub>/Cd(ClO<sub>4</sub>)<sub>2</sub> and 1 mM KBr



<sup>4</sup>He radiolysis of aqueous 1 M HCO<sub>2</sub><sup>-</sup> solutions with NaNO<sub>3</sub>/Na<sub>2</sub>SeO<sub>4</sub>/Cd(ClO<sub>4</sub>)<sub>2</sub> and 1 mM KBr



**References:**


- Pimblott, S.M. et al., *Energy loss by non-relativistic electrons and positrons in liquid water*. Nuclear Instruments and Methods in Physics Research Section B: Beam Interactions with Materials and Atoms, 2002, **194**(3): p. 237-250.
- Pimblott S.M. & La Verne J.A., *Stochastic Simulation of the Electron Radiolysis of Water and Aqueous Solutions*, Journal of Physical Chemistry A, 1997, **101**: p. 5828-38.
- Huerta Parajon, M.; et al., *H Atom Yields in the Radiolysis of Water*. Radiation Physical Chemistry, 2008 (in press).
- Pastina, B. et al., *Dependence of Molecular Hydrogen Formation in Water on Scavengers of the Precursor to the Hydrated Electron*. J. Phys. Chem. A, 1999, **103**: p. 5841-46.

**Acknowledgements:**


- British Nuclear Decommissioning Authority.
- Office of Basic Energy Sciences of the U.S. Department of Energy.
- The University of Manchester, UK.
- Radiation Laboratory at The University of Notre Dame, IN, USA.



Presented at the Gordon Conference in Radiation Driven Processes in Physics, Chemistry and Biology, Waterville Valley Resort, Waterville Valley, NH, USA, July 6-11, 2008.



**MANCHESTER**  
1824



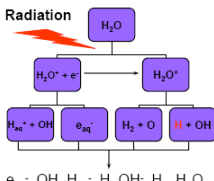
## Hydrogen atom yields in the radiolysis of water

**M. Huerta Parajon<sup>a,b</sup>, Jay A. LaVerne<sup>a</sup> & Simon M. Pimblott<sup>b</sup>**  
 a University of Notre Dame, Notre Dame, IN 46556, USA  
 b University of Manchester, Manchester, M13 9PL, UK  
 E-mail: [Monica.Huerta@postgrad.manchester.ac.uk](mailto:Monica.Huerta@postgrad.manchester.ac.uk), [Jay.LaVerne@nd.edu](mailto:Jay.LaVerne@nd.edu), [Simon.Pimblott@manchester.ac.uk](mailto:Simon.Pimblott@manchester.ac.uk)

**Introduction:**

H atom is one of the most important species generated after radiolysis of water due to the fragmentation of the water excited state.

**Radiation**



$e_{aq}^- + OH, H_{aq}^+, H, OH, H_2, H_2O_2$

The measurement of hydrogen atom yields is difficult. We adopted two different methods using GC and MS techniques.

In the first method, H atoms produced after radiolysis of water abstract atomic hydrogen from selected solutes to generate  $H_2$ . H atom yields are then calculated from the difference between the  $H_2$  yields when solute is added and when it is not.

**$H_2$  generation after water irradiation:**

$$H_2O^+ + e^- \rightarrow H_2O^{\bullet+} \rightarrow H_2 + O$$

$$e^- + H_2O \rightarrow \dot{H}_2O^- \rightarrow H_2 + O$$

$$H_2O + e^- \rightarrow \dot{H}_2O^{\bullet-} \rightarrow H + OH (+H_2O) \rightarrow H_2 + OH + OH$$

$$\bullet H + e_{aq}^- \rightarrow \dot{H}_2$$

$$\bullet H + \bullet H \rightarrow H_2$$

$$e_{aq}^- + e_{aq}^- \rightarrow H_2$$

$H_2^{\bullet}$

**Addition of selected solutes:**

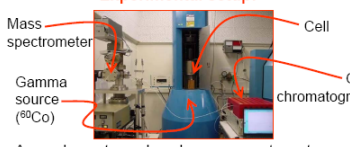
$$\bullet H + RH \rightarrow H_2 + \bullet R \quad RH = HCO_2^-, CH_3OH$$

$$\text{Total } H_2 \text{ measured} = H_2^0 + H_2 (\bullet H)$$

In the second method, HD is formed quantitatively by direct abstraction of D atoms from deuterated solutes.

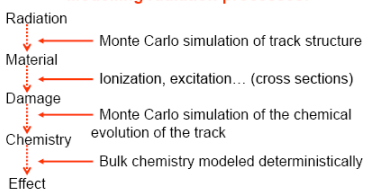
$$\bullet H + RD \rightarrow HD + \bullet R \quad RD = DCO_2^-, CD_3OH$$

**Experimental setup:**



A gas chromatograph and a mass spectrometer are connected inline with the sample cell placed in the gamma source.

**Modelling radiation processes:**



**Results:**

**HCO<sub>2</sub><sup>-</sup> + 1 mM NaNO<sub>3</sub> + 1 mM KBr**

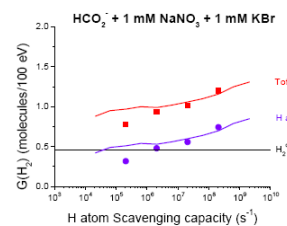


Figure 1. Production of  $H_2$  in the gamma radiolysis of aqueous formate solutions as a function of the formate scavenging capacity for H atoms:  $\blacksquare$  Total  $H_2$ ,  $\bullet$  Hydrogen atom. The black line is the  $H_2^0$  yield determined in water with 1 mM  $NO_3^-$  and no formate. Coloured lines are the results of the Monte Carlo calculations.

**DCO<sub>2</sub><sup>-</sup> + 1 mM NaNO<sub>3</sub> + 1 mM KBr**

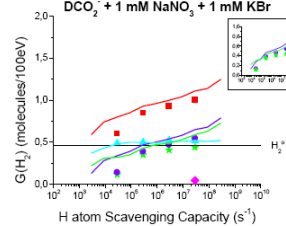


Figure 2. Production of  $H_2$  in the gamma radiolysis of aqueous deuterated formate solutions as a function of the deuterated formate scavenging capacity for H atoms:  $\blacksquare$  Total  $H_2$ ,  $\bullet$  H atom,  $\blacktriangle$   $H_2$ ,  $\blacklozenge$  HD and  $\blacklozenge$   $D_2$ . The black line is the  $H_2^0$  yield determined in water with 1 mM  $NO_3^-$  and no deuterated formate. Coloured lines are the results of the Monte Carlo calculations.

**CH<sub>3</sub>OH + 1 mM NaNO<sub>3</sub> + 1 mM KBr**

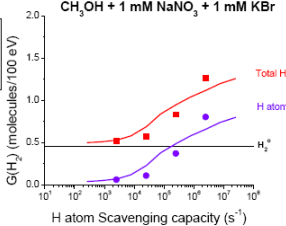


Figure 3. Production of  $H_2$  in the gamma radiolysis of aqueous methanol solutions as a function of the methanol scavenging capacity for H atoms:  $\blacksquare$  Total  $H_2$ ,  $\bullet$  Hydrogen atom. The black line is the  $H_2^0$  yield determined in water with 1 mM  $NO_3^-$  and no methanol. Coloured lines are the results of the Monte Carlo calculations.

**CD<sub>3</sub>OH + 1 mM NaNO<sub>3</sub> + 1 mM KBr**

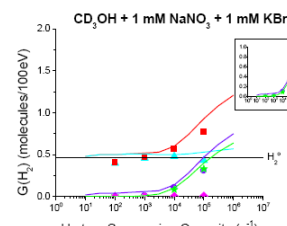


Figure 4. Production of  $H_2$  in the gamma radiolysis of aqueous deuterated methanol solutions as a function of the deuterated methanol scavenging capacity for H atoms:  $\blacksquare$  Total  $H_2$ ,  $\bullet$  H atom,  $\blacktriangle$   $H_2$ ,  $\blacklozenge$  HD and  $\blacklozenge$   $D_2$ . The black line is the  $H_2^0$  yield determined in water with 1 mM  $NO_3^-$  and no deuterated methanol. Coloured lines are the results of the Monte Carlo calculations.

**10 mM HCO<sub>2</sub><sup>-</sup> + NaNO<sub>3</sub> + 1 mM KBr**

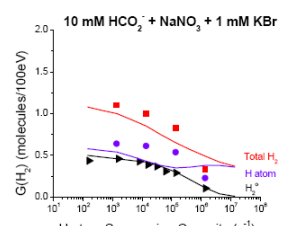


Figure 5. Production of  $H_2$  in the gamma radiolysis of 10 mM aqueous formate solutions with different added concentrations of nitrate as a function of the nitrate scavenging capacity for H atoms:  $\blacksquare$  Total  $H_2$ ,  $\bullet$  H atom. The black line and dots are the  $H_2^0$  yield determined in water varying the concentration of  $NO_3^-$  and no formate addition. Coloured lines are the results of the Monte Carlo calculations.

**10 mM DCO<sub>2</sub><sup>-</sup> + NaNO<sub>3</sub> + 1 mM KBr**

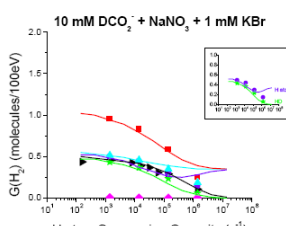


Figure 6. Production of  $H_2$  in the gamma radiolysis of 10 mM aqueous deuterated formate solutions and different added concentrations of nitrate as a function of the nitrate scavenging capacity for H atoms:  $\blacksquare$  Total  $H_2$ ,  $\bullet$  H atom,  $\blacktriangle$   $H_2$ ,  $\blacklozenge$  HD,  $\blacklozenge$   $D_2$ . The black line and dots are the  $H_2^0$  yield determined in water varying the concentration of  $NO_3^-$  and no deuterated formate addition. Coloured lines are the results of the Monte Carlo calculations.

**References:**

- Pimblott, S.M. et al. *Energy loss by non-relativistic electrons and positrons in liquid water*. Nuclear Instruments and Methods in Physics Research Section B: Beam Interactions with Materials and Atoms. 2002. 194(3): p. 237-250.
- Pimblott S.M. & La Verne J.A., *Stochastic Simulation of the Electron Radiolysis of Water and Aqueous Solutions*, Journal of Physical Chemistry A, 1997, 101: p. 5828-38.
- Huerta Parajon, M.; et al., *H Atom Yields in the Radiolysis of Water*. Radiation Physical Chemistry, 2008 (in press).

**Acknowledgements:**

- Nuclear Decommissioning Authority.
- Office of Basic Energy Sciences of the U.S. Department of Energy.
- The University of Manchester.
- The University of Notre Dame.

## APPENDIX B

### Yields and standard errors

1.1	Introduction.....	179
1.2	Gamma radiolysis.....	179
1.2.1	Variation of formate.....	179
1.2.2	Variation of nitrate.....	180
1.2.3	Variation of selenate.....	183
1.3	<sup>1</sup> H radiolysis.....	185
1.3.1	No addition of hydrogen atom scavenger.....	185
1.3.2	Variation of nitrate.....	186
1.3.3	Variation of selenate.....	187
1.4	<sup>4</sup> He radiolysis.....	189
1.4.1	No addition of hydrogen atom scavenger.....	189
1.4.2	Variation of nitrate.....	190
1.4.3	Variation of selenate.....	193

## 1.1 Introduction

Three or more measurements were made for each experimental point. The associated errors to the experimental values are smaller than the symbol used to represent each point. The error associated with the scatter of the experimental measurements is expected to be significantly larger than errors introduced by other parameters such as change in humidity (as measurements were made in different seasons and laboratories) or change of nylon cords used to connect the sample cell with the GC and MS (which may cause better isolation). Every measurement with their respective averages and standard deviations are presented in this appendix.

## 1.2 Gamma radiolysis

## 1.2.1 Variation of sodium formate

<b>[HCO<sub>2</sub>]</b>	<b>1 mM</b>	<b>10 mM</b>	<b>100 mM</b>	<b>300 mM</b>	<b>1 M</b>
<b>[NaNO<sub>3</sub>]</b>	<b>G(Total H<sub>2</sub>) (molecules / 100 eV)</b>				
<b>1 mM</b>	0.8579	0.9493	1.0226	1.1049	1.2101
	0.7864	0.9338	1.0134	1.0813	1.1921
	0.8123	0.9326	1.0051	1.0848	1.1924
	0.7230	0.9219			
	0.6842				
<b>Average</b>	<b>0.7728</b>	<b>0.9344</b>	<b>1.0137</b>	<b>1.0904</b>	<b>1.1982</b>
<b>Std.Dev. (±)</b>	<b>0.0695</b>	<b>0.0113</b>	<b>0.0088</b>	<b>0.0127</b>	<b>0.0103</b>
<b>24 mM</b>	0.6812	0.5838	0.7934	0.9600	0.8992
	0.6412	0.8163	0.7696	0.9458	0.8806
	0.6409	0.8278	0.9013	0.9591	0.8815
<b>Average</b>	<b>0.6544</b>	<b>0.7426</b>	<b>0.8214</b>	<b>0.9550</b>	<b>0.8871</b>
<b>Std.Dev. (±)</b>	<b>0.0232</b>	<b>0.1377</b>	<b>0.0702</b>	<b>0.0079</b>	<b>0.0105</b>

<b>[HCO<sub>2</sub>]</b>	<b>1 mM</b>	<b>10 mM</b>	<b>100 mM</b>	<b>300 mM</b>	<b>1 M</b>
<b>[Na<sub>2</sub>SeO<sub>4</sub>]</b>	<b>G(Total H<sub>2</sub>) (molecules / 100 eV)</b>				
<b>1 mM</b>	0.8651	0.9012	0.9483	0.9495	1.0938
	0.8661	0.8946	0.9373	0.9532	1.1218
	0.8660	0.8937	0.9429	0.9980	1.1257
<b>Average</b>	<b>0.8657</b>	<b>0.8965</b>	<b>0.9428</b>	<b>0.9669</b>	<b>1.1138</b>
<b>Std.Dev. (±)</b>	<b>0.0006</b>	<b>0.0041</b>	<b>0.0055</b>	<b>0.0270</b>	<b>0.0174</b>
<b>100 mM</b>	0.6623	0.7144	0.7737	0.8562	0.9806
	0.6619	0.7180	0.7766	0.8414	0.9728
	0.6357	0.7106	0.7754	0.8170	0.9827
<b>Average</b>	<b>0.6533</b>	<b>0.7143</b>	<b>0.7752</b>	<b>0.8382</b>	<b>0.9787</b>
<b>Std.Dev. (±)</b>	<b>0.0153</b>	<b>0.0037</b>	<b>0.0015</b>	<b>0.0198</b>	<b>0.0052</b>

## 1.2.2 Variation of nitrate

<b>[HCO<sub>2</sub>]</b>	<b>10 mM</b>	<b>1 M</b>
<b>[NaNO<sub>3</sub>]</b>	<b>G(Total H<sub>2</sub>) (molecules / 100 eV)</b>	
<b>1 mM</b>	0.8640	1.2034
	0.8633	1.2145
	0.8571	1.2007
<b>Average</b>	<b>0.8615</b>	<b>1.2062</b>
<b>Std.Dev. (±)</b>	<b>0.0038</b>	<b>0.0073</b>
<b>10 mM</b>	0.7933	1.1415
	0.7793	1.1529
	0.7680	1.1467
<b>Average</b>	<b>0.7802</b>	<b>1.1470</b>
<b>Std.Dev. (±)</b>	<b>0.0127</b>	<b>0.0057</b>
<b>100 mM</b>	0.6676	1.0127
	0.6594	1.0206
	0.6363	1.0147
<b>Average</b>	<b>0.6544</b>	<b>1.0160</b>
<b>Std.Dev. (±)</b>	<b>0.0163</b>	<b>0.0041</b>
<b>300 mM</b>	0.4326	0.8530
	0.4297	0.8512
	0.4143	0.8476
<b>Average</b>	<b>0.4255</b>	<b>0.8506</b>
<b>Std.Dev. (±)</b>	<b>0.0098</b>	<b>0.0028</b>
<b>1 M</b>	0.1959	0.6402
	0.2355	0.5976
	0.2032	0.6140
<b>Average</b>	<b>0.2115</b>	<b>0.6173</b>
<b>Std.Dev. (±)</b>	<b>0.0211</b>	<b>0.0215</b>
<b>3 M</b>		0.4078
		0.4303
		0.3966
<b>Average</b>		<b>0.4116</b>
<b>Std.Dev. (±)</b>		<b>0.0171</b>

<b>[DCO<sub>2</sub>]</b>	<b>10 mM</b>			
<b>[NaNO<sub>3</sub>]</b>	<b>G(Total H<sub>2</sub>)</b> molecules/100eV	<b>G(H<sub>2</sub>)</b> molecules/100eV	<b>G(HD)</b> molecules/100eV	<b>G(D<sub>2</sub>)</b> molecules/100eV
<b>1 mM</b>	0.8592	0.3918	0.4670	0.0005
	0.7547	0.4122	0.3425	0.0000
	0.7349	0.4134	0.3196	0.0018
<b>Average</b>	<b>0.7829</b>	<b>0.4058</b>	<b>0.3764</b>	<b>0.0008</b>
<b>Std.Dev.</b>	<b>0.0668</b>	<b>0.0122</b>	<b>0.0793</b>	<b>0.0010</b>
<b>10 mM</b>	0.7628	0.3354	0.4250	0.0023
	0.7067	0.3767	0.3300	0.0000
	0.6246	0.3763	0.2474	0.0010
<b>Average</b>	<b>0.6981</b>	<b>0.3628</b>	<b>0.3341</b>	<b>0.0011</b>
<b>Std.Dev.</b>	<b>0.0695</b>	<b>0.0237</b>	<b>0.0889</b>	<b>0.0012</b>
<b>100 mM</b>	0.5056	0.2439	0.2611	0.0006
	0.4577	0.2544	0.2033	0.0000
	0.4312	0.2605	0.1700	0.0007
<b>Average</b>	<b>0.4648</b>	<b>0.2529</b>	<b>0.2115</b>	<b>0.0004</b>
<b>Std.Dev.</b>	<b>0.0377</b>	<b>0.0084</b>	<b>0.0461</b>	<b>0.0004</b>
<b>300 mM</b>	0.3449	0.2040	0.1394	0.0015
	0.3023	0.1893	0.1117	0.0013
	0.2762	0.1919	0.0836	0.0007
<b>Average</b>	<b>0.3078</b>	<b>0.1951</b>	<b>0.1116</b>	<b>0.0011</b>
<b>Std.Dev.</b>	<b>0.0347</b>	<b>0.0079</b>	<b>0.0279</b>	<b>0.0004</b>
<b>1 M</b>	0.1446	0.1034	0.0411	0.0001
	0.1418	0.1057	0.0360	0.0001
	0.1433	0.1129	0.0304	0.0000
<b>Average</b>	<b>0.1432</b>	<b>0.1074</b>	<b>0.0358</b>	<b>0.0000</b>
<b>Std.Dev.</b>	<b>0.0014</b>	<b>0.0049</b>	<b>0.0053</b>	<b>0.0000</b>

[DCO <sub>2</sub> ]	1 M			
[NaNO <sub>3</sub> ]	G(Total H <sub>2</sub> ) molecules/100eV	G(H <sub>2</sub> ) molecules/100eV	G(HD) molecules/100eV	G(D <sub>2</sub> ) molecules/100eV
1 mM	0.9209	0.2880	0.5389	0.0940
	0.9118	0.2804	0.5385	0.0928
	0.8933	0.2819	0.5197	0.0916
<b>Average</b>	<b>0.9086</b>	<b>0.2835</b>	<b>0.5324</b>	<b>0.0928</b>
<b>Std.Dev.</b>	<b>0.0141</b>	<b>0.0040</b>	<b>0.0110</b>	<b>0.0012</b>
10 mM	0.8347	0.2305	0.5148	0.0894
	0.8426	0.2402	0.5138	0.0887
	0.8495	0.2367	0.5222	0.0906
<b>Average</b>	<b>0.8423</b>	<b>0.2358</b>	<b>0.5169</b>	<b>0.0896</b>
<b>Std.Dev.</b>	<b>0.0074</b>	<b>0.0049</b>	<b>0.0046</b>	<b>0.0010</b>
100 mM	0.7187	0.1637	0.4708	0.0842
	0.7295	0.1605	0.4783	0.0906
	0.7186	0.1622	0.4683	0.0881
<b>Average</b>	<b>0.7223</b>	<b>0.1622</b>	<b>0.4725</b>	<b>0.0876</b>
<b>Std.Dev.</b>	<b>0.0063</b>	<b>0.0016</b>	<b>0.0052</b>	<b>0.0032</b>
300 mM	0.6120	0.1172	0.4089	0.0859
	0.6076	0.1204	0.4022	0.0850
	0.5966	0.1139	0.3959	0.0868
<b>Average</b>	<b>0.6054</b>	<b>0.1172</b>	<b>0.4023</b>	<b>0.0859</b>
<b>Std.Dev.</b>	<b>0.0080</b>	<b>0.0032</b>	<b>0.0065</b>	<b>0.0009</b>
1 M	0.4266	0.0625	0.2858	0.0782
	0.4064	0.0623	0.2667	0.0774
	0.4039	0.0597	0.2661	0.0781
<b>Average</b>	<b>0.4123</b>	<b>0.0615</b>	<b>0.2729</b>	<b>0.0779</b>
<b>Std.Dev.</b>	<b>0.0124</b>	<b>0.0016</b>	<b>0.0112</b>	<b>0.0004</b>

## 1.2.3 Variation of selenate

<b>[HCO<sub>2</sub><sup>-</sup>]</b>	<b>10 mM</b>	<b>1 M</b>
<b>[Na<sub>2</sub>SeO<sub>4</sub>]</b>	<b>G(Total H<sub>2</sub>) (molecules / 100 eV)</b>	
<b>1 mM</b>	0.8335	1.2369
	0.8360	1.2042
	0.8062	1.1979
<b>Average</b>	<b>0.8252</b>	<b>1.2130</b>
<b>Std.Dev.</b>	<b>0.0165</b>	<b>0.0209</b>
<b>10 mM</b>	0.7704	1.1083
	0.8138	1.1034
	0.7811	
<b>Average</b>	<b>0.7884</b>	<b>1.1416</b>
<b>Std.Dev.</b>	<b>0.0226</b>	<b>0.0034</b>
<b>100 mM</b>	0.7503	0.9113
	0.7207	0.8970
	0.6833	0.9139
<b>Average</b>	<b>0.7181</b>	<b>0.9074</b>
<b>Std.Dev.</b>	<b>0.0336</b>	<b>0.0091</b>
<b>300 mM</b>	0.5692	0.6682
	0.5551	0.7483
	0.5566	0.6748
<b>Average</b>	<b>0.5603</b>	<b>0.6971</b>
<b>Std.Dev.</b>	<b>0.0078</b>	<b>0.0445</b>
<b>1 M</b>	0.2736	0.4669
	0.3215	0.4590
	0.2801	0.4434
<b>Average</b>	<b>0.2917</b>	<b>0.4564</b>
<b>Std.Dev.</b>	<b>0.0260</b>	<b>0.0119</b>

[DCO <sub>2</sub> ]	10 mM			
[Na <sub>2</sub> SeO <sub>4</sub> ]	G(Total H <sub>2</sub> ) molecules/100eV	G(H <sub>2</sub> ) molecules/100eV	G(HD) molecules/100eV	G(D <sub>2</sub> ) molecules/100eV
1 mM	0.8632	0.4322	0.4301	0.0010
	0.8492	0.4633	0.3852	0.0007
	0.8375	0.4611	0.3753	0.0011
<b>Average</b>	<b>0.8500</b>	<b>0.4522</b>	<b>0.3968</b>	<b>0.0010</b>
<b>Std.Dev.</b>	<b>0.0129</b>	<b>0.0174</b>	<b>0.0292</b>	<b>0.0002</b>
10 mM	0.7975	0.3697	0.4276	0.0002
	0.8168	0.3854	0.4300	0.0014
	0.8128	0.3904	0.4214	0.0010
<b>Average</b>	<b>0.8090</b>	<b>0.3818</b>	<b>0.4264</b>	<b>0.0009</b>
<b>Std.Dev.</b>	<b>0.0102</b>	<b>0.0108</b>	<b>0.0044</b>	<b>0.0006</b>
100 mM	0.6495	0.2776	0.3694	0.0025
	0.6417	0.2720	0.3679	0.0018
	0.6495	0.2810	0.3675	0.0009
<b>Average</b>	<b>0.6469</b>	<b>0.2769</b>	<b>0.3683</b>	<b>0.0017</b>
<b>Std.Dev.</b>	<b>0.0045</b>	<b>0.0045</b>	<b>0.0010</b>	<b>0.0008</b>
300 mM	0.4549	0.1764	0.2778	0.0007
	0.4654	0.1857	0.2791	0.0007
	0.4585	0.1842	0.2735	0.0009
<b>Average</b>	<b>0.4596</b>	<b>0.1821</b>	<b>0.2768</b>	<b>0.0007</b>
<b>Std.Dev.</b>	<b>0.0053</b>	<b>0.0050</b>	<b>0.0029</b>	<b>0.0001</b>
1 M	0.2268	0.0806	0.1462	0.0000
	0.2292	0.0951	0.1335	0.0005
	0.2323	0.0996	0.1324	0.0003
<b>Average</b>	<b>0.2294</b>	<b>0.0918</b>	<b>0.1374</b>	<b>0.0003</b>
<b>Std.Dev.</b>	<b>0.0028</b>	<b>0.0099</b>	<b>0.0077</b>	<b>0.0003</b>



1.3  $^1\text{H}$  radiolysis

## 1.3.1 No addition of hydrogen atom scavenger

<b>[NaNO<sub>3</sub>]</b>	<b>G°(H<sub>2</sub>)</b>
<b>1 mM</b>	0.7724
	0.7673
	0.7686
<b>Average</b>	<b>0.7694</b>
<b>Std.Dev.</b>	<b>0.0026</b>
<b>10 mM</b>	0.6050
	0.6294
	0.6232
<b>Average</b>	<b>0.6192</b>
<b>Std.Dev.</b>	<b>0.0127</b>
<b>30 mM</b>	0.5432
	0.5635
	0.5806
<b>Average</b>	<b>0.5624</b>
<b>Std.Dev.</b>	<b>0.0187</b>
<b>100 mM</b>	0.4652
	0.4836
	0.4571
<b>Average</b>	<b>0.4686</b>
<b>Std.Dev.</b>	<b>0.0135</b>
<b>300 mM</b>	0.3200
	0.3232
	0.3158
<b>Average</b>	<b>0.3197</b>
<b>Std.Dev.</b>	<b>0.0037</b>
<b>1 M</b>	0.1423
	0.1476
	0.1480
<b>Average</b>	<b>0.1460</b>
<b>Std.Dev.</b>	<b>0.0032</b>

## 1.3.2 Variation of nitrate

<b>[HCO<sub>2</sub><sup>-</sup>]</b>	<b>10 mM</b>
<b>[NaNO<sub>3</sub>]</b>	<b>G(Total H<sub>2</sub>) (molecules / 100 eV)</b>
<b>1 mM</b>	1.2111
	1.1899
	1.1994
<b>Average</b>	<b>1.2001</b>
<b>Std.Dev. (±)</b>	<b>0.0106</b>
<b>10 mM</b>	1.0415
	1.0438
	1.0474
<b>Average</b>	<b>1.0442</b>
<b>Std.Dev. (±)</b>	<b>0.0030</b>
<b>100 mM</b>	0.8119
	0.8171
	0.8025
<b>Average</b>	<b>0.8105</b>
<b>Std.Dev. (±)</b>	<b>0.0074</b>
<b>300 mM</b>	0.5470
	0.5435
	0.5413
<b>Average</b>	<b>0.5439</b>
<b>Std.Dev. (±)</b>	<b>0.0029</b>
<b>1 M</b>	0.2604
	0.2563
	0.2540
<b>Average</b>	<b>0.2569</b>
<b>Std.Dev. (±)</b>	<b>0.0033</b>

<b>[DCO<sub>2</sub>]</b>	<b>1 M</b>			
<b>[NaNO<sub>3</sub>]</b>	<b>G(Total H<sub>2</sub>)</b> molecules/100eV	<b>G(H<sub>2</sub>)</b> molecules/100eV	<b>G(HD)</b> molecules/100eV	<b>G(D<sub>2</sub>)</b> molecules/100eV
<b>1 mM</b>	1.1445	0.6164	0.4628	0.0654
	1.1165	0.5998	0.4490	0.0677
	1.1411	0.6055	0.4675	0.0681
<b>Average</b>	<b>1.1340</b>	<b>0.6072</b>	<b>0.4597</b>	<b>0.0671</b>
<b>Std.Dev.</b>	<b>0.0153</b>	<b>0.0084</b>	<b>0.0096</b>	<b>0.0015</b>
<b>10 mM</b>	1.0287	0.5033	0.4548	0.0706
	1.0605	0.5304	0.4754	0.0546
	1.0273	0.5088	0.4501	0.0684
<b>Average</b>	<b>1.0389</b>	<b>0.5142</b>	<b>0.4601</b>	<b>0.0646</b>
<b>Std.Dev.</b>	<b>0.0188</b>	<b>0.0143</b>	<b>0.0135</b>	<b>0.0087</b>
<b>100 mM</b>	0.8522	0.3587	0.4242	0.0693
	0.8603	0.3611	0.4272	0.0720
	0.8498	0.3514	0.4269	0.0715
<b>Average</b>	<b>0.8541</b>	<b>0.3571</b>	<b>0.4261</b>	<b>0.0709</b>
<b>Std.Dev.</b>	<b>0.0055</b>	<b>0.0051</b>	<b>0.0017</b>	<b>0.0014</b>
<b>300 mM</b>	0.7008	0.2629	0.3666	0.0714
	0.6966	0.2607	0.3644	0.0716
	0.6951	0.2581	0.3650	0.0720
<b>Average</b>	<b>0.6975</b>	<b>0.2605</b>	<b>0.3653</b>	<b>0.0716</b>
<b>Std.Dev.</b>	<b>0.0029</b>	<b>0.0024</b>	<b>0.0012</b>	<b>0.0003</b>
<b>1 M</b>	0.4561	0.1383	0.2507	0.0671
	0.4489	0.1346	0.2469	0.0674
	0.4443	0.1315	0.2457	0.0672
<b>Average</b>	<b>0.4498</b>	<b>0.1348</b>	<b>0.2478</b>	<b>0.0672</b>
<b>Std.Dev.</b>	<b>0.0059</b>	<b>0.0034</b>	<b>0.0026</b>	<b>0.0001</b>

## 1.3.3 Variation of selenate

<b>[HCO<sub>2</sub>]</b>	<b>10 mM</b>
<b>[Na<sub>2</sub>SeO<sub>4</sub>]</b>	<b>G(Total H<sub>2</sub>) (molecules / 100 eV)</b>
<b>1 mM</b>	1.1726
	1.1661
	1.1513
<b>Average</b>	<b>1.1633</b>
<b>Std.Dev.</b>	<b>0.0109</b>
<b>10 mM</b>	1.0516
	1.0733
	1.0454
<b>Average</b>	<b>1.0568</b>
<b>Std.Dev.</b>	<b>0.0147</b>
<b>100 mM</b>	0.7972
	0.7990
	0.8036
<b>Average</b>	<b>0.7999</b>
<b>Std.Dev.</b>	<b>0.0033</b>
<b>300 mM</b>	0.5982
	0.5923
	0.5928
<b>Average</b>	<b>0.5944</b>
<b>Std.Dev.</b>	<b>0.0033</b>
<b>1 M</b>	0.3198
	0.3140
	0.3309
<b>Average</b>	<b>0.3216</b>
<b>Std.Dev.</b>	<b>0.0086</b>

1.4  $^4\text{He}$  radiolysis

## 1.4.1 No addition of hydrogen atom scavenger

<b>[NaNO<sub>3</sub>]</b>	<b>G°(H<sub>2</sub>)</b>
<b>1 mM</b>	1.3108
	1.2642
	1.2080
<b>Average</b>	<b>1.2610</b>
<b>Std.Dev.</b>	<b>0.0515</b>
<b>10 mM</b>	1.1506
	1.1690
	1.1531
<b>Average</b>	<b>1.1576</b>
<b>Std.Dev.</b>	<b>0.0100</b>
<b>30 mM</b>	1.0732
	1.0660
	1.0821
<b>Average</b>	<b>1.0737</b>
<b>Std.Dev.</b>	<b>0.0081</b>
<b>100 mM</b>	1.0126
	1.0093
	1.0146
<b>Average</b>	<b>1.0122</b>
<b>Std.Dev.</b>	<b>0.0027</b>
<b>300 mM</b>	0.9214
	0.9302
	0.9371
<b>Average</b>	<b>0.9296</b>
<b>Std.Dev.</b>	<b>0.0079</b>
<b>1 M</b>	0.7103
	0.7115
	0.7201
<b>Average</b>	<b>0.7140</b>
<b>Std.Dev.</b>	<b>0.0053</b>
<b>3 M</b>	0.2039
	0.1922
	0.1957
<b>Average</b>	<b>0.1973</b>
<b>Std.Dev.</b>	<b>0.0060</b>

## 1.4.2 Variation of nitrate

<b>[HCO<sub>2</sub><sup>-</sup>]</b>	<b>10 mM</b>	<b>1 M</b>
<b>[NaNO<sub>3</sub>]</b>	<b>G(Total H<sub>2</sub>) (molecules / 100 eV)</b>	
<b>1 mM</b>	1.4195	1.3874
	1.3542	1.3502
	1.3853	1.3716
<b>Average</b>	<b>1.3863</b>	<b>1.3698</b>
<b>Std.Dev. (±)</b>	<b>0.0326</b>	<b>0.0187</b>
<b>10 mM</b>	1.2554	1.3098
	1.2513	1.3205
	1.2513	1.3262
<b>Average</b>	<b>1.2527</b>	<b>1.3188</b>
<b>Std.Dev. (±)</b>	<b>0.0023</b>	<b>0.0083</b>
<b>30 mM</b>		1.2748
		1.2928
		1.2888
<b>Average</b>		<b>1.2855</b>
<b>Std.Dev. (±)</b>		<b>0.0094</b>
<b>100 mM</b>	1.1012	1.2044
	1.0998	1.1618
	1.1002	1.2197
<b>Average</b>	<b>1.1004</b>	<b>1.1953</b>
<b>Std.Dev. (±)</b>	<b>0.0007</b>	<b>0.0300</b>
<b>300 mM</b>	0.8764	1.0265
	0.8447	1.0117
	0.8410	1.0283
<b>Average</b>	<b>0.8540</b>	<b>1.0222</b>
<b>Std.Dev. (±)</b>	<b>0.0194</b>	<b>0.0091</b>
<b>1 M</b>	0.5070	0.6457
	0.5534	0.6419
		0.6490
<b>Average</b>	<b>0.5302</b>	<b>0.6455</b>
<b>Std.Dev. (±)</b>	<b>0.0328</b>	<b>0.0036</b>

<b>[DCO<sub>2</sub>]</b>	<b>10 mM</b>			
<b>[NaNO<sub>3</sub>]</b>	<b>G(Total H<sub>2</sub>)</b> molecules/100eV	<b>G(H<sub>2</sub>)</b> molecules/100eV	<b>G(HD)</b> molecules/100eV	<b>G(D<sub>2</sub>)</b> molecules/100eV
<b>1 mM</b>	1.4563	1.3190	0.1344	0.0028
	1.4472	1.3029	0.1443	0.0000
	1.3917	1.2551	0.1366	0.0000
<b>Average</b>	<b>1.4317</b>	<b>1.2923</b>	<b>0.1384</b>	<b>0.0009</b>
<b>Std.Dev.</b>	<b>0.0350</b>	<b>0.0332</b>	<b>0.0052</b>	<b>0.0016</b>
<b>10 mM</b>	1.3606	1.2302	0.1304	0.0000
	1.3558	1.2170	0.1388	0.0000
	1.3540	1.2279	0.1261	0.0000
<b>Average</b>	<b>1.3568</b>	<b>1.2250</b>	<b>0.1317</b>	<b>0.0000</b>
<b>Std.Dev.</b>	<b>0.0034</b>	<b>0.0070</b>	<b>0.0065</b>	<b>0.0000</b>
<b>100 mM</b>	1.1557	1.0786	0.0718	0.0052
	1.0691	0.9997	0.0694	0.0000
	1.0757	1.0097	0.0660	0.0000
<b>Average</b>	<b>1.1001</b>	<b>1.0294</b>	<b>0.0690</b>	<b>0.0017</b>
<b>Std.Dev.</b>	<b>0.0482</b>	<b>0.0430</b>	<b>0.0029</b>	<b>0.0030</b>
<b>300 mM</b>	0.7941	0.7133	0.0228	0.0580
	0.7566	0.7223	0.0310	0.0032
	0.7692	0.7389	0.0303	0.0000
<b>Average</b>	<b>0.7733</b>	<b>0.7248</b>	<b>0.0280</b>	<b>0.0204</b>
<b>Std.Dev.</b>	<b>0.0191</b>	<b>0.0130</b>	<b>0.0046</b>	<b>0.0326</b>
<b>1 M</b>	0.4218	0.4089	0.0117	0.0012
	0.4220	0.4112	0.0108	0.0000
	0.3858	0.3772	0.0086	0.0000
<b>Average</b>	<b>0.4099</b>	<b>0.3991</b>	<b>0.0104</b>	<b>0.0004</b>
<b>Std.Dev.</b>	<b>0.0208</b>	<b>0.0190</b>	<b>0.0016</b>	<b>0.0007</b>
<b>3 M</b>	0.2062	0.2028	0.0027	0.0006
	0.1981	0.1962	0.0017	0.0002
	0.2017	0.2001	0.0014	0.0002
<b>Average</b>	<b>0.2020</b>	<b>0.1997</b>	<b>0.0019</b>	<b>0.0003</b>
<b>Std.Dev.</b>	<b>0.0041</b>	<b>0.0033</b>	<b>0.0007</b>	<b>0.0003</b>

<b>[DCO<sub>2</sub>]</b>	<b>1 M</b>			
<b>[NaNO<sub>3</sub>]</b>	<b>G(Total H<sub>2</sub>)</b> molecules/100eV	<b>G(H<sub>2</sub>)</b> molecules/100eV	<b>G(HD)</b> molecules/100eV	<b>G(D<sub>2</sub>)</b> molecules/100eV
<b>1 mM</b>	1.3595	1.0456	0.2905	0.0235
	1.4014	1.0787	0.2958	0.0269
	1.3999	1.0648	0.3083	0.0267
<b>Average</b>	<b>1.3869</b>	<b>1.0630</b>	<b>0.2982</b>	<b>0.0257</b>
<b>Std.Dev.</b>	<b>0.0238</b>	<b>0.0166</b>	<b>0.0092</b>	<b>0.0019</b>
<b>10 mM</b>	1.2995	0.9858	0.2851	0.0286
	1.2933	0.9704	0.2929	0.0301
	1.3201	0.9878	0.3039	0.0283
<b>Average</b>	<b>1.3043</b>	<b>0.9813</b>	<b>0.2940</b>	<b>0.0290</b>
<b>Std.Dev.</b>	<b>0.0140</b>	<b>0.0095</b>	<b>0.0095</b>	<b>0.0009</b>
<b>100 mM</b>	1.0701	0.7707	0.2782	0.0212
	1.1244	0.8196	0.2784	0.0264
	1.1057	0.8038	0.2767	0.0252
<b>Average</b>	<b>1.1001</b>	<b>0.7981</b>	<b>0.2778</b>	<b>0.0242</b>
<b>Std.Dev.</b>	<b>0.0276</b>	<b>0.0250</b>	<b>0.0009</b>	<b>0.0027</b>
<b>300 mM</b>	0.9180	0.6493	0.2424	0.0263
	0.8928	0.6257	0.2393	0.0278
	0.9041	0.6354	0.2430	0.0257
<b>Average</b>	<b>0.9050</b>	<b>0.6368</b>	<b>0.2416</b>	<b>0.0266</b>
<b>Std.Dev.</b>	<b>0.0126</b>	<b>0.0119</b>	<b>0.0020</b>	<b>0.0011</b>
<b>1 M</b>	0.5409	0.3648	0.1523	0.0238
	0.5672	0.3825	0.1586	0.0261
	0.5574	0.3760	0.1583	0.0231
<b>Average</b>	<b>0.5552</b>	<b>0.3744</b>	<b>0.1564</b>	<b>0.0243</b>
<b>Std.Dev.</b>	<b>0.0133</b>	<b>0.0090</b>	<b>0.0036</b>	<b>0.0016</b>



## 1.4.3 Variation of selenate

<b>[HCO<sub>2</sub><sup>-</sup>]</b>	<b>10 mM</b>	<b>1 M</b>
<b>[Na<sub>2</sub>SeO<sub>4</sub>]</b>	<b>G(Total H<sub>2</sub>) (molecules / 100 eV)</b>	
<b>1 mM</b>	1.3504	1.3997
	1.3677	1.4076
	1.3553	1.3768
<b>Average</b>	<b>1.3578</b>	<b>1.3947</b>
<b>Std.Dev. (±)</b>	<b>0.0089</b>	<b>0.0160</b>
<b>10 mM</b>	1.3202	1.3882
	1.3283	1.3868
	1.3240	1.3893
<b>Average</b>	<b>1.3242</b>	<b>1.3881</b>
<b>Std.Dev. (±)</b>	<b>0.0040</b>	<b>0.0013</b>
<b>30 mM</b>		1.3413
		1.3643
		1.3539
<b>Average</b>		<b>1.3531</b>
<b>Std.Dev. (±)</b>		<b>0.0115</b>
<b>100 mM</b>	1.2534	1.2715
	1.2496	1.2692
	1.2348	1.2673
<b>Average</b>	<b>1.2459</b>	<b>1.2693</b>
<b>Std.Dev. (±)</b>	<b>0.0098</b>	<b>0.0021</b>
<b>300 mM</b>	0.9508	1.0658
	0.9534	1.0925
		1.0790
<b>Average</b>	<b>0.9521</b>	<b>1.0791</b>
<b>Std.Dev. (±)</b>	<b>0.0018</b>	<b>0.0133</b>
<b>1 M</b>	0.5085	0.6660
	0.5054	0.6493
	0.4985	0.6309
<b>Average</b>	<b>0.5041</b>	<b>0.6487</b>
<b>Std.Dev. (±)</b>	<b>0.0051</b>	<b>0.0175</b>

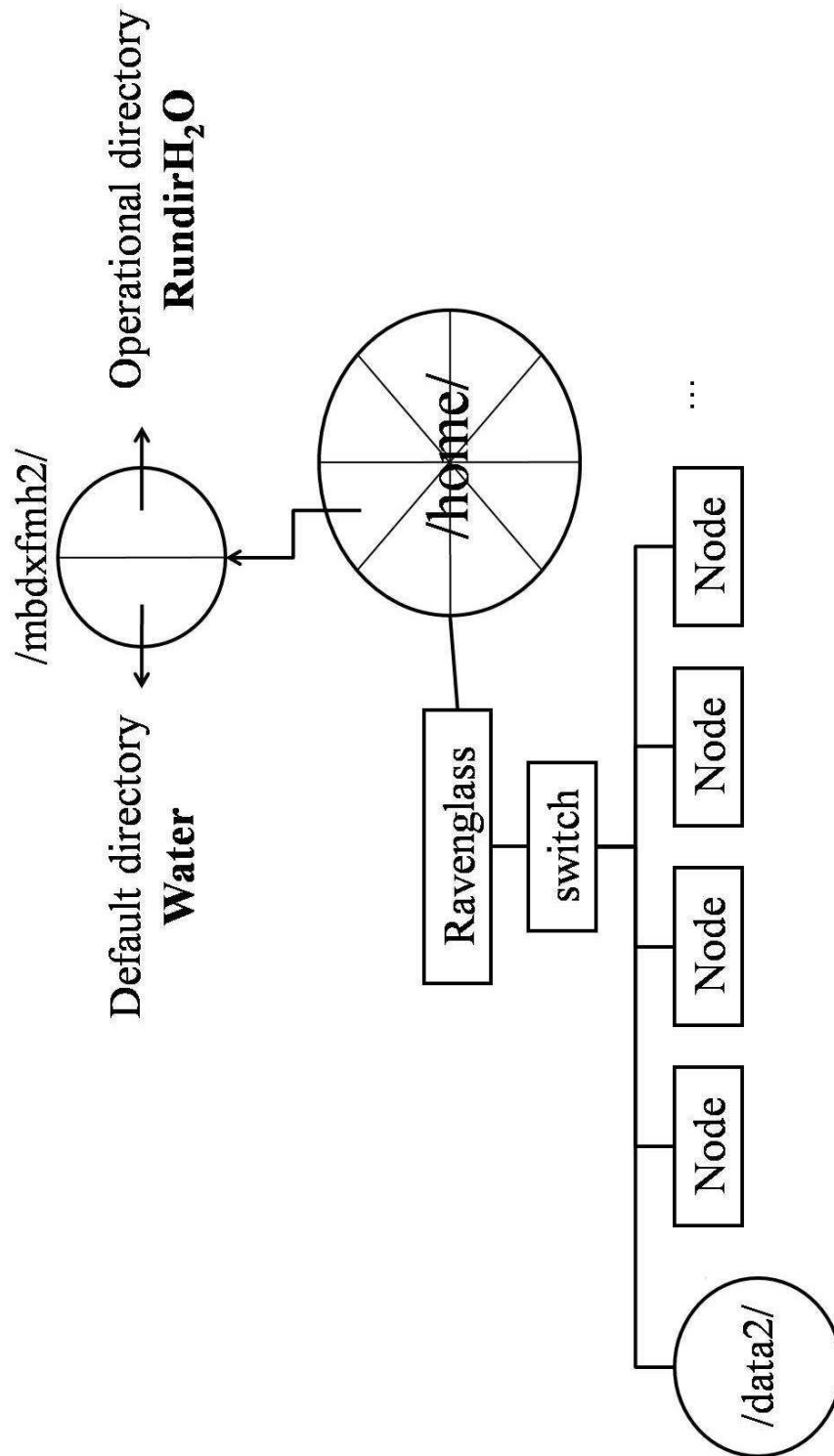
<b>[DCO<sub>2</sub>]</b>	<b>10 mM</b>			
<b>[Na<sub>2</sub>SeO<sub>4</sub>]</b>	<b>G(Total H<sub>2</sub>)</b> molecules/100eV	<b>G(H<sub>2</sub>)</b> molecules/100eV	<b>G(HD)</b> molecules/100eV	<b>G(D<sub>2</sub>)</b> molecules/100eV
<b>1 mM</b>	1.3687	1.2706	0.0921	0.0060
	1.3607	1.2784	0.0823	0.0000
	1.3316	1.2466	0.0850	0.0000
<b>Average</b>	<b>1.3536</b>	<b>1.2652</b>	<b>0.0864</b>	<b>0.0020</b>
<b>Std.Dev.</b>	<b>0.0195</b>	<b>0.0166</b>	<b>0.0051</b>	<b>0.0035</b>
<b>10 mM</b>	1.2861	1.1973	0.0884	0.0004
	1.2704	1.1845	0.0851	0.0009
	1.2856	1.1988	0.0868	0.0000
<b>Average</b>	<b>1.2807</b>	<b>1.1935</b>	<b>0.0868</b>	<b>0.0004</b>
<b>Std.Dev.</b>	<b>0.0089</b>	<b>0.0079</b>	<b>0.0017</b>	<b>0.0004</b>
<b>100 mM</b>	1.0614	0.9986	0.0627	0.0001
	1.0004	0.9388	0.0616	0.0000
	1.0570	0.9945	0.0625	0.0000
<b>Average</b>	<b>1.0396</b>	<b>0.9773</b>	<b>0.0623</b>	<b>0.0000</b>
<b>Std.Dev.</b>	<b>0.0340</b>	<b>0.0334</b>	<b>0.0006</b>	<b>0.0000</b>
<b>300 mM</b>	0.7415	0.7044	0.0363	0.0007
	0.7646	0.7289	0.0357	0.0000
	0.7713	0.7356	0.0357	0.0000
<b>Average</b>	<b>0.7591</b>	<b>0.7230</b>	<b>0.0359</b>	<b>0.0002</b>
<b>Std.Dev.</b>	<b>0.0156</b>	<b>0.0164</b>	<b>0.0003</b>	<b>0.0004</b>
<b>1 M</b>	0.4340	0.4203	0.0137	0.0000
	0.4325	0.4168	0.0157	0.0000
	0.4212	0.4070	0.0142	0.0000
<b>Average</b>	<b>0.4292</b>	<b>0.4147</b>	<b>0.0146</b>	<b>0.0000</b>
<b>Std.Dev.</b>	<b>0.0070</b>	<b>0.0069</b>	<b>0.0010</b>	<b>0.0000</b>

# APPENDIX C

## Command Scripts

1.1	Ravenglass layout.....	196
1.2	TS_MHP.com.....	197
1.3	run_ravenglass.com.....	199

## 1.1 Ravenglass layout



## 1.2 TS\_MHP.com (Used to submit job to computer cluster)

```
#!/bin/csh
```

```
setenv TOP "/home/ravenglass/mbdxfmh2/"
setenv HOME "/home/ravenglass/mbdxfmh2/"
setenv HOME1 $HOME"Water/"
setenv FRNT "1mM_NaNO3_H2O2_"
```

Setting environmental variables

Job name

```
# Directory
cd $HOME
```

Move to users home directory

```
# Present directory
pwd
```

```
# Compile programs
# cd $HOME"Programs"
ifort -O1 -o ranchange.exe
$TOP"/MyPrograms/Ranchange/ranchange.f"
ifort -O1 -CB -DH=C -DA=D -DD -Iinclude -o Tracksim_coord.exe
/home/ravenglass/mbdsssp5/MyPrograms/Hydrotrack/Source/*.F
ifort -O1 -CB -Iinclude -o PhysicoChem.exe
/home/ravenglass/mbdsssp5/MyPrograms/PhysicoChem/Source/*.f
ifort -O1 -CB -Iinclude -o PhysicoChem_full.exe
/home/ravenglass/mbdsssp5/MyPrograms/PhysicoChem/Source/*.f
ifort -O1 -CB -pc32 -Iinclude -o Kinetics_new.exe
/home/ravenglass/mbdsssp5/MyPrograms/Kinetics3/Source_new/*.f
ifort -O1 -CB -Iinclude -o TrackReduce.exe
$TOP"/MyPrograms/TrackReduce/Source/trk_conv5.f"
```

```
# Directory
cd $HOME"RundirH2O"
```

Compile programs

```
pwd
```

```
# Fragmentation datafile
rm ssrp_trk.frg
cp $HOME1"em.frg" ssrp_trk.frg
```

```
# Simulation methods
rm simuln_methods.dat
cp $HOME1"simuln_methods_rt.dat" simuln_methods.dat
```

```
# Chemistry datafile
rm ssrp_trk.dat
cp $HOME1"Chemistry/MHP_NO3-_may09.dat" ssrp_trk.dat
```

```
# Submit file
rm run.com
cp $HOME1"run_ravenglass.com" run.com
```

Command file

```
Loop begins
```

```
set i = -1
while ( $i < 99 )
@ i = $i + 1
```

Number of nodes

Copying info from default directory to operational directory

```
echo $i
```

```
if ( $i < 10 ) then
```

```
# Job name
setenv JOB_NAME $FRNT"0"$i
```

```
else
```

```
# Job name
setenv JOB_NAME $FRNT$i
```

→ Different jobname for each node

```
endif
```

```
# Remove old dump file
rm $JOB_NAME".dump"
```

→ Clean up information dump files

```
# Track datafile
rm $JOB_NAME"_track.dat"
cp $HOME1"Ion/track.dat" $JOB_NAME"_track.dat"
```

→ Radiation energy and type

```
# New random Number
rm $JOB_NAME".dat"
$TOP'Programs/ranchange.exe'
cp rnseeds.dat $JOB_NAME".dat"
```

→ Generate new random number seeds for each node

```
# Submit file
rm $JOB_NAME
cp run.com $JOB_NAME
```

→ Creates individual command script for each node

```
# Submit job
qsub $JOB_NAME
# ./ $JOB_NAME
```

→ Submit job to node

```
end
```

———— Loop ends

```
exit
```

### 1.3 run\_ravenglass.com (Used to run simulations on cluster node)

```
#!/bin/csh -f
```

```
setenv TOP '/home/ravenglass/mbdxfmh2/'
setenv HOME '/home/ravenglass/mbdxfmh2/'
setenv HOME1 $HOME'Water/'
setenv HOME2 $HOME'RundirH2O/'
setenv JOB_NAME $PBS_JOBNAME
setenv NREAL 100
```

Setting environmental variables

Number of tracks simulated on this node

```
cd /data2/mbdxfmh2/
```

Move to scratch memory space of the cluster

```
mkdir $JOB_NAME'_dir'
```

Create operational directory in scratch memory space

```
cd $JOB_NAME'_dir'
```

Move to directory

```
# Present directory
```

```
pwd
```

Echos to log file directory name

```
# Setup
```

```
# Random number seeds
cp $HOME2$JOB_NAME'.dat' rnseeds.dat
rm -f rnseeds.old
cp rnseeds.dat rnseeds.old
```

```
# Restart info
rm -f ssrp_trk.rst
cp $HOME1'restart.rst' ssrp_trk.rst
```

```
# Simulation methods
rm simuln_methods.dat
cp $HOME1'simuln_methods_rt.dat' simuln_methods.dat
```

```
# Track file location
rm track.inp
cp $HOME1'track.inp' track.inp
```

Input variables to run program

```
# Cross-section files
rm xsectns_H2Oliq.dat
cp $HOME1'xsectns_H2Oliq.dat' xsectns_H2Oliq.dat
```

```
# Medium data
rm medium_param.dat
cp $HOME1'medium_298.dat' medium_param.dat
```

```
# Track datafile
rm track.dat
# cp $HOME1'track.dat' track.dat
cp $HOME2$PBS_JOBNAME'_track.dat' track.dat
```

Type of radiation

```
rm trk_conv.inp
cp $HOME1'trk_conv.inp' trk_conv.inp
```

```
# Fragmentation distribution
rm -f ssrp_trk.frg
cp $HOME2'ssrp_trk.frg' ssrp_trk.frg
```

Fates of ionization and  
excitation events

```
# Chemistry datafile
# in TS file
rm -f ssrp_trk.dat
cp $HOME2'ssrp_trk.dat' ssrp_trk.dat
```

Input data (chemistry)

Input variables to run program

```
# Kinetics run file
rm ssrp_trk.inp
cp $HOME1'ssrp_trk.inp' ssrp_trk.inp
```

Verification file

```
# Time files
rm reorg*.inp
cp $HOME1'reorg1.inp' reorg1.inp
cp $HOME1'reorg2.inp' reorg2.inp
cp $HOME1'reorg3.inp' reorg3.inp
cp $HOME1'reorg4.inp' reorg4.inp
cp $HOME1'reorg5.inp' reorg5.inp
cp $HOME1'reorg6.inp' reorg6.inp
cp $HOME1'reorg7.inp' reorg7.inp
cp $HOME1'reorg8.inp' reorg8.inp
cp $HOME1'reorg9.inp' reorg9.inp
# cp $HOME1'reorg10.inp' reorg10.inp
# cp $HOME1'reorg11.inp' reorg11.inp
# cp $HOME1'reorg12.inp' reorg12.inp
# cp $HOME1'reorg13.inp' reorg13.inp
# cp $HOME1'reorg14.inp' reorg14.inp
```

Times at which arrays describing  
chemical species are reorganized

```
echo " Finished setup "
```

```
pwd
```

Loop begins

```
set i = 0
while ( $i < $NREAL )
@ i = $i + 1
```

```
$TOP'Programs/Tracksim_coord.exe' < track.inp
$TOP'Programs/PhysicoChem.exe' < trk_conv.inp
```

Track structure (energy,  
ionization and excitation)

Type of ionization and  
excitation

```
$TOP'Programs/Kinetics_new.exe' < ssrp_trk.inp
$TOP'Programs/TrackReduce.exe' < reorg1.inp
```

Chemistry

Clean up

```
$TOP'Programs/Kinetics_new.exe' < ssrp_trk.inp
$TOP'Programs/TrackReduce.exe' < reorg2.inp
```

```
$TOP'Programs/Kinetics_new.exe' < ssrp_trk.inp
$TOP'Programs/TrackReduce.exe' < reorg3.inp
```

```
$TOP'Programs/Kinetics_new.exe' < ssrp_trk.inp
$TOP'Programs/TrackReduce.exe' < reorg4.inp
```

```
$TOP'Programs/Kinetics_new.exe' < ssrp_trk.inp
$TOP'Programs/TrackReduce.exe' < reorg5.inp
```

```
$TOP'Programs/Kinetics_new.exe' < ssrp_trk.inp
$TOP'Programs/TrackReduce.exe' < reorg6.inp
```



```
$TOP'Programs/Kinetics_new.exe' < ssrp_trk.inp
$TOP'Programs/TrackReduce.exe' < reorg7.inp
```

```
$TOP'Programs/Kinetics_new.exe' < ssrp_trk.inp
$TOP'Programs/TrackReduce.exe' < reorg8.inp
```

```
STOP'Programs/Kinetics_new.exe' < ssrp_trk.inp
STOP'Programs/TrackReduce.exe' < reorg9.inp
```

```
# $TOP'Programs/Kinetics_new.exe' < ssrp_trk.inp
# $TOP'Programs/TrackReduce.exe' < reorg10.inp
```

```
# $TOP'Programs/Kinetics_new.exe' < ssrp_trk.inp
# $TOP'Programs/TrackReduce.exe' < reorg11.inp
```

```
# $TOP'Programs/Kinetics_new.exe' < ssrp_trk.inp
# $TOP'Programs/TrackReduce.exe' < reorg12.inp
```

```
# $TOP'Programs/Kinetics_new.exe' < ssrp_trk.inp
# $TOP'Programs/TrackReduce.exe' < reorg13.inp
```

```
# $TOP'Programs/Kinetics_new.exe' < ssrp_trk.inp
# $TOP'Programs/TrackReduce.exe' < reorg14.inp
```

```
$TOP'Programs/Kinetics_new.exe' < ssrp_trk.inp
```

```
rm ssrp_trk.oldd
cp ssrp_trk.dump ssrp_trk.oldd
rm sumtrack.oldd
cp sumtrack.dump sumtrack.oldd
```

Cleaning old data dump files and rewriting with new information

```
end
```

Loop ends

```
# Rename output files
cat track.dat > test.res
cat sumtrack.res >> test.res
cat ssrp_trk.dat >> test.res
cat ssrp_trk.res >> test.res
rm $HOME2$JOB_NAME'_Results.res'
mv test.res $HOME2$JOB_NAME'_Results.res'
mv ssrp_trk.kin0 $HOME2$JOB_NAME'_Kinetics0.res'
mv ssrp_trk.kin1 $HOME2$JOB_NAME'_Kinetics1.res'
mv ssrp_trk.kin2 $HOME2$JOB_NAME'_Kinetics2.res'
mv facin.dat $HOME2$JOB_NAME'_Yields.dat'
```

Output results

```
rm $HOME2$JOB_NAME'.dump'
cp ssrp_trk.dump $HOME2$JOB_NAME'.dump'
```

Store information (produce much more than output in results files)

```
rm * → Remove all information on the scratch memory space
```

```
cd /data2/mbdxfmh2/ → Move to top directory in scratch memory space
```

```
rmdir $JOB_NAME'_dir' → Remove operational directory from scratch memory space
```

```
exit
```